Combined Neural Network and CFD Modelling of Extreme Storm Surges

Von der
Fakultät Architektur, Bauingenieurwesen und Umweltwissenschaften
der Technischen Universität Carolo-Wilhelmina
zu Braunschweig

zur Erlangung des Grades eines
Doktoringenieur (Dr.-Ing.)
genehmigte

Dissertation

von
Mohamed Fathy Tawfeek Ramadan Tayel
geboren am 01.01.1981
aus Beheira, Ägypten

Eingereicht am: 21. Mai 2015
Disputation am: 08. September 2015

Berichterstatter: Prof. Hocine Oumeraci
Prof. Jürgen Jensen

2015

To my beloved family and sons

„Gedruckt bzw. veroffentlicht mit Unterstutzung des Deutschen
Akademischen Austauschdienstes“

Preface

Over the last 5 years, it has been my fortune to meet many nice people who have provided me with their time, knowledge, support, companionship and patience. This thesis is a result of a long and complex process involving chaotic brainstorms, discussion, feedbacks and motivations from those people.

I would like to gratefully acknowledge the financial support by German Academic Exchange Service (DAAD) for pursuing the doctoral studies in the frame of the GERLS 2009/2010 programme (German Egyptian Research Long-term Scholarship).

First of all, I would like to thank my promotor and supervisor, Prof. Oumeraci, for providing me this opportunity to conduct my PhD at LWI. He has not only given me with deep thought, fresh innovation, critical feedbacks, but he also offered me full support and strong motivation. His valuable guidance and nice communication made doing research with him attractive and pleasant. Without these contributions from him, I would never have come to this stage.

My deep gratitude goes to Prof. Jensen from Research Institute for Water and Environment-University of Siegen, for his valuable support in the evaluation reports for the DAAD, valuable advices and feedbacks. His sharing of data, especially at the beginning of the study, provides inputs and suggestions for my research.

My thanks also go to Dr. Plüß from the Federal Waterways Engineering and Research Institute (BAW) for providing a computational TELEMAC-grid for the entire North Sea (2006) with the related bathymetry and boundary conditions data. He also offered the computational support to run the simulations by providing the 8 cores computer in BAW. Moreover, his guidance and help with JANET/DAVIT software to deal with TELEMAC2D input/output data. Without this initial support from him, it would be harder to use TELEMAC2D in such reasonable time period.

I am also very grateful to Dr. Gönnert from the Agency of Roads, Bridges and Waters, Dr. Weisse and Dr. Meyer from Helmholtz-Zentrum Geesthacht (HZG) in Hamburg for sharing their data and all their support, especially at the beginning of the study.

Finally, I would like to express my deepest gratitude to my parents and my small family in Egypt. They always give me love and encouragement from miles away. I owe everything to them, without their ever-lasting love and support; I never would have completed this PhD study.

Braunschweig, May 2015 Mohamed Fathy Tawfeek Tayel

Kurzfassung

Genaue Vorhersagen der Sturmflut sind von entscheidender Bedeutung für viele Küstengebiete. Dies gilt umso mehr, da mit weiterem zunehmendem Nutzungsdruck auf die Küstengebiete, die bereits heute stark besiedelt sind und beträchtliche Sachwerte aufweisen, die Schäden durch extreme Sturmfluten sehr hoch sein können. Vor allem entlang der Nordseeküste werden zuverlässige Sturmflutvorhersagen benötigt, da ein Großteil der Küstengebiete nicht nur unter dem Meeresspiegel liegt, sondern auch häufigen Stürmen ausgesetzt ist. Der Beitrag der Wechselwirkungen zwischen den verschiedenen Sturmflutkomponenten zum resultierenden Extremwasserstand ist noch nahezu vollständig unbekannt, da die Wechselwirkungen in der Regel nicht-linear und nicht-stationär sind. Derzeit kann die Natur dieser nicht-linearen Wechselwirkungen und deren Beitrag zur Extremsturmflut noch nicht durch herkömmliche numerische hydrodynamische oder statistische Modelle allein gelöst werden. Alternativ wird ein pragmatischer datengesteuerten Ansatz vorgeschlagen, beispielhaft für Cuxhaven und Sylt, der die Vorhersagen des CFD-Modells TELEMAC und die nichtlinearen autoregressive Inputs mit exogenen wiederkehrenden neuronalen Netzen (NARX) in einem Hybridmodell kombiniert. Das Hybridmodell TELEMAC –NARX ermöglicht, den Beitrag der nichtlinearen Wechselwirkungen zwischen den Sturmflutkomponenten implizit zu bestimmen. Dadurch wird auch ermöglicht, die Korrektur der oft beträchtlichen Fehler der Ergebnisse der CFD-Modelle hinsichtlich Höhe und Eintrittszeit der Wasserstände zu korrigieren. Die Vorhersage des Hybridmodells wird durch die beobachteten Wasserstände von 1999 bis 2007 in Cuxhaven und Sylt validiert. Im Durchschnitt ergeben sich für die Ergebnisse des Hybridmodells an beiden Standorten eine Wurzel des mittleren quadratischen Fehlers (RMSE) von 0,14 m und ein Korrelationskoeffizient von 0,99. Der maximale Beitrag der nichtlinearen Wechselwirkung $(\eta_{NL})_{max}$ bei Cuxhaven, die 21% der höchsten Sturmflut ($(\eta_{all})_{max}$ = 7,21 m NN) aller in 1991 bis 2007 eingetretenen Extremsturmfluten erreicht, ist niedriger als der Beitrag bei Sylt mit 25,80% bezogen auf die höchste ($(\eta_{all})_{max}$ = 5,66 m NN) der Extremsturmfluten im gleichen Zeitraum. In den meisten extremen Sturmflutereignissen dieser Studie führte die Berücksichtigung der nicht linearen Wechselwirkungen der Sturmflutkomponenten zu niedrigeren Sturmflutwasserständen als die, die aus der linearen Überlagerung der Komponenten resultierten. Jedoch, unter bestimmten Bedingungen, führten die nicht linearen Wechselwirkungen zu höheren Sturmfluten als die lineare Überlagerung (z.B. Sturmflut vom Januar 2000 bei Cuxhaven und Sylt).

Zusätzlich zum mittleren Meeresspiegelanstieg könnte sich die Bedrohung durch extreme Sturmfluten infolge veränderter Stürme als einer der dramatischsten Auswirkungen des Klimawandels erweisen. Die zeitlichen Änderungen der Signale des Klimawandels hinsichtlich der Sturmfluten für das Emissionsszenario A1B 2070-2100 in Cuxhaven und Sylt, werden anhand des neuen Hybridmodells eingeschätzt. Die Erhöhung der extremen Sturmfluten infolge des Klimawandels ist von Bedeutung für die Deutsche Bucht und die niederländische Küste, jedoch mit einer beträchtlichen Abnahme für die Mitte der Nordsee und entlang der britischen Ostküste. Die maximale Sturmfluten für das A1B-Szenario bei Cuxhaven und Sylt sind höher als die maximalen Sturmfluten ($(\eta_{EFN})_{max}$) an beiden Standorten von 1991 bis 2007, mit jeweils 0,19 m (4,8%) für Cuxhaven und 0,54 m (17,9%) für Sylt. Die künftige Zunahme der Häufigkeit extremer Sturmfluten allein wäre für viele Küstenanlagen unbedeutend. Dies ist jedoch nicht der Fall für die Zunahme der Höhe und Dauer der Sturmfluten, die zu einer Reduzierung der Sicherheit der Anlagen führen würden.

Abstract

Accurate predictions of storm-tide are of vital importance for many coastal areas. Especially with further increasing pressure on the coastal areas, already with a high population density and highly valuable assets, the costs of extreme storm-tide damage can be very high. Particularly along North Sea coasts, reliable storm-tide predictions are of crucial importance as a large portion of the coastal zones is not only below mean sea level but also characterized by frequent storms. The contribution of the mutual interactions between the various storm-tide components to the resulting extreme water level is still almost fully unknown as these interactions are generally nonlinear and non-stationary. Currently, the nature of these mutual nonlinear interactions and their contributions to the extreme storm-tide cannot yet be solved by conventional hydrodynamic models or statistical models alone. Alternatively, a pragmatic data-driven approach is proposed and exemplarily implemented in Cuxhaven and Sylt, which combines the predictions of hydrodynamic model (TELEMAC) and nonlinear autoregressive with exogenous input (NARX) recurrent neural networks model. This approach, called hybrid TELEMAC-NARX model, can implicitly account for the nonlinear interactions among all storm-tide components. This enables the substantial errors in both magnitude and timing of the results predicted by the hydrodynamic model to be corrected. The prediction of the hybrid model is validated using the observed water level (1999-2007) at Cuxhaven and Sylt, the average performance of the hybrid models at both sites has a root mean square error of 0.14 m and a correlation coefficient of 0.99. The maximum effect of the nonlinear interaction $(\eta_{NL})_{max}$ at Cuxhaven, which reaches 21% from the highest physical limit of extreme storm-tide (1991-2007) $(\eta_{all})_{max}$ =7.21 m NN, is lower than its counterpart of 25.80% from $(\eta_{all})_{max}$ =5.66 m NN at Sylt. In the most extreme storm-tide events considered in this study, the contribution of the nonlinear interaction resulted in smaller extreme water levels than those obtained through linear superposition of extreme storm-tide components. However, under certain conditions, the nonlinear interactions might result in higher storm-tides than those resulting from the linear superposition (e.g. storm of January 2000 at Cuxhaven and Sylt).

As one of the most dramatic impacts of climate change in addition to the increase of mean sea level rise, the threat by extreme storm-tides might increase mainly due to the change in wind climate under emission scenario (A1B 2070-2100). The increase of the magnitude of the extreme surge-tide due to climate change is significant for the German Bight and the Netherlands coasts, while it decreases significantly for the middle of the North Sea and along the UK east coast. The temporal variations of the climate change signals for storm-tide at the two pilot sites, Cuxhaven and Sylt, are assessed using the new hybrid model. The maximum storm-tide under the A1B scenario at Cuxhaven and Sylt are higher than the maximum of storm-tide $((\eta_{EFN})_{max})$ at both sites in (1991-2007) by 0.19 m (4.8 %) and 0.54 m (17.9 %), respectively. The future increase in frequency of extreme storm-tide events alone, which is not significant, would be less relevant for many coastal facilities whereas the increase in duration and/or magnitude of extreme events (both are significant) could decrease their safety.

Table of Contents

List of Figures

List of Tables

List of Notations and Symbols

τ	hour	the time delay
ε	m^2/s^2	turbulent dissipation
α	degree	the steepest slope at a point
$(\eta_{rd})_{max}$	m	maximum contribution of river discharge at Sylt or Cuxhaven
$(\eta_{su\text{-}t\ TEL})_{A1B\_2}$	m	surge-tide under future meteorological condition A1B_2 (2070-2100)
$(\eta_{su\text{-}t\ TEL})_{C20\_2}$	m	surge-tide under control meteorological condition C20_2 (1970-2000)
$(\eta_{su\text{-}t\ TEL})_{H20}$	m	surge-tide under hindcast meteorological condition H20 (1970-2000)
$(V_n + u_n)$	-	the value of the equilibrium argument of the tidal constituent
$\vec{\tau}$	kg/m s^2	Friction stress at sea bottom
$\Delta^x_{C20\_2}(100)$	m	bias signal of surge-tide as difference between the mean value $P^x_{C20\_2}(100)$ in the control simulation (C20_2) and the corresponding mean value $P^x_{H20}(100)$ from the hindcast simulation (H20)
$\Delta^x_{C20\_2}(99.5)$	m	bias signal of surge-tide as difference between $P^x_{C20\_2}(99.5)$ in the control simulation (C20_2) and the corresponding mean value $P^x_{H20}(99.5)$ from the hindcast simulation (H20)
$\Delta f\_w^{Cuxhaven}_{A1B\_2}$	hour/year	differences in strong winds (≥ 17.2 m/s) frequencies between the end of 21st century (2070-2100) and the reference control climate (1970-2000) at Cuxhaven
$\Delta f\_w^{Sylt}_{A1B\_2}$	hour/year	differences in strong winds frequencies (≥ 17.2 m/s) between the end of 21st century (2070-2100) and the reference control climate (1970-2000) at Sylt
$\Delta^x(100)$	m	climate change signal of surge-tide as difference between the mean value $P^x_{A1B\_2}(100)$ in the climate change simulation (A1B_2) and the corresponding mean value $P^x_{C20\_2}(100)$ from the control simulation (C20_2)
$\Delta^x(99.5)$	m	climate change signal of surge-tide as difference between the mean value $P^x_{A1B\_2}(99.5)$ in the climate change simulation (A1B_2) and the corresponding mean value $P^x_{C20\_2}(99.5)$ from the control simulation (C20_2)
$(\eta_{all})_{max}$	m	linear superpostion of the extracted highest peaks of predicted storm-tide components including the nonlinear interaction highest peak
$(\eta_{all})_{min}$	m	linear superpostion of the extracted lowest troughs of predicted storm-tide components including the nonlinear interaction lowest trough
$(\eta_{EFN})_{max}$	m	the extracted highest peak of predicted storm-tide by NARX ensemble
$(\eta_{es})_{max}$	m	the extracted highest peak of predicted external surge by TELEMAC2D
$(\eta_{es})_{min}$	m	the extracted lowest trough of predicted external surge by TELEMAC2D
$(\eta_L)_{max}$	m	the extracted highest peak of predicted storm-tide by independent linear superposition of storm-tide components without considering their nonlinear interaction
$(\eta_{NL})_{max}$	m	highest peak of nonlinear interaction
$(\eta_{NL})_{min}$	m	lowest trough of nonlinear interaction
$(\eta_{OB})_{max}$	m	the extracted highest peak of observed storm-tide at Cuxhaven or Sylt

$(\eta_{\text{su-t TEL}})_{\max}$	m	the extracted highest peak of predicted surge-tide by TELEMAC2D
$\vec{n_f}$	-	the normal vector to the bottom
$\vec{n_s}$	-	the normal vector of a solid boundary
$\bar{\eta}_b$	m	mean water surface elevation due to wave set-up at the breaker line
$\bar{\eta}_{\max}$	m	mean water surface elevation due to wave set-up at the mean shoreline
$\bar{\eta}_s$	m	mean water surface elevation due to wave set-up at the Stillwater shoreline
$[RMSL]_{max}$	m	the maximum increase of relative mean sea level rise at Cuxhaven and Sylt in 2092
C_c	$m^{1/2}/s$	Chezy friction coefficient
C_f	$m^{1/2}/s$	real friction coefficient
f_n	-	nodal factor of the tidal constituent
g_k	-	the error gradient at iteration k that used to update the X_k in backpropagation algorithm
$\vec{k}$	rad/m	Wave number vector
$s_j^{m'}$	-	the error signal of neuron (j) in the layer m', which is computed based on whether or not neuron j is in the output layer
S_{tot}	$Jule/Hz^2.rad$	total source/sink term that represents all physical processes that generate, dissipate, or redistribute wave action density
S_{wx}, S_{wy}	m/s^2	forcing components due to wind surge
u_{wind}. v_{wind}	m/s	Velocity components of wind speed
X_k	-	the combined weights and biases vector at iteration k in order to minimize the ANN error
α_s	-	the learning rate used to adapts the ANN weights according to the gradient error
$\bar{\eta}$	m	mean water surface elevation about still-water level
η_A	m	predicted storm-tide by Type-A NARX model at Cuxhaven or Sylt
η_{at}	m	astronomical tides generated in the North Atlantic Ocean
η_B	m	predicted storm-tide by Type-B NARX model at Cuxhaven or Sylt
η_{cor}	m	coriolis force effect
η_{ds}	m	external or deep surges generated at northern parts of the North Sea
η_{EFN}	m	predicted storm-tide by the EFN at Cuxhaven or Sylt
η_{es}	m	external surges effect on water level
η_L	m	linearly superposed TELEMAC2D results of tide, storm surge, external surge and river discharge effects independently
η_{mor}	m	long-term morphological change effect on water level
η_{NL}	m	the nonlinear interaction effect between extreme storm-tide components as the linear addition of η_{NLT} and η_{NLE}
η_{NLE}	m	the complementary nonlinear effects by the EFN as the difference between η_{EFN} and $\eta_{\text{su-t TEL}}$
η_{NLT}	m	the approximated nonlinear effects by TELEMAC2D as the difference between $\eta_{\text{su-t TEL}}$ and η_L
η_{ob}	m	observed storm-tide
η_Q	m	River discharge effect on water level
η_r	m	basin resonance effect on water level
η_R	m	predicted storm-tide results at Sylt by the Relational NARX model
η_{rd}	m	river discharge effect on water level
η_{slp}	m	pressure setup
η_{slr}	m	long-term sea level rise effect on water level
η_{ss}	m	storm surges effect on water level

$\eta_{st\text{-}t\ TEL\text{-}TOM}$	m	predicted storm-tide results of the coupled models TELEMAC2D for hydrodynamic and TOMAWAC for the wave propagation
$\eta_{st\text{-}t}$	m	storm-tide water level
$\eta_{su\text{-}t\ TEL}$	m	predicted surge-tide by TELEMAC2D without including the wave setup effect
$\eta_{su\text{-}t}$	m	surge-tide water level
η_t	m	tide effect on water level
η_w	m	wave set-up (difference between mean and still water level)
η_{wa}	m	wave propagation along the North Sea area
η_{ws}	m	wind setup
ρ_{air}	Kg/m3	Air density
A_n	m	amplitude of the tidal constituent
$\vec{u}$	m/s	Flow velocity vector
$z_i(t)$	-	the output signal of the i^{th} neuron in the hidden layer at time (t) for NARX network
a	-	the generated output vector by any layer in the ANN
a_j	-	The output signal of an individual artificial neuron j
a_{wind}	-	dimensionless quantity represented by the drag coefficient
b	-	the bias vector for any layer in the ANN
b_j	-	bias associated with an artificial neuron j
C	m/s	the wave velocity
CC	-	correlation coefficient
C_g	m/s	the wave group velocity
D_m	degree	Mean wave direction by TOMAWAC
d_u	-	the input-memory orders
d_y	-	the output-memory orders
E	m	the total error as the difference between the target vector and the generated output vector by the ANN
e_q	m	the error in the q^{th} exemplar or pattern
F	$(m^2/hz)/deg$	Directional spectral density of waves
FCOR	rad/s	the Coriolis coefficient
f_{di}	Hz	Discretized Wave frequency by TOMAWAC
F_f	kg m/s^2	Friction force at sea bottom
f_r	Hz	intrinsic or relative wave frequency
f_W	Hz	Wave frequency
F_x,F_y	m/s^2	Components of Wave driving force that affect the flow
g	m/s^2	acceleration due to gravity
G_n	degree	phase lag of the tidal constituent behind the phase of the corresponding constituent at Greenwich
H	m	Wave height
h	m	still water depth
h_b	m	still water depth at breaker line
H_b	m	Breaker wave height
Hessian	-	the Hessian for the sum-of-square error function
H_{os}	m	offshore significant wave height
H_s	m	significant wave height
$IW^{i,j}$	-	Input weight matrix of the ANN input layers, while superscripts i and j are used to identify the source connection (j) and the destination (i) connection
J	-	the Jacobean of the error function
K	-	iteration number used during the ANNs learning to minimize the

		error function
K^*	m^2/s^2	turbulent kinetic energy
K_i, k_j	rad/m	Components of Wave number vector
L	m	wavelength
$LW^{i,j}$	-	Layer weight matrix of the ANN layers , while superscripts i and j are used to identify the source connection (j) and the destination (i) connection
M_2	m	the main lunar semidiurnal tidal constituent
MQ	m^3/s	mean river discharge
N	$Jule/Hz^2.rad$	directional spectrum of wave action N ($Jule.Hz^{-2}.rad^{-1}$)
N	-	number of the input layer's neurons in the NARX network
Na^+	-	Positive sodium ions
ND	-	the number of wave directions included by TOMAWAC
NF	-	the number of wave frequencies included by TOMAWAC
n_j	-	The net signal serves as input to the activation function of an individual artificial neurons
p	-	the input vector of the ANN
p	-	the number of artificial neurons in the output layer of the developed ANN
P_a	Pascal	Sea surface pressure
Q	m^3/s	fresh water river discharge
q	-	the number of training examples or patterns as pairs of inputs and its target outputs
R	-	the number of elements in the input vector of the ANN
$\Re$	-	the set of real numbers
R_{dr}	km	Rossby deformation radius
S	-	the number of artificial neurons in a layer of the ANN
S_{bf}	$Jule/Hz^2.rad$	bottom friction-induced energy dissipation
S_{br}	$Jule/Hz^2.rad$	bathymetric breaking-induced energy dissipation
S_{ds}	$Jule/Hz^2.rad$	whitecapping-induced energy dissipation
S_h	m/s^2	source or sink of fluid
S_{in}	$Jule/Hz^2.rad$	wind-driven wave generation
S_{nl}	$Jule/Hz^2.rad$	non-linear quadruplet interactions
S_p	m/s^2	Pressure setup
S_{tr}	$Jule/Hz^2.rad$	non-linear triad interactions
S_x and S_y	m/s^2	source or sink term of the momentum in u and v
S_{xx} S_{xy} S_{yx} S_{yy}	N/m^2	the component of radiation stress tensor
T	g/l	the passive (non-buoyant) tracer
t	s	time
ta	-	target or observed vector for the ANN that used during training phase
t_j	-	The target signal of an individual artificial neuron
T_m	s	Mean wave period by TOMAWAC
T_N	hours	basin resonance period
T_W	s	wave period
u,v	m/s	Flow velocity components in x and y directions
$u_m(t)$	-	the (m) input variable of the ANNs model at discrete time step t
v_t	m^2/s	the coefficients of momentum
v_T	m^2/s	the coefficients of tracer diffusion
$w_{i,j}$	-	the connection weight between two neurons , while subscripts i and j are used to identify the source connection (j) and the destination (i) connection
w_{ij}	-	the connection weight from the i-th artificial neuron in the preceding

		layer to the current layer neuron j
W^j	-	the synaptic weight matrix of layer (j) in the ANN
x,y	-	Orthogonal Cartesian direction
x_b	m	horizontal distance between the breaker line and the Stillwater shoreline
y(t)	-	the generated output vector by the output layer of the ANN at time t
z	m	Free surface elevation
δ_{ij}	-	the Kronecker symbol (δ_{ij} =1 if i=j and 0 elsewhere)
$\zeta_{(c,t)m}$	m	modelled tide by TELEMAC2D at crests or trough points
$\zeta_{(c,t)r}$	m	real-tidal level at crests or trough points
ζ_m	m	modelled tide by TELEMAC2D
ζ_r	m	real-tidal level at at time t_i
θ	-	implicitation coefficient for nonlinear terms of shallow water equations in TELEMAC2D
θ_{di}	degree	Discretized wave direction by TOMAWAC
θ_W	degree	the direction of wave propagation relative to North=0 degree
μ	-	a parameter governing the step size of the Levenberg-Marquardt algorithm
ρ	Kg/m^3	Water density
σ	m	standard deviation
σ_{dis}	rad/s	the relative (intrinsic) angular frequency
Φ, λ	degree	latitude and longitude of the North Sea
ω	rad/s	angular velocity of the Earth
ω_n	Hz	frequency of the tidal constituent
Hi	-	number of hidden layer's neurons in the NARX network
$f()$	-	the activation function of the artificial neuron
$d\_w_S^x(\geq 99)$	hour	extreme wind duration (wind speed > annual 99% percentile) at mesh point x that is either Cuxhaven or Sylt under s conditions, which is hindcast or control meteorological conditions 1991-2000
$\Delta d_{A1B\_2}^x(\geq 99.5)$	hour	climate change signal of mean duration for extreme surge-tide events as difference between the mean value $d_{A1B\_2}^x(\geq 99.5)$ in the climate change simulation (A1B_2) and the corresponding mean value $d_{C20\_2}^x(\geq 99.5)$ from the control simulation (C20_2)
$\Delta d_{C20\_2}^x(\geq 99.5)$	hour	bias signal of mean duration for extreme surge-tide events as the difference between the mean value $d_{C20\_2}^x(\geq 99.5)$ in the control simulation (C20_2) and the corresponding mean value $d_{H20}^x(\geq 99.5)$ from the hindcast simulation (H20)
$\Delta ds_{A1B\_2}^x(\geq 99.5)$	hour	climate change signal of mean duration for extreme storm-tide events as difference between the mean value $ds_{A1B\_2}^x(\geq 99.5)$ in the climate change simulation (A1B_2) and the corresponding mean value $ds_{C20\_2}^x(\geq 99.5)$ from the control simulation (C20_2)
$\Delta ds_{C20\_2}^x(\geq 99.5)$	hour	bias signal of mean duration for extreme storm-tide events as the difference between the mean value $ds_{C20\_2}^x(\geq 99.5)$ in the control simulation (C20_2) and the corresponding mean value $ds_{H20}^x(\geq 99.5)$ from the hindcast simulation (H20)
$\Delta f_{A1B\_2}^x(\geq 99.5)$	event/year	climate change signal of mean frequency for extreme surge-tide events as difference between the mean value $f_{A1B\_2}^x(\geq 99.5)$ in the climate change simulation (A1B_2) and the corresponding mean value $f_{A1B\_2}^x(\geq 99.5)$ from the control simulation (C20_2)
$\Delta f_{C20\_2}^x(\geq 99.5)$	event/year	bias signal of mean frequency for extreme surge-tide events as the

		difference between the mean value $f^{x}_{C20\_2}(\geq 99.5)$ in the control simulation (C20_2) and the corresponding mean value or $f^{x}_{H20}(\geq 99.5)$ from the hindcast simulation (H20)
$\Delta fs^{x}_{A1B\_2}(\geq 99.5)$	event/year	climate change signal of mean frequency for extreme storm-tide events as difference between the mean value $fs^{x}_{A1B\_2}(\geq 99.5)$ in the climate change simulation (A1B_2) and the corresponding mean value $fs^{x}_{A1B\_2}(\geq 99.5)$ from the control simulation (C20_2)
$\Delta fs^{x}_{C20\_2}(\geq 99.5)$	event/year	bias signal of mean frequency for extreme storm-tide events as the difference between the mean value $fs^{x}_{C20\_2}(\geq 99.5)$ in the control simulation (C20_2) and the corresponding mean value or $fs^{x}_{H20}(\geq 99.5)$ from the hindcast simulation (H20)
$\Delta s^{x}_{C20\_2}(99.5)$	m	bias signal of storm-tide as difference between $Ps^{x}_{C20\_2}(99.5)$ in the control simulation (C20_2) and the corresponding mean value $Ps^{x}_{H20}(99.5)$ from the hindcast simulation (H20)
$\Delta s^{x}(99.5)$	m	climate change signal of storm-tide as difference between the mean value $Ps^{x}_{A1B\_2}(99.5)$ in the climate change simulation (A1B_2) and the corresponding mean value $Ps^{x}_{C20\_2}(99.5)$ from the control simulation (C20_2) at mesh point x that represents either Cuxhaven or Sylt
$[Ps^{x}_{A1B\_2}(99.5)]_{max}$	m	highest effect by 99.5th percentile of mean annual storm-tide at each of Cuxhaven and Sylt under future realization (A1B_2), including $[RMSL]_{max}$
$\mathrm{P}^{\mathrm{x}}_{\mathrm{A1B\_2}}(99.5)$	m	mean of $\mathrm{P}^{\mathrm{xn}}_{\mathrm{A1B\_2}}(99.5)$
$\mathrm{P}^{\mathrm{xn}}_{\mathrm{A1B\_2}}(99.5)$	m	annual 99.5th percentile of surge-tide under future meteorological condition (A1B_2) for years n= 2070-2100 at every mesh point x in the North Sea model
$\mathrm{P}^{\mathrm{x}}_{\mathrm{C20\_2}}(99.5)$	m	mean of $\mathrm{P}^{\mathrm{xn}}_{\mathrm{C20\_2}}(99.5)$
$\mathrm{P}^{\mathrm{xn}}_{\mathrm{C20\_2}}(99.5)$	m	annual 99.5th percentile of surge-tide under control meteorological condition (C20_2) for years n= 1970-2000 at every mesh point x in the North Sea model
$\mathrm{P}^{\mathrm{x}}_{\mathrm{H20}}(99.5)$	m	mean of $\mathrm{P}^{\mathrm{xn}}_{\mathrm{H20}}(99.5)$
$\mathrm{P}^{\mathrm{xn}}_{\mathrm{H20}}(99.5)$	m	annual 99.5th percentile of surge-tide under hindcast meteorological condition (H20) for years n= 1970-2000 at every mesh point x in the North Sea model
$\mathrm{Ps}^{\mathrm{x}}_{\mathrm{A1B\_2}}(99.5)$	m	mean of $\mathrm{Ps}^{\mathrm{xn}}_{\mathrm{A1B\_2}}(99.5)$
$\mathrm{Ps}^{\mathrm{xn}}_{\mathrm{A1B\_2}}(99.5)$	m	annual 99.5th percentile of storm-tide under future meteorological condition (A1B_2) for years n= 2070-2100 at mesh point x that represents either Cuxhaven or Sylt
$\mathrm{Ps}^{\mathrm{x}}_{\mathrm{C20\_2}}(99.5)$	m	mean of $\mathrm{Ps}^{\mathrm{xn}}_{\mathrm{C20\_2}}(99.5)$
$\mathrm{Ps}^{\mathrm{xn}}_{\mathrm{C20\_2}}(99.5)$	m	annual 99.5th percentile of storm-tide under control meteorological condition (C20_2) for years n= 1991-2000 at mesh point x that represents either Cuxhaven or Sylt
$\mathrm{Ps}^{\mathrm{x}}_{\mathrm{H20}}(99.5)$	m	mean of $\mathrm{Ps}^{\mathrm{xn}}_{\mathrm{H20}}(99.5)$
$\mathrm{Ps}^{\mathrm{xn}}_{\mathrm{H20}}(99.5)$	m	annual 99.5th percentile of storm-tide under hindcast meteorological condition (H20) for years n= 1991-2000 at mesh point x that represents either Cuxhaven or Sylt
$\mathrm{Ps}^{\mathrm{x}}_{\mathrm{S}}(99.5)$	m	mean of $\mathrm{Ps}^{\mathrm{xn}}_{\mathrm{S}}(99.5)$
$\mathrm{Ps}^{\mathrm{xn}}_{\mathrm{S}}(99.5)$	m	annual 99.5th percentile of storm-tide where S is either hindcast, control or future meteorological conditions (H20, C20_2 or A1B_2, respectively) for years n= 1991-2000 (H20 and C20) or 2070-2100, respectively, at mesh point x that represents either Cuxhaven or Sylt

$P_s^x(99.5)$	m	mean of $P_s^{xn}(99.5)$
$P_S^{xn}(99.5)$	m	annual 99.5th percentile of surge-tide where S is either hindcast, control or future meteorological conditions (H20, C20_2 or A1B_2, respectively) for years n= 1970-2000 (H20 and C20) or 2070-2100, respectively, at every mesh point x in the North Sea model
$CI_d^x(\geq 99.5)$	hour	confidence interval for the mean duration $d_{H20}^x(\geq 99.5)$ at every mesh point x with a statistical significance level of 95% using student's t test
$CI_f^x(\geq 99.5)$	event/year	confidence interval for the mean frequency $f_{H20}^x(\geq 99.5)$ at every mesh point x with a statistical significance level of 95% using student's t test
$CIs_d^x(\geq 99.5)$	hour	confidence interval for the mean duration $ds_{H20}^x(\geq 99.5)$ at every mesh point x with a statistical significance level of 95% using student's t test
$CIs_f^x(\geq 99.5)$	event/year	confidence interval for the mean frequency $fs_{H20}^x(\geq 99.5)$ at every mesh point x with a statistical significance level of 95% using student's t test
$CIs^x(99.5)$	m	confidence interval for the mean of $Ps_{H20}^{xn}(99.5)$ at every mesh point x with a statistical significance level of 95% using student's t test
$CI^x(99.5)$	m	confidence interval for the mean of $P_{H20}^{xn}(99.5)$ at every mesh point x with a statistical significance level of 95% using student's t test
$d_{A1B\_2}^x(\geq 99.5)$	hour	mean of $d_{A1B\_2}^{xn}(\geq 99.5)$
$d_{A1B\_2}^{xn}(\geq 99.5)$	hour	annual duration of extreme surge-tide events, which exceed annual 99.5th percentile and cover one or more hourly intervals, under future meteorological condition (A1B_2) for years n= 2070-2100 at every mesh point x in the North Sea model
$d_{C20\_2}^x(\geq 99.5)$	hour	mean of $d_{C20\_2}^{xn}(\geq 99.5)$
$d_{C20\_2}^{xn}(\geq 99.5)$	hour	annual duration of extreme surge-tide events, which exceed annual 99.5th percentile and cover one or more hourly intervals, under control meteorological condition (C20_2) for years n= 1970-2000 at every mesh point x in the North Sea model
$d_{H20}^x(\geq 99.5)$	hour	mean of $d_{H20}^{xn}(\geq 99.5)$
$d_{H20}^{xn}(\geq 99.5)$	hour	annual duration of extreme surge-tide events, which exceed annual 99.5th percentile and cover one or more hourly intervals, under hindcast meteorological condition (H20) for years n= 1970-2000 at every mesh point x in the North Sea model
$ds_{A1B\_2}^x(\geq 99.5)$	hour	mean of $ds_{A1B\_2}^{xn}(\geq 99.5)$
$ds_{A1B\_2}^{xn}(\geq 99.5)$	hour	annual duration of extreme storm-tide events, which exceed annual 99.5th percentile and cover one or more hourly intervals, under future meteorological condition (A1B_2) for years n= 1991-2000 at mesh point x that represents either Cuxhaven or Sylt
$ds_{C20\_2}^x(\geq 99.5)$	hour	mean of $ds_{C20\_2}^{xn}(\geq 99.5)$
$ds_{C20\_2}^{xn}(\geq 99.5)$	hour	annual duration of extreme storm-tide events, which exceed annual 99.5th percentile and cover one or more hourly intervals, under control meteorological condition (C20_2) for years n= 1991-2000 at mesh point x that represents either Cuxhaven or Sylt
$ds_{H20}^x(\geq 99.5)$	hour	mean of $ds_{H20}^{xn}(\geq 99.5)$
$ds_{H20}^{xn}(\geq 99.5)$	hour	annual duration of extreme storm-tide events, which exceed annual 99.5th percentile and cover one or more hourly intervals, under hindcast meteorological condition (H20) for years n= 1991-2000 at mesh point x that represents either Cuxhaven or Sylt
$f_{A1B\_2}^x(\geq 99.5)$	event/year	mean of $f_{A1B\_2}^{xn}(\geq 99.5)$

$f^{xn}_{A1B\_2}(\geq 99.5)$	event/year	annual frequency of extreme surge-tide events, which exceed annual 99.5th percentile and cover one or more hourly intervals, under future meteorological condition (A1B_2) for years n= 2070-2100 at every mesh point x in the North Sea model
$f^{x}_{C20\_2}(\geq 99.5)$	event/year	mean of $f^{xn}_{C20\_2}(\geq 99.5)$
$f^{xn}_{C20\_2}(\geq 99.5)$	event/year	annual frequency of extreme surge-tide events, which exceed annual 99.5th percentile and cover one or more hourly intervals, under control meteorological condition (C20_2) for years n= 1970-2000 at every mesh point x in the North Sea model
$f^{x}_{H20}(\geq 99.5)$	event/year	mean of $f^{xn}_{H20}(\geq 99.5)$
$f^{xn}_{H20}(\geq 99.5)$	event/year	annual frequency of extreme surge-tide events, which exceed annual 99.5th percentile and cover one or more hourly intervals, under hindcast meteorological condition (H20) for years n= 1970-2000 at every mesh point x in the North Sea model
$fs^{x}_{A1B\_2}(\geq 99.5)$	event/year	mean of $fs^{xn}_{A1B\_2}(\geq 99.5)$
$fs^{xn}_{A1B\_2}(\geq 99.5)$	event/year	annual frequency of extreme storm-tide events, which exceed annual 99.5th percentile and cover one or more hourly intervals, under future meteorological condition (A1B_2) for years n= 1991-2000 at mesh point x that represents either Cuxhaven or Sylt
$fs^{x}_{C20\_2}(\geq 99.5)$	event/year	mean of $fs^{xn}_{C20\_2}(\geq 99.5)$
$fs^{xn}_{C20\_2}(\geq 99.5)$	event/year	annual frequency of extreme storm-tide events, which exceed annual 99.5th percentile and cover one or more hourly intervals, under control meteorological condition (C20_2) for years n= 1991-2000 at mesh point x that represents either Cuxhaven or Sylt
$fs^{x}_{H20}(\geq 99.5)$	event/year	mean of $fs^{xn}_{H20}(\geq 99.5)$
$fs^{xn}_{H20}(\geq 99.5)$	event/year	annual frequency of extreme storm-tide events, which exceed annual 99.5th percentile and cover one or more hourly intervals, under hindcast meteorological condition (H20) for years n= 1991-2000 at mesh point x that represents either Cuxhaven or Sylt
$\Delta s^{x}_{C20\_2}(100)$	m	bias signal of storm-tide as difference between the mean value $Ps^{x}_{C20\_2}(100)$ in the control simulation (C20_2) and the corresponding mean value $\mathrm{Ps}^{x}_{H20}(100)$ from the hindcast simulation (H20)
$\Delta s^{x}(100)$	m	climate change signal of storm-tide as difference between the mean value $Ps^{x}_{A1B\_2}(100)$ in the climate change simulation (A1B_2) and the corresponding mean value $Ps^{x}_{C20\_2}(100)$ from the control simulation (C20_2) at mesh point x that represents either Cuxhaven or Sylt
$[\Delta s^{x}(100)]_{max}$	m	The highest increase of $\Delta s^{x}(100)$ at Cuxhaven and Sylt
$[Ps^{x}_{A1B\_2}(100)]_{max}$	m	highest effect by maximum percentile of mean annual storm-tide at each of Cuxhaven and Sylt under future realization (A1B_2), including $[RMSL]_{max}$
$\mathrm{P}^{x}_{A1B\_2}(100)$	m	mean of $\mathrm{P}^{xn}_{A1B\_2}(100)$
$\mathrm{P}^{xn}_{A1B\_2}(100)$	m	annual maximum percentile of surge-tide under future meteorological condition (A1B_2) for years n= 2070-2100 at every mesh point x in the North Sea model
$\mathrm{P}^{x}_{C20\_2}(100)$	m	mean of $\mathrm{P}^{xn}_{C20\_2}(100)$
$\mathrm{P}^{xn}_{C20\_2}(100)$	m	annual maximum percentile of surge-tide under control meteorological condition (C20_2) for years n= 1970-2000 at every mesh point x in the North Sea model
$\mathrm{P}^{xn}_{C20\_2}(100)$	m	annual maximum percentile of storm-tide under control meteorological condition (C20_2) for years n= 1991-2000 at mesh point x that

		represents either Cuxhaven or Sylt
$P_{H20}^{x}(100)$	m	mean of $P_{H20}^{xn}(100)$
$P_{H20}^{xn}(100)$	m	annual maximum percentile of surge-tide under hindcast meteorological condition (H20) for years n= 1970-2000 at every mesh point x in the North Sea model
$Ps_{A1B\_2}^{x}(100)$	m	mean of $Ps_{A1B\_2}^{xn}(100)$
$Ps_{A1B\_2}^{xn}(100)$	m	annual maximum percentile of storm-tide under future meteorological condition (A1B_2) for years n= 2070-2100 at mesh point x that represents either Cuxhaven or Sylt
$Ps_{C20\_2}^{x}(100)$	m	mean of $Ps_{C20\_2}^{xn}(100)$
$Ps_{H20}^{x}(100)$	m	mean of $Ps_{H20}^{xn}(100)$
$Ps_{H20}^{xn}(100)$	m	annual maximum percentile of storm-tide under hindcast meteorological condition (H20) for years n= 1991-2000 at mesh point x that represents either Cuxhaven or Sylt
$Ps_{S}^{x}(100)$	m	mean of $Ps_{S}^{xn}(100)$
$Ps_{S}^{xn}(100)$	m	annual 100th percentile of storm-tide where *S* is either hindcast, control or future meteorological conditions (H20, C20_2 or A1B_2, respectively) for years n= 1991-2000 (H20 and C20) or 2070-2100, respectively, at mesh point x that represents either Cuxhaven or Sylt
$P_{S}^{x}(100)$	m	mean of $P_{S}^{xn}(100)$
$P_{S}^{xn}(100)$	m	annual 100th percentile of surge-tide where *S* is either hindcast, control or future meteorological conditions (H20, C20_2 or A1B_2, respectively) for years n= 1970-2000 (H20 and C20) or 2070-2100, respectively, at every mesh point x in the North Sea model
$CIs^{x}(100)$	m	confidence interval for the mean of $Ps_{H20}^{xn}(100)$ at every mesh point x with a statistical significance level of 95% using student's t test
$CI^{x}(100)$	m	confidence interval for the mean of $P_{H20}^{xn}(100)$ at every mesh point x with a statistical significance level of 95% using student's t test

Abbreviations

AN	The artificial neuron
ANNs	Artificial Neural Networks
BAW	Federal Waterways Engineering and Research Institute.
BER	bed elevation range
BODC	British Oceanographic Data Centre
BPN	back-propagation neural network
DDM	Data-driven modelling
EFN	ensemble fitting neural network
EPSPs	excitatory or positive postsynaptic potential
FE	Finite element
GCMs	General circulation climate models
GUI	Graphical user interface
HZG	Helmholtz-Zentrum Geesthacht
LNHE	Labouratoire National d'Hydraulique et Environment
LWI	Leichtweiß-Institute for Hydraulic Engineering and Water Resources
MHW	Mean High Water
MLP	multilayer perceptron
MSE	Mean Square Error
MWL	mean water level
NARX	Nonlinear Autoregressive with eXogeneous inputs neural network
NCEP	National Centers for Environmental Prediction
NHN	Normalhöhennull
NN	Normal Null
PSP	postsynaptic potential
RCMs	Regional climate models
RMSE	root mean square of error
RMSE	Root Mean Square Error
RMSLr	Relative Mean Sea Level rise
RMS_{tp}	Root Mean Square error of turning points
RMS_{ts}	Root Mean Square Error of time series
SANN	STATISTICA Automated Neural Networks
SI	Scatter Index
SLP	sea level Pressure
SWL	still water level
TDL	time delay line block
TLU	Threshold Logic Unit proposed by mcculloch & Pitts, (1943)

1 Introduction

1.1 Motivation

Settlements in coastal lowlands are especially vulnerable to storm surges, tides and waves associated with climate change and sea level rise. However, these lowlands are often densely settled and the population living there is growing rapidly. Furthermore, the value of the coastal ecosystems represents almost 40% of the value of all marine and terrestrial ecosystems (Oumeraci, 2000). An area of about 40.000 km² along the North Sea coast encompasses coastal lowlands, home to more than 16 million people and major economic activities (Hofstede, 2004). During extreme storm-tides, large areas of flood-prone coastal lowlands can be, and have been, flooded (Woth, 2006), causing loss of life and property. One of the most catastrophic events in the North Sea occurred on February 1962; at Hamburg >300 people lost their lives and damages of 1.6 billion EUR (Brönnimann et al., 2013), when the coastlines of the southern part of the North Sea were hit by a severe storm-tide. Due to the particular wind direction and to the coincidence of the storm surge with the astronomical spring tide (even if not the highest of the month), water levels exceeded any value previously observed (5.7 m above mean sea level at Hamburg (Brönnimann et al., 2013)). Moreover, the maximum of the storm-tide from February 1962 had an additional portion of 90 cm for parts of the German Bight, coming as a long external surge wave from the Atlantic (Woth, 2006), resulting in that disastrous flood. Nevertheless, the negative extreme storm-tides are less well documented but, these events pose a severe threat to the navigation of large vessels in shallow water and may have an effect on sediment transport (Burlace, 1986).

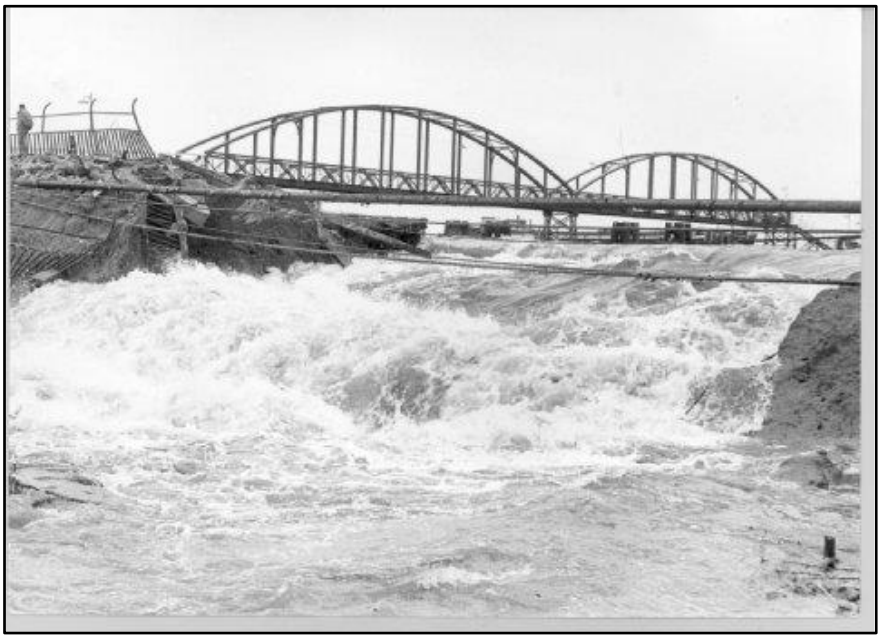

Figure 1.1: Broken dyke after the storm surge in Hamburg in February 1962. Source: Hamburger Morgenpost, reprinted with permission (Brönnimann et al., 2013).

The tremendous increase in offshore and onshore activities requires the development of improved modelling techniques for the prediction and hindcast of extreme storm-tide during storms. Reliable prediction of extreme storm-tides is vital for the life cycle design and management of coastal, harbour and offshore structures. Moreover, it is uncertain whether nature has enough time to "implement" the worst physical combinations of all components for the generation of the most extreme events ("perfect storm-tide"). The prediction of extreme storm-tide is a very complex engineering problem including diverse components, such as storm surge, tides, waves, coastal topography and in estuarine zones also river discharge. These components are well understood but not or not completely and properly taken into account by the existing prediction models for storm-tide, even by assuming that a good bathymetry and wind forcing are available. The greatest difficulties towards the determination of "the maximum physically possible storm-tide" essentially arise from the fact that the nonlinear interactions between the various components (Chen, Liu, & Hsu, 2012; DERM , 2009; Higaki, Hayashibara, & Nozaki, 2009; Horsburgh & Wilson, 2007; Prandle & Wolf, 1978; Wolf, 2009) are still unknown. Despite the now routine approaches of linking the tide and surge components in present operational storm-tide models and the substantial progress in recent research of air-sea interactions and on the coupling of surge and wind-wave models, a proper process-based coupling of all components will certainly take decades to be implemented in the current numerical models. For example, the wind-wave interaction and bottom friction effects on storm-tide, especially when tides and storm surges as long waves enter shallow water, are still under further research. Furthermore serious difficulties arise from the unstationarity of the processes involved; particularly those are long–term (e.g. climate change) and from the problems associated with extrapolation of observations to 10^{-2}-10^{-5} years of extreme events with statistical distributions without any physical base. In fact, it is well known that decisions based in wrong numbers resulting from sophisticated analyses (e.g. extreme value theory and multivariate analysis) may represent an additional hazard (Oumeraci, 2004).

1.2 Objectives

The tentative main objective of this PhD study is the development of a new hybrid modelling approach, which combines Data-Driven models (DDMs), such as Artificial Neural Networks (ANNs), with the hydrodynamic numerical models that apply to coastal areas and estuaries as simple "operational", low cost modelling tools in order to:

(i). account for the high nonlinearity of the processes at two sites in the North Sea, Germany. For a selected site representative of an estuary area (e.g. Cuxhaven) and a selected site representative of an open coast area (e.g. Sylt),

(ii). determine the worst extreme water levels, which is physically possible in the 21st century under the projected climatic change for the North Sea area.

(iii). relate and predict extreme water levels at Sylt using Cuxhaven data. Since long-term water level observations at Sylt may be not available in the past, it is valuable and cost effective for a coastal engineering study to establish the relationship with the available water levels at Cuxhaven.

1.3 Methodology

The tentative methodology, which will be specified in more details as a key result of Chapter 2, is briefly illustrated in Figure 1.2.

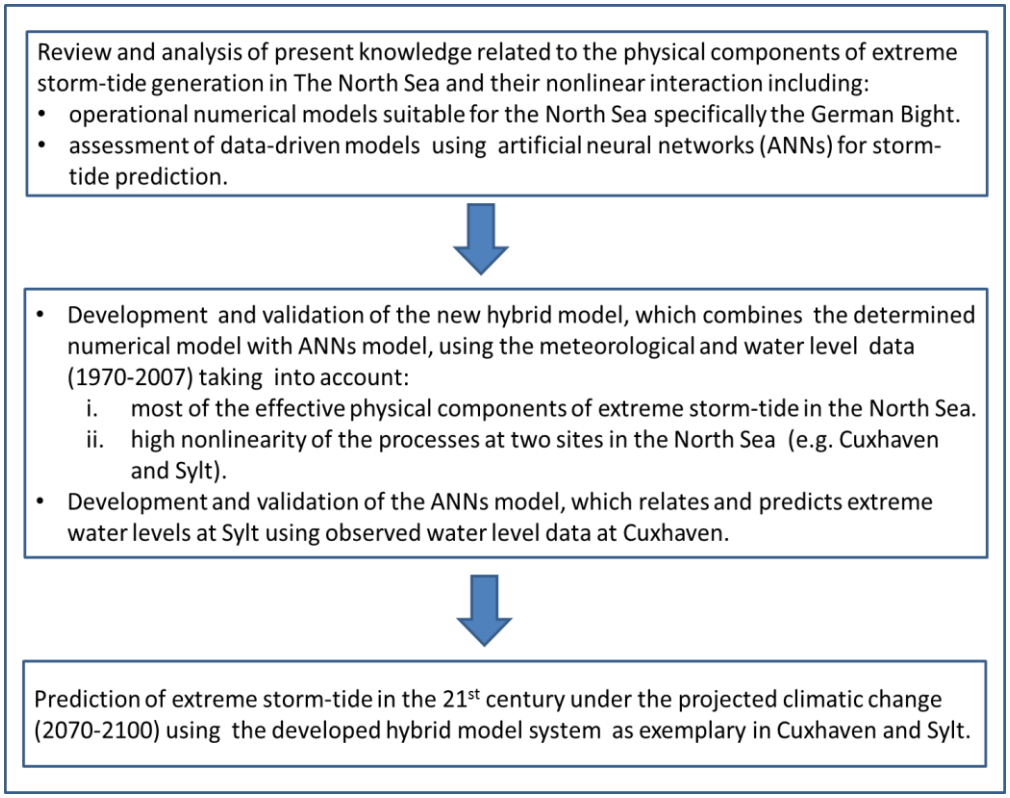

Figure 1.2: Tentative methodology of the PhD study.

First, the present knowledge related to the classification of extreme storm-tide components as a basis for the understanding of the processes involved in the nonlinear interaction and its generation will be reviewed (chapter 2). Particular emphasis will be put on the available models that can be used for building the new hybrid model system.

Second, the numerical implementation of the selected CFD models, their calibration and validation against the observed data at the two study sites is prescribed (chapter 3). This is followed by the identification of the most relevant components of the resulting storm-tide at both sites, which allows us to save computation time.

Third, as the processes involved in the generation of extreme storm-tide are very complex and the relationships between the components are nonlinear, numerical/statistical models alone are not able to provide proper and accurate predictions. Therefore, a more efficient computational tool (“ hybrid model system”) needs to be developed and validated using meteorological forcing (1970-2007), which will be obtained from available data of the past meteorological events (“hindcast conditions”). Moreover, a relational ANNs model will be developed to retrieve missing data at Sylt using observed water level from Cuxhaven, which accounts for the differences in the nonlinear phase and amplitude of water level between the two sites (chapter 4).

Forth, the new hybrid model will be driven by meteorological forces (2070-2100), which will be obtained from scenario for future meteorological events "future conditions" (chapter 5). The emission scenario widely used between 2070 and 2100 is SRES A1B, where SRES is the IPCC Special Report on Emission Scenarios. This illustrates the hybrid model capability to estimate the effects of future climate change and of the relative mean sea level rise on the storm-tide.

Finally, the results of the implementation, verification and application of the new hybrid model as well as those of the selected numerical models are summarised and conclusions are drawn. Furthermore, recommendations are provided for the application of the hybrid system, including the outline of possible future research topics (chapter 6).

2 Current State of Knowledge and Modelling

The tremendous increase in offshore and onshore activities requires the development of improved modelling techniques for both hindcast and forecast of extreme water levels during storms. On the coastlines of the North Sea, a combination of high tides, storm surges, wind waves, external surges from the Atlantic and their mutual interactions generally represent the major sources of coastal flood risks. The contribution of the mutual interactions between the various components still remains the least understood. In shallow water, both man-made and natural marine systems are much affected by extreme storm-tide due to the non-stationary nature of the contributing components and the nonlinear interactions between those processes. A proper physically-based coupling of all components will probably take decades to be implemented in the current operational hydrodynamic models ("knowledge-driven" models). Meanwhile, rather a more pragmatic data-driven approach is required to complement the "knowledge-driven" models describing the behaviour of physical systems. The objective of this chapter is to review the knowledge on the physical behaviour of extreme storm-tide in order to better understand the most relevant processes and their interactions. This will allow to identify the knowledge gaps and to specify more precisely the objectives and methodology of the PhD study (as tentatively formulated in Chapter 1) towards the development of a new hybrid modelling approach by combining knowledge-driven with data-driven models and taking implicitly into account the nonlinear interaction between the contributing components. Such a model is expected to bridge the knowledge gaps and to assess the contributions of these nonlinear interactions to the resulting extreme storm-tide. Moreover, reliable prediction of the extreme water levels is vital for the life cycle design and management of coastal, harbour and offshore structures. Therefore, this chapter needs to address the review and analysis of the following aspects:

- Study area (North Sea with a focus on the German Bight) and the main prevailing types of meteorological storms.
- Classification of extreme storm-tide components in the North Sea.
- Physically-based and data-driven storm-tide models for the North Sea.

From the results of this literature study implications for the planned research will be drawn, thus allow to specify more precisely the objectives and methodology of the PhD study towards the development of a new hybrid modelling approach which efficiently combines neural network techniques with conventional numerical methods.

2.1 The North Sea area and prevailing storms

The North Sea is one of the world's largest shelf seas with surface area of 575.300 km^2 (Velema, 2010). It is surrounded by the east coasts of Scotland and England to the west, while the northern and central European mainland to the east and south. Therefore, it lies between seven countries (UK, France, Belgium, Netherlands, Germany, Denmark and Norway). The North Sea is around 960 km long and 580 km wide and very shallow in the south, with an average depth from 25 to 35 m. The depth increases as moving up north, where the deepest point in

the North Sea is found in a shore-parallel trench located near the Norwegian coast, with depths over 500 m (Velema, 2010). This topography influences the system of eigen-oscillations of the North Sea (especially resonance to tidal forcing) and water level rise during storm surges. The shallow topography of the North Sea supports nonlinear effects caused by energy dissipation at the bottom and changing depths due to tidal waves. These processes are stronger than the nonlinearity due to momentum advection (Sündermann & Pohlmann, 2011). As a result tidal curves and figures are severely non-harmonic. The bathymetry of the North Sea is shown in Figure 2.1. Shallow water processes have a large influence on the water level and wave height for the German Bight coasts, located in the southeastern part.

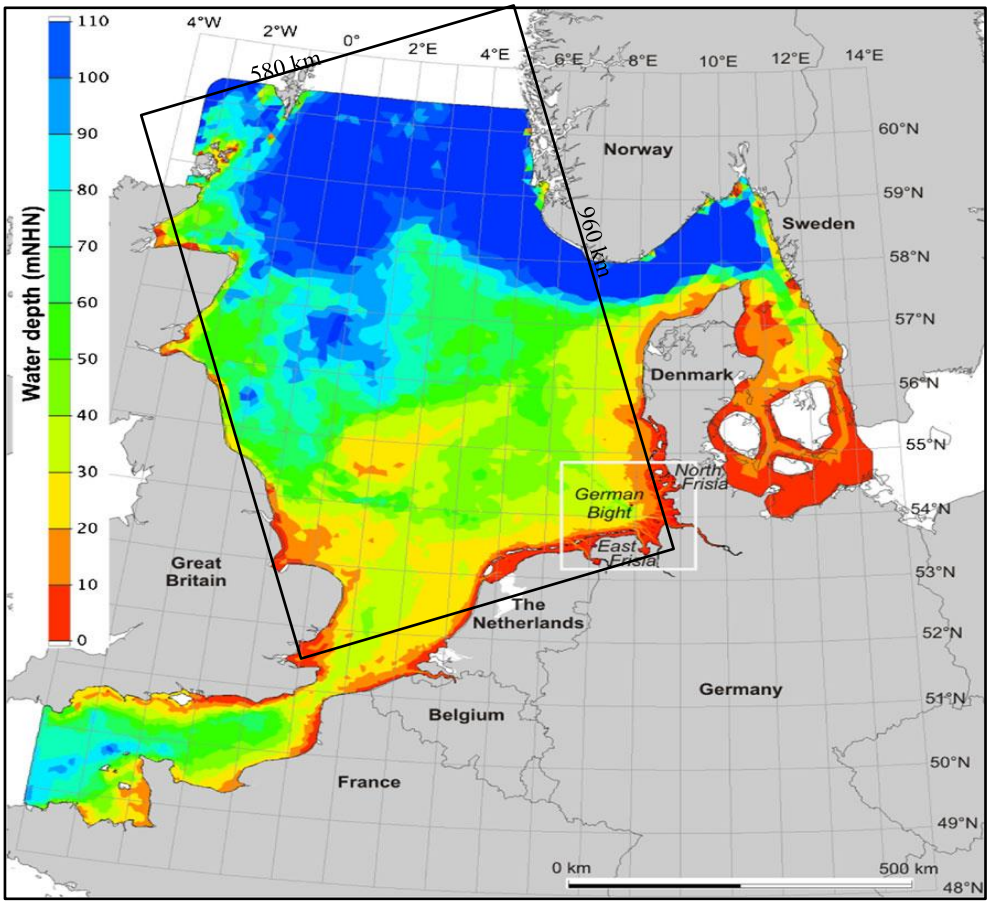

Figure 2.1: Topography of the North Sea as represented by an unstructured model grid. The study area of the German Bight is depicted by the white rectangle. Water depths are given relative to the German chart datum of mNHN (Normalhöhennull, in m) (Kösters & Winter, 2013).

The bed elevation range (BER), which is the range of morphological activity throughout the data-collection period, has been calculated and mapped to describe the decadal morphodynamic activity of the German Bight based on bathymetric data from the years 1984 to 2006 by Kösters & Winter (2013) (see Figure 2.2). These have shown that the highest morphological activity can be found in the outer estuary tidal channels of the East Frisian coast and along the German west coast. Considering the known distribution of tidal currents and wave energy along the German Bight coastline, it was hypothesized that the main morphodynamics drivers

along the East Frisian coast are the tidal currents, whereas the high morphologic activity along the North Frisian coast can also be related to wave forcing (Kösters & Winter, 2013).

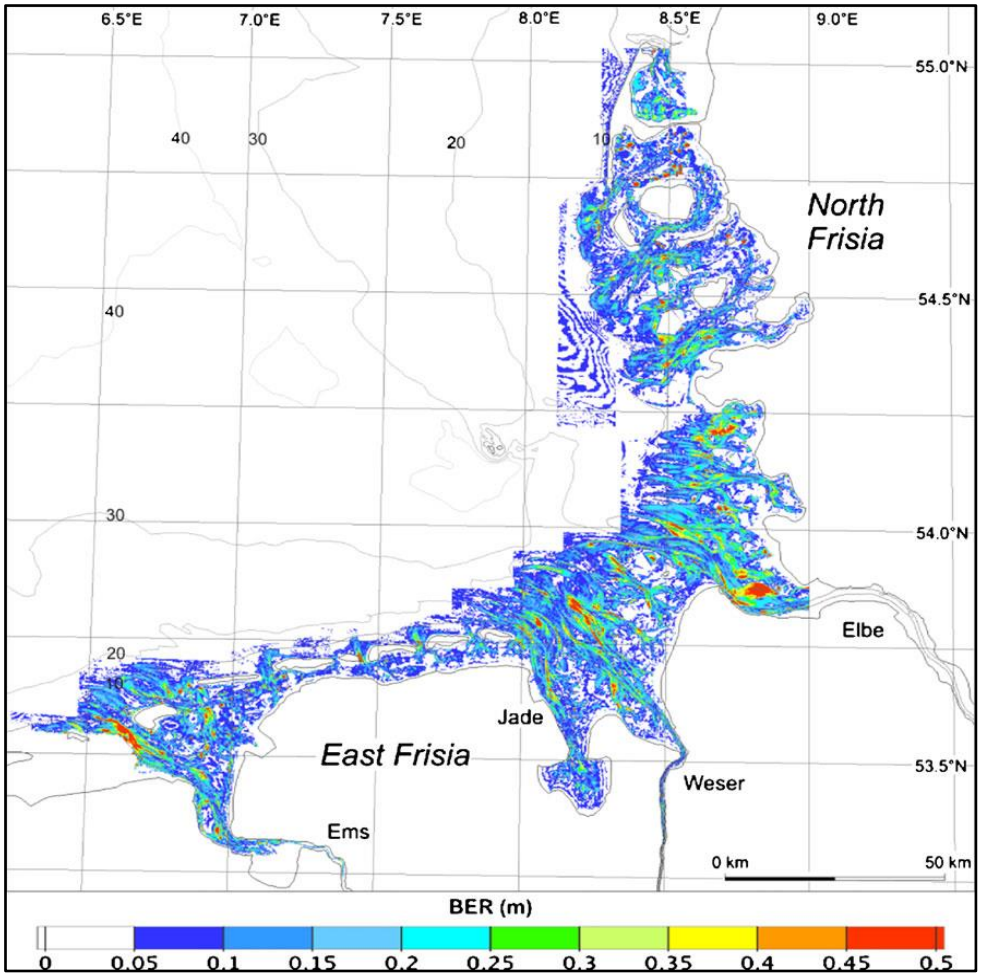

Figure 2.2: Average bed elevation range (m/year) based on bathymetric data (1984–2006) as integral measure of morphological changes (Kösters & Winter, 2013).

The North Sea links up with the Atlantic Ocean to the north and also the southwest, via the English Channel. The open connection with the Atlantic (mainly through the northern entrance, less than through the English Channel) allows the free exchange of momentum, energy and matter between the two seas. Planetary waves generated by astronomical and atmospheric forces in the ocean penetrate over the shelf break into the North Sea, where they produce tides and external surges. To the east it indirectly connects with the Baltic Sea (siek, 2011) through the Skagerrak, which is located between Denmark and Norway (approximately 100 km wide). Therefore, the North Sea is characterized by a broad connection to the ocean, meanwhile by strong continental impacts from north-western Europe. This results in a substantial interplay of oceanic influences (e.g. tides, the external surge and North Atlantic low pressure systems) and continental ones (e.g. freshwater discharge). At the southern landward boundaries, the North Sea is connected with four rivers (Elbe, Weser, EMS and Westerschelde). The long-term average discharge of Elbe is 856 m^3 s^{-1} and it is 358 m^3 s^{-1} for Weser. While the other

two rivers (EMS and Westerschelde) have long-term average discharge less than 88 m^3 s^{-1} (van Beusekom et al., 2001).

The North Sea is located in the northern hemisphere latitudinal belt of the atmospheric extra-tropical cyclones region (usually between 30° and 60° latitude from the equator). Therefore, a storm is defined as a severe cyclonic windstorm that is associated with areas of low atmospheric pressure (<10000 Pascal). The meteorological conditions are affected by the path and the velocity of the depression systems, which have a large spatial scale (average about 1600 km (Aguado & Burt, 2007)), moving across the sea. These storms, which have a westerly direction for this region, travel with the jet stream across the North Atlantic towards Europe. So they are rarely motionless and commonly travel about 1200 kilometres in one day.

The late autumn and winter seasons are the times of storms in Europe as a result of pressure differences between two locations. This is due to the higher differences in temperature during these seasons between the North Pole area and the tropics than the differences during summer. The extra-tropical cyclone begins as a weak disturbance somewhere along the frontal zone (stationary front), where cold air from polar region meets warm air from the south (see Figure 2.3) (Stage a). The collision of these two air masses results in the uplift of the warm air into the upper atmosphere creating a cyclonic spin around a low pressure centre in counter clockwise direction due to the Coriolis force (Stage b). Associated with this centre is the cold and warm fronts. During the middle stages of cyclogenesis, the storm intensifies and the pressure at the storm's centre drops. Cold fronts usually move along the Earth's surface at velocities greater than the warm front. As a result, the late stages of cyclogenesis occur when the cold front overtakes the warm front causing the air in the warm sector to be lifted into the upper atmosphere (Stage c). The resulting boundary between the cold and cool air masses is called an occluded front. A day or two after occlusion the occluded front dissipates, winds subside, and a stationary front forms on the surface of the Earth again (Stage a).

Most of the storms are already generated in the Atlantic Ocean, where the starting point can differ greatly. The very strong onshore winds at all parts of the North Sea coast lead to over more than one tidal cycle persistent storm-tide curves. Therefore, a notable storm surge on the German coast can only be generated for storm depression tracks across the 8° longitude between 55° and 65° latitude. The track location of the storm depression when passing the 8th degree of longitude is crucial for the development of the storm surges on the German North Sea coast and for typing the storm surge. If the Track of the storm from the North Atlantic is south of 55th or north of the 65th latitude, there might be no danger to the German North Sea coast, but for the neighboring coasts (e.g. the Holland surge in 1953 south of the 55° latitude). The North Sea is mainly affected by three types of meteorological storms, which may potentially generate extreme storm-tide (Petersen & Rohde, 1979). These storm types, namely the Jutland type, the Scandinavian type and the Skagerrak type, are depicted in Figure 2.4 along with their associated storm surge characteristics.

1. *Jutland-type:* developed over Newfoundland, traveling mostly very fast in easterly direction from England over the North Sea to Jutland between 57 ° and 55° latitude. It results in strong southwesterly winds, shifting to westerly and finally to northwest

winds. It is associated with storm surges of medium height and narrow curve, which occur rarely (e.g. the storm surge of 2/3 Jan.1976).

2. *Scandinavia-type:* is a slow-moving depression system formed over Greenland and Iceland and traveling towards the southeast, crossing Scandinavia between the 60th and 65th degree of latitude. Deep pressure systems from the Scandinavia type cause long, persistent storms with winds from northwesterly directions over the North Sea. Usually, the highest wind speeds are not as strong as those from the Jutland type but the storm-tide curve, derived from tide gauge observations, includes more than one high tide. The storm surge generated by this storm type has the widest surge curve, and is lower and less frequent (e.g. 16/17. Feb 1962 storm surge).
3. *Skagerrak-Type:* is located between the other two types, traveling usually from west-northwest to east-southeast. It crosses the 8th degree of longitude, which lies just in front of the western coast of Schleswig-Holstein, between the tip of Denmark and the 60th degree of latitude. These storms generate the highest water levels with medium width surge curve that occur most often (e.g. storm surge of 27. Oct 1936).

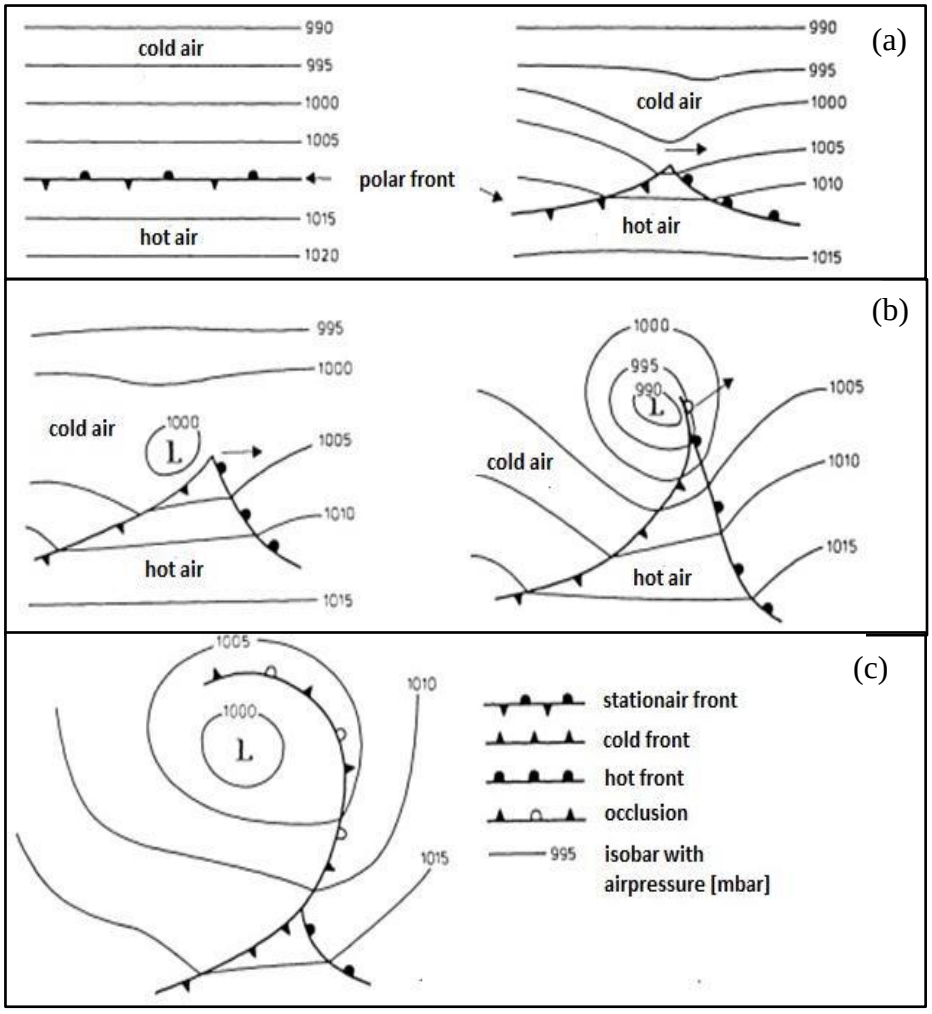

Figure 2.3: Extratropical cyclone development from birth (a) to death (c), which lasts between 3 and 10 days (De Jong, 2012).

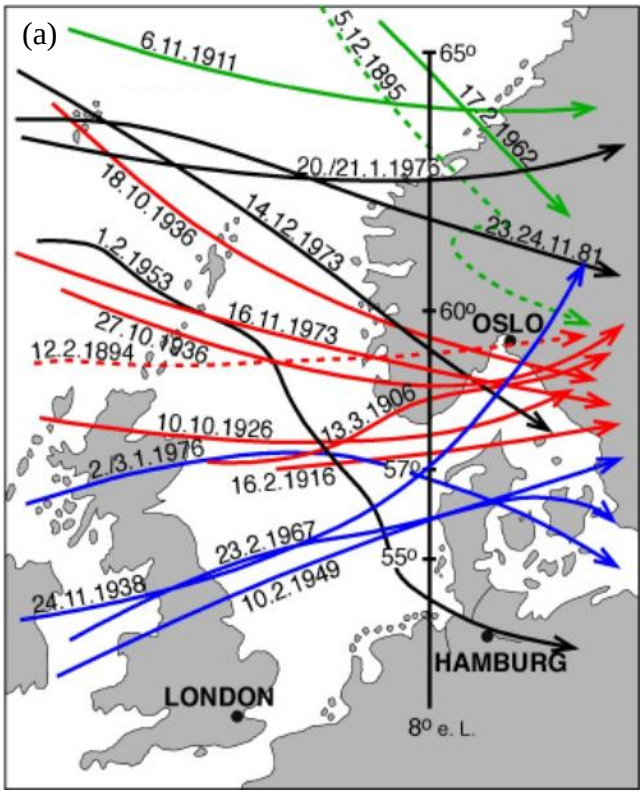

Figure 2.4: Storm depression tracks, which cause strong storm surges at the North Sea Coast (modified from (Petersen & Rohde, 1979) . Types of depression systems as coloured: Blue: Jutland type, red: Skagerrak type, green: Scandinavian type, black: mixed types.

2.2 Classification of extreme storm-tide components

Extreme water levels at an open coast may consist of the following six components (Walton & Dean, 2009): (i)wind setup due to wind shear at the water surface, (ii) pressure setup due to the atmospheric pressure decrease over the spatial extent of the storm system, (iii) wave setup caused by wind-induced waves transferring momentum to the water column, (iv) Coriolis forced set up or set down due to the effects of the rotation of the earth acting on the wind driven alongshore current at the coast, (v) seiche due to resonance effects initiated by moving wind system, and (vi) an astronomical tide component. In the North Sea, the external surges that are generated outside and then propagate to the interested area also contribute nonlinearly to the resulting extreme storm-tide level. Therefore, the extreme storm-tide is a consequence of different determinants and their complex nonlinear interactions. Extreme storm-tide components can be classified according to generation forces into stochastic components, which are generally of meteorological nature, and deterministic components (see Figure 2.15).

2.2.1 Stochastic components

These components have a time scale in the order of individual storm event ranging from a few hours to 4 or 6 days.

a) Wind setup and inverse barometric effect

Typically, the most important component of a storm-tide is definitely the wind setup, which is combined with the pressure setup due to the natural formation of the meteorological storm systems. The wind setup is generated primarily by a strong wind. Northerly or north-westerly winds are notorious in this respect for the North Sea (long fetch), while easterly or westerly wind directions have moderate fetch. The northerly wind can blow the full length of the North Sea without interruption and sweep the water up against the German coast. The wind setup for the southern North Sea coasts is mainly around 150-200 cm (De Jong, 2012). The pressure effect is often described as the inverted-barometer (IB) effect, the water level decreases by one centimeter for each hPa increase in pressure. It can reach up to about 10-20 cm, depending on the pressure difference and the distance between the storm center and the point of measurement. The combination of wind and pressure setup can raise or lower the water level by up to several meters, generating a storm surge as shown in Figure 2.5 (Siek, 2011). Storm surges in the German North Sea coast are usually caused by strong local winds (wind speed ≥ 17.2 m/s) from northwesterly directions blowing over the shallow shelf areas in the German Bight (depths ≤40 m; along the coastlines ≤10 m) occurring when the low pressure systems travel farther eastward into the Scandinavian/Baltic area (Dangendorf et al., 2014). These winds cause an effect of water pile up with surges of up to more than four meters (Dangendorf et al., 2014). By definition, a storm surge in the North Sea is a water level 1.5 m above Mean High Water (MHW) or higher (Jensen et al., 2008). Two types of North Sea storm surges can be distinguished. The wind-induced type occurs after north-westerly winds have continued for a prolonged period of time, causing wind setup in the south-eastern coast of North Sea. Storm surges generated by wind setup are easy to predict, with a warning lead time of 18 to 24 hours. By contrast, the extra-tropical cyclone type of surge is much more difficult to predict because in this case a small low-pressure system with hurricane force winds tracks across the British Islands at high speed, intensifying over the North Sea.

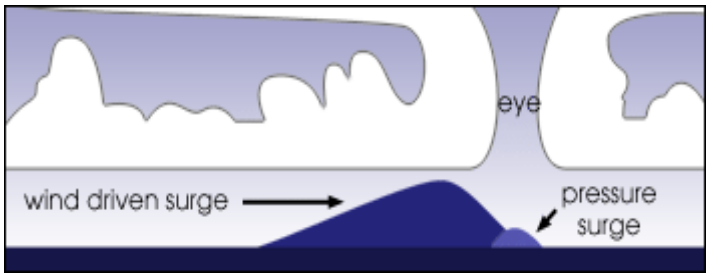

Figure 2.5: Storm surge component as combination of wind and pressure setup (Siek, 2011).

The amplitude of storm surge depends on several factors including:

- *Intensity, duration and direction of wind*: especially in extra-tropical storms
- *Bottom friction*: which limits the growth of the long storm surge waves, and this must be accounted for in numerical models (Carter, 1985; Bijl, 1997).
- *Coastline geometry*: the concave shape of the bay coast is likely to enhance surge levels.

- *Coriolis Effect:* This apparent force affects all oceanic and atmospheric movement in coordinates that rotate with the earth. In a basin with the dimensions of the North Sea, the rotation of the earth affects all storm-tide components. The Rossby radius (Pedlosky, 1982) for the North Sea is ca. 270 km; so that it is necessary to take into account the inertia effect of this force.

b) External surge

Under certain weather conditions an external surge can be generated in the North Atlantic, pushing additional water masses into the North Sea basin (Gönnert, 2001). External surges are generated in the Northeastern Atlantic due to air pressure variations that are induced by fast passing cyclones. They may generate noticeable waves at the water surface as well as internal waves in the water body. The propagation of an external surge into the North Sea takes place preferably when the track of the causative cyclone leads from the sea areas between Ireland and Iceland to Mid-Norway causing strong winds to the north of Scotland. These waves propagate to the North Sea similar to a tidal wave, but independently of the tide phase and any periodic regularity, and travel through the North Sea in counterclockwise direction (Pugh, 1996) as shown in Figure 2.6. They are affected by the earth rotation (Coriolis force) and by the rapidly decreasing depth. External surges will increase (or decrease), if the cyclone track shifts southward (or northward) and influence the water body of the North Sea. These factors are accentuated as the external surge moves southward down the east coast of Britain (Roger A. Flather, 2000). The study of 73 external surges which occurred in the years from 1971 to 1995, showed that the residual contribution of external surge in Cuxhaven without the wind effects must be interpreted by 10 cm to 109 cm (Gönnert & Thumm, 2010). The extreme storm-tide in February 1962 had an additional contribution of 90 cm for some sites in the German Bight, coming as a long wave from the Atlantic, resulting in a disastrous flood (Timmerman, 1975).

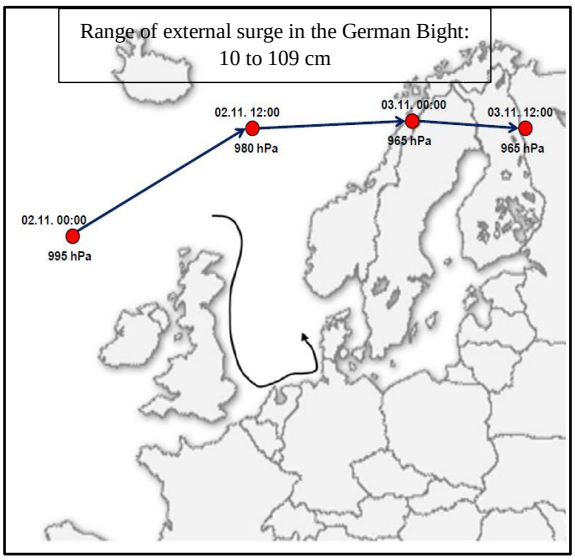

Figure 2.6: External surge propagation in the North sea (3.11.1971 14:00 MET) (Sossidi et al., 2010).

c) Wave setup

Ocean waves transform both in terms of their heights (H) as well as their shapes as they propagates onshore. These transformations result in a fall and a rise in the mean water level (MWL) respectively outside and inside of the surf zone, the so-called wave set down and set up (Figure 2.7). It is well known that wave set down and setup can be explained through the concept of the wave radiation stress (Longuet-Higgins & Stewart, 1964), which is the forcing from ocean waves on the mean body of water. The cross-shore increase of the wave radiation stress (S_{xx}) outside the surf zone is balanced with a decrease in a hydrostatic pressure forcing on the mean body of water and thus by a fall in MWL seaward of the breaker line; whereas the wave setup inside the surf zone is generated by the cross-shore decay of the wave radiation stress landward of the wave breaking point (Figure 2.7). Wave setup can cause an increase in mean water level elevation ($\bar{\eta}$) on the order of 20% or more of the offshore breaking wave height (H_b) and can thus be a significant portion of the overall storm water level during storms inside the surf zone (Weaver & Slinn, 2004). At the German Bight, a field wave setup experiment was conducted on the Island of Sylt (Hansen, 1978), who noted that the maximum wave setup is approximately 50% of the significant breaking wave height or 30% of the offshore significant wave height "H_{OS}". In Hoernum South of Sylt, the offshore significant wave height is 2 m and reaches 5 m during the storm (Mewis, 2006). On the other hand, wave setdown is small and constitutes approximately 5% of the breaking wave height.

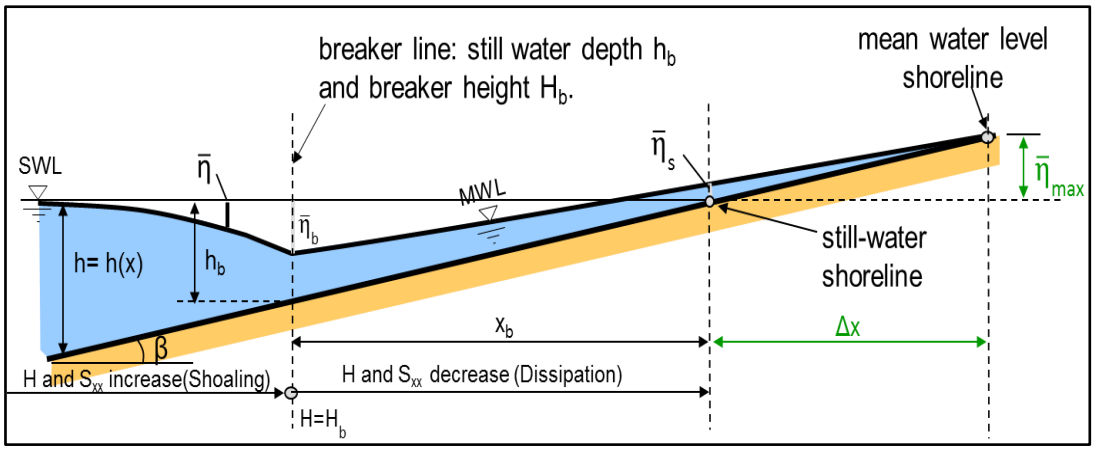

Figure 2.7: Wave set up and set down – definition sketch (Oumeraci, 2009).

d) River discharge

The water levels in the estuaries of the German rivers Ems, Weser and Elbe are influenced by variations of the discharge and changes of the tidal dynamics in the North Sea. The most important river in the German bight is the Elbe, with long-term average discharge 856 m^3/s, minimum discharge145 m^3/s and maximum discharge 3620 m^3/s. The amounts of water discharge (MQ) in large rivers are related primarily to: (i) drainage basin size, (ii) large-scale atmospheric circulation dynamics and (iii) topography

An estuary has typically three main sections as illustrated in Figure 2.8(b): a lower (or marine) estuary, in free connection with the open sea; a middle estuary, where the mixing of saline and fresh water occur; and upper (or fluvial) estuary, usually dominated by freshwater influences. However, the upper estuary is subject to daily tidal rise and fall, like the rest of estuary (Open University, 1999). The impacts of the water level changes at the North Sea gauges (Borkum, Lighthouse "Alte Weser" and Helgoland) show that, the Mean low Water (MLW) is increasing from the North Sea into the estuaries Ems, Weser and Elbe continuously up to the respective tidal border, where the discharge takes effect (Figure 2.8(a)). The smaller the distance to the tidal border is, the more dominant the effect of the discharge on the water levels becomes (Jensen et al., 2003). The effect of the Mean Low Water (MLW) in the North Sea gauges for the MLW of the Ems, Weser and Elbe gauges can only be determined at the gauges Emden, Bremerhaven and Cuxhaven. At the gauges sited more upstream in the estuary, there is only a small influence due to the MLW of the North Sea gauges (Jensen et al., 2003). For the Elbe river (Figure 2.8(b)) an increase of the dedicated discharge (MQ) by 1 m^3/s at the gauge Neu Darchau causes an increase of 0.1 cm in the MLW at Bunthaus (Jensen et al., 2003). Hence, the effect of river discharge on the water level during storms is almost negligible at Cuxhaven especially with the small discharge amounts.

2.2.2 Deterministic components

a) Tidal level effect

Tides, caused by the gravitational effect of sun and moon, are periodic and very predictable. The North Sea is a marginal sea, so the tidal motions are not the result of the direct action of the tide-gravitational forces. In fact, the observed tide in the North Sea is a co-oscillating response to the tidal waves generated in the North Atlantic Ocean (Otto et al., 1990; Velema, 2010), which propagate around the coast in counter clockwise direction taking the form of long gravity waves. The main tidal constituents are expressed by waves which enter and exit the North Sea through the northern and western open-sea boundaries with the North Atlantic Ocean (see Figure 2.1). The main tidal constituent in the North Sea is the M_2-tide with period of 12 hours and 24 minutes (see Figure 2.9). Near the coast of Scotland and England it propagates almost as a perfect Kelvin wave. This can be seen in the rectangular pattern of the co-tidal and co-range lines in Figure 2.9 (Dyke, 2007). Conservation of energy flux requires an increase in tidal height and current amplitude as water depths decrease. The increase in tidal currents gives rise to strong bottom friction and generation of intense turbulence, dissipating a large amount of energy and mixing the water column. Much of the tidal energy is dissipated in the Southern shallow part, but a portion is reflected as a damped wave, propagating northward along the continental coast. When the incoming and reflected tidal waves are superimposed together, three elevation amphidromic points (EAPs) are generated. One located in the Southern Bight and two are displaced progressively eastward from the mid-distance as the reflected wave is damped gradually when travelling northward (Butler et al., 2007; Debernard et al., 2003). Therefore, the North Sea has a complex tidal regime due to the combined effects of Coriolis and frictional forces with the geometry of the North Sea region. In addition, when

water becomes shallower, higher harmonics of astronomical constituents are generated by bottom friction and non-linear effects. These higher harmonics are referred to as shallow water constituents (Doodson, 1973). For example, the dominant semidiurnal M2 tide in shallow regions leads to a significant quarter-diurnal harmonic (M_4) due to nonlinear effects, namely, advection, wave drift, quadratic bottom friction, and time-dependent viscosity (siek, 2011).

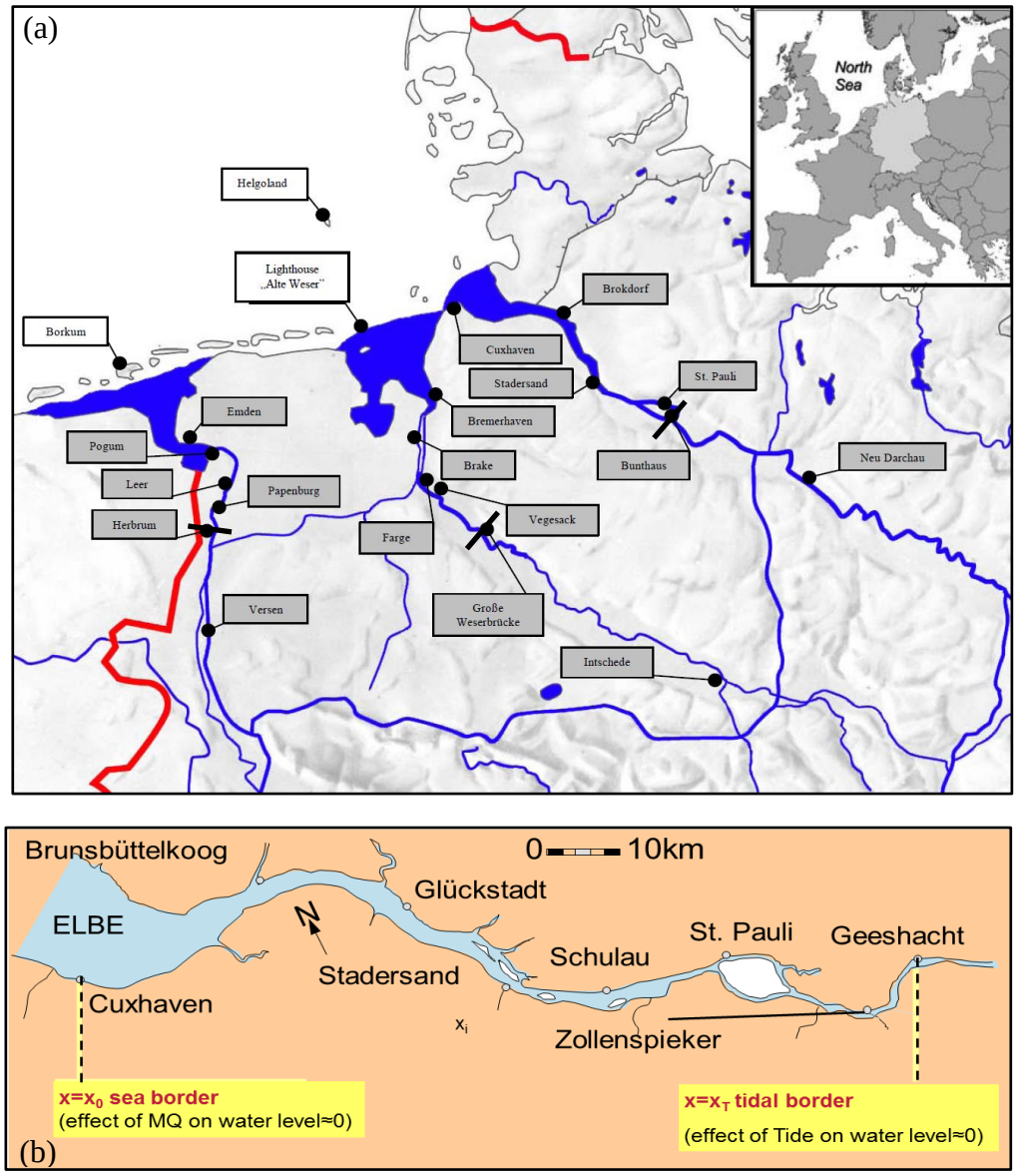

Figure 2.8: Tidal border Herbrum, Grosse wasserbrueke and Bunthaus of the Ems, Weser and Elbe rivers respectively (a) (Jensen et al., 2003).The effective borders of the North Sea tides and Elbe River discharge in the Elbe's estuary area (b) (Oumeraci, 2009).

The mean tidal range increases from 2.2 m in the entrance of the Ems-Dollart estuary to nearly 3 m in the offshore area of Jade, Weser and Elbe estuaries and decreases to about 1.8 m in the offshore area of North Frisia. The highest tidal range at the German North Sea coast occurs close to the landward border of the Lower Weser estuary in Bremen with about 4 m on the average (Niemeyer et al., 1996). If the storm makes landfall during high tide, the effect is

a higher water level than if the surge hits the shore during low tide. Tide and surges are not linearly additive, but interactive (Khan, 1995). It has long been recognized that in shallow water areas with a large tidal range, the nonlinear effects of tide-surge interaction are important. The peak of the storm surge in the southern North Sea tends to 'avoid' predicted tidal high water, due to the speeding up of the tidal wave propagation in the presence of the deeper water caused by the surge level (see Figure 2.10) and other subtle changes are caused by bottom friction (Wolf, 2009).

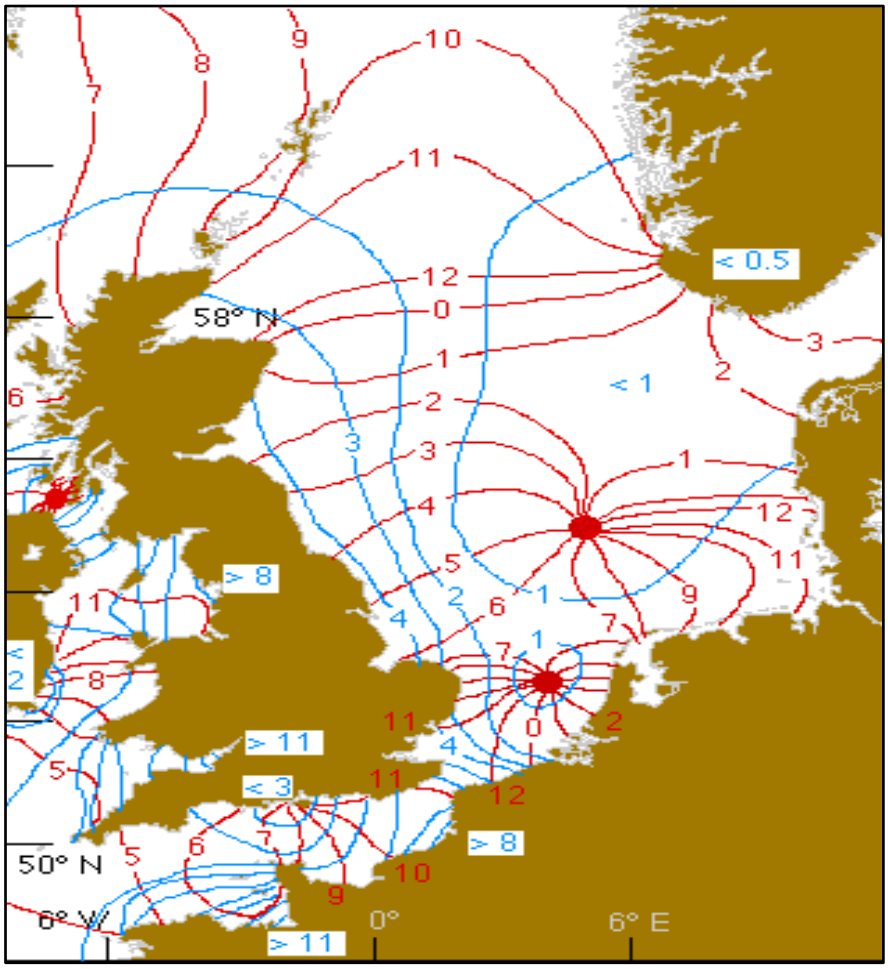

Figure 2.9: Tides in the North Sea as derived from observations. Red lines are co-phase lines of the M_2 tide, labelled in hours after the moon's transit through the meridian of Greenwich, there are thus only 25 minutes between the co-phase lines labelled 12 and 0. Blue lines give the mean tidal range at spring tide (co-range lines as the sum of M_2 and S_2) (Tomczak, 2002).

b) Seiche

In semi-enclosed seas, a standing wave or seiche can arise as a result of incoming long waves from sea generated by direct external forcing (e.g., atmospheric pressure, wind, and tide). The North Sea often experiences a lengthwise seiche with a period of about 34.5 hours (Weenink, 1956). Moreover, it responds to the twice-daily tide driving from the north of Scotland and also through the Straits of Dover, the wave-pattern breaks up into three seiches (see Fig-

ure 2.9). At the ends of a seiche, there are dramatic tides, with 4 metres difference between high and low tide. In the middle, at what's called the node, the tides are much less dramatic with only 1.5 metres between high and low water.

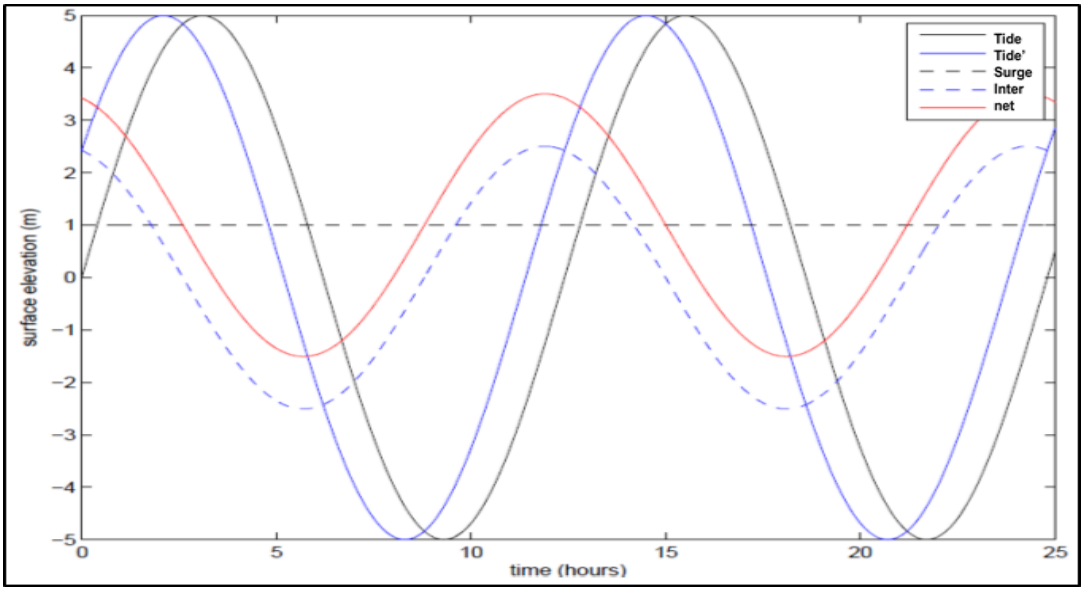

Figure 2.10: Illustration of tide-surge interaction. Undisturbed predicted tide (Tide) is solid black line, phase advanced tide (Tide') is solid blue line, undisturbed meteorological surge (Surge) is dashed black line, tide-surge interaction (Inter) is dashed blue line, net storm surge is solid red line (Wolf, 2009).

The seiche component for the storm surge in the North Sea occurred once in December 1954. Two storm surges "twin" occurred during the period of 21-24 of December. The period between the maxima of the two storms (about 35 hours) was such as to cause almost complete resonance for the North Sea (Weenink, 1956). Normally, the storms of the North Sea have wind variations at time scales shorter than the resonance period in order to complicate the response(De Jong, 2012).

2.2.3 Climate change effect and long term components

a) Climate change effect on storm surge and waves

Today, we live in a period where increasing greenhouse gas (GHG) concentrations in the atmosphere are beginning to change the global climate. There is considerable uncertainty regarding the future emissions of GHG and associated aerosols, as the amount of these emissions depends upon the character and scale of future economic activity, which is difficult to predict. General Circulation Models (GCMs) estimates an increase in global temperatures in the range from 1.1 to 6.4^{o}C at the end of 21st century, which depends on emissions scenario (Meehl et al., 2007). An increase in global temperatures of this magnitude is likely to have a significant impact on climate processes operating at various scales, from global and hemispherical scale processes to the regional and local scale surface environmental variables

(Fealy et al., 2012). Storm surge climate depends strongly on the meteorological conditions and those differ significantly when various future development scenarios are considered. Additionally, the same scenario simulated with difference global/regional circulation models can lead to considerable differences in the atmospheric and consequently storm surge climate (Beniston et al., 2007; Gaslikova et al., 2013). These uncertainties were partly addressed in recent studies of the North Sea. These studies comprise different analysis time horizons and a wide spectrum of models and scenarios. The study from Woth (2006) was based on 30-year time-slice simulations with various combinations of 2 global and 4 regional circulation models under two scenarios (SRES A2, B2). Despite the scenario-induced and model-related uncertainties, there was an agreement among the different realizations that the high percentiles of storm surge heights increase in the German Bight toward the end of the 21st century. The results suggest that under future climate conditions storm surge extremes have larger changes for the continental coast while differences are generally smaller and not statistically different from zero along the UK coast. In the western part of the continental coast the increase is primarily a result of more frequent extremes while in the eastern part, from the German Bight up to Denmark, changes in the duration and the intensity of the extremes become more important. Within the German Bight the 99.5th storm surge percentile along the 10 m bathymetry line is increased significantly in all scenario simulations by 20–30 cm which corresponds to a rise of around 20% surge heights (see Figure 2.11). In a real world these differences would have different implications for coastal protection. A stand-alone increase in the frequency of extreme events would be less relevant for many coastal facilities, but an increase in duration and magnitude of extreme events could stretch their security limits.

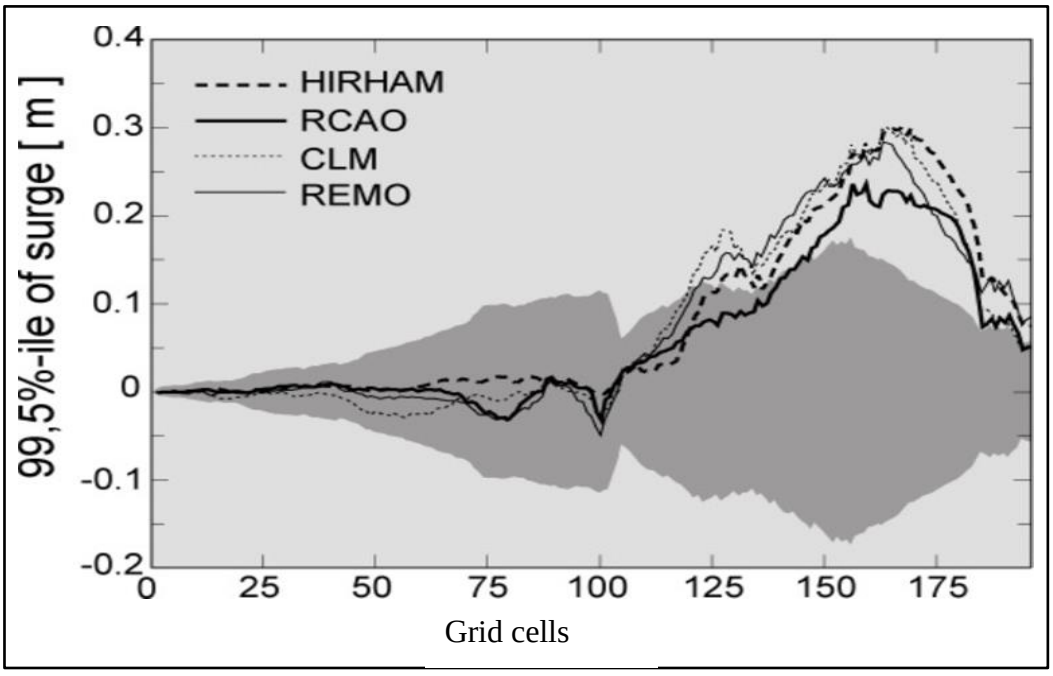

Figure 2.11: Climate change signals of interannual mean of the 99.5th percentile of storm surge for all four ensemble members under A2 scenario. The signals are compared to 95% confidence bands reflecting the inter-annual variability in the hindcast. Depicted are grid cells located on the 10 m depth line along the North Sea coast beginning with 1 in Scotland and ending with 196 in Denmark, with the german bight (130-175) (Woth et al., 2006).

Debernard and Røed (2008) considered the Special Report on Emission Scenarios (SRES) A1B, A2 and B2 with circulation models and found an increase of about 6-10 % for the high storm surge percentiles for the south-eastern part of the North Sea. Moreover, along the North Sea east coast and in the Skagerrak the annual 99-percentiles of significant wave height increase of about 6-8%, and these results are robust across the various choices in global models and emission scenarios.

With the increasing computer power and computational resources in the last 5 years, the studies turned their attention to the transient runs (2001–2100) and greater amount of realizations with the aim to investigate rather the system internal natural variability than the uncertainties due to different scenarios and models. Gaslikova et al. (2013) investigated the possible future storm surge climates in the southeastern North Sea (German Bight) based on transient simulations (1961–2100) under two IPCC emission scenarios (SRES A1B and B1) and two initial conditions. The climate change scenarios were regionalized with the regional climate model CCLM (Lautenschlager et al., 2009). Possible sea level rise in the North Sea is not taken into account. Comparing the 30-year averages of the annual 99 percentiles of the wind-induced water levels between the four climate realizations and the respective control climates, a small tendency toward an increase is inferred for all climate change realizations toward the end of the 21st century. Concerning the German Bight, the climate change signals are higher for the North Frisian coastal areas (about 10 %) than for the East Frisian ones (about 8 %). This is consistent with an increase in frequency of strong westerly winds. Considering the whole time series (1961–2100) for selected areas, this tendency is superimposed with strong decadal fluctuations. It is found that uncertainties are related not only to the used models and emission scenarios but also to the initial conditions pointing to the internal natural variability.

b) Long term effect of bathymetry

The bathymetry of the shelf and near-shore region plays an important role for the water level measured at the coastline. The magnitude of the wind setup is dependent on the depth and width of the continental shelf (Weaver & Slinn, 2004). On the continental shelf, where the water depth is smaller, the storm surge wave travels much slower than in deep water and a significant transfer of energy from the storm system to the water wave occur and quickly builds up to several meters amplitude on the shallow continental shelf. The southeastern part of the North Sea is shallower with an average of 22m water depth (Figure 2.1). Also a number of local factors due to the morphology contribute to the modification/amplification of storm surge such as the effect of islands, convergence effects and storm track with shore line. Kösters & Winter (2013) and Winter (2011) studied the spatial distribution of BER in the German North Sea coast, in which the BER values reveal the depth effect on the time scale of morphological evolution. The annual bed topographies are based on data down to a water depth of 20 m; areas deeper than 20 m are the same for the various years in 1982 to 2008 (Kösters & Winter, 2013). The deeper the water is (more than 10m), the longer and less topographical changes are likely (see Figure 2.2). So, the surge-tide simulations are most reliable for the deeper parts of the North Sea with water depths greater than 10 m where the topological changes might not be considered. Moreover, satisfying results of water level heights are

obtained when the coast is steep, which is the case for large parts of the east coast of Great Britain (R. A. Flather & Smith, 1998). In case of the southern and south-western North Sea, where the coast is flat and large areas are mudflats, water level heights can realistically be modelled up to the 10 m depth line without taking into account topographical changes (Gaslikova et al., 2013; Woth et al., 2006). Therefore, the future changes in today's topography does not need to be taken into account in future storm-tide simulations, since at both concerned sites (Cuxhaven and Sylt) the water depth is greater than 20 m.

c) Long term effect of relative sea level rise

In the time of a warming climate, sea level rise is one of the major consequences that we have to cope with. Extreme water levels generally occur during a combination of a spring tide and a storm surge. An increase in the sea level will, of course, affect extreme levels directly. Moreover, changes in the relative sea level and hence water depth can also influence the tidal component by changing its wavelength, and modifying the propagation and dissipation of tidal energy. Increased water depth also affects the generation, propagation and dissipation of the storm surge component, possibly reducing slightly the surge magnitude. (Woth, 2006) used the projections provided by the IPCC (Houghton et al., 2001) for the mean sea level rise, which is added to the change caused by meteorological forcing. For the mid-term time horizon 2030, an increase of 9 cm was used for the two scenarios A2 and B2, while the increase reached 33 cm for A2 and 29 cm for B2 by 2085. The uncertainty of these numbers was given by the IPCC as about ±5 cm and ±20 cm for the different time horizons, which accounts for different global climate models and emission scenarios. It was assumed that mean sea level rise and changing storm surge height are independent and may simply be added. The storm related change of mean maximum surge level change at the Cuxhaven for the end of the 21st century varied between 42 cm to 61 cm with a mean value, across all models and scenarios, of 50 cm.

On large temporal scales, storm-tide is affected by Relative Mean Sea Level rise (RMSLr) as observed from long tidal gauge records (e.g Cuxhaven). Recently many studies that analysed sea level changes at different spatial scales with different methods, clearly point to the existence of considerable regional variability in the rates of sea level change (e.g. Domingues et al., 2008; Mitrovica et al., 2009; Wahl et al., 2010, 2011). Moreover, the temporal behaviour for sea level rise at both sites in the German Bight is different from those of wider regional and global changes (Mudersbach et al., 2012; Wahl et al., 2013). The projections provided by the IPCC AR4 are used for most coastal planning purposes considering the mean sea level rise, so the differences at interested sites (e.g. Cuxhaven and Sylt) from the global mean changes are ignored. Wahl et al. (2011, 2013) analyzed the RMSLr at Cuxhaven and Sylt by combined high-resolution water level data and tidal peaks over the last 166 years using the k-factor approach and Monte Carlo autoregressive padding (MCAP). The results show that higher rates of relative sea level rise are detected for the eastern part of the German Bight (e.g. Sylt) than for the southern part (e.g. Cuxhaven) especially during the period 1950-2008. Since relative sea level changes can also vary spatially due to variations in vertical land movement, where their results indicating higher rates of subsidence for the eastern part than the southern

part of the German Bight (Wahl et al., 2010; Wahl, Jensen, Frank, et al., 2011; Wahl et al., 2013). The estimated long-term trend of RMSLr for the period 1937-2008 at Cuxhaven is 2.1±0.3 mm/year, while it is 2.0±0.3 mm/year at Sylt. The mean sea level at both sites is expected to increase with approximately 0.20±0.03 m in year 2092 with respect to the MSL (1991-2000) of 0.121 m and 0.027 m at Cuxhaven and Sylt, respectively. These estimated long-term trends at both sites are different when shorter periods are considered but with higher standard error. In the deeper water parts, an expected sea level rise can be linearly superimposed on the other extreme water level components as the water depth is more than 10 m (Lowe & Gregory, 2005; Woth, 2006; Sterl et al., 2009; Howard et al., 2010; Gaslikova et al., 2013).

Arns et al. (2015) investigated the impact of mean sea level rise (SLR) on extreme water levels using a numerical model (MIKE 21 flexible mesh) that covers the entire North Sea, but has its highest spatial resolution in the northern part of the German Bight (1 km). A 40-year hindcast covering the period 1970 to 2009 (include 65 extreme events) is conducted using observed mean sea level (MSL) changes, tides and atmospheric forcing as boundary conditions. The model reproduces the observed water levels well for this control period. A second 40-year run is then conducted considering the same atmospheric forcing but adding +0.54 m to the MSL to explore the effects of sea level rise on storm surges in the investigation area. Figure 2.12 shows that the difference between the two runs of surge-tide (residuals) are generally above 0 cm with most locations showing significant positive changes in addition to SLR. Large height residuals are mostly found in the region bounded by latitudes 54.4 and 54.9, where the water is very shallow (Wadden Sea). The largest increase reaches the order of 15 cm (in addition to the MSL changes). Two additional model runs were conducted (with and without SLR) where atmospheric forcing was neglected, i.e. the effect of SLR on astronomical tidal water levels is investigated. Figure 2.12 shows that changes in tidal water levels from SLR are up to three times larger compared to the model run with meteorological forcing included. This indicates that water level residuals in the northern German Bight are mainly caused by nonlinear changes in the tidal components. Taking atmospheric forcing into account, by contrast, partly compensates tidal high water increases by surge reduction due to increases in the water depth. Moreover, the occurrence of high water levels becomes earlier under model run with SLR. This is a result from water depth increases causing reduced shallow water effects and friction.

2.2.4 Nonlinear interaction between storm-tide components

Storm surge impacts are not simply linearly related to maximum water level but rely on more complex, non-linear interactions between tide–surge conditions, the associated wind wave field and thresholds to landscape change (Spencer et al., 2015). Generally, observed water level at a given location and time can be considered as a sum of components (Roger A. Flather & Williams, 2000):

water level = mean sea level + tide + storm surge + nonlinear interactions (2.1)

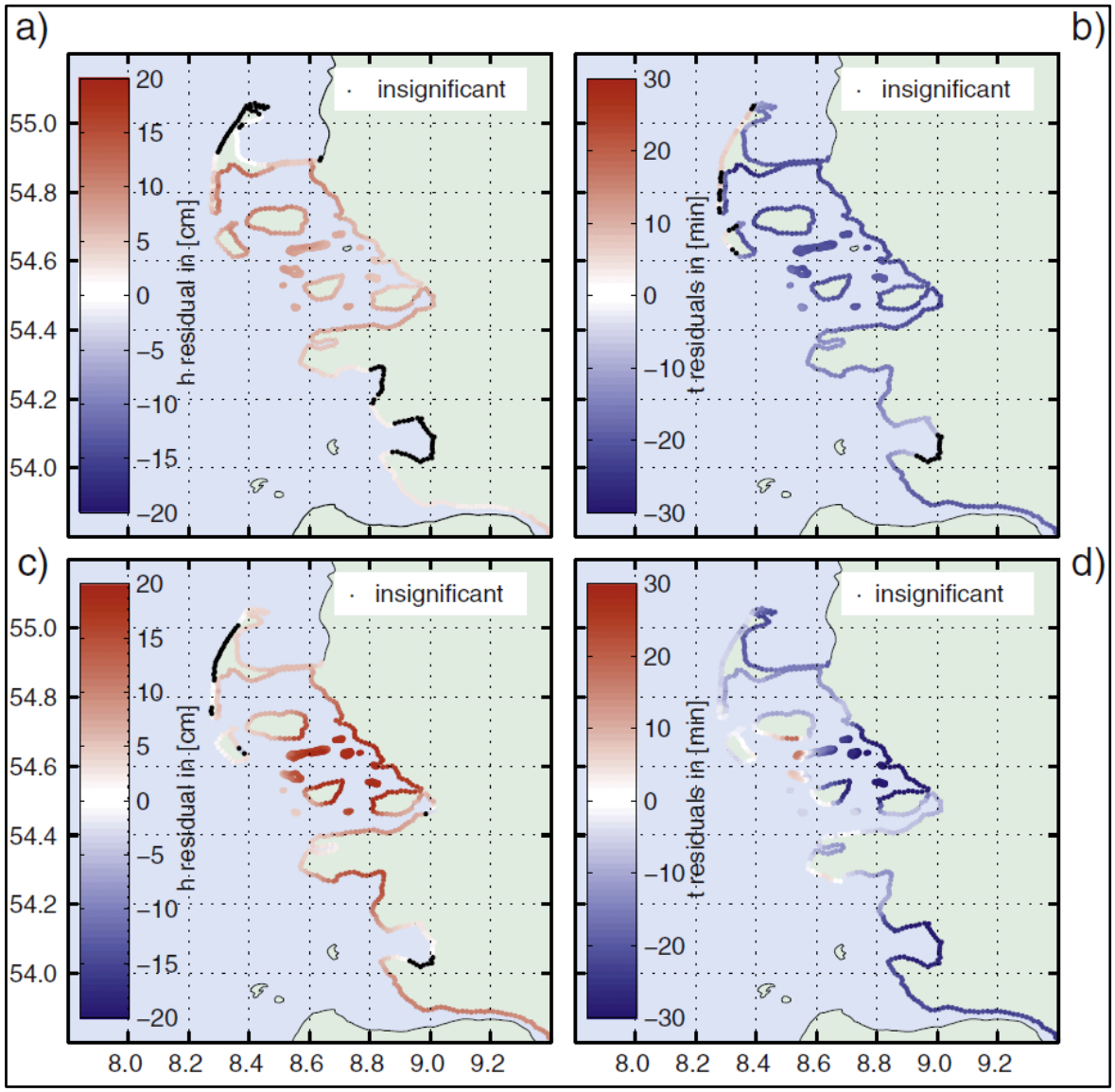

Figure 2.12: Effect of sea level rise on extreme surge-tide (a), time of surge-tide occurrence (b), astronomical tide (c), time of tide occurrence (d) averaging all 65 events. The black dots show locations where changes were found to be insignificant (Arns et al., 2015).

Prandle and Wolf (1978) considered an analytical solution of two progressive waves along a semi-infinite channel. They showed that the nonlinear interaction caused by quadratic friction was the largest, followed by the shallow water terms and nonlinear momentum advection terms. The interaction effect contributed by bottom friction increased with decreasing water depth and was proportional to the product of surge and tide. They concluded that the surge height increased at rising tide and decreased at high tide due to this interaction. Wolf (1981) used a 1-D analytical model to show that the shallow water effect became dominant over

quadratic friction for tidal amplitudes in excess of 3 m and in depths of 10 m or less. Wolf (2009) demonstrated that in the southern North Sea, the surge peak tends to modify the predicted high tide due to the change of the propagation speed when the surge modified the total depth (see Figure 2.10).

Within the XtremRisK project, Goennert and Sossidi (2011) developed an empirical method to assess extreme events, which takes the hydrodynamics of storm-tide into account. With this method, the components of a storm surge, tide, external surge, and their interaction were analyzed. The focus lies on the analysis of: (i) the highest observed occurrence of each component and (ii) the interaction between tide and wind surge and the interaction between storm surge and external surge using empirical, statistical and numerical methods (iii) the calculation of an extreme storm surge event based on the result of the analyses. This approach is presented with the example of Cuxhaven (see Figure 2.13). The wind surge curve was calculated by subtracting the astronomical tide from the observed tide, as well as by subtracting the mean tide from the observed tide. The effect of the astronomical dissimilarity on the wind surge can be identified by means of these two wind surge curves. The astronomical dissimilarity in combination with the wind surge of 3.70 m reduces to 10 cm for Cuxhaven. Only the external surges that occurred without a coinciding storm surge are taken into account. The average decrease in these external surges between Aberdeen and Cuxhaven is about 30%. The storm surge curve consists of the wind surge curve, the external surge curve and an astronomical tide curve that reflects the mean tide condition plus the ascertained effect of the astronomical dissimilarity (see Figure 2.13).

Figure 2.14 shows the relative contribution of the different components for the German Bight. Storm surge, tide and external surge components have the largest contribution to the observed storm-tide outside of the surf zone in the German Bight. The wind surge maximum can occur in all tidal phases, but mostly occurs around tidal low water. The highest wind surge event at the tidal gauge of Cuxhaven which was not influenced by an external surge reached a height of 4.15 m. This occurred in January 1976 around low tide (Goennert & Sossidi, 2011). The maximum height of an external surge recognized at Cuxhaven was 1.09 m. This external surge reached 1.08m in Aberdeen and it did not coincide with a storm surge. The highest external surge that coincided with a storm surge reached a peak level of 1.00m at Cuxhaven. The highest tidal range occurred at Cuxhaven with about 3 m on the average.

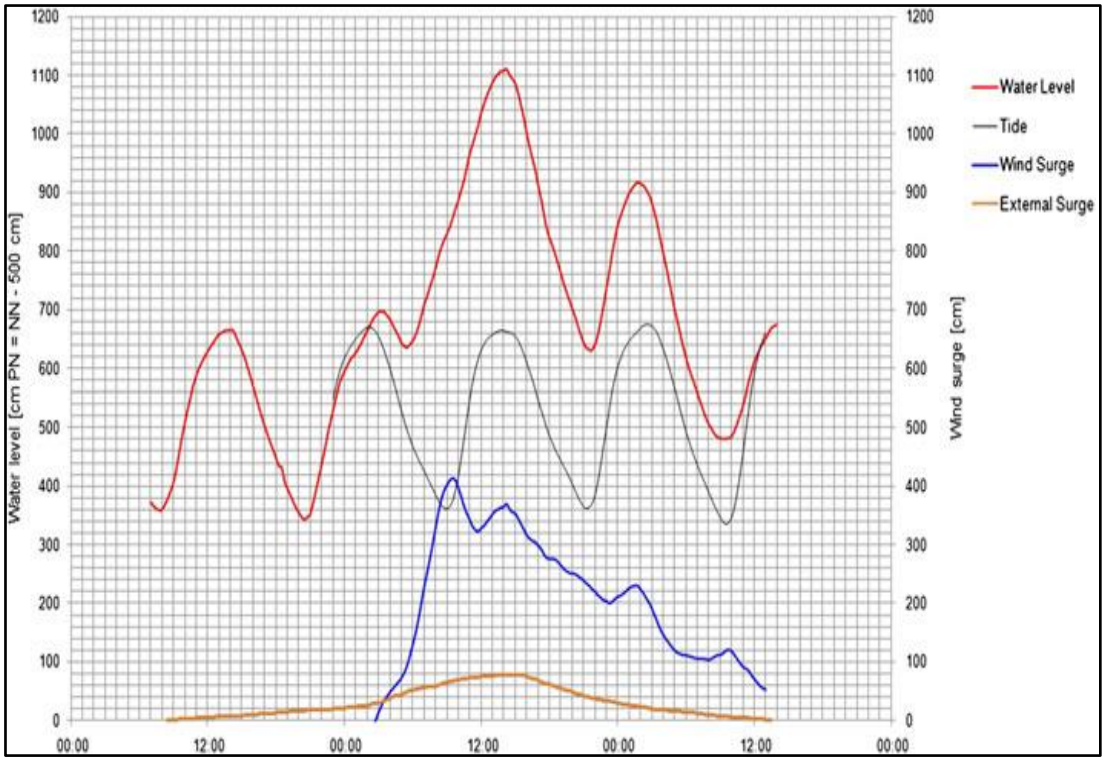

Figure 2.13: Extreme storm surge and its components at the tidal gauge of Cuxhaven (Goennert & Sossidi, 2011).

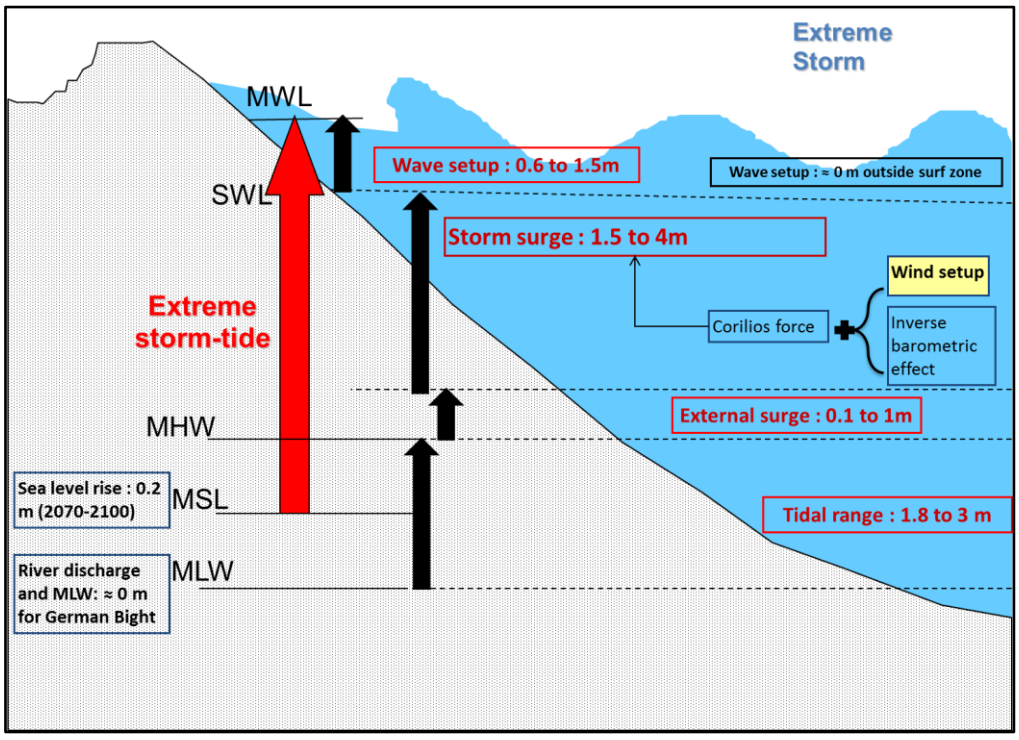

Figure 2.14: Relative contribution of the different storm-tide components for the German Bight.

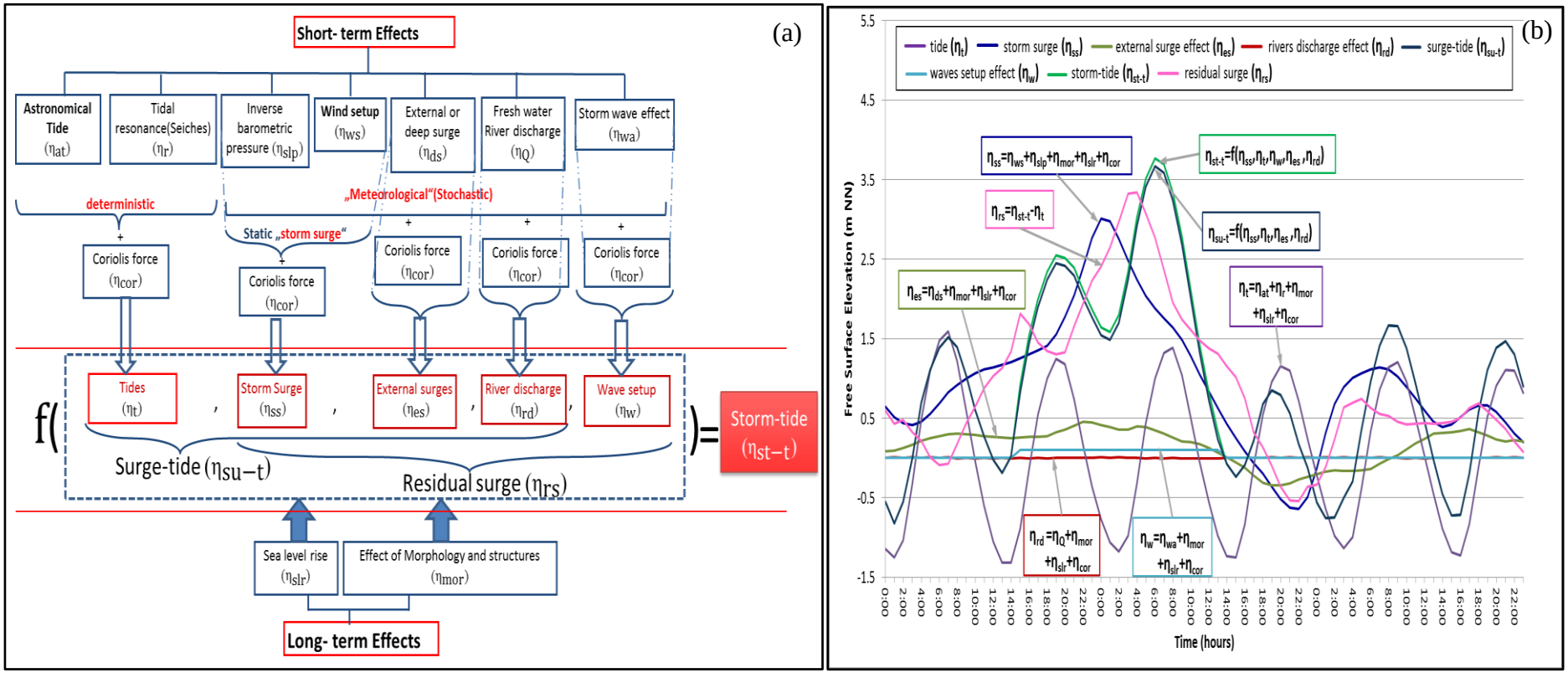

Storm surge (η_{ss}): the change in water level due to the action of the storm as a combination of atmospheric pressure and wind setups.
Tide (η_t): the normal rise and fall of the water due to earth's gravitational interaction with the moon and sun, which is affected by the natural resonance (seiches) of the semi enclosed basins like the North Sea.
Storm-tide or extreme storm surge (η_{st-t}): is the mean water level generated by the nonlinear combination of a storm surge, wave setup or setdown, external forces and astronomical tide.
Surge-tide (η_{su-t}): the change in water level due to the nonlinear combination of storm surge, external forces and astronomical tide only without wave effects.
Residual surge (η_{rs}): the difference between observed storm-tide (η_{OB}) and the predicted astronomical tides (η_t).

Figure 2.15: Main components contributing nonlinearly to the generation of extreme storm-tide and used terminology along with classification of storm-tide components (a) (modified from (Oumeraci, 2009)) , Exemplary illustration of the time series of the components (b).

Extreme storm-tide components can be classified into three categories based on the forcing responsible for their generation as depicted in Figure 2.15:

(i) *Meteorological factors:* with non-stationary and stochastic characteristics such as wind speed and direction, storm characteristics and its track, sea level pressure, and rivers discharge.
(ii) *Deterministic factors:* such as astronomical tides and tidal resonance, which may greatly affect the tidal ranges in a shelf sea like the North Sea, depending on geometry, friction and rotation.
(iii) *Local factors in a shallow water region*: such as local bathymetry changes, roughness of the continental shelf and shoreline geometry. In the North Sea, the external surges generated outside and then propagating to the interested area contribute also nonlinearly to the resulting extreme storm-tide level.

The storm surge, the tide and the external surge components have the largest contribution to the observed storm-tide in the North Sea area, especially inside the German Bight. The storm surge contribution for the southern North Sea coasts is mainly around 1.5-4.0 m, while the tide contribution ranges from 1.0 to 3.0 m. The external surge contribution in Cuxhaven (without the effect of storm surge) varies from 10 cm to 109 cm (Gönnert & Thumm, 2010).

The wave setup is primarily present in and near the coastal surf zone. So, the wave setup has approximately no contribution outside the surf zone to the water level, because the source of the momentum flux to the water column is limited to the white capping-induced energy dissipation. The selected two sites for this study (Cuxhaven and Sylt) are located far outside of the surf zone with water depth greater than 20 m. Hence, the contribution of the wave setup to the observed storm-tide at both sites is almost negligible.

On the southern boundary of the North Sea area, the fresh water discharges of the four main rivers (Westerschelde, Ems, Weser, and Elbe) have approximately no effect on the water level in the German Bight especially for smaller river discharges. The Mean low Water (MLW) is increasing from the North Sea to the estuaries from the rivers Ems, Weser and Elbe continuously up to the respective tidal border, where the effect of the river discharge dominates. For the Elbe river (Figure 2.8), an increase of the dedicated discharge (MQ) by 1 m^3/s at the gauge Neu Darchau causes an increase of 0.1 cm in the MLW near the tidal border at Bunthaus (Jensen et al., 2003)

The German Bight is shallow with an average water depth of 22 m. So the time scale of morphological evolution becomes larger and its effect smaller as the water is getting deeper i.e. more than 10 m (Woth, 2006; Gaslikova et al., 2013). In storm-tide simulations, the future changes in today's bathymetry may not be taken into account, since at both interested sites (Cuxhaven and Sylt) the water depth is greater than 20 m.

The relative sea level changes vary spatially due to variations in vertical land movement. The eastern part of the German Bight (e.g. Sylt) has higher rates of subsidence than the southern part (e.g. Cuxhaven) (Wahl et al., 2013). The estimated long-term trend of RMSLr (1937-2008) at Cuxhaven is 2.1±0.3 mm/year, while it is 2.0±0.3 mm/year at Sylt. The mean sea

level at both sites is expected to increase with approximately 0.20±0.03 m in 2092 with respect to the MSL (1991-2000) of 0.121 m and 0.027 m at Cuxhaven and Sylt, respectively. Moreover, the expected sea level rise can be linearly superimposed on the predicted storm-tide as the water depth is larger than 10 m (Lowe & Gregory, 2005; Woth, 2006; Sterl et al., 2009; Howard et al., 2010; Gaslikova et al., 2013).

Storm surge impacts are not simply linearly related to maximum water level, but rather depend on the more complex, nonlinear interactions between all components (see Figure 2.15). The nonlinear interactions are caused by quadratic friction as the water depth decrease as well as by the shallow water terms and nonlinear momentum advection terms. Goennert and Sossidi (2011) developed a method to assess the nonlinear interaction of the storm surge, tide and external surge components which resulted in a lower water level than that obtained by linear superposition of these three components.

2.3 Storm-tide models for the North Sea

The safety of the large variety of applications (design of coastal defenses against flooding, offshore structures for gas and oil extraction, schemes for generating power from the energy in the North Sea) is reflected by the crucial importance of an improved understanding and of the capability of our models to accurately simulate and predict extreme storm-tide. Over the past two decades, the operational numerical storm-tide models have significantly been improved, which particularly represent a substantial contribution to the improvement of the studies related to the mitigation of flood risk and coastal zone management. These models, however, approximate partially or fully omit the effect of the nonlinear interactions among the components of extreme storm-tide (see Figure 2.15), which has been shown to overestimate the maximum water level (Goennert & Sossidi, 2011), and to incorrectly predict the time of its arrival (Higaki et al., 2009)(DERM, 2009). Therefore, the purpose of this section is to briefly review and analyse the most relevant numerical knowledge-based models (CFD models) and data-driven models (DDMs) available for the North Sea in order to build a new hybrid modelling approach by combining numerical models with data-driven models in order to take into account the nonlinear interaction between the contributing components. The requirements and selection criteria to identify the most suitable CFD models depend on the characteristics of the storm surge model like:

1. Space resolution of the model for better representation of coastal and shallow water areas, since the nonlinear interaction is mainly due to bottom friction and the complexity of the shallow areas. Therefore, the modelled area discretization with finite element mesh is preferable to nested grids with finite difference.
2. Required computational resources and time of the model for forecasting purposes as part of operational system. The implementation of parallel processing capabilities in CFD models provides the possibility of simulation on multiprocessor PCs in reasonable time.
3. Representation of storm-tide components (Figure 2.15), which change in space and time, as forcing terms in the model and lateral open boundary.

The most suitable type of DDMs for storm-tide in the North Sea depends on:

1. Use of short to moderate time series of observed data at interested sites
2. Suitability for the long term prediction of storm-tide.

This section will proceed as follows:

1. Comparative analysis of the state-of-art numerical storm-tide models available for the North Sea area with the objective of identifying the most suitable numerical model to be considered as a part of the prospective hybrid modelling approach.
2. Review of the approaches in data-driven modelling (statistical and ANN methods) to select a complementary model for the chosen numerical model in step 1.

2.3.1 Numerical storm-tide prediction models for the North Sea

Essentially, the coastal floods due to storm-tide can be predicted with an accuracy that depends on the accuracy of the meteorological forecasts. An appropriate numerical weather model can predict the motion of atmospheric depression with a satisfactory accuracy in a range of several days. The wind and air surface pressure fields predicted by this model can be utilized as some driving forces of the sea motion in a numerical storm-tide model (Gaslikova et al., 2013; Chini, 2012; siek, 2011; Woth, 2006). The storm-tide models are basic parts of the operational oceanographic systems, used for a real time prediction of surges, tides and waves in the North Sea. The basis of the widely used numerical storm-tide model is the Navier-Stokes shallow water equations, stating the physical laws of mass and momentum conservations (Chen, Liu, & Hsu, 2012; DERM , 2009; Higaki, Hayashibara, & Nozaki, 2009; Horsburgh & Wilson, 2007; Prandle & Wolf, 1978; Wolf, 2009). These equations are inherently nonlinear. Nevertheless, the numerical models are based on several assumptions due to the limited knowledge of the underlying processes (e.g. energy dissipation associated with bed resistance). Such assumptions are usually expressed in empirical forms that require the values of one or more parameters to be identified through calibration process. Moreover, these models are discretized either by finite difference or finite element with the nonlinear momentum advection terms, nonlinear bottom stress effects, and/or nonlinear shallow water effects are either approximated or fully omitted. This treatment of the nonlinear terms has been shown to overestimate the maximum water level, and to incorrectly predict the time of its arrival (Higaki et al., 2009)(DERM, 2009). Furthermore, the effect of wave-induced setup is not considered in the storm-tide estimation despite its importance inside the surf zone.

The operational surge-tide models created and run in different countries around the North Sea are compared and presented in Table 2.1. Each of these models has its limitations and weaknesses. It is noticeable that most of the operational surge-tide models were developed between 1990 and 2000. Moreover, they used nested grids and finite difference discretization to represent the modelled area, which requires more computation time and resources.

Recently, a number of advances on physically-based storm-tide modeling have been implemented. These improvements include: parallel processing (provide possibility of simulation

on multiprocessor PCs in reasonable time), refining computational grids, utilizing more accurate calibration of models with better data and using improved numerical schemes. These advances were applied successfully to TELEMAC2D (part of TELEMAC system (Hervouet, 2007; Hervouet & Van Haren, 1994)) and DELFT3D (Deltares, 2010).

The software suite Delft3D simulates the surge-tide in a two dimensional, depth-integrated configuration. The deterministic mathematical model solves the three-dimensional shallow water equations and the continuity equations by use of an implicit finite-difference-scheme. Non-stationary hydrodynamic processes driven by tidal forces and meteorological boundary conditions can be solved on a staggered curvilinear model grid (see Table 2.1), which may require the use of nested grids technique for interested areas. Moreover, the non-linear terms in the coupled continuity equation and momentum equations are removed by linearisation of the fluxes in time (Deltares, 2010). It was recently integrated the Simulating Wave Nearshore (SWAN) model in order to enable an efficient and a direct coupling between e.g. circulation models (wave driven currents) and sediment transport models (stirring by wave breaking) (Siek, 2011).

Bruss et al. (2011) investigated the processes involved during conditions of extreme water levels (tide, three major storm surges, several external surges and an increase in the mean sea level) in Cuxhaven using DELFT3D. The different processes were analyzed individually and adverse combinations including the approximated nonlinear interactions between them were simulated yielding new scenarios. They found that the effects of these processes interaction seem to be reduced in the approximated nonlinear superposition with high absolute water levels. Among the new scenarios, the superposition of the storm surge of January 1976 with the external surge of December 1990 and the mean spring high tide of November 1990 leads to the highest water level in Cuxhaven. It is not the storm of the highest ‘standalone surge’ of February 1967 which leads to the highest scenario when superimposed with the other processes. Despite the iterative maximization of the water level peaks to spring high tide, the actual highest water levels of the scenarios appear ~30 min before spring high tide, which is due to the approximated nonlinear interactions between the processes in DELFT3D.

TELEMAC2D solves the non-conservative form of the shallow water equations using an unstructured grid, so the refinement of interested area is applicable without the use of nested grids. It considers the propagation of long waves such as surge and tide, including non-stationary meteorological conditions and any source or sink of momentum within the domain. The nonlinear terms in the solved equations are computed with implicitation coefficient approximated to first order, in this way the continuous equations are transformed into a linear discrete system which is solved using an iterative procedure (solver) based on the conjugate gradient method. Furthermore, it has the option for coupling the surge-tide, waves (TOMAWAC (Benoit, 2003; Benoit et al., 2001) and ARETMIS (Aelbrecht et al., 1997)) and sediment transport (SISYPHE(Villaret, 2010)). The Coastal Division of the Federal waterways Engineering and Research Institute in Hamburg (BAW) used the TELEMAC2D model to simulate the tidal dynamics in the North Sea and in particular, in the German Bight (Plüß, 2004). This model is utilized in-house to generate the boundary conditions for estuary modelling and to estimate tidal and storm surge dynamics.

Table 2.1: Comparison of surge-tide models for the North Sea (modified from (Siek, 2011; Takayama, 2002)).

Country	Model's Acronym	Operating and developing Institutions	Model type (Dimension)	Resolution	Type of application	Forcing	Lateral open boundary
Germany	BSHcmod	Federal Maritime and Hydrographie Agency of Germany Bundesamt für Seeschiffahrt und Hydrographie (BSH)	3D Baroclinic models covering North Sea, Baltic Sea and English Channel	Nested grid with size of about 10km for whole region, while 1.8km grid size is used for the German Bight, Kattegat and western Baltic Sea. 14 z levels.	operational Once per day to forecast T+12h	Meteoforecast data from global and local area models of the Germany's National Meteorological Service Deutscher Wetterdienst (DWD) with space resolution 30km/15km	14 tidal harmonics & external surges, calculated by 2D Northeast Atlantic model & river runoff.
	BSHsmod	Water level prediction service of BSH for German stations	2D tide-surge model	10km resolution and covers only North Sea	operational Twice per day to forecast T+00h and T+84h	Tides and DWD meteorological forecasts	
	TELEMAC2D	Bundesanstalt für Wasserbau Dienststelle Hamburg (BAW) Developed by (LNHE) france	2D surge-tide model	Unstructured grid covers only North Sea	scientific	Recalculations in the context of HIPOCAS (Hindcast-simulations in cooperation with the GKSS)	Tide and external surge from Aberdeen
Netherlands	Dutch Continental Shelf Model (DCSM), based on "WAQUA" system (renamed to DELFT3D-flow)	Developed by Delft Hydraulics and Rijkswaterstaat run by KNMI -Koninklijk Nederlands Meteorologisch Instituut (Royal Netherland Meteorological Institute) and Rijksinstituut voor Kust en Zee (RIKZ)	2D tide-surge model covering northwest Europian shelf with Data Assimilation (Kalman Filter)	staggered curvilinear grid with approximately grid size is 8 km.	operational 4 times per day	10m wind and surface pressure from KNMI HIRLAM atmospheric model.	10 tidal harmonics and surge elevation

Table 2.1: Cont.

Country	Model's Acronym	Operating and developing Institutions	Model type (Dimension)	Resolution	Type of application	Forcing	Lateral open boundary
Denmark	MIKE21	Developed byDanish HydraulicInstitute (DHI) andrun by DanishMeteorologicalInstitute (DMI)	2D nestedmodel, coveringNorth Sea,Skaggerak,Danish Belts andBaltic region.	3 different grids with 18 km, 6 km and 2 km.	operational Twice a day to predict at the moment and after 36 h	10 m wind and atmospheric pressure at MSL, from UKMO LAM (LimitedAreaModel) are used.	10 tidal constituents at the area from Scotland to Norway and in the Dover strait
UK	CS3	Developed by the Proudman Oceanographic Laboratory (POL) and run by UK Meteorological Office	3D tide-surge model. The interaction with the tides is taken into account	$1/6^{O}$ longitude and $1/9^{O}$ latitude, 15 z levels. Covers northwest Europian shelf 48N to 63N 12W to 13E	operational 4 runs per day for 6h hindcast + 36h forecast	Wind and surface atmospheric pressure from limited area atmospheric model (LAM) of the UK Meteorological Office	15 tidal harmonics and external surge, which is estimated as hydrostatic
Baltic Sea Baltic collaboration **Sweden** **Finland** **Poland** **Germany** **Denmark**	HIROMB HIgh Resolution Baroclinic Ocean model of the Baltic	Developed by BSH and SMHI and based on 3-D model of BSH and run by SMHI	3D primitive equation mode with 24 layers increasing thickness from 4m for the surface mixed layer to 60m for the deeper layers, including an equation of boundary layer dynamics and a viscous-plastic ice model.	Nested grids, with 22km grid size for North Sea and finer grid size 5.5km east of 60 E, covered the eastern North Sea, Skagerrak, Katterat and Baltic Sea	Daily 48h forecast of sea level additionally to current, temperature, salinity and ice condition	Atmospheric pressure, wind speed and direction, humidity, temperature and cloud coverage from HIRLAM at DNMI; fresh water inflow from 80 major river Outlets; Wind waves enhance mixing and mass transport in the surface layer from outputs of HYPAS (Hybrid Parametric wave prediction model for Shallow water) wind wave model	The water level at open boundary between the Atlantic and North Sea, produced by coarse grid storm surge model for the northeast Atlantic.

2.3.2 Prediction of storm-tides using data-driven models

Tide-surge interaction at a local scale is very important because it is most apparent in shallow-water areas where large surges may be generated. The nonlinear interaction between the storm-tide components may significantly change the design return period of the design water level for coastal defenses against flooding (Siek, 2011). In practice this interaction is difficult to describe in terms of analytical models and some knowledge can be gained from the numerical models (Siek, 2011). Alternative techniques are based on the analysis of the observed data characterizing the underlying processes of "storm-tide". Models using these approaches are primarily defined on the basis of relations between system state variables (input, internal and output variables) with only a limited knowledge of the details about the physical behaviour of the system. Such models are called data-driven models, since the nonlinear interaction is encoded naturally in the observed storm-tide data series. During the recent decade, such models became quite popular due to the redundant availability of data. The approaches in data-driven modelling generally originate from statistical methods and artificial intelligence based approaches such as Artificial Neural Networks (ANNs).

a) Statistical methods

These methods analyze the distribution of the positive and/or negative surges relative to the high and low waters from long time series of the observations at certain sites (at least 20 years). Moreover, statistical modelling exploits large spatial scale variables with a direct or indirect link to surge statistics, such as the spatial distribution of monthly sea level pressure (Woth, 2006).

Joseph (2009) examined the individual components of the total water level, namely the wave height, tide and surge, across the North Sea. The total water level for each sea state was rarely measured (longest duration 20 years at K13 site in the middle of the North Sea (53°13'04"N 03°13'13"E)) and long duration data sets of such measurements were not readily available. The relationship between these components was explored and Monte Carlo simulations method was proposed to combine the individual components, taking into account their joint probability. Using the longest data, at K13, the maximum total water level in the 20 year data set is 10.50 m. extrapolating the total water level measurements to various return periods results in Table 2.2:

Table 2.2: Summary of extrapolated total water levels at K13 (in the middle of the North Sea), the extrapolated total water level (found by fitting a Weibull distribution to the total water level records) (Joseph, 2009).

Return Period [years]	*Extrapolated Total Water Level [m, rel MSL]*	Monte Carlo
20 [duration of measured data]	10.47	----
100	11.60	11.86
10,000	14.65	15.57

Arns and Jensen (2013) investigated the use of a coastal regionalization approach to determine extreme water level probabilities, especially for areas where only few or no water level measurements exist. As a case study, the coastline of Schleswig-Holstein in the German Wadden Sea was used. The extreme value analyses (EVA) in the German Bight were performed based on the Cuxhaven records (1918-2009). The regionalization is based on a numerical multi-decadal model hindcast of water levels (MIKE 21) for the entire North Sea. Predicted water levels from the hindcast are bias-corrected using the information from the available tide gauge records. The bias-correction is transferred to the water levels predicted at every coastal and island model grid point in the study area. Using the recommendations on conducting extreme value analyses, water return levels along the entire northern German coastline are estimated. They estimated the heights and occurrence probabilities of extreme events such as floods or extreme still water levels. Two direct approaches were used, namely the block maxima (BM) method with generalized extreme value distribution (GEV) and the peaks over threshold (POT) method with generalized Pareto distribution (GPD). The performance of the GEV and the GPD was tested by focusing on the robustness and stability of the particular distribution (see Figure 2.16). The stability of the POT method was analyzed by applying the 99.7th percentile based threshold, which was identified to be most appropriate for the tide gauges in the German Bight. As shown in Arns et al. (2013), the GEV with r = 1 value/yr is stable when a long record is used. This behaviour changes from 1938 onwards, when the GEV derived return water level estimates begin to stagger, with large discrepancies of up to 0.9 m in the resulting return water levels. To obtain reliable and stable return water level estimates for the German Bight using the GEV, they recommend using datasets which start in 1937 or earlier. The GEV derived return water levels for the period from 1918 to 2008 were considered as "reference truth". The stability of the GPD indicates that, in contrast to all cases of the GEV, the GPD leads to very stable return water level estimates until the starting year for the sample creation in 1977. Using a sample that does not include the1976s values creates unstable results leading to lower return water level estimates. With the starting year in 1997 or later, return water levels increase again.

Wahl (2012); Wahl, Jensen, & Mudersbach (2011) and Wahl, Mudersbach, et al. (2011) developed a methodology for exceedance probabilities for storm-tide scenarios based on multivariate statistics supported by the knowledge of the physics of the constitutive components and their possible superposition. Hereby, effects such as changes in storm induced water levels and storm surge durations, among other effects, are taken into account. The associated uncertainties were explicitly considered by using a probabilistic approach. For this analysis, tide gauge observations from 1900 until 2010 have been digitized and analyzed. For every storm surge curve, 25 parameters are determined, and for each parameter, an (extreme value) statistical distribution was assigned. With these results, Monte-Carlo simulations for 1,000,000 events were performed in order to generate a sample of extreme storm-tide at Cuxhaven (Figure 2.17). The methodology enables to assign joint probabilities for both, observed and synthetic storm-tide events, which are used for the calculation of failure probabilities of flood defense structures and the probability of flooding. As shown in Figure 2.17, the parameters "highest turning point" (S) and "intensity/fullness" (F) were used, which were also considered for the statistical assessment of the simulation results. The rank correlation (Kendall's

RC) is found to be RC= 0.43[−] for the observations and RC= 0.44[−] for the simulation results at Cuxhaven. This highlights that the stochastic storm-tide model leads to reasonable results. In a further step by Wahl et al. (2015), all relevant loading parameters for coastal structures along the German North Sea coastline (i.e. storm surge and wave parameters) were jointly analyzed with different multivariate statistical models. A trivariate fully nested Archimedean Copula model was constructed to additionally include relevant wave parameters in the statistical assessment. Here, the significant wave height was chosen as a representative wave parameter. It was jointly analyzed with the two important storm surge parameters for Westerland on the west side of Sylt Island.

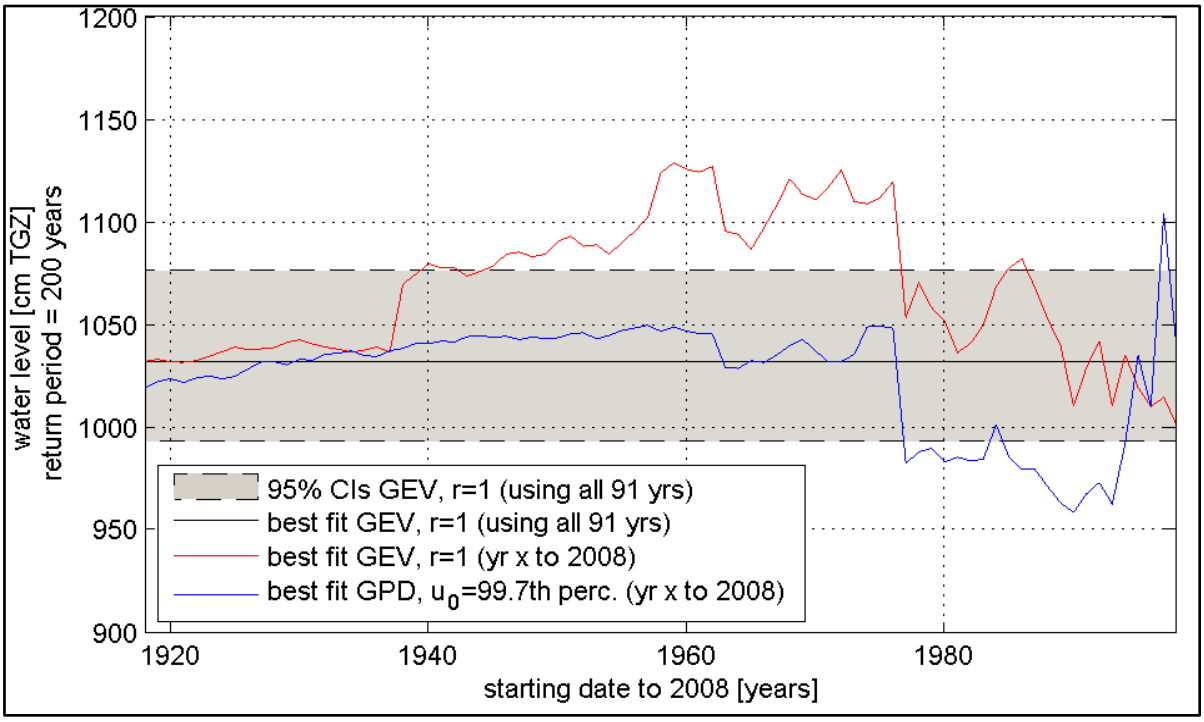

Figure 2.16: Stability of GPD (U_0=99.7th perc.) and GEV (r=1 val/yr) estimates at Cuxhaven station(Arns & Jensen, 2013).

b) Neural network based simulation of storm-tides

Traditional methods such as harmonic analysis, least mean squares method, and hydrodynamic models have disadvantages in that they require excessive data, are time consuming, and are tedious to carry out (Rakshith et al., 2014). In the last two decades, Artificial Neural Networks (ANNs) have been widely applied in coastal engineering (i) for solving various problems related to time series forecasting of water levels, waves and tides, (ii) for predicting sea-bed liquefaction and scour depth and (iii) for estimating design parameters of coastal and marine structures. The ability of ANNs to learn highly complex interrelationship based on observed data sets by means of learning algorithms (along with built-in error tolerance and less required data) makes them a powerful data-driven modelling tool in the research community (Rakshith et al., 2014) with advantageous capabilities such as nonlinearity, adaptivity, function approximation and parallel information processing mechanism (Haykin, 1999).

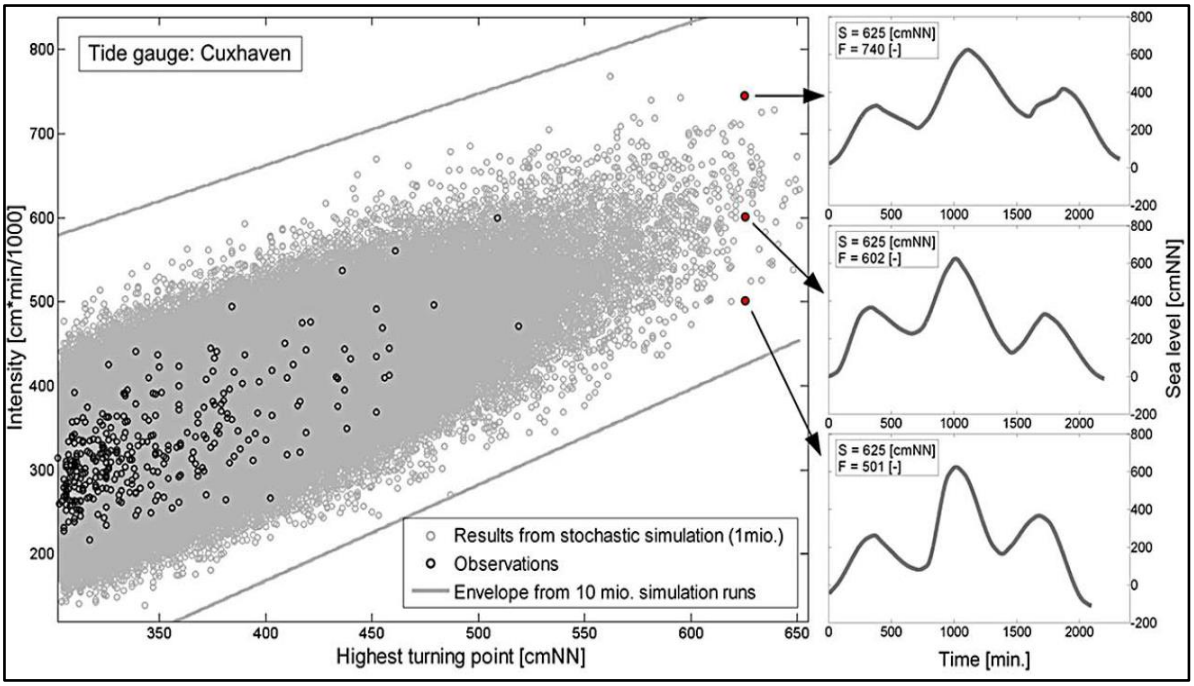

Figure 2.17: Results from simulating 10 million storm surges, represented by the parameters "highest turning point" and "intensity" for the tide gauges of Cuxhaven and selected high resolution and stochastically simulated storm surge curves (right) (Wahl, Mudersbach, et al., 2011).

Prouty et al. (2008) developed an ANNs to predict storm surge magnitudes and arrival times at selected locations in the North Sea. The model predicts storm surges based solely on past measured surge residuals at one or more tidal stations. The research focuses on the performance of the model at the Sheerness tide station near the entrance of the River Thames in the UK. The ANN uses input from both the target station and an additional station located where the peak of the storm surge has just passed to take advantage of the specificity of surge propagation in the North Sea. The ANN was trained to relate surge at the primary station from measured surge at a secondary station. The optimal secondary location was correlated to the forecast interval and the storm surge's propagation time between the secondary and primary station. Moreover, they used ANN ensembles to reduce variance and minimize error. The ensemble forecasting method averages results from multiple ANN models trained based on different model initializations. A significant result of this research was the ANN's ability to accurately predict maximum water surface elevations. A single ANN model had a 4-hour forecast error of 0.017 m, while a simple [1,1] ensemble model using 20 repetitions performed better with an average 4-hour forecast error of 0.008 m. When over-training is included to reduce the model bias, the error is further reduced to 0.004 m. ANN ensemble model performances for predicting maximum storm surge were however less impressive. Best results were obtained for ensembles of [30,1] models with an average 4-hour forecast error of 0.68 m.

Bajo and Umgiesser (2010) developed an operational surge forecast system based on a combination of hydrodynamic model and ANN model in order to improve predictions at Venice (Figure 2.18). In their study the hydrodynamic model provides a five-day forecast for the Mediterranean Sea (so the ANN is only used for short-term prediction improvement). Then,

results near Venice are extracted and improved using a neural network. They consider the total water level as the sum of the surge and of the astronomic tide. The tide-surge nonlinear interaction and wave set-up were not computed in the operational system. Their method reduced by half the average error of the hydrodynamic model for the first day forecast and maintains good performances also for longer forecasts (up to 3 days).

Siek and Solomatine (2011) developed a real-time data assimilation technique using Nonlinear AutoRegressive with eXogenous inputs (NARX) neural network to re-analyze and improve chaotic model forecasts in the North Sea. The chaotic model with data assimilation has demonstrated a pronounced capability for reliable and accurate forecasting that outperforms standard chaotic model, ANN (MLP) model and the European numerical storm surge models. For 48-hours ahead forecasting at Hoek van Holland station during stormy period (RMSE=2.43 cm see Table 2.3), the chaotic models with NARX data assimilation (every 6 hours) outperforms the standard chaotic model (RMSE=15.21 cm) and the KNMI numerical model with ensemble Kalman filter (EnKf) data assimilation (RMSE=11.62 cm).

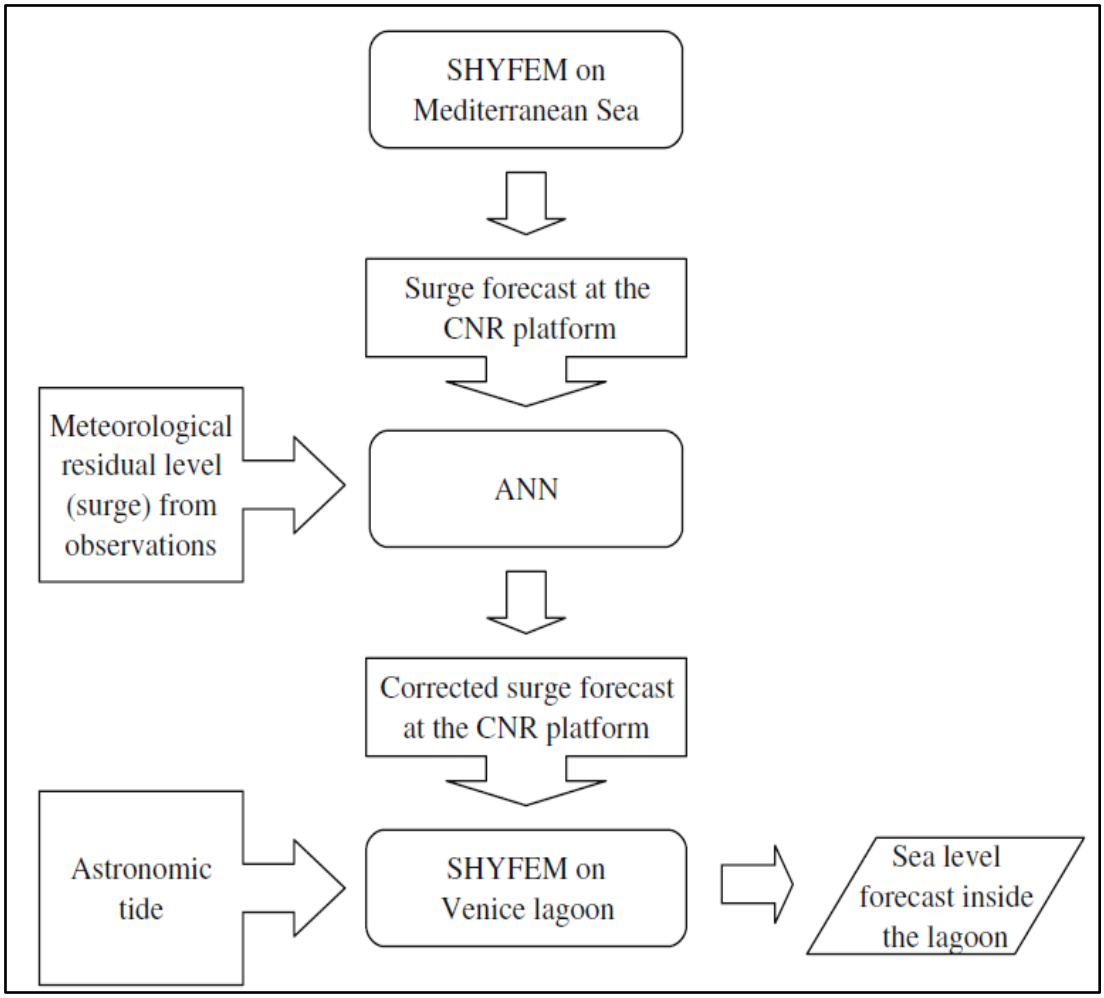

Figure 2.18: Diagram of the operational chain. The Shallow water HYdrodynamic Finite Element Model (SHYFEM) is applied on two different grids. Between the two simulations the artificial neural network (ANN) is applied to correct the results of the first simulation at *Acqua Alta* (CNR platform) close to Vince lagoon (Bajo & Umgiesser, 2010).

Shreenivas and Pradnya (2012) predicted the water levels with a lead time of few hours to a day using the technique of artificial neural networks. Instead of using the previous and current values of observed water level time series directly as input and output, the water level anomaly (difference between the observed water level and harmonically predicted tidal level) is calculated for each hour and the ANN model was developed using this time series. The network predicted anomaly is then added to harmonic tidal level to predict the water levels. The exercise is carried out at six locations, two in The Gulf of Mexico, two in The Gulf of Maine and two in The Gulf of Alaska along the USA coastline. The ANN models performed reasonably well for all forecasting intervals at all the locations. The ANN models were also run in real time mode for a period of eight months. Considering the hurricane season in Gulf of Mexico the models were also tested particularly during hurricanes.

Table 2.3: Performance comparison of the 48-hours ahead chaotic model forecasts for different frequency of data assimilation using NARX neural network (Siek & Solomatine, 2011).

Chaotic Model with Different Frequency of Data Assimilation Using NARX (RMS errors in cm)	6hr	12hr	24hr
Non-stormy period			
No. tapped input delays	20	20	20
No. hidden nodes	20	20	20
RMSE	2.05	1.93	2.08
Stormy period			
No. tapped input delays	20	20	19
No. hidden nodes	17	20	14
RMSE	2.43	1.63	3.65

An innovative approach of artificial neural networks (ANN) was used by Pashova et al. (2013) as a nonparametric modeling framework for the nonlinear sea level forecasting and filling the missing values in the daily sea level series. They developed two types of the artificial neural network (ANN) architectures FeedForward Backpropagation (FFBP) and recurrent Echo state network (ESN). In some cases, the ANN can be used as an alternative to the traditional methods, for filling in missing values in the time series. The sea level data are derived from the records spanning a 5-years of the tide gauge Burgas, which is located on the western Black Sea coast. Most of the data gaps include time periods from 1 to 3-4 days up to 1 to 3 weeks. The achieved results have shown that the performance of ANN models is better than that of the conventional numerical models and that they are very promising for the real-time filling of missing data in the time series.

Rakshith et al. (2014) predicted water level at Karwar, located at the west coast of India, using Non-linear Auto Regressive eXogenous input (NARX). It has the advantage that generated output is fed back to the network input creating a loop. Conceptually, it differs than static ANN in the fact that it uses the target given to it also as an input. Predictions were carried out for various prediction durations using the weekly and monthly data sets. It was found that at Karwar, one year ’s prediction can be successfully carried out using one month data as an input with correlation coefficient (‘CC’) greater than 0.97 (see Table 2.4). The developed model was further applied to predict water level at New Mangalore Port Trust, Panambore, along the

west coast of India, which is 260 km south of Karwar. The results with 'CC' value greater than 0.96 are encouraging.

Table 2.4: Mean square error 'mse' in cm and correlation coefficient 'CC' values for water level predictions of one month, 3, 6, and 12 months' duration using one month water level as input. Network structure refers to input-neurons, hidden-neurons and number of predicted months (Rakshith et al., 2014).

Network structure	mse		CC	
	Training	Simulation	Training	Simulation
1-1-1	21.99	31.71	0.99539	0.99574
1-5-3	13.97	32.38	0.99705	0.99389
1-7-6	13.62	105.89	0.99745	0.97875
1-10-12	12.49	110.13	0.99772	0.97775

The operational surge-tide models developed and implemented in different countries for the North Sea are comparatively shown in Table 2.1. Most of these models use nested grids and finite difference discretization to represent the modelled area, requiring more computation time and resources. Recently, a number of advances on numerical storm-tide models have been achieved including: parallel processing (provide possibility of simulation on multiprocessor PCs in reasonable time), refining computational grids and using improved numerical schemes. These advances were applied successfully to TELEMAC2D (unstructured grid) and DELFT3D (curvilinear grid). Moreover, these models can integrate wave models to account for wave-induced setup due to its importance in storm-tide estimation for sites with depth less than 10 m inside the surf zone. The BAW in Hamburg used the TELEMAC2D model to simulate surge and tidal dynamics in the North Sea and in particular, the German Bight (Plüß, 2004). This may provide the mesh grid, bathymetry, boundary conditions data and support which are required to setup the North Sea model for this study. Therefore, the CFD model TELEMAC2D is an appropriate candidate among the free open-source tools that can be used as part of storm-tide prediction at the interested sites (Cuxhaven and Sylt).

The contribution of the mutual interactions between the various components of extreme storm-tide still remains the most unknown, despite the now routine approximating the nonlinear interaction between tide, external surge and internal surge component in the current numerical storm-tide models. The numerical models are based on vertically integrated hydrodynamic equations governing the flow in the sea. These models are discretized either by finite differences or finite elements. The nonlinear momentum advection terms, nonlinear bottom stress effects, and/or nonlinear shallow water effects are either approximated or omitted. This treatment of the nonlinear terms has been shown to overestimate the maximum water level, and to incorrectly predict the time of its arrival (Higaki et al., 2009)(DERM, 2009). Statistical and ANNs models (data-driven models (DDMs)) have been widely applied in coastal engineering in the last two decades for solving various problems related to time series forecasting of water levels. DDMs became quite popular due to the redundant availability of observed data. Moreover, the nonlinear interaction is encoded naturally in the observed storm-tide data series, which are used for training or data fitting by DDMs.

Statistical models require long time series of observed water level data (generally more than 20 years), which is usually not available for all coastal sites, especially in the developing countries. Furthermore, serious difficulties arise from the non-steadiness of the processes involved and from the problems associated with extrapolation of observations to 10-2-10-5 years of extreme events with statistical distributions without any physical base. It is well known that decisions based on wrong numbers resulting from sophisticated analyses (e.g. extreme value theory and multivariate analysis) without physically-based support may represent an additional hazard (Oumeraci, 2004).

Artificial neural networks (ANNs), which are able to approximate implicitly any non-linear mathematical functions (Hornik, 1993), allow plausible simulations of complex systems' behaviour without any preceding knowledge of the internal relations among their components (Haykin, 1999). Static ANNs were applied for water level and storm surge prediction (Bajo & Umgiesser, 2010; Pashova et al., 2013; Prouty et al., 2008) for short term periods (up to one month), provided that a reasonably large amount of good quality observed data are collected. On the other hand, dynamic ANNs such as NARX networks were used for long term predictions of storm-tides, e.g. one year prediction using only one month as input (Rakshith et al., 2014). NARX has the advantage to feed back the generated output into the network input creating a loop. Conceptually, as the target output is assigned, also as a delayed input, this improves the NARX predictably for long-term periods. Siek (2011) found that the chaotic model with NARX data assimilation has demonstrated a significant capability for storm-tide forecasting that outperforms standard chaotic models, ANN (static) models and the European numerical storm surge models.

The aforementioned existing methods have a number of advantages and disadvantages, thus providing opportunities and space for improvements. So in this research, a combination of the strengths of ANN methodology (NARX models) with those of numerical modelling (TELEMAC2D) can provide a powerful and computationally efficient operational model system for storm-tide prediction at selected sites (Cuxhaven and Sylt). In this way, the nonlinear interaction of the different extreme storm-tide components is considered implicitly and corrects the substantial errors in both magnitude and timing of the peak extreme surge water level. Moreover, this combination will reduce the amount of training data for NARX models.

2.4 Summary and Implications for the PhD Study

As depicted in Figure 2.15, extreme storm-tide components can be classified into three categories based on the forcing responsible for their generation: meteorological factors, deterministic factors and local factors in a shallow water region. Moreover, the external surges that are generated outside and then propagate into the North Sea contribute also nonlinearly to the resulting extreme storm-tide level.

On the southern boundary of the North Sea area, the fresh water discharges of the four main rivers (Westerschelde, Ems, Weser, and Elbe) have approximately no effect on the water level in the German Bight especially for smaller river discharges (Jensen et al., 2003). The storm

surge, tide and external surge components have the largest contribution to the observed storm-tide in the North Sea area especially inside the German Bight. The wave setup is primarily present in and near the coastal surf zone. So, the wave setup has approximately no contribution outside the surf zone to the water level. The selected two sites for this study (Cuxhaven and Sylt) are located far outside of the surf zone with water depth greater than 20 m. Hence, the contribution of the wave setup to the observed storm-tide at both sites is almost negligible in such a large water depth. Furthermore, the time scale of bathymetry evolution is getting longer and its effect is smaller as the water is getting deeper i.e. more than 10 m (Woth, 2006; Gaslikova et al., 2013). Therefore, for such large water depths the future changes in today's bathymetry do not need to be taken into account in storm-tide simulations.

The mean sea level is expected to increase with approximately 0.20±0.03 m in year 2092 (Wahl et al., 2013; Mudersbach et al., 2012) with respect to the MSL (1991-2000) of 0.121 m and 0.027 m at Cuxhaven and Sylt, respectively. Moreover, the expected sea level rise can be linearly superimposed on the predicted storm-tide as the water depth is larger than 10 m (Lowe & Gregory, 2005; Woth, 2006; Sterl et al., 2009; Howard et al., 2010; Gaslikova et al., 2013).

Currently, the nature of the mutual nonlinear interactions between all components of the extreme storm-tide cannot yet be solved by conventional numerical models or statistical models alone. The numerical models are discretized either by finite difference or finite element with the nonlinear terms are approximated. This treatment of the nonlinear terms has been shown to overestimate the maximum water level, and to incorrectly predict the time of its arrival (Higaki et al., 2009)(DERM, 2009). On other hand, the statistical models require long time series of observed water level data (more than 20 years), which is usually not available for all coastal sites, especially in developing countries. Furthermore, It is well known that decisions based in wrong numbers resulting from sophisticated analyses (e.g. extreme value theory and multivariate analysis) may represent an additional hazard (Oumeraci, 2004). In a number of other studies, Artificial Neural Networks (ANNs) have been successfully employed for the prediction of water levels, waves and storm surge for short-term periods (Bajo & Umgiesser, 2010; Makarynskyy et al., 2004; Mandal & Prabaharan, 2006; Prouty et al., 2008; Tissot et al., 2002). These studies emphasize the ability of ANNs to improve predictions as compared to the hydrodynamic/statistical models. However, predictability of any static ANNs model has limitations, especially for long-term predictions (non-stationary processes).

The dynamic ANNs such as NARX networks were used for long term prediction of storm-tide e.g. one year prediction using only one month as input (Rakshith et al., 2014). They have powerful dynamical representational capabilities (Lin et al., 1996).

The combination of the strengths of ANN methodology (NARX models) with those of numerical modelling (TELEMAC2D and TOMAWAC) may provide a powerful and computationally efficient operational model system for storm-tide prediction at interested sites (Cuxhaven and Sylt). This combination can reduce the amount of training data required for the NARX model and also account for the nonlinear interaction among all storm-tide components.

2.5 Specification of Objectives and Methodology

In this PhD study, a hybrid modelling approach for storm-tide predictions will be developed by combining knowledge-based numerical models (NM) and data-driven models (DDMs). This approach focuses on using the best features of these models for simulations at almost-real-time. Based on the results of the state of the art review, particularly those related to the strengths and limitations of the hydrodynamic models and (DDMs), the research methodology is specified more precisely to achieve the objectives of the PhD study including:

(i) Development of the hybrid (TELEMAC-NARX) models as exemplarily for the interested two sites in the German Bight (Cuxhaven and Sylt) to predict extreme storm-tide accurately, which account for the high nonlinearity between the contributing components (Figure 2.15). The results from TELEMAC will be included as input for the NARX model, thus consequently reducing the amount of the data required for NARX training.

(ii) Development of a relational NARX model to retrieve missing water level data at one site (e.g. Sylt) using available observed water level data at a neighbouring site (e.g. Cuxhaven), which will acquire implicitly the nonlinear relationship between the recovered site (Sylt) and the source site (Cuxhaven).

(iii) Estimation of the extreme storm-tide, which is physically possible in the 21st century, by considering the effects of future climate change projection (e.g. between 2070 and 2100) and relative mean sea level rise using the developed hybrid TELEMAC-NARX model system, exemplarily for the two selected sites in the German Bight (Cuxhaven and Sylt).

Figure 2.19 shows an overview of the specified methodology adopted in this research study, which may be summarized as follows:

- *State of the art review:* A comprehensive analysis of the current knowledge is conducted to identify the knowledge gaps, missing components and shortcomings of the existing storm-tide modelling techniques. This also includes the classification of extreme storm-tide components as a basis for the understanding of process involved in the nonlinear interaction and its generation. Based on the results obtained from the analysis of the available knowledge, the models that can be used for building the new hybrid system are determined. TELEMAC system is chosen for the numerical modelling of storm-tide over the North Sea, while the nonlinear interaction between components is complemented using two NARX models at Cuxhaven and Sylt (See previous sections of this chapter).
- *Installation, validation and configuration of the CFD model system (TELEMAC)*: The cooperation with BAW and Helmholtz zentrum Geesthacht (HZG) are established successfully to provide the bathymetry grid, boundary conditions and meteorological data for the North Sea area during past (1970-2007) and future (2070-2100). The installation and configuration of TELEMAC system version 6p2 will be performed in order to run in parallel mode on the Intel 8 cores computer “erebos1” that is provided by BAW as a computational support. The flow and wave propagation over the North

Sea will be simulated using the chosen flow model TELEMAC2D and the wave propagation model TOMAWAC, which includes a detailed validation against field measurements obtained at different sites within the interested area (German Bight).

- *Development of hybrid modelling approach*: Based on the capabilities shown by NARX models for extreme water level prediction (see Section 2.3.2(b)), the hybrid modelling approach will be developed and implemented as follows:
  - *Development of the new hybrid TELEMAC-NARX model*: two types of models (Types A &B) for hindcasting the extreme water levels (1970-2007) will be developed for Cuxhaven and Sylt: (i) using NARX neural network model alone (Type-A), (ii) combining the NARX models with hydrodynamic numeric models (TELEMAC2D and TOMAWAC) (Type-B). Ensembles methods of Types A and B (hybrid TELEMAC-NARX) models will be developed to reduce the variance and to minimize errors, especially for extreme storm-tide events. The observed water level data series are used for the NARX training process, so these data naturally contains the relevant information about the nonlinear interaction of extreme storm-tide components. The ensemble models are able to extract the contribution of the nonlinear interaction between the different extreme storm-tide components at both sites by subtracting the results of the hydrodynamic models (linear superposition of each storm-tide components) from the ensemble results.
  - *Development of the relational NARX model*: to retrieve missing data at Sylt using observed water level from Cuxhaven (2000-2007), a NARX model will be developed to account for the differences in the nonlinear phase and amplitude of water level between the two sites (principally due to the storm surge, tide and external surge). Especially, the two sites are separated by a distance of more than one hundred kilometers, and both sites are affected by the same storms and storm-tide components.

Prediction of extreme storm-tide in the 21st century under the projected climatic change: The developed hybrid TELEMAC-NARX model system is exemplarily used for two sites in the German Bight (Cuxhaven and Sylt). This is to illustrate its capability to estimate the effects of future climate change projections (e.g.between 2070 and 2100) and of the relative mean sea level rise on the storm-tide. As global circulation models (GCMs) show systematic errors (bias) between the hindcast and control surge predictions (1960-1990) (Woth, 2006), the difference between the mean of future and control simulations at both sites will represent the response of the storm-tides to the applied emission scenario (A1B_2). This difference and the expected relative Mean Sea Level rise (RMSLr) at both sites are linearly added to the mean of hindcasted storm-tide by the hybrid model (1970-2000), which represents the highest possible extreme storm-tide in the 21st century.

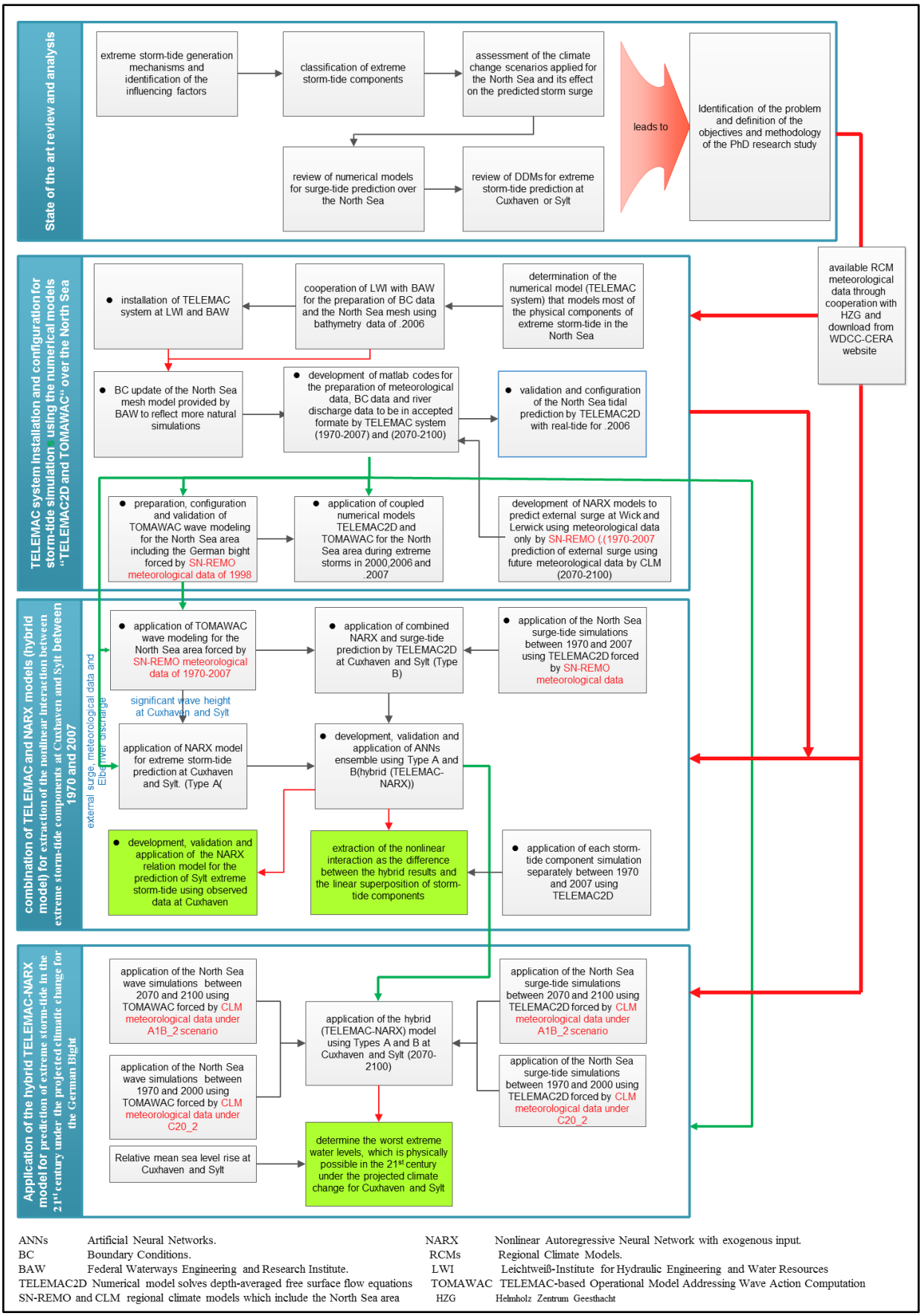

Figure 2.19: Specified methodology of the PhD study.

3 Storm-tide simulations using the numerical models “TELEMAC2D and TOMAWAC“ for the North Sea

Numerical models have great importance in the studies that are dealing with coastal development and coastal zone management. They may be considered as valuable modelling tools for decision-making and for an improved understanding of the physical processes observed in the North Sea such as those associated with storm-tides. The variety of applications (e.g. design and operation of coastal defenses against flooding, offshore structures for gas and oil extraction, ocean wave energy devices) is reflected in the importance of understanding, physically simulating and numerically predicting the effects due to storm surge, waves and tidal forcing. Based on the results obtained from the analysis of the available knowledge (chapter 2), the models that can be used for building the new hybrid system are TELEMAC model system for the numerical modelling of storm-tide over the North Sea, while the nonlinear interaction between components is complemented using two NARX models at Cuxhaven and Sylt (chapter 4). Therefore, the objectives of this chapter are

(i) to introduce the TELEMAC model system as an operational modelling tool for the hydrodynamic and wave propagation over the North Sea using the flow model TELEMAC2D (Hervouet, 2007; Hervouet & Van Haren, 1994) and the wave propagation model TOMAWAC (Benoit, 2003; Benoit et al., 2001), respectively, and

(ii) to carry out simulations of storm-tides in the North Sea using both flow and wave models, including a detailed validation against field measurements obtained at different sites within the study areas in the German Bight.

To achieve the first objective, the theoretical background and the main features of both flow and wave models are briefly outlined, including a brief overview of the governing equations and the definition of different input and output files. The second objective is achieved through the preparation of the required input data and the setup for both models as well as through the comparison between the calculated results and the dataset available at different sites in the German Bight (Cuxhaven, Sylt and Helgoland).

3.1 Theoretical background and description of the numerical models used for the storm-tide simulations in the North Sea

3.1.1 An introduction to the TELEMAC model system

The storm-tide in the German Bight, which is located in the southeastern part of the North Sea, is dominated by storm surges, tide, external surges and other physical processes (see Figure 2.15). Therefore, the transfer of waves, tides and external surges from offshore to the coastline, with the aim of assessing the effect of offshore processes on local storm surges,

nearshore waves and rivers discharge, should be conducted using state-of-the-art numerical models. The modeling system TELEMAC (Hervouet, 2007) is capable of simulating various processes separately or simultaneously for free-surface flow, wind wave propagation and further related problems. TELEMAC simulates these processes using finite element or finite-volume methods on an unstructured grid. Hence, areas of special interest can be refined, which reduce the computational time and increase representation of the area geometry. So, this allows the modeler to avoid the need of the systematic use of embedded models, as it is for instance the case with the finite-difference models.

TELEMAC was developed by the National Hydraulics and Environmental Laboratory (Labouratoire National d'Hydraulique et Environment- LNHE) of the Research and Development Directorate of France Electricity Board (EDF-DRD). It is designed for the use in fields of free surface hydrodynamics, sedimentology, water quality, waves and underground flows. TELEMAC consists of several numerical models (see Figure 3.1), which are one-, two- and three-dimensional. The numerical algorithms of TELEMAC are stored in a single FE-library (Bibliothµeque d'Elements Finis (BIEF)) that is shared by all models. This provides the following features:

- Consistency is ensured throughout the entire TELEMAC system, thus allowing models to be coupled internally and externally.
- The user is offered a set of subroutines that are specific to each model. These subroutines are all in FORTRAN90 and may be easily modified to meet the users’ specific requirements: prescription of initial conditions or complex boundary conditions, introduction of new functions, coupling with other modelling systems.
- The improvement of codes are suitable for users without getting into the basic details of finite element algorithms (i.e. programing abstraction).
- A parallel version is available for use on multiprocessor computers or clusters of workstations (automatic domain breakdown operations).

The pre- and post-processing tools (Figure 3.1), which can be utilized with or embedded in TELEMAC, are particularly powerful and they normally feature a Graphical User Interface (GUI). The FUDAA-PREPRO software (developed from the FUDAA platform by the Research, Computing and Modelling Department of CETMEF) is a complement to the TELEMAC system, which covers most of the pre-processing tasks and the basic graphical output of the results. The grid generator MATISSE is embedded in TELEMAC. Other pre-processors like JANET (developed by smile consult GmbH, Hannover) and Blue-Kenue (developed by the National Research Council (NRC), Canada) can also be used for grid generation, in which case the STBTEL module of TELEMAC acts as interface to import the generated mesh. The model results can be processed using Mermaid Matlab Tools (http://www.mathworks.com/matlabcentral/fileexchange/25021-telemac-tools) and other post-processors like DAVIT (developed from smile consult GmbH, Hannover).

TELEMAC has been open source since July 2010 and can be downloaded from the internet site (http://opentelemac.org), so it can be compiled and run on both UNIX and Intel computers under Windows operating system. For the purpose of this thesis, the source code of TELEMAC version 6p2 was downloaded and compiled to run the simulations in 64-bit processing under "windows7 64 bit as operating system" in parallel mode (Tayel & Oumeraci, 2012a). It has been installed on the Intel 8 cores computer "erebos1" that is provided by the Federal Waterways Engineering and Research Institute (BAW) as a computational support. The hydrodynamics and wave propagation over the North Sea are simulated using the flow model TELEMAC2D and the wave model TOMAWAC, respectively.

3.1.2 Flow model TELEMAC2D

a) Governing equations

TELEMAC2D uses the Finite Element (FE) technique to solve the non-conservative form of shallow water equations, also called the Saint-Venant equations (first derived by him in 1871). The Saint-Venant equations are a depth-averaged simplification of the full three-dimensional Navier-Stokes equations. The major assumptions may be summarized as follows: (i) the fluid is Newtonian, incompressible and vertically homogeneous, (ii) the pressure distribution is hydrostatic. These equations apply when the horizontal length scale is much larger than the vertical length scale. The continuity (Eq. (3.1)) and momentum equations (Eq. (3.2) and (3.3)) are written with the water depth (h) and flow velocity components (u,v) averaged on the vertical dimension (z) as the unknown terms (Ata & Hervouet, 2012; Hervouet, 2007) but the transport of a passive tracer (T) (Eq. (3.4)) and turbulence (k^*-ε model Eq. (3.5) and (3.6)) can be also taken into consideration.

$$\frac{\partial h}{\partial t}+\vec{u}.\vec{\nabla}(h)+h\,\mathrm{div}(\vec{u})=S_h \qquad \text{continuity} \qquad (3.1)$$

$$\frac{\partial u}{\partial t}+\vec{u}.\vec{\nabla}(u)=-g\frac{\partial Z}{\partial x}+S_x+\frac{1}{h}\mathrm{div}\left(h\nu_t\vec{\nabla}u\right) \qquad \text{momentum along x} \qquad (3.2)$$

$$\frac{\partial v}{\partial t}+\vec{u}.\vec{\nabla}(v)=-g\frac{\partial Z}{\partial y}+S_y+\frac{1}{h}\mathrm{div}\left(h\nu_t\vec{\nabla}v\right) \qquad \text{momentum along y} \qquad (3.3)$$

$$\frac{\partial T}{\partial t}+\vec{u}.\vec{\nabla}(T)=S_T+\frac{1}{h}\mathrm{div}\left(h\nu_T\vec{\nabla}T\right) \qquad \text{tracer conservation} \qquad (3.4)$$

where u and v are velocity components (m/s) in x and y directions, $\vec{u}$ is the velocity vector $\vec{u}=(u,v)$, h is the depth (m), T is the passive (non-buoyant) tracer (g/l), ν_t and ν_T are the coef-

ficients of momentum and tracer diffusion, respectively (m^2/s), g is the gravitational acceleration (m/s^2), t is the time (s), z is the elevation of free surface (m), S_h is the source or sink of fluid (m/s), S_T is the source or sink of tracer (g/l/s), S_x and S_y are some source or sink term of the momentum in u and v (m/s^2), respectively, which may include friction, Coriolis, and wind force.

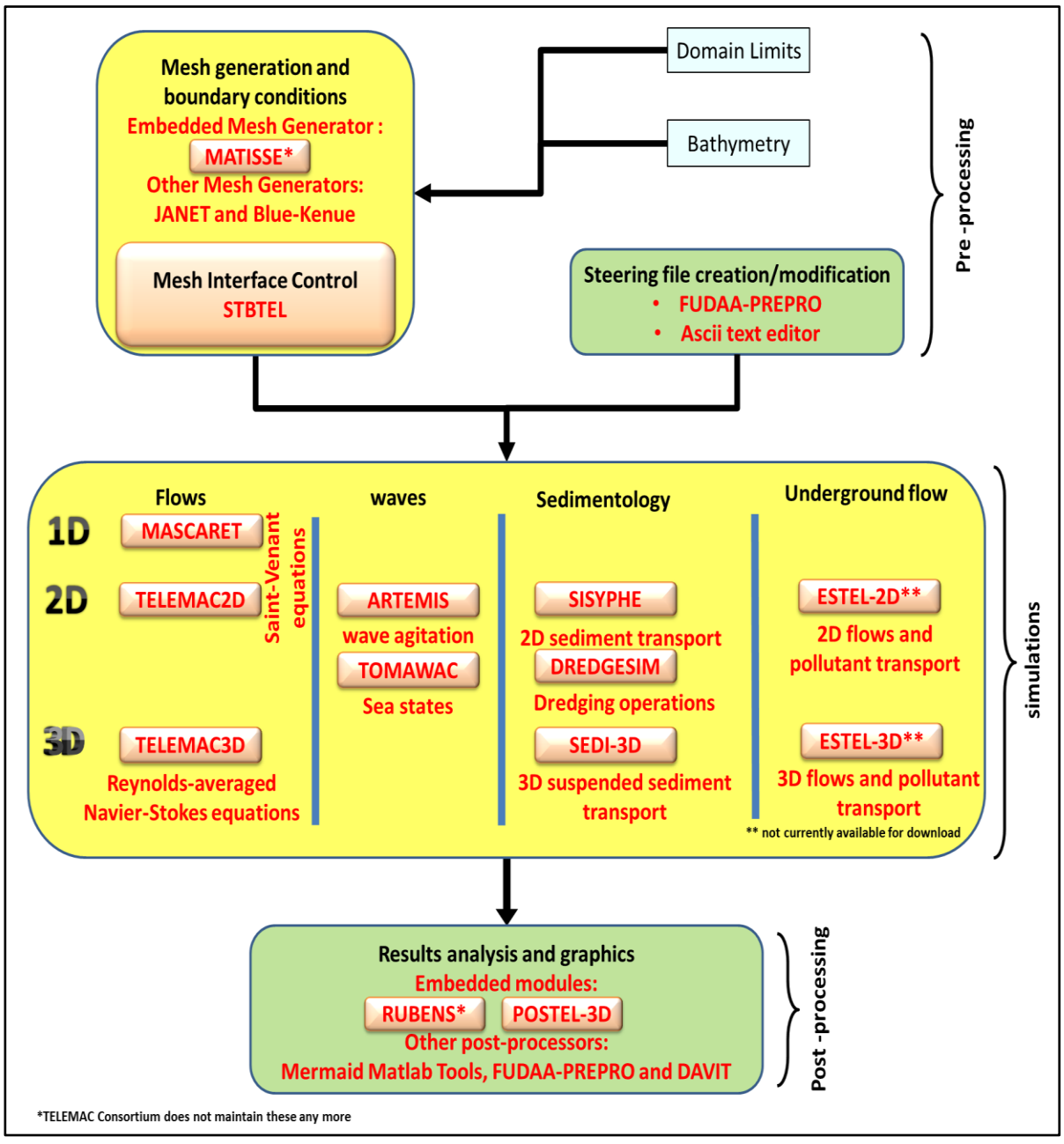

Figure 3.1: Organisation structure of the TELEMAC modelling system.

The turbulence in an estuary, which intensifies diffusion, is the key factor that causes mixing of inflowing fresh water and seawater. This turbulence is generated by currents arising from river flow, tides, or both (Ramachandran, 2010). Turbulent viscosity may be given in TE-

LEMAC2D by the user or is determined by a model simulating the transport of turbulent quantities k^* (turbulent kinetic energy) and ε (turbulent dissipation), for which the equations are as follows (Ata & Hervouet, 2012; Hervouet, 2007):

$$\frac{\partial k^*}{\partial t} + \vec{u}.\vec{\nabla}(k^*) = \frac{1}{h}\mathrm{div}\left(h\frac{\nu_t}{\sigma_{k^*}}\vec{\nabla}k^*\right) + P\text{-}\varepsilon + P_{k^*v} \tag{3.5}$$

$$\underbrace{\frac{\partial \varepsilon}{\partial t}}_{\text{rate of change}} + \underbrace{\vec{u}.\vec{\nabla}(\varepsilon)}_{\text{convection}} = \underbrace{\frac{1}{h}\mathrm{div}\left(h\frac{\nu_t}{\sigma_\varepsilon}\vec{\nabla}k^*\varepsilon\right)}_{\text{diffusion}} + \underbrace{\frac{\varepsilon}{k^*}\left(C_{1\varepsilon}P\text{-}C_{2\varepsilon}\varepsilon\right) + P_{\varepsilon v}}_{\text{production and destruction}} \tag{3.6}$$

b) Numerical resolution schemes

TELEMAC2D solves the equations on an unstructured grid using the spatial discretization of triangular elements with a finite element method. The equations are discretized in space by decomposing the unknown variables into linear functions. Although the formulation of the equations is non-conservative, the discretization ensures an exact conservation of the water mass (Chini, 2012; Hervouet, 2007). There are two principal options for the equations resolution:

1. *coupled method:* the continuity equation and the momentum equation are treated simultaneously, or
2. *wave equation method:* the velocity components are eliminated from the continuity equation (using a value obtained from the momentum equation) in order to get a wave equation only depending on the water depth. This technique increases the calculation speed but has the disadvantage of smoothing the results.

Based on the equations solved, TELEMAC2D can consider the propagation of long waves such as surge and tide, including an approximation of the non-linear interaction between them. The numerical solution of these equations is based upon the fractional step method with two steps: (i) Advection and (ii) Propagation, diffusion and source terms (representing the wind, Coriolis force, bottom friction and any source or sink of momentum within the domain) (Ata & Hervouet, 2012). The main choice concerns the schemes used for solving the advection step such as method of characteristics and Streamline Upwind Petrov Galerkin method (SUPG).

The propagation, diffusion and source terms are then used to compute the final state at the end of each time step, where a semi-implicit time discretization allows the elimination of the non-linearity in the equations. The nonlinear terms are computed with implicitation coefficient θ in the propagation step, according to Eq. (3.7) (Galland et al., 1991).

$$f = \theta f^{n+1} + (1-\theta)f^n \tag{3.7}$$

Therefore, the continuous equations are transformed into a linear discrete system which is solved using an iterative procedure (solver) based on the conjugate gradient method. The solver is used for the hydrodynamic propagation step, the tracer diffusion step and solving the turbulence model system.

c) Courant Number Management

The quality of the simulation results is influenced considerably by the value of the Courant number, which is the number of grid cells crossed by a water particle during a time step, $c_r = C\Delta t / \Delta x$, where C is the propagation velocity. Experience shows that if the Courant number is above 7 or 8, the accuracy of the results will decrease. It is hard to keep the value of the Courant number under 7, especially in sea models with a large tidal range, so that TELEMAC2D can automatically executes intermediate time steps in order to keep it below a given value specified by the user.

d) Turbulence modelling

TELEMAC2D provides four options of different complexity for turbulence modelling. The simplest option is to set a constant viscosity coefficient. In other hand, the Elder's model (Elder, 1959) assumes a non-isotropic velocity dependent depth mean viscosity value (in the flow direction and the direction normal to the flow) (Chini, 2012). The third option involves using a k^*-ε model that solves the transport equations for k^* (turbulent energy) and ε (turbulent dissipation). Equations (Eq. (3.5) and (3.6)) are solved by a fractional step method, with convection of turbulent variables being processed at the same time as the hydrodynamic variables, while the diffusion and production-dissipation of k^* and ε are being processed in another step. Use of the k^*-ε model requires a finer mesh than the constant viscosity model and thus increases the required computation time.

e) Treatment of bottom friction

Bottom friction is a major unknown in environmental studies and can be represented empirically (Hervouet, 2007). It can be modeled in TELEMAC2D using a linear or nonlinear law.

Linear law: it is rarely applied because it does not represent real physics as the friction forces are generally a quadratic function of the velocity.

nonlinear laws of friction: the friction stress ($\vec{\tau}$) (see Eq. (3.8)) is in the direction of the current and can be represented as follow:

$$\vec{\tau} = -\rho \frac{c_f}{2} |u| \vec{u} \qquad (3.8)$$

Friction coefficient C_f is rarely used. It is usually replaced by other coefficients such as Chezy coefficient C_c, which is related to C_f by $C_c = \frac{2g}{C_f}$ (unit: $m^{1/2}\ s^{-1}$). The friction force at the bottom F_f is equal $\frac{1}{\rho h}\vec{\tau}.\vec{n_f}$, where $\vec{n_f}$ is the normal vector to the bottom and its positive magnitude is equal to the cosine reciprocal of the steepest slope at a point ($1/\cos(\alpha)$).The friction law of Chezy was established for a uniform flow but it is extended to all types of flow (Hervouet, 2007). We get the following Chezy formula for the shear force at the bottom:

$$F_f = -\frac{1}{\cos(\alpha)}\frac{g}{hC_c^2}|u|\vec{u} \qquad (3.9)$$

TELEMAC2D can use also other coefficients such as Manning and Strickler (see Hervouet, 2007).

f) Treatment of tidal flats

Tidal flats are the areas besides the estuary that are periodically become dry or wet depending on the propagation of tides and storm surges, or flooding wave. *Three methods* are proposed in TELEMAC2D to take into account the presence of tidal flats in the computational domain. *In the first method*, the tidal flats are detected and the free surface gradient ($-g\vec{\nabla}(Z)$) is corrected. *In the second method*, the tidal flat areas are removed from the computation domain. *In the third method*, processing is performed in the same way as in the first method, but a porosity term is added to half-dry mesh elements inside the tidal flat area. Therefore, it can avoid the generation of parasitic driving terms that should not be included, which appear in the areas of tidal flats from forces like the gradient of atmospheric pressure.

g) Model inputs

- *Simulation control panel*

TELEMAC2D reads the physical and numerical inputs given by the user in the "steering file", which is the control panel of the model simulation. The steering file comprises a number of keywords with their values, which are assigned according to the appropriate physical conditions of the modeled area. During a computation, TELEMAC2D uses a series of input and output files. Therefore, the steering file has also the links to external files.The complete list of all files are presented in TELEMAC2D manual (Ata & Hervouet, 2012).

- *Geometry mesh file*

TELEMAC2D requires as main input also a finite element mesh of triangle grid elements, which have the bathymetric data at each node covering the area to be modelled. Therefore, the

creation of bathymetry mesh is the first step to be taken during the modelling process in order to define the nodes where the computation of the model variables takes place.

- *Prescription of initial conditions*

Initial conditions describe the model state at the start of simulation with time t=0 s. TELEMAC2D provides a continued computation; so the initial state is the last time step of the result file of the previous computation. In other cases, the initial state must be defined by the user. The simplest is done using keywords in the “steering file”, or by programming in more sophisticated ones.

- *Prescription of boundary conditions*

The boundary conditions of the study domain can either be liquid or solid. The solid boundary is impermeable, which does not allow discharge across the boundary. That can be written as:

$$\vec{u}.\vec{n_s}=0 \tag{3.10}$$

where $\vec{n_s}$ is the normal vector of the solid boundary.

The liquid boundary supposes the existence of fluid domain that does not form part of the calculation domain but one that can influence it. This influence has to be translated into boundary conditions, which are prescribed by the user for each point in a liquid boundary. They concern the dependent variables of TELEMAC2D: water depth, the two components of velocity (or flowrate) and the tracer. In other hand, the boundary conditions of k^* and Epsilon variables in the turbulence model are determined by TELEMAC2D.

In some cases, all the necessary information concerning the boundary conditions is not available. This is usual for coastal domains where only the values of the sea level on several points are known. This kind of model is referred to as an “under-constrained” model. To solve this problem, the Thompson method uses the method of characteristics to calculate the missing values. For example, TELEMAC2D will compute the velocity at the boundary in the case of a prescribed elevation.

The Thompson method can also be used for “over-constrained” models (too much information specified at the boundary). If the velocity information and the level information are not consistent, too little or too much energy is going into the model. Therefore, the Thompson technique computes a new value for the velocity and performs small adjustments to cancel the inconsistencies in the information. For example, the flow related to the tidal forcing in maritime applications induces a temporal shift in the velocity direction. So, a liquid boundary node can be successively an inflow or an outflow node due to tides. The temporal shift in the boundary conditions can be implemented. However, a phase lag may appear between the inner velocity and imposed velocity at the boundary, which leads to a numerical reflection. This phase lag may be due to a delay in the inner flow due to bottom friction and the complexity of

the bathymetry. Therefore, the Thompson method allows modifying the velocity consistently with water depth.

h) Model outputs

TELEMAC2D can generate at the end of a successful simulation several output files: the result file, the listing printout, the formatted results file and the binary results file.

The result file has all the information about the mesh geometry, then the computed values for all the printout variables and all the mesh points at each printout time step. It is stored in a Serafin format. The first graphic printout time step is determined using the Steering file.

During the simulation, TELEMAC2D displays the listing printout of the current time step, the mass balance in the domain and the error involved in its calculation. The formatted and binary results files can be used to provide data to the other models as well.

3.1.3 Wave propagation model TOMAWAC

a) Governing equations

The purpose of the TOMAWAC is modelling the generation and the spatio-temporal evolution of waves at the sea surface. The main physical process of interest is the sea state or water waves, these two terms being used interchangeably (Benoit, 2011).The water waves generally correspond to the water waves induced by wind in the sea. The wave period (T_W) ranges typically from 2.5 to 25 s (frequency $f_W=1/T_W$= 0.04 to 0.4 Hz). The sea state can take different forms depending on the weather (calm sea or storm) or by the wave nature (wind sea or swell). Sea-state modelling is a major task in coastal and ocean engineering. It describes the generation, propagation and dissipation of water waves in coastal and ocean waters.

TOMAWAC is a time-stepping (i.e. non-stationary) phase averaged spectral wave transformation model, which is part of the TELEMAC finite element modelling suite. The acronym TOMAWAC derives from "TELEMAC-based operational model Addressing Wave Action Computation”. The model is a third generation wave model, since it does not require any parameterization on the spectral or directional distribution of power (or action density). In the general case of wave propagation in an unsteady medium (sea currents and/or water levels varying in time and space), the directional spectrum of the variance density is no longer conserved rather the directional spectrum of wave action N ($Jule.Hz^{-2}.rad^{-1}$) (Benoit, 2011) . TOMAWAC solves the conservation equation of the wave action density N over an unstructured triangular finite element mesh where the independent parameters can been chosen as time t, geographical position x & y, relative (intrinsic) angular frequency $\sigma_{dis} = 2\pi f_r$ (where f_r is the intrinsic or relative wave frequency)**,** and direction of wave propagation θ_w. In horizontal Cartesian co-ordinates, the conservation equation for wave action can be written as (Benoit, 2011):

$$\frac{\partial \tilde{N}}{\partial t}+\vec{\nabla}.\left(\vec{c_g}\tilde{N}\right)=\frac{S_{tot}}{\sigma_{dis}}$$

or

$$\frac{\partial \tilde{N}}{\partial t}+\dot{x}\frac{\partial \tilde{N}}{\partial x}+\dot{y}\frac{\partial \tilde{N}}{\partial y}+\dot{\theta_w}\frac{\partial \tilde{N}}{\partial \theta_w}+\dot{f_r}\frac{\partial \tilde{N}}{\partial f_r}=\frac{S_{tot}}{\sigma_{dis}} \quad (3.11)$$

where $\tilde{N}(x, y, \sigma_{dis}, \theta_w, t)=\frac{2\pi\sigma_{dis}}{C\,C_g}N(x, y, k_x, k_y, t)$ with $\vec{k}=(k_x, k_y)=(|k|\sin\theta_w, |k|\cos\theta_w)$ is the wave number vector that is related to angular frequency σ_{dis} by the dispersion relation in the zero-current case by $\sigma_{dis}^2=g|k|\tanh(|k|h)$, $\vec{\nabla}$ is the four-dimensional differential operator in the x, y, σ_{dis}, θ_w-space, c is the phase velocity of waves. $\vec{c_g}=(\frac{\partial x}{\partial t},\frac{\partial y}{\partial t},\frac{\partial \sigma_{dis}}{\partial t},\frac{\partial \theta_w}{\partial t})=(c_x,c_y,c_{\sigma_{dis}},c_{\theta_w})=(\dot{x},\dot{y},2\pi\dot{f_r},\dot{\theta_w})$ is the propagation velocity of a wave group. The right-hand side contains S_{tot} (see Eq. (2.1)), which is the source/sink term that represents all physical processes that generate, dissipate, or redistribute wave action density (see section 3.1.3(c)):

$$S_{tot}=\underbrace{S_{in}+S_{ds}+S_{nl}}_{\text{Deep Water Source/Sink Terms}}+\underbrace{S_{bf}+S_{br}+S_{tr}}_{\text{Shallow Water Source/Sink Terms}} \quad (3.12)$$

S_{in}: wind-driven wave generation

S_{ds}: whitecapping-induced energy dissipation

S_{nl}: non-linear quadruplet interactions

S_{bf}: bottom friction-induced energy dissipation

S_{br}: bathymetric breaking-induced energy dissipation

S_{tr}: non-linear triad interactions.

Eq. (3.11) is an equation of transport where the spatial transfer rates $\dot{x}$ and $\dot{y}$ represent the spatial wave propagation and shoaling. The directional transfer rate $\dot{\theta_w}$ models the refraction-induced change of wave propagation direction, which is generated by the spatial variations of the wave propagation environment that can result either from water depth changes or current gradients. The relative frequency transfer rate $\dot{f_r}$ models the shifts in wave frequency due to sea level variations in space and time and/or the current variations in space. The last term is zero when there is no temporal variation of the sea level (i.e. water depth) and the current is uniform. The transfer rates, as computed from the linear wave theory, are as follow (Benoit, 2011; Chini, 2012):

$$\dot{x}=c_g \sin\theta_w + u \tag{3.13}$$

$$\dot{y}=c_g \cos\theta_w + v \tag{3.14}$$

$$\dot{\theta_w}=-\frac{\sigma_{dis}}{\sinh 2|k|\,h}\left(\cos\theta_w \frac{\partial h}{\partial x}-\sin\theta_w \frac{\partial h}{\partial y}\right)-\sin\theta_w \cos\theta_w \frac{\partial u}{\partial x} + \sin^2\theta_w \frac{\partial u}{\partial y}-\cos^2\theta_w \frac{\partial v}{\partial x}+\sin\theta_w \cos\theta_w \frac{\partial v}{\partial y} \tag{3.15}$$

$$2\pi\dot{f_r}=\frac{\sigma_{dis}\,|k|}{\sinh 2|k|h}\left(\frac{\partial h}{\partial t}+u\frac{\partial h}{\partial x}+v\frac{\partial h}{\partial y}\right)-\sin^2\theta_w \frac{\partial u}{\partial x}-\sin\theta_w \cos\theta_w \frac{\partial u}{\partial y}- \sin\theta_w \cos\theta_w \frac{\partial v}{\partial x}-\cos^2\theta_w \frac{\partial v}{\partial y} \tag{3.16}$$

Given $N(x, y, k_x, k_y, t) = \frac{C\,C_g}{2\pi\sigma_{dis}^2} F(x, y, \sigma_{dis}, \theta_w, t)=BF$ with F is the directional variance spectrum, it is possible to consider the radiation stress contribution to the mean flux of horizontal momentum (Eq. (3.2) and (3.3)). The radiation stress tensor, S_{ij}, can be defined as follow (Longuet-Higgins & Stewart, 1964):

$$S_{ij}=\rho g \int_0^{2\pi}\int_0^{+\infty}\left[\frac{C_g}{C}\frac{k_i k_j}{k^2}+\left(\frac{C_g}{C}-\frac{1}{2}\right)\delta_{ij}\right]\times F(\theta_w,f_w)\,d\theta_w\,df_w \tag{3.17}$$

where i and j point to the two horizontal coordinates x and y. δ_{ij} is the Kronecker symbol (δ_{ij} =1 if i=j and 0 elsewhere). The horizontal components of radiation forcing term, S_{rad}, are added to Eq. (3.2) and (3.3), which are solved by TELEMAC2D:

$$S_{rad}=-\frac{1}{\rho h}\begin{pmatrix}\frac{\partial S_{xx}}{\partial x}+\frac{\partial S_{xy}}{\partial y}\\ \frac{\partial S_{yx}}{\partial x}+\frac{\partial S_{yy}}{\partial y}\end{pmatrix} \tag{3.18}$$

b) Application domain of TOMAWAC model

TOMAWAC can be applied from the deeper ocean up to the coastal zone. Its application range is determined by relative depth h/L, wherein L denotes the wave length corresponding to the peak spectral frequency for irregular waves. The application domain of TOMAWAC includes:

- *Deep water zone*, characterized by large water depths (i.e. $\frac{h}{L} > 0.5$). The principal physical processes are: wind-driven wave generation, white capping dissipation and non-linear quadruplet interactions;
- *Intermediate water depth zone* with a relative water depth h/L =0.05 and 0.5. In addition to the above processes, bottom friction, shoaling (wave growth due to a bottom rise) and the effects of refraction due to bathymetry and/or to currents are to be taken into account;
- *Shallow water zone*, including shoals or nearshore areas with a relative water depth h/L <0.05. For these shallow water areas, such physical processes as bottom friction, bathymetric breaking and non-linear triad interactions between waves should be included.

The application domain of TOMAWAC does not include harbour areas and, more generally, the cases in which the effects of reflection and/or diffraction on structures cannot be neglected. For those applications, the ARTEMIS model of the TELEMAC system is suitable.

Several factors take part in the evolution of sea-state and interact to various extents with the waves. TOMAWAC models the following interactions:

- *Wave-bathymetry interaction*: the submarine relief data entered into TOMAWAC are time-independent, while the sea level can change in time. TOMAWAC can take into account refraction, shoaling, bottom friction and bathymetric breaking;
- *Wave-atmosphere interaction*: this interaction represents the main mechanism in wave generation. It contributes to energy dissipation processes (white capping, wave propagation against the wind, etc.) and it is involved in energy transfers. To represent the unsteady behaviour of this interaction, TOMAWAC requires wind fields at 10 m height (specification of the two horizontal velocity components) with a time step that is adapted to the modelled weather event. These wind fields can be obtained either by a meteorological models or from satellite measurements;
- *Wave-current interaction*: sea currents (generated either by the tide or by oceanic circulations) may significantly affect waves depending on their intensity. They modify the refractive wave propagation direction, reduce or increase the wave height according to their direction of propagation in comparison with that of waves, and can affect the wave periods if they exhibit a marked unsteady behaviour. In TOMAWAC, the current flow field is represented by the horizontal components of the depth-averaged flow velocity at the nodes of the computational grid. TOMAWAC models frequency

changes caused either by the Doppler effect or by unsteady currents, as well as by a non-homogeneous current field.

The above interactions with their processes modify the total wave energy and the directional spectrum distribution of this energy (i.e. the shape of the directional spectrum of energy). Numerical modelling of these various processes is not yet mature, though some of them are now well known. The theoretical modelling of these processes is described in detail in the TOMAWAC User's manual (Benoit, 2011).

c) Numerical aspects of TOMAWAC

- *Spatial discretization*

In TOMAWAC, the spatial discretization is performed using the finite elements technique (and in all the models of the TELEMAC system as well). This avoids the use of nested grids for nearshore applications, where complex bathymetry and irregular shoreline often require a refined resolution. So, a large maritime area can be discretized using a number of triangular elements whose size may be varied according to the desired resolution on the same grid.

- *Spectro-angular discretization*

At each time step, the propagation frequencies f_{di} and directions θ_{di} of the action density spectrum is discretized at each node. The range of wave directions [0°, 360°] is discretized in a number of equally spaced directions (ND). This number of wave directions is specified by the user (usually 12 to 72). The directions are defined as follows:

$$\theta_{di} = \frac{(i-1).360}{ND} \text{ with i between 1 and ND} \tag{3.19}$$

The discretization of the wave frequency follows a geometrical series (see Eq.(3.20)), for which the minimal frequency (f_1), the frequential ratio (qr) and the number of frequencies (NF) are specified by the user (usually 15 to 30).

$$f_{di} = f_1 . qr^{i-1} \text{ with i between 1 and NF} \tag{3.20}$$

A 2-dimensional grid of (ND.NF) points by the discretization of θ_{di} and f_{di} is used at each node, which is represented in polar a coordinate system. In this grid, the wave frequencies are measured radially and the propagation direction corresponds to the value of an angle in relation to the axis selected by the user as (vertical or horizontal)

- *Numerical schemes*

The wave action balance equation is solved in TOMAWAC through a fractional step method, including:

- firstly, a convection step (left-hand side of the wave action equation (Eq. (3.11))) is performed, in which an intermediate solution is calculated without the source terms:

$$\frac{\partial(BF)}{\partial t}+\vec{c_g}.\vec{\nabla}(BF)=0 \qquad (3.21)$$

Eq. (3.21) is solved in TOMAWAC by means of the method of characteristics (Benoit, 2011). The characteristics curves have to be computed only once at the beginning of computation due to the fact that the convector field $\vec{c_g}$ is not time dependent when there is no tide. At each time step, the convection step is thus reduced to an interpolation, which allows saving computing time.

- Secondly, a source terms integration step (right-hand side of Eq. (3.11)) is performed, the new solution is calculated from the intermediate solution taking into account only the effect of the source terms:

$$\frac{\partial(BF)}{\partial t}=B.S_{tot} \qquad (3.22)$$

The source terms integration is carried out through a semi-implicit scheme:

$$\frac{F^{n+1}-F^{*}}{\Delta t}=\frac{S_{tot}{}^{n+1}+S_{tot}{}^{*}}{2} \qquad (3.23)$$

where the exponent * denotes the values of the variables after the propagation step (but before the source term integration step) and the exponent n+1 denotes the values of the variables after the source term integration step. This scheme is inspired by the semi-implicit scheme used in the WAM model (WAMDI Group, 1988).

d) Model inputs

- *Simulation control panel*

TOMAWAC reads the physical and numerical inputs given by the user in the "steering file", which has the same role as for TELEMAC2D. The steering file has the links to external files. The main files used in TOMAWAC computation are the same as those used by TELEMAC2D. the complete list of all files are presented in TOMAWAC manual (Benoit, 2011).

- The geometry mesh file

TOMAWAC can simulate the changes in the action density spectrum at each node of the same geometry mesh used by TELEMAC2D. In TOMAWAC the wave direction spectrum is split

into a finite number of propagation frequencies f_i and directions θ_i. The balance equation of wave action density is solved for each component (f_i, θ_i). Each component of the action density spectrum changes in time under the effects of the software-modelled processes.

- *Prescription of initial conditions*

The variance density directional spectrum is computed as the product $F(f_{di}, \theta_{di}) = E(f_{di}) . D(\theta_{di})$, where $E(f_{di})$ is the variance density spectrum and $D(\theta_{di})$ denotes the angular distribution function. Table 3.1 shows all the available options in TOMAWAC for computing the initial frequency distribution and directional distribution of the waves using the integer keyword TYPE OF INITIAL DIRECTIONAL SPECTRUM.

- *Prescription of boundary conditions*

Two different boundary conditions are proposed in TOMAWAC, an imposed wave spectrum or free conditions. The free boundary absorbs fully the wave energy. It may be:

- *Liquid boundary*: it is assumed that the waves propagate beyond the domain and nothing else enters it.
- *Solid boundary*: it is assumed that the shore fully absorbs the wave energy, depending on whether waves are entering or exiting the computational domain.

In the second option, the wave action spectrum is strictly imposed at each point along the boundary with a prescribed value. This boundary condition allows wave energy to enter the computational domain.

The boundary conditions are specified using the boundary conditions file (CONLIM), the steering file and the user subroutine LIMWAC.f.

e) Model outputs

At the end of a successful simulation, TOMAWAC can generate several output files: the 2D result file, the listing printout, the global results file and the punctual or spectrum results file. These files have the same roles as TELEMAC2D output files.

Table 3.1: Types of initial action density spectrum as proposed in TOMAWAC (Benoit, 2011).

Key-word value		Spectrum	Constants being used
0		Zero spectrum	none
1	Wind≠ 0	- Frequencies: Jonswap according to wind - Directions: unimodal about the wind ($\theta_1 = \theta_w$)	f_{pmax}, γ, σ_a, σ_b, Fetch, s_1
	Wind = 0	Zero spectrum	none
2	Wind≠ 0	- Frequencies: Jonswap according to wind - Directions: unimodal about the wind ($\theta_1 = \theta_w$)	f_{pmax}, γ, σ_a, σ_b, Fetch, s_1
	Wind = 0	- Frequencies: parameterised Jonswap (α, f_p) - Directions: parameterised unimodal (same spectrum at every point)	α_{phil}, f_p, γ, σ_a, σ_b, s_1, θ_1
3	Wind≠ 0	- Frequencies: parameterised Jonswap (α) - Directions: unimodal about the wind ($\theta_1 = \theta_w$)	α_{phil}, f_p, γ, σ_a, σ_b, s_1
	Wind = 0	Zero spectrum	none
4	Wind≠ 0	- Frequencies: parameterised Jonswap (α, f_p)	α_{phil}, f_p, γ, σ_a, σ_b, s_1, θ_1, s_2, θ_2, λ
	Wind = 0	- Directions: parameterised angular distribution function. Same spectrum at every point	α_{phil}, f_p, γ, σ_a, σ_b, s_1, θ_1, s_2, θ_2, λ
5	Wind≠ 0	- Frequencies: parameterised Jonswap (H_{m0}) - Directions: unimodal about the wind ($\theta_1 = \theta_w$)	H_{m0}, f_p, γ, σ_a, σ_b, s_1
	Wind = 0	Zero spectrum	none
6	Wind≠ 0	- Frequencies: parameterised Jonswap (H_{m0}, f_p)	H_{m0}, f_p, γ, σ_a, σ_b, s_1, θ_1, s_2, θ_2, λ
	Wind = 0	- Directions: parameterised angular distribution function. Same spectrum at every point	
7	Wind≠ 0	- Frequencies: parameterised TMA (H_{m0}, f_p)	H_{m0}, f_p, γ, σ_a, σ_b, s_1, θ_1, s_2, θ_2, λ
	Wind = 0	- Directions: parameterised angular distribution function. Same spectrum at every point	

The TELEMAC system has proved state-of-the-art and useful software system. It is suitable for a wide range of applications. It consists of several numerical models (see Figure 3.1), which are designed for the use in the fields of free surface hydrodynamics, sedimentology, water quality, waves and underground flows. TELEMAC models can utilize multiprocessor computers to run in parallel version and the code can be modified by users to program particular functions of a simulation. The numerical algorithms of TELEMAC models are collected into a single finite element library (BIEF), which offers the cross-linking/coupling of the boundary conditions definition, the temporal and spatial discretization, the solved equations

and their solution methods or output variables. These capabilities make TELEMAC (version 6.2 in parallel processing mode) an appropriate operational model system for the assessment of storm surges, tide, external surges and other physical processes. These phenomena are dominating in the South-Eastern part of the North Sea (see Figure 2.15). The hydrodynamics and wave propagation over the North Sea can be simulated using the flow model TELEMAC2D and the wave propagation model TOMAWAC, respectively.

TELEMAC2D solves the non-conservative form of shallow water equations, with h (depth) and u, v (flow velocity components) as the unknown. It considers the propagation of long waves such as surge and tide, including an approximation of the non-linear interaction between them. The numerical solution of these equations is based upon the fractional step method with two steps: (i) Advection and (ii) Propagation, diffusion and source terms (representing the wind, Coriolis force, bottom friction and any source or sink of momentum within the domain).

TOMAWAC solves the wave action density (N) conservation equation (Eq. (3.11)). It can model the processes of spatial propagation of waves over relatively large distances, refraction due to spatial variations in bathymetry and current, shoaling due to spatial variations in seabed and current. Moreover, it can also describe the processes of generation by unsteady wind fields, dissipation by white capping, dissipation by depth induced wave breaking, dissipation by seabed friction and non-linear wave-wave interactions (quadruplets and triads). The application domain of TOMAWAC does not include harbour areas and cases in which the effects of reflection and/or diffraction on structures are relevant. Eq. (3.11) for N is solved in TOMAWAC through a fractional step method. Firstly, a convection step is performed by calculating an approximate solution without the source terms (Eq.(3.12)). Secondly, the integration step of the source terms is performed by calculating the next time step solution from the intermediate solution. The source and sink terms are classified as linear and non-linear terms in N, in which a Taylor's expansion is made for the non-linear terms keeping only the first-order terms.

As both TELEMAC2D and TOMAWAC models are parts of the TELEMAC system, they share the same geometry and boundary conditions files to run the simulations. Therefore, the wave state simulation by TOMAWAC can be coupled with the flow model TELEMAC2D.

3.2 Surge-tide and wave propagation modelling for the North Sea area

The hydrodynamic conditions in the North Sea are driven by tides, on top of which the water level is affected by local surge, Atlantic external surge and waves during storm conditions (see Figure 2.15). Furthermore, the water levels in the estuaries of the German rivers (Ems, Weser and Elbe) may be affected by variations in the river discharge.

Storm-tide in the North Sea is related mainly to weather conditions that induce water level alterations by combined effects of extreme wind and atmospheric pressure. This section shows how TELEMAC2D and TOMAWAC models are implemented to the North Sea area,

including the hydrodynamic conditions that may affect the generation of surge-tides. The implementation includes the following steps:

- Preparation of the required bathymetry mesh, boundary conditions and meteorological data in order to carry out the hydrodynamic and wave propagation modelling for the North Sea area.
- Validation of the tidal simulation for the North Sea by TELEMAC2D in 2006 using real-tide (based on observed water level measurements) at Cuxhaven, Sylt and Helgoland.
- Implementation of surge-tide simulations using TELEMAC2D, taking into account the different physical processes that may affect the surge-tide. On the other hand, the predicted wave parameters by TOMAWAC in 1998 will be compared with the measured parameters at Sylt.

The numerical storm-tide simulation results identify the effective contribution of each component to the extreme water level at the two interested sites, Cuxhaven and Sylt. Therefore, the components with negligible contributions can be not included in the past (1970-2007) and/or future (2070-2100) numerical simulations, which saves the computation time.

3.2.1 Geometry mesh file

The creation of the bathymetry mesh file for the North Sea domain is the first step to be taken during the modelling process in order to define the nodes, where computation of the model variables takes place. The nonlinear nature of the North Sea storm-tide is mainly due to the complexity of the geometry and bathymetry of this shallow shelf sea. Moreover, the open boundary of the regional North Sea model has to be shifted away from the shallow area in order to avoid ill-posed open boundary forcing (YU, 1993).

The main advantage of TELEMAC with finite element technique is the high flexibility in the mesh refinement process. Therefore, the key areas can be represented in more detail and the areas near the open sea can be kept with coarser elements. The bathymetry mesh file of the North Sea area is kindly provided by BAW, which is an updated version in 2006 based on (Plüß, 2004). It is supplied in Gauss-Kruger zone 3 coordinate system. ‘JANET’, the mesh processing software that allows generation of triangulated irregular mesh, has been used to create the bathymetry mesh on which Telemac2D and TOMAWAC will solve the governing equations. A minimum inter-node distance of 80 m has been defined in the German estuaries to have more accuracy and computation nodes near the southern boundary. Near the outer open sea, the grid size is set up to 26 km in northern of the Dogger Bank to reduce the computation time. The model region extends

- North:From Wick (λ = 3° 5 ' W, φ = 58° 27' N) along a line north to the latitude (φ = 60°) and following this latitude eastward to Lerwick (λ = 1° 8' W, φ = 60° 9' N) up to Norway
- West: Along a line from Plymouth / Ile de Batz, following the longitude λ = 4° 5' W

- East: In the Baltic Sea along the 13th longitude (East) into the Mecklenburg Bay
- in the German estuaries:
  - Ems up to Papenburg,
  - Weser up to the weir „große Weserbrücke" and
  - Elbe up to the weir at Geesthacht

The mesh consists of 41891 nodes and 70564 elements, it covers the following extend according to Gauss-Kruger zone 3:

- Easting: from 253936 m to 3781870.15 m and
- Northing: from 5441363.5 m to 6755029.46 m.

The boundaries of the bathymetry mesh by BAW are updated using FUDAA pre-processor to represent the hydrodynamic conditions in the North Sea mesh model naturally (see Figure 3.2). The solid segments in the northern and eastern boundaries are removed, since it could prohibit the full propagation of tide and/or external surge inside the area. Moreover, the fresh water discharge of the adjacent rivers / estuaries is prescribed at each river section. The discharge data of Westerschelde, Ems, Weser, and Elbe rivers from 1960 to 2007 are kindly provided by BAW.

3.2.2 Preparation of boundary conditions and meteorological data for the North Sea model

a) Meteorological data

The effect of meteorological forces (essentially wind and pressure) modifies, to a great extent, the regular tidal movements in the North Sea. TELEMAC2D requires the 10 m height wind and sea level pressure (SLP) fields in order to simulate the storm surge component. The wave propagation model TOMAWAC requires mainly the 10 m height wind to simulate the main source of wave energy by wind (S_{in}).

The meteorological forces should have sufficient accuracy and resolution in order to get the storm surge and wave fields satisfactorily modeled. The hourly zonal and meridional wind speed components along with the hourly Sea Level Pressure (SLP) fields are kindly provided by Helmholtz-Zentrum Geesthacht (HZG) in netcdf format for each month between 1958 and 2007. The hourly wind speed components and SLP fields are regionalized with regional climate model (RCM) SN-REMO (0.5^o x 0.5^o horizontal resolution) (von Storch et al., 2000), which is forced on boundaries with atmospheric NCEP re-analyses. The RCM SN-REMO is set up for running on a rotated grids with North Pole located at (-170^o longitude, 32.5^o latitude), which differ from the geographical North Pole (0^o longitude, 90^o latitude). So, the regionalized meteorological conditions are rotated back to geographical coordinate system with the North Pole of (0^o longitude, 90^o latitude). These re-rotated meteorological conditions are transformed afterward to "3-degree Gauss-Kruger zone 3" coordinate system, which is used by the North Sea geometry grid in TELEMAC2D and TOMAWAC.

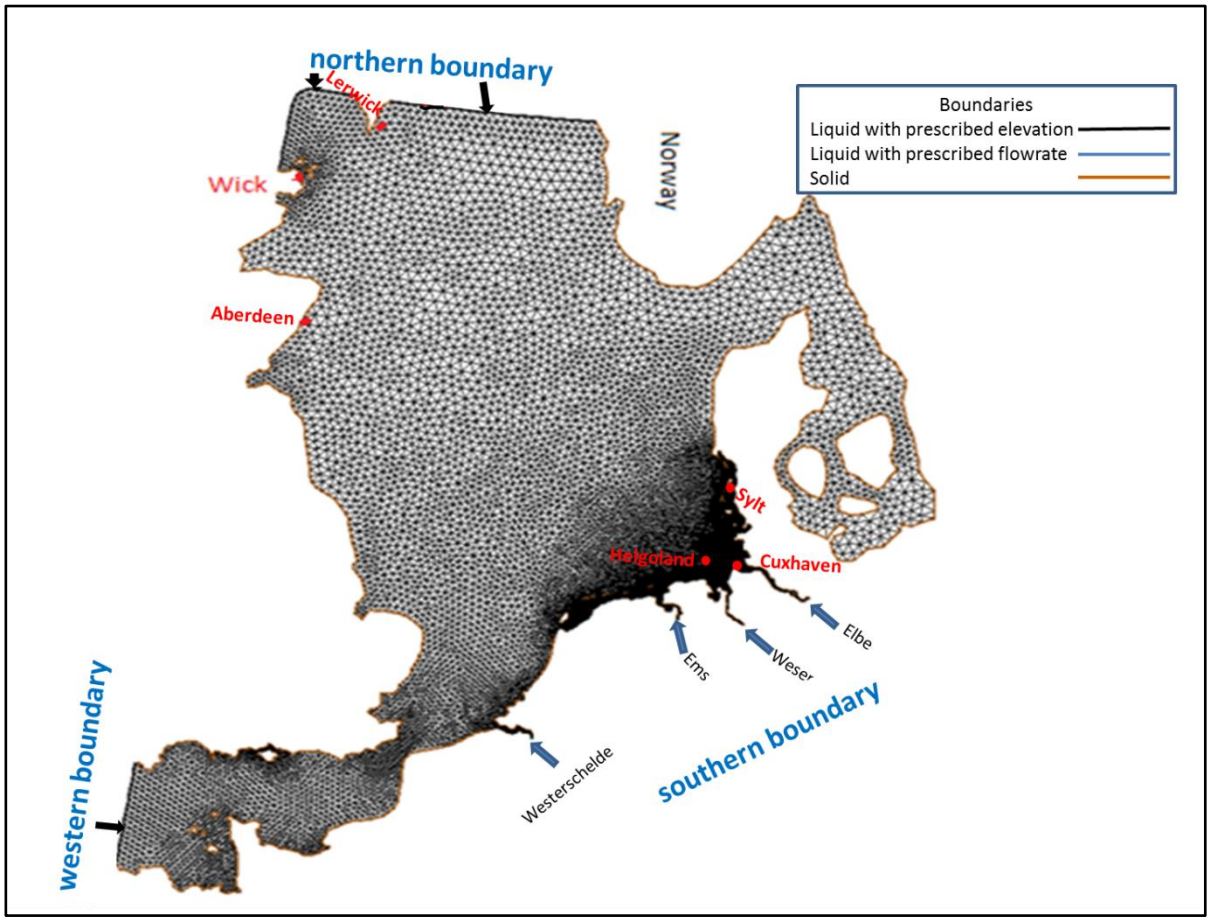

Figure 3.2: Geometry mesh of the North Sea mesh in TELEMAC2D with the prescribed water elevation at open-sea and flow rate of fresh water discharge at southern boundaries (modified from updated version in 2006 by(Plüß, 2004)).

The coverage domain of the RCM SN-REMO is much larger than the geometry mesh of the North Sea. It extends from 10.3° W to 70.73° E and from 29.6° N to 67.8° N using a finite difference mesh with resolution of 50 km. In order to use the monthly meteorological data by the RCM SN-REMO over the North Sea mesh, two interpolations are performed (see Figure 3.3):

(i) in space over the computation grid (Figure 3.2) and stored in serafin format for each year between 1970 and 2007 (Tayel & Oumeraci, 2012b)
(ii) in time during the surge-tide and/or wave propagation simulation at the internal computation time step by TELEMAC2D and/or TOMAWAC, respectively.

Therefore, after interpolation in space of the hourly wind speed components and SLP fields, a linear temporal interpolation is performed at each computational time step inside TELEMAC2D by the modified subroutine METEO.f (Tayel & Oumeraci, 2012b). On the other hand, TOMAWAC reads only the hourly wind speed components from the Serafin files and perform the temporal interpolation at each time step without modification to its subroutines.

b) External surge from the Atlantic

The contribution of the external surge from the Atlantic must be properly considered for a precise simulation of the water elevation in the North Sea model domain. For this purpose, the external surge at Aberdeen is linearly added to the tidal level with time shifts of about 45 minutes to the north-west part of the northern boundary and about 2 hours for the other part between Scotland and Norway (see Figure 3.2). Doing so, the external surge is constant in space at each time step for the two parts of the northern open sea boundary but the observed external surge is higher at the north-west part than between Scotland and Norway.

The suitable sites for considering the external surge of the North Sea model are Wick and Lerwick because they have zero time shifts from the northern boundary and reflect the observed external surge variability in space (see Figure 3.2). Two ANNs models called NARX (Nonlinear AutoRegressive eXogenous inputs) are developed to predict the external surges at wick and Lerwick using wind and pressure data as input. The NARX models for both sites are used to fill the gaps in observed external surge data between 1970 and 2007. Moreover, they will also be used to predict the external surge between 2070 and 2100 for future surge-tide realization (see chapter 5).

For Wick and Lerwick, the construction of each NARX model is performed in two phases. The first phase deals with the determination of the optimum number of input variables time series lags that should be included as input, also the optimum architectural parameters and best training algorithm using STATISTICA Automated Neural Networks (SANN) tool in STATISTICA package version 10 from Statsoft Inc.. In the second phase, the final NARX model is developed using the neural networks toolbox in Matlab 2013b for further structural parameters configuration and modifications that are based on the optimum structure obtained by SANN.

Finally, the two NARX models prediction results are validated in terms of correlation coefficient (CC), root mean square of error (RMSE) and standard deviation (σ) using observed external surge data at Wick and Lerwick.

- *Input variables selection and preparation for the developed NARX models*

The NARX models in the learning phase also implicitly capture the nonlinear relation between the meteorological forces as input data and the external surge at Wick and Lerwick as output using a moderate time span (approximately 10 years) of the observed external surge at each site. The observed data between 1969 and 2007 for both sites are downloaded from the British Oceanographic Data Centre (BODC) website http://www.bodc.ac.uk/. The observed external surge for Wick contains data gaps and improbable values mostly in 1970, 1971 and 1985, while it is the case for Lerwick in 1999 and 2000. A subset of the observed external surge data at each site for learning and validating the models are selected such that it does not contain gaps and/or a substantial amount of doubtful observed values. This criterion is fulfilled for Wick data between 1990 and 1997, while the suitable data for Lerwick is between 1972 and 1984. The downloaded data for each year of the above selected periods (Wick(1990-1997) and Lerwick (1972-1984)) is recorded with time interval between 15 minutes and 1

hour, which is temporally interpolated in order to be synchronized with observed meteorological data every hour.

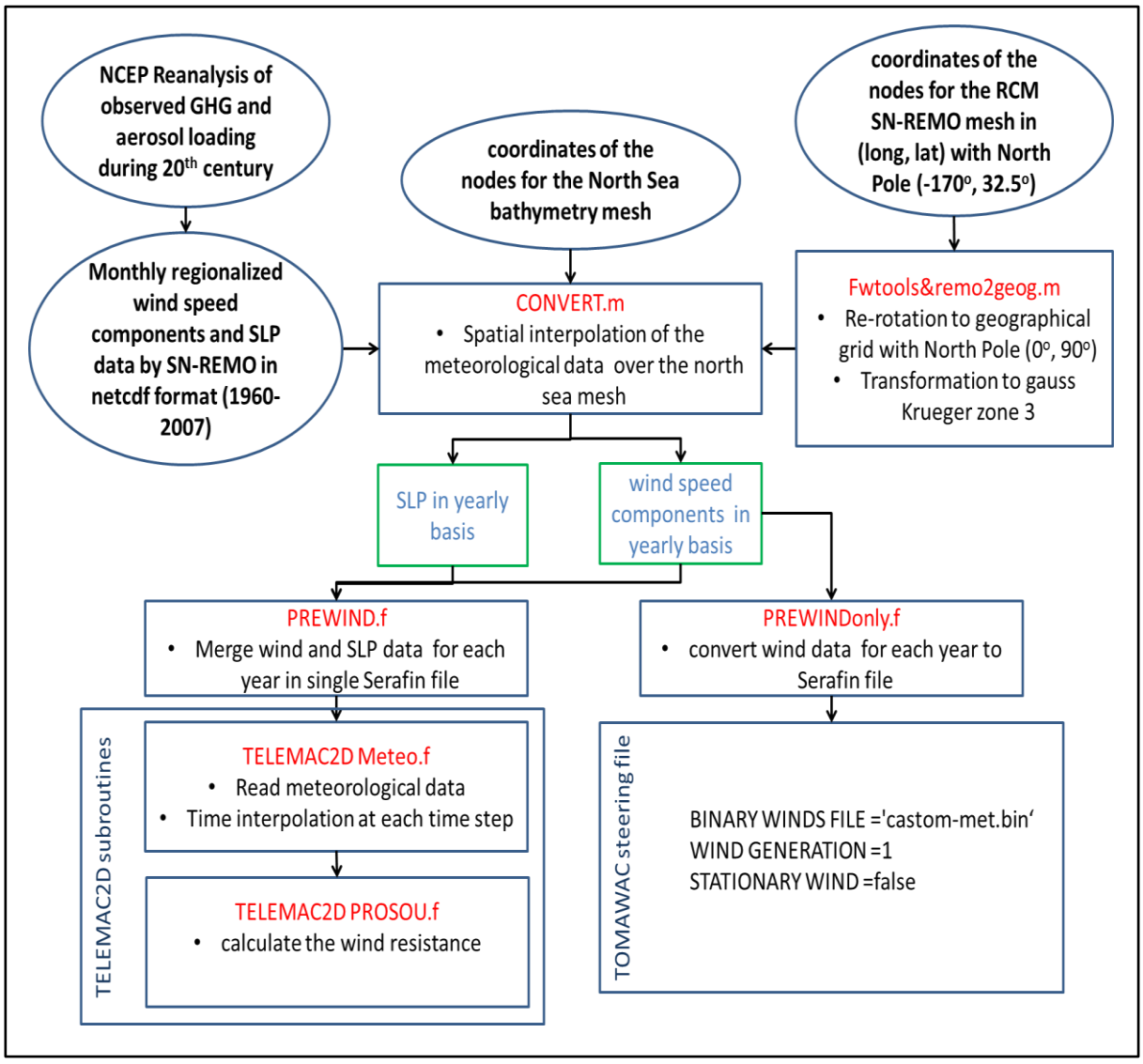

Figure 3.3: Interpolation scheme of meteorological data for the North Sea model, where the developed/modified codes (except remo2geog.m and Fwtools are free software) are in red and their functions are in black (Tayel & Oumeraci, 2012b).

Table 3.2 shows the input and output data for the two developed NARX models at Wick and Lerwick. The input deck of the two NARX models consists of the two wind speeds components in east-west direction (wind U component or zonal component) and in south-north direction (wind V component or meridional component) in addition to the sea level pressure. These three types of meteorological data are extracted from the RCM SN-REMO wind and SLP fields using the spatial interpolation at Wick and Lerwick every hour.

Table 3.2: Input and output for the developed NARX models at Wick and Lerwick.

Description	Wick	Lerwick
Input	• Time series of wind U component. • Time series of wind V component. • Time series of sea level pressure. • Time series of observed external surge.	• Time series of wind U component. • Time series of wind V component. • Time series of sea level pressure. • Time series of observed external surge.
output	Time series prediction of external surge every hour	Time series prediction external surge every hour
Training period	1990 to 1997	1972 to 1984
Prediction period	1999,2000 and from 2070 to 2100	1970,1971,1985 and from 2070 to 2100

- *Identification of ANNs optimum parameters using SANN*

SANN is used to automatically search for the various combinations of architectural parameters for the developed ANNs models, to additionally obtain the optimum lags in the time series of the input variables that should be included. The different ANNs models using SANN are developed through the following three stages:

Stage 1- Data Selection and construction of ANNs models by using SANN

The span periods of the used learning data for Wick and Lerwick are from 1990 to 1997 and from 1972 to 1984, respectively. Three independent series of data among the available data series should be selected (training, validation and testing series) such that the training series contains most of the extreme events (Jayawardena & Fernando, 2001). Therefore, the above selected learning data sets for both sites are divided randomly in three series: the training series, the validation series and test series, which represent respectively 70%, 15% and 15% of the data. Figure 3.4 shows the input and output variables (see Table 3.2) along with the modified structural parameters for the designed ANNs by SANN at Wick. For both sites, only the regression (Eq. (4.12)) and time series regression (Eq. (4.13)) types are used in the develop-

ment of their ANNs models. The input variables (u_m) for both ANN models, which are developed by SANN, do not include the previous observed external surge as input.

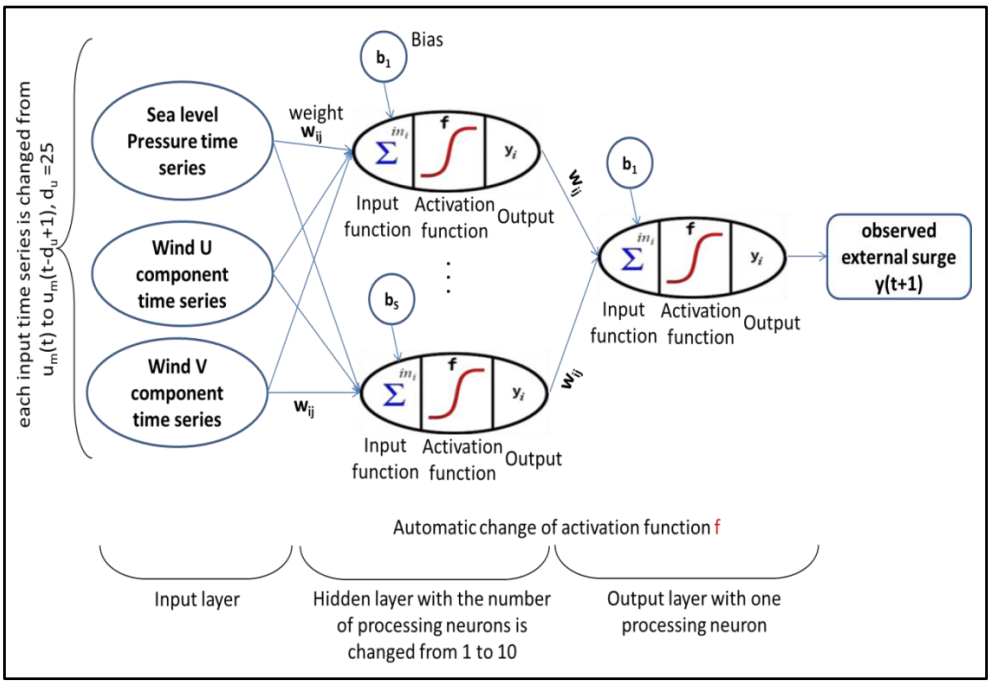

Figure 3.4: Change of the architectural parameters of SANN models for Wick (the same in case of Lerwick) (see Eqs. (4.12) and (4.13).

Stage 2- SANN and ANN model training

From an initially random configuration of weights and biases (i.e., a random point on the error surface), SANN automatically use several training algorithms in order to incrementally seek for the global minimum. For Wick and Lerwick, the optimum architecture of the two types of models is determined by training many MLP networks that have different architectural parameters. For each model type, 25 trials are carried out. In such a way, the time lags of input variables are changed from 0 to 24. In each trial, several MLP networks are trained by varying (i) the number of neurons in the hidden layer from 1 to 10 neurons, (ii) the type of activation function (identity, logistic, tangent sigmoid, exponential and sine functions) in the hidden and output layers.

Stage 3- Determination of the optimum ANN architectural parameters

In each trial for the two ANN models at Wick and Lerwick, only the best network based on the test set performance is selected. The results of the ANN models for Wick indicate an increase in the correlation coefficient and stable decrease in Sum Square of Error (SSE) until inputs time lag d_u=14 hours, while for Lerwick the same behaviour is observed but only until d_u=7 hours.

The optimum number of neurons in the hidden layer for the best selected MLP neural network is 3 neurons for both sites. Moreover, the candidate types of activation function for neurons in

the hidden layer is tangent sigmoid (tansig), while the output layer has only one neuron with linear activation function.

- *Implementation of the NARX models for Wick and Lerwick*

The SANN time series analysis generates a static feed forward MLP and all the dynamic information learned from the past memories of the output (feedback) path is discarded. The output (feedback) path is implemented using NARX neural networks (see section 4.2.3). For developing the final NARX models at both sites, the optimum architectural parameters of the number of hidden layer neurons with 3 neurons, the time lags of the input variables with d_u=14 hours for Wick and d_u=7 hours for Lerwick are used.

Figure 3.5 shows the NARX architecture for Wick and Lerwick with tansig and linear activation functions in the hidden and output layers, respectively. The development of each NARX model is implemented using the built-in Matlab Levenberg-Marquardt algorithm. The training for each model is repeated 30 times because of the random weight and bias initializations. The prediction results from the NARX models are "validated" in terms of correlation coefficient (CC), Root Mean Square of Error (RMSE), mean and standard deviation (σ) using the observed external surge in 1998 for Wick and Lerwick. The "validation" results from both NARX models at Wick and Lerwick are listed in Table 3.3. It is obvious from this table that the NARX model at Lerwick performs better than the other NARX model at Wick (lower RMSE and higher correlation for Lerwick). For the NARX model in Lerwick, the lowest RMSE is 0.06 m with correlation of 0.88, while it has an RMSE of 0.09 m and a correlation coefficient of 0.83 in Wick.

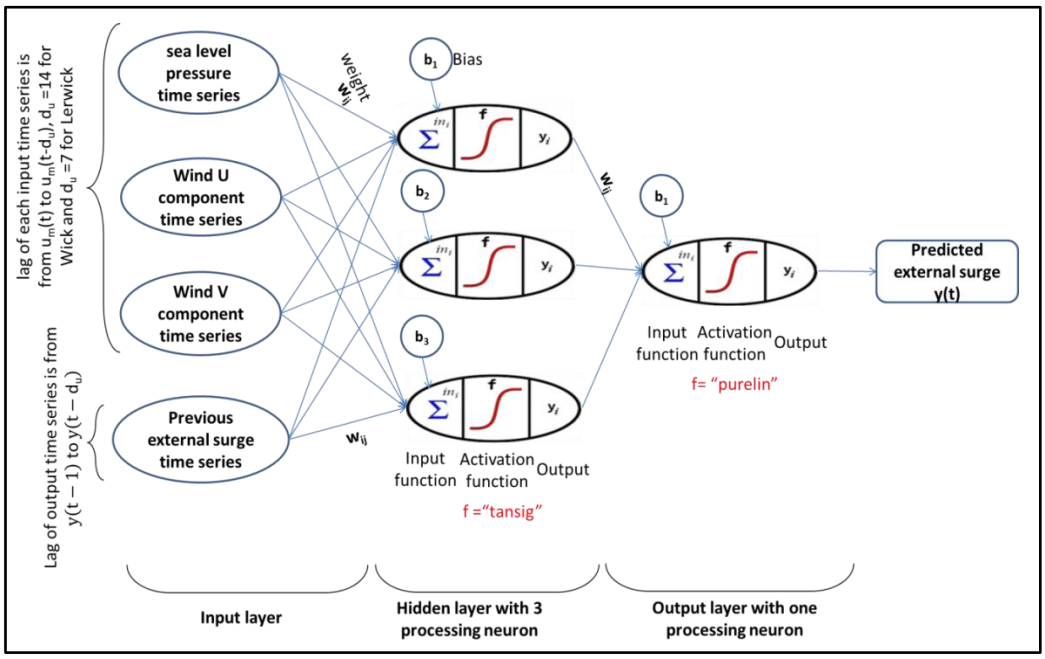

Figure 3.5: Schematic representation of NARX neural network with 3 input variables (see Table 3.2), tansig and linear activation functions in the hidden and output layers, respectively.

Table 3.3: Standard deviation (σ), Root Mean Square Error (RMSE) and correlation coefficient (CC) results for predicted external surge by NARX models at Wick and Lerwick over the whole year 1998.

Station / parameter	Wick		Lerwick	
	observed	**predicted**	**observed**	**predicted**
Mean (m)	0.03	0	0.03	0
RMSE (m)	0	0.09	0	0.06
Standard deviation σ (m)	0.15	0.12	0.12	0.11
Correlation coefficient CC	1	0.83	1	0.88

Figure 3.6 compares the temporal variations of the predicted external surge during January 1998 by each NARX model at Wick and Lerwick with the observed external surge. The NARX model in Lerwick shows a relatively good performance during this period, which might indicate about the more accurate prediction of input meteorological data by SN-REMO at Lerwick. Moreover, the extreme events predicted by both NARX models occurred at the time of observed external surge events. This provides an indication of the nonlinear capability of both NARX models in predicting external surge at both sites. On the other hand, the NARX models at both sites produce a smoothed nonlinear prediction of the external surge. It might be further enhanced, if the observed wind and SLP data at both sites are used instead of the predicted by SN-REMO. Moreover, the addition of the predicted external surge by surge-tide model (TELEMAC2D) covering the North Atlantic to the input deck might increase the prediction performance.

c) Astronomical tide at open-sea boundaries

The observed tides in the North Sea are a co-oscillating response to the tides generated in the North Atlantic Ocean (Banner, 2011). These co-oscillating tides are expressed by waves, which enter and exit the North Sea through the northern and western open boundaries with the North Atlantic Ocean (Figure 3.2). Therefore, the prediction of the boundary tidal level from 1970 to 2007 and during the future surge-tide realization between 2070 and 2100 are taken into account, when the tidal wave propagates from the open boundary up to the German coast. The complicated nature of tides in the North Sea area is mainly due to the complexity of the geometry and bathymetry for this shallow shelf sea. Regional North Sea models are often suffering from ill-posed open boundary forcing; this is the reason why the open boundary has to be shifted away from the shallow area (YU, 1993). This allows to reduce the number of tidal constituents in the open boundaries to the main tidal constituents only.

The tidal analysis begins by extracting the tidal constituents from the tidal level records. The basis for the harmonic analysis is the assumption that tidal variations can be represented by a number of harmonic constituents. It determines the amplitude and phase of the individual cosine curves (called tidal constituents), which are identified by their periods in mean solar hours. Finding the tidal harmonic constituents at each node location of an open boundary allows the prediction of tidal level at that boundary. An application of harmonic analysis is to

select the proper harmonic constituents to fit tidal level (η_t) at certain location according to Eq. (3.24) (Dronkers, 1964)

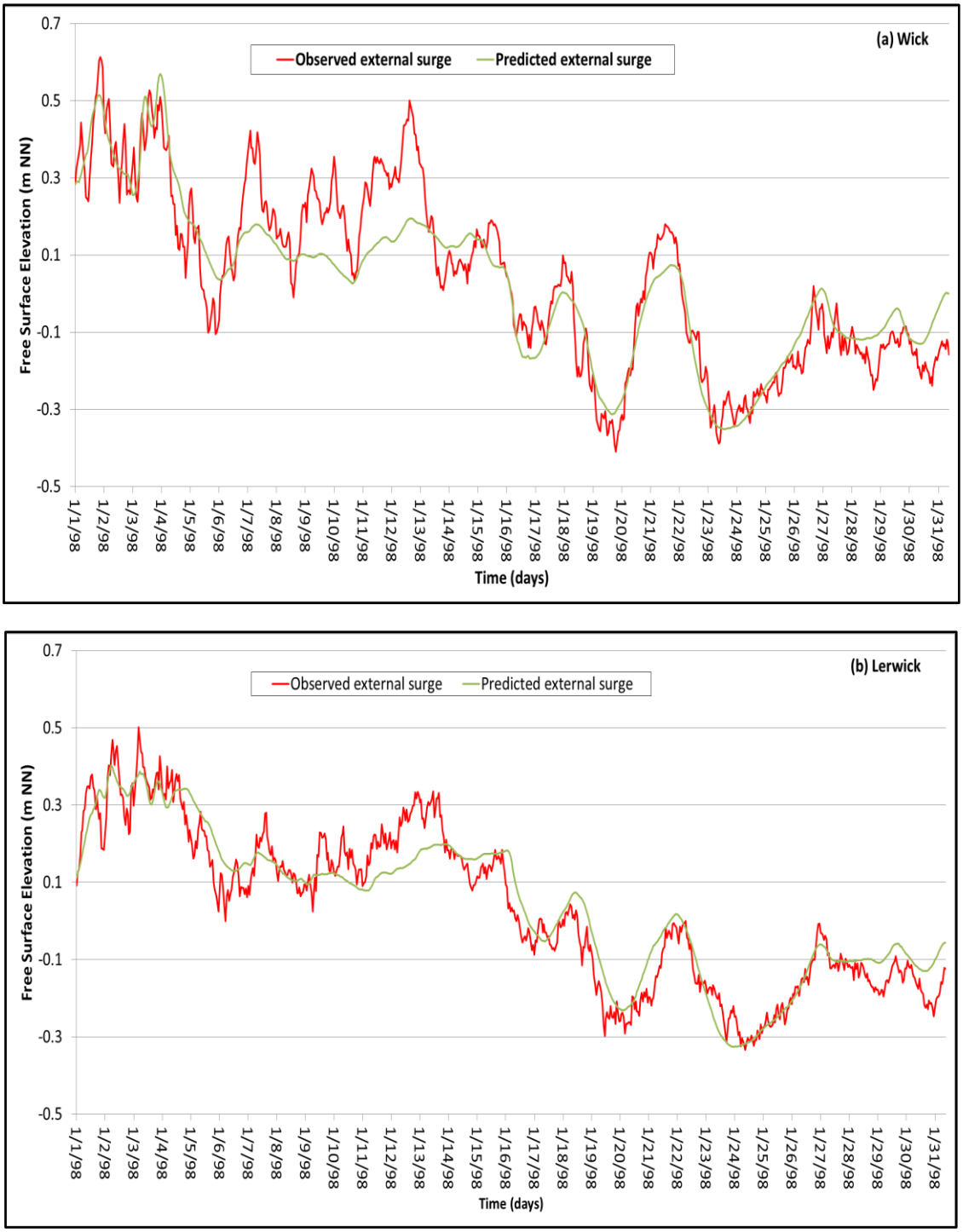

Figure 3.6: Comparison of the predicted external surge by NARX models during January 1998 at Wick (a) and Lerwick (b) with the observations at each site.

$$\eta_t = \sum_{n=1}^{N} f_n A_n \cos[\omega_n t - G_n + (V_n + u_n)] \quad (3.24)$$

where t is time, referred to 0 hour of Greenwich Mean Time (GMT); n is the index of the tidal constituent; A_n is the amplitude of the tidal constituent; f_n is the nodal factor of the tidal constituent; ω_n is the frequency of the tidal constituent; G_n is the phase lag of the tidal constituent behind the phase of the corresponding constituent at Greenwich; $(V_n + u_n)$ is the value of the equilibrium argument of the tidal constituent; V_n is the uniformly changing part of the constituent phase at the Greenwich Meridian; and u_n is the nodal adjustments of the tidal constituent (YU, 1993).

The tidal level at each node of the northern and western open-sea boundaries (78 nodes) needs to be prescribed for the North Sea model (Figure 3.2) taking into account the main eight tidal constituents (Q1, O1, P1, K1, N2, M2, S2, K2). At the open-sea boundaries, the tidal level records at each node in 2006 are kindly provided by BAW, which are predicted by BSH model covering the North Atlantic Ocean. For these nodes, the tidal level are predicted during the periods 1970-2007 and 2070-2100 using "Tidal Analysis Toolbox" (Pawlowicz et al., 2002) through the following two steps:

(i) For each node in the the northern and western open-sea boundaries, the harmonic constituents are calculated based on the tidal level in 2006 using the developed Matlab script "tidalanalysis.m" (Tayel & Oumeraci, 2012b).
(ii) The main harmonic constituents for each node that obtained in step (i) are used as input to predict the tidal level with the developed Matlab script "prepare.m" (Tayel & Oumeraci, 2012b). It makes a loop over all open-sea boundary nodes to generate the tidal levels every 15 minutes (see Figure 3.9). The modified TELEMAC2D subroutine SL.f, which is provided by BAW, is used during the simulation to read the data.

d) River discharge

The water levels in the estuaries of the German rivers Ems, Weser and Elbe may be affected by variations in their discharge and changes of the tidal dynamics in the North Sea. The daily fresh water discharges of the four main rivers (Westerschelde, Ems, Weser, and Elbe) in the southern North Sea from 1960 to 2007 are kindly supplied by BAW. The rivers discharge data are temporally interpolated every 15 minutes in order to be synchronized with the predicted tidal level.

3.2.3 Tidal simulation for the North Sea using TELEMAC2D

The tidal oscillation in the North Sea, which is regular and deterministically predictable, is dominated by the semidiurnal lunar tide M2. The propagation of tidal waves into the North Sea basin is deformed due to friction, so that shallow water tides arise, especially in the sallow

southern part. In order to build the 2D-Hydrodynamic model of the North Sea area, the domain bathymetry and bottom friction have to be calibrated using real-tide prediction (based on observed water level measurements). The tidal simulation for the North Sea by TELEMAC2D in 2006 is validated with the real-tide at Cuxhaven, Sylt and Helgoland. The purpose from this tide case is to guide the setup of the real case with influence of meteorological forces and other boundary conditions for the North Sea model.

a) General Model Settings

- *Definition of domain geometry*

The definition of the North Sea domain geometry is based on the bathymetry data imported at the beginning of the mesh generation process in JANET (see section 3.2.1). The bathymetry mesh file used for the North Sea modelling is updated with the bathymetry data of 2006, which is based on HIPOCAS (Hindcast-simulations in cooperation with the GKSS) project (Plüß, 2004). Moreover, the modeled area is extended by shifting the northern open-sea boundary further away from the shallow part.

Both geometry and boundary condition files, which are generated during the mesh creation by JANET, are provided by BAW. These files are updated to reflect the natural conditions of the modelled area boundaries using FUDAA preprocessor (see Figure 3.2). The bathymetry mesh uses the coordinate system of Gauss-Kruger zone 3. In this case the Saint-Venant equations (Eq.(3.1) to Eq.(3.3)) are solved in a Cartesian coordinate system without running the computation in spherical coordinates.

- *Initial conditions*

The initial free surface elevation in the domain is considered as a constant; therefore the keyword INITIAL ELEVATION is set in the steering file to 0.60 m. Water depth h at each point is calculated as the difference between the bottom elevation and the free surface elevation in the domain; both of them are referred to Normal Null (NN).

- *Boundary conditions*

The definition of boundary sides and their physical characteristics have been established in the boundary condition file during the mesh generation process. The physical boundaries of the model domain can be either liquid or solid. Generally, an impermeable condition exists for the solid boundaries, which does not allow any discharge across the boundary. Liquid boundary conditions can be either imposed water level or discharge flow rate that varies over the time or constant.

For the North Sea, the time varying tidal level has been considered at the northern and western open-sea boundaries (see Figure 3.2). This was obtained by predicting the tidal level for these boundaries (see section 3.2.2(c)), and extracting the time series of tidal level at each node in the open-sea boundaries. Therefore, a liquid boundary file with imposed tidal level values of 2006 has been prescribed and generated (Tayel & Oumeraci, 2012b) to simulate the tidal dy-

namics in the North Sea model. A free liquid boundary condition is set for the horizontal velocity components (u, v). Moreover, the Thompson method are used for these boundaries in the steering file to avoid the numerical reflection problem due to the phase lag between the inner simulated tidal level and imposed tide at the boundaries. The rest of the points in the contour of the domain are considered as part of the solid boundary.

- *Friction law and Coriolis effect*

For the tidal simulation in the North Sea, the energy dissipation is controlled by the bottom friction. Therefore, a good estimation of the friction coefficient value will have a determinant effect on the performance of the predicted tide. The Chezy formula is chosen for bottom friction (see section 3.1.2(e)). The friction coefficient is usually considered as a function of the water depth for tidal simulations in large domains. The TELEMAC2D subroutine STRCHE.f (Tayel & Oumeraci, 2012b) is implemented to define a variable Chezy coefficient according to the following equations (Giardino & Monbaliu, 2003):

$$C_c = \begin{cases} 65 & \text{for } h<40 \text{ m} \\ 65+(h-40) & \text{for } h>40\text{m and } h<65\text{m} \\ 90 & \text{for } h>65\text{m} \end{cases} \quad (3.25)$$

When modelling large domains, it is necessary to take into account the effect of the Coriolis force on the moving masses. This is done by activating the logical keyword CORIOLIS inside the steering file. The components of the Coriolis force FU and FV in the momentum equations are thus

$$\begin{aligned} FU &= FCOR*u \\ FV &= -FCOR*v \end{aligned} \quad (3.26)$$

where $FCOR = 2\omega \sin(\lambda)$ (rad/s) is the Coriolis coefficient with $\omega = 7.27 * 10^{-5}$ rad/s being the angular velocity of the Earth and λ is the latitude (degree) The Coriolis coefficient for the North Sea model is set to $FCOR = 1.078*10^{-4}$(rad/s).

b) Flow model options for tidal simulation in 2006

The variables defined for graphic print outs are the east (u) and north (v) velocity components, the free surface elevation, and the water depth (h). The printout of the results for all variables are set at every hour to demonstrate the response of the system to the tide influence.

A simulation of the tide in 2006 is carried out, which is the same period for the time series of the tidal level imposed at the open-sea boundaries. The time step Δt in the flow model should satisfy the courant number criterion, thus Δt is kept constant to 60 seconds so that the maximum courant number remains below 7.

The constant viscosity option has been chosen for the modelling of the turbulence in the southern estuaries. The keyword "VELOCITY DIFFUSIVITY", which represents the overall viscosity coefficient (molecular & turbulent viscosity), has a definite effect on the extent and shape of the recirculation. Following the HIPOCAS project, the value of the viscosity coefficient is 0.1 m^2/s , which is defined inside the steering file, while the coefficient of viscosity for southern rivers estuaries of the North Sea is change in space using the subroutine " CORVIS.f" that is provided by BAW.

The mass balance is checked over the entire domain during the simulations. This option allows computing the flow through the boundaries of the domain (liquid or solid) and the relative error on mass-conservation for each time step. The method of characteristics and conservative scheme & SUPG are chosen to solve the advection step for the velocity components and the water depth, respectively. The accuracy required during the solution of the propagation step was kept as 1.10^{-4}.

c) Results of tidal simulations

The model trials with different Chezy's coefficients affect the tidal level results inside the German Bight. 22 different trials are implemented to get an acceptable compromise between the predicted and real-tidal levels. In these trials, the performance is determined using the correlation coefficient (CC), standard deviation (σ), Root Mean Square Error of time series (RMS_{ts}) and RMS error of turning points (RMS_{tp}) (Giardino & Monbaliu, 2003) as follow:

$$\mathrm{RMS_{ts}} = \left[\frac{1}{N}\sum_{1}^{N}[\xi_r(t_i) - \xi_m(t_i)]^2\right]^{1/2} \tag{3.27}$$

where N is the total number of measurements; ζ_r is the real-tidal level at at time t_i ; ζ_m is the modelled tide by TELEMAC2D at the same time t_i;

$$\mathrm{RMS_{tp}} = \left[\frac{1}{N_{(c,t)}}\sum_{1}^{N_{(c,t)}}\left[\xi_{(c,t)r} - \xi_{(c,t)m}\right]^2\right]^{1/2} \tag{3.28}$$

where $N_{(c,t)}$ is the total number of turning point values (crests and troughs), $\zeta_{(c,t)r}$ is the surface elevation of real-tide at crests or trough points, $\zeta_{(c,t)m}$ is the modelled tidal elevation at crest or trough points.

The best performance is obtained by dividing the North Sea model domain to 4 subdomains according to depth as follows:

$$C_c = \begin{cases} 70 & \text{for } h<20 \text{ m} \\ 65+(h-20) & \text{for } h>20\text{m and } h<40\text{m} \\ 60+(h-40) & \text{for } h>40\text{m and } h<65\text{m} \\ 85 & \text{for } h>65\text{m} \end{cases} \quad (3.29)$$

The real-tide data of Cuxhaven, Sylt and Helgoland stations are compared with the simulation output by TELEMAC2D (see Table 3.4). The real-tide data is based on harmonic analysis of observed water level in 2006 for each station. It is noticeable from Table 3.4 that the tide simulation by TELEMAC2D reproduces almost exactly the real-tide for the three stations in the German Bight. The correlation between real tide and predicted tide in each station reaches 0.99, while the $RMSE_{ts}$ ranges from 0.08 m at Cuxhaven (see Figure 3.7) to 0.11 at Helgoland.

Table 3.4: Tidal simulations using TELEMAC2D in 2006.

Station / parameter	Cuxhaven	Sylt	Helgoland
$RMSE_{ts}$ (m)	0.08	0.10	0.11
$RMSE_{tp}$ (m)	0.07	0.08	0.09
Correlation coefficient	0.99	0.99	0.99
Standard deviation σ for real-tide (m)	1.02	0.72	0.82
Standard deviation σ for predicted tide (m)	1.03	0.77	0.82

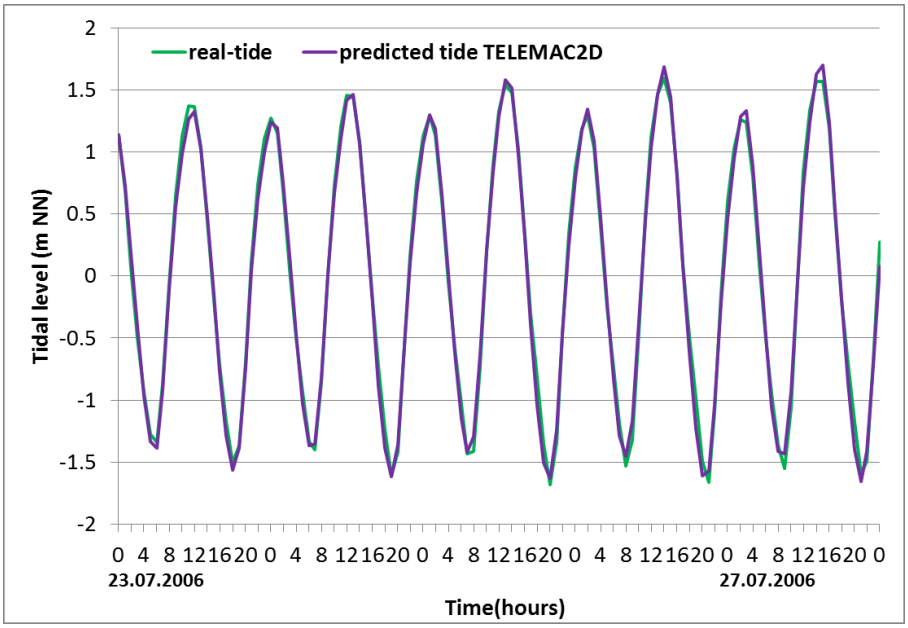

Figure 3.7: Comparison of tide simulation using TELEMAC2D and real-tide at Cuxhaven.

3.2.4 Surge-tide simulation for the North Sea using TELEMAC2D

The combination of tidal and meteorological conditions in interaction with the external surge is required for the evaluation of past (1970-2007) and future (2070-2100) surge-tide events in the North Sea. The emphasis of this section lies on the implementation of surge-tide simulation using TELEMAC2D by taking into account the diverse physical processes that may affect the surge-tide. Therefore, the tidal simulation in the previous section 3.2.3 builds the basis for surge-tide modelling after defining the friction coefficient value according to water depth in 4 subdomains of the North Sea (see Eq. (3.29)). Only the boundary conditions should be updated to include the external surge and the southern rivers discharge in addition of considering wind and pressure.

a) General Model Settings

The setup of the geometry mesh, initial conditions, friction law, Coriolis force and control options for the flow model in the tide case (see section 3.2.3) are used for the surge-tide simulation in 2006 by TELEMAC2D.

- *Boundary conditions*

For the surge-tide simulations by TELEMAC2D $\eta_{su\text{-}t\ TEL}$, the boundary conditions of the North Sea model are prescribed using all extreme storm-tide components (see Figure 2.15). These boundary conditions are shown in Figure 3.8.

On the northern open sea boundary, the tidal level on each node and the external surge either from Wick or Lerwick stations are linearly added.

On the western boundary (West border: France-England) only the tidal water level is prescribed at each node. So, the influence of the shallow water can be taken into account when the tidal wave plus external surge propagate from the open boundary up to the German coast. The Thompson method is used for open-sea boundaries in the steering file to avoid numerical reflection problems due to the phase lag between the inner simulated water level and the imposed water level at the boundaries.

On the southern onshore edge of the estuaries the fresh water discharge of the adjacent rivers are prescribed at each river section.

For the North Sea, the time varying tidal level and external surge are considered at the northern open-sea boundary (see Figure 3.8), while at the western boundary only tide is taken into account. These were obtained by predicting the tidal level and external surge (see tion 3.2.2), and extracting the time series of the tidal level at each node at the open-sea boundaries with the external surge time series from Wick and Lerwick added to the northern boundary only. Therefore, a liquid boundary file with the imposed water level values of 2006 are prescribed and generated including rivers discharge time series (Figure 3.9). A free liquid boundary condition is set for the horizontal velocity components (u, v).

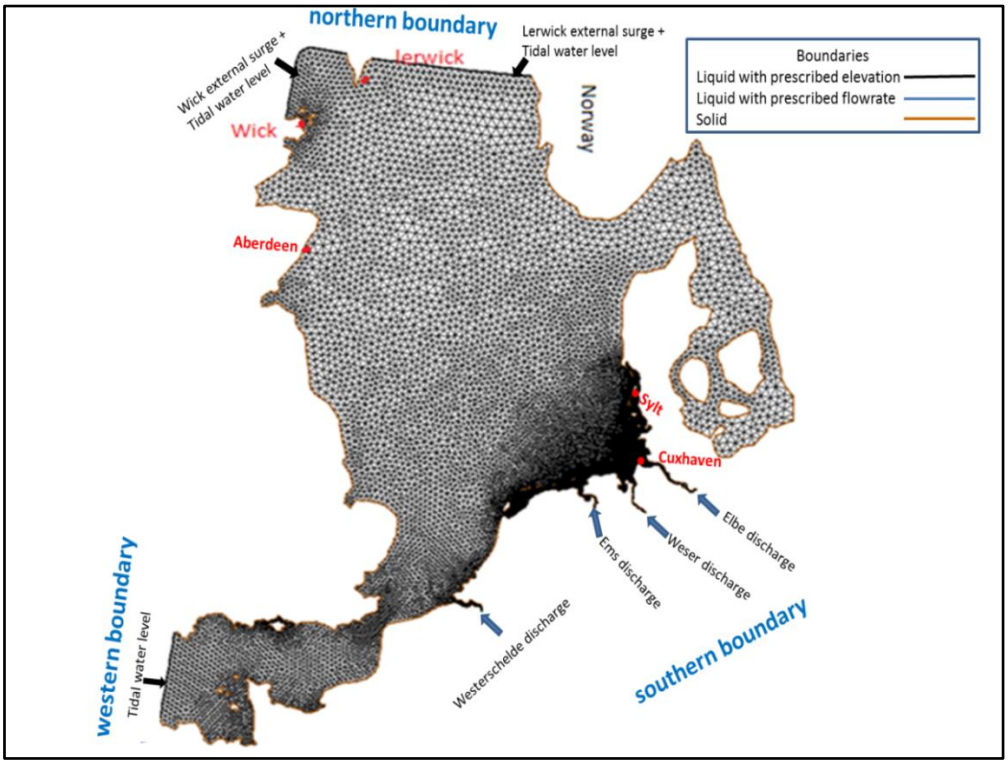

Figure 3.8: Boundary conditions of the North Sea mesh in TELEMAC2D with water level prescribed at the open-sea and with flow rate of fresh water discharge prescribed at southern boundary.

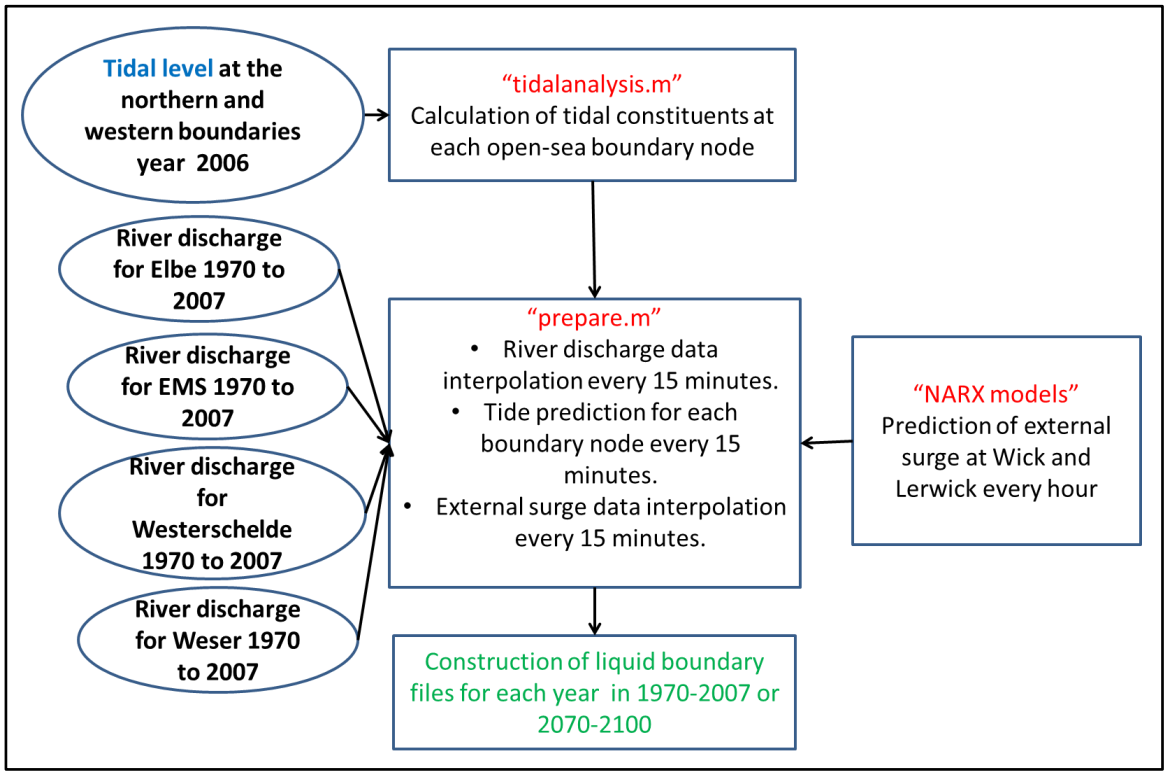

Figure 3.9: Construction of liquid boundary files data for surge-tide simulations including external surge, tide and river discharges.

- *Wind and atmospheric pressure setups*

The influence of a wind blowing on the water surface can be taken into account by TELEMAC2D through adding to the right hand side of Eqs. (3.2) and (3.3) a forcing term due to wind, S_{wx} and $S_{wy,}$ (m/s^2) as follows (Giardino & Monbaliu, 2003):

$$S_{wx}= \frac{1}{h}\frac{\rho_{air}}{\rho} a_{wind} u_{wind} \sqrt{u_{wind}^2+v_{wind}^2} \tag{3.30}$$

$$S_{wy}= \frac{1}{h}\frac{\rho_{air}}{\rho} a_{wind} v_{wind} \sqrt{u_{wind}^2+v_{wind}^2} \tag{3.31}$$

where ρ_{air} and ρ are the air and water densities (kg/m^3), respectively. a_{wind} is a dimensionless quantity represented by the drag coefficient.

The logical keyword WIND inside the steering file determines whether this influence is to be taken into account. If so, the coefficient $(\rho_{air}/\rho)\, a_{wind}$ is then provided with the keyword COEFFICIENT OF WIND INFLUENCE. This coefficient can be calculated as a function of wind-velocity. The subroutine PROSOU.f is modified (Tayel & Oumeraci, 2012b) to define a_{wind} according to the formula used by the Institute of Oceanographic Sciences (United Kingdom):

$$\begin{cases} \text{for } |\vec{u}_{wind}|<5\ m/s & a_{wind}=0.565.10^{-3} \\ \text{for} 5< |\vec{u}_{wind}|<19.22\ m/s & a_{wind}=(-0.12+0.137|\vec{u}_{wind}|).10^{-3} \\ \text{for } |\vec{u}_{wind}|<19.22\ m/s & a_{wind}=2.513.10^{-3} \end{cases} \tag{3.32}$$

Atmospheric pressure is taken into account by setting the keyword AIR PRESSURE to true. When the atmospheric pressure P_a (unit: Pascal = kg m^{-1} s^{-2}) is considered, TELEMAC2D simply adds to the right side of the momentum equation the term S_p (m/s^2).

$$S_p=-\frac{1}{\rho h}\overrightarrow{grad}(P_a) \tag{3.33}$$

For surge-tide simulations in the North Sea, the size of the domain and the simulation duration requires that wind velocity and sea level Pressure (SLP) are used, which vary in space and time. Therefore, the two subroutines PREWIND.f and Meteo.f have been used to interpolate wind velocity components and SLP fields in space and time over the entire computational mesh (see section 3.2.2(a))

b) Results of surge-tide simulations

The observed extreme water level in the German bight at Cuxhaven and Sylt during the storm of November 2006 is compared with the surge-tide predicted for the same storm by TELEMAC2D (see Figure 3.10 and Figure 3.11). This storm is a typical low-pressure area (p_a < 100000 Pascal) moving from west to east across the central North Sea and associated with strong onshore winds causing a strong surge. The mean wind speed during this storm is 17 m/s, and the mean wind direction is 300°. The meteorological characteristics at Cuxhaven during the storm of November 2006 differ slightly from those at Sylt. This storm occurred in conjunction with a neap tide in Cuxhaven and Sylt, while the observed external surge at Wick is much less important. Since the external surge propagates from Wick to Cuxhaven and Sylt, its effect on the two sites occurs after the time of its maximum at Wick. The effects of wave setup and river discharge on the water level during this storm are almost negligible (see section 3.2.5(d)), especially for relatively low waves and small river discharges.

Figure 3.10 and Figure 3.11 show the temporal variations of the meteorological conditions for Cuxhaven and Sylt respectively during the storm of November 2006. These variables as prescribed in Table 4.3 are the two wind speed components and sea level pressure, tides, significant wave heights, external surges, Elbe river discharge (for Cuxhaven only), $\eta_{su\text{-}t\ TEL}$ and the observed storm-tide at the two pilot sites Cuxhaven and Sylt. The two wind speed components and sea level pressure are the interpolated values at Cuxhaven and Sylt which are extracted from the RCM SN-REMO. Furthermore, the Elbe river discharge at Neu Darchau and the external surges at Wick were extracted from the recorded measurements. The tides at the selected sites were calculated using the harmonic analysis of the observed water level. Only the significant wave height (H_s) and the $\eta_{su\text{-}t\ TEL}$ were simulated by the wave propagation model TOMAWAC and the hydrodynamic model TELEMAC2D respectively under the effect of the meteorological force of SN-REMO. The observed water level at the two pilot sites η_{OB} contains all of the components and implicitly their nonlinear interaction (η_{NL}). The highest η_{OB} peaks during the storm of January 2006 at Cuxhaven and Sylt, which reach 3.81 m and 2.21 m respectively, overestimate those calculated by $\eta_{su\text{-}t\ TEL}$ of 2.97 m and 2.09 m respectively. Moreover, the approximation of the nonlinear interaction between the components by TELEMAC2D η_{NLT} , which approximates the nonlinear interaction, shifts in the arrival time of highest $\eta_{su\text{-}t\ TEL}$ peak of 2.23 m by -9 hours at Sylt (see Figure 3.11).

Figure 3.12 shows the difference between the predicted storm-tide by $\eta_{su\text{-}t\ TEL}$ and the linear storm-tide (η_L), which is the linear superposition of storm surge, tide, external surge, wave setup and rivers effect that are simulated individually by TELEMAC, as the approximated nonlinear interaction by TELEMAC2D (η_{NLT}) during the storm of November 2006 at Cuxhaven and Sylt. Furthermore, the difference between the η_{OB} and $\eta_{su\text{-}t\ TEL}$, which complements the η_{NLT} (η_{NLE}), is calculated. The η_L peaks, which occur directly before the time of maximum observed storm-tide ($(\eta_{OB})_{max}$) at both sites, overestimate both the η_{OB} and $\eta_{su\text{-}t\ TEL}$peaks. The approximated nonlinear interaction η_{NLT}, which is considered by $\eta_{su\text{-}t\ TEL}$,

decreases the η_L peak at both sites by -0.18 m. This coincides with more decrease by the η_{NLE} of -0.36 m at Cuxhaven and -0.44 m at Sylt. Therefore, the small decrease by η_{NLT} does not affect strongly the mean water level (MWL) of $\eta_{su\text{-}t\ TEL}$ and the following peaks will propagate under less pronounced shoaling effect than the η_{OB} peak, which increases the height of $(\eta_{OB})_{max}$ and delays its arrival time more than $\eta_{su\text{-}t\ TEL}$ peak. For example the $(\eta_{OB})_{max}$ is delayed by 2 hours than $\eta_{su\text{-}t\ TEL}$ peak at Sylt.

Some statistical parameters have been calculated in order to compare the simulated and measured values of free surface elevation at Cuxhaven and Sylt in 2006. The different statistical parameters are presented in Table 3.5. The performance values at Sylt are better than those at Cuxhaven, which might be the better prediction of meteorological conditions by SN-REMO at open coast (e.g. Sylt) than near land (e.g. Cuxhaven). The standard deviation of $\eta_{su\text{-}t\ TEL}$ at Sylt, which is 0.69 m, is representative of the η_{OB}, meanwhile the correlation coefficient is almost equal to its value at Cuxhaven of 0.96.

Table 3.5: Statistical parameters calculated at Cuxhaven and Sylt between simulated and measured values in 2006 of free surface elevation.

Station / parameter	Cuxhaven		Sylt	
	observed	**predicted**	**observed**	**predicted**
Mean (m)	0.13	0.16	0.07	0.11
RMSE (m)	0	0.29	0	0.20
Standard deviation σ (m)	1.10	0.97	0.71	0.69
Correlation coefficient CC	1	0.97	1	0.96

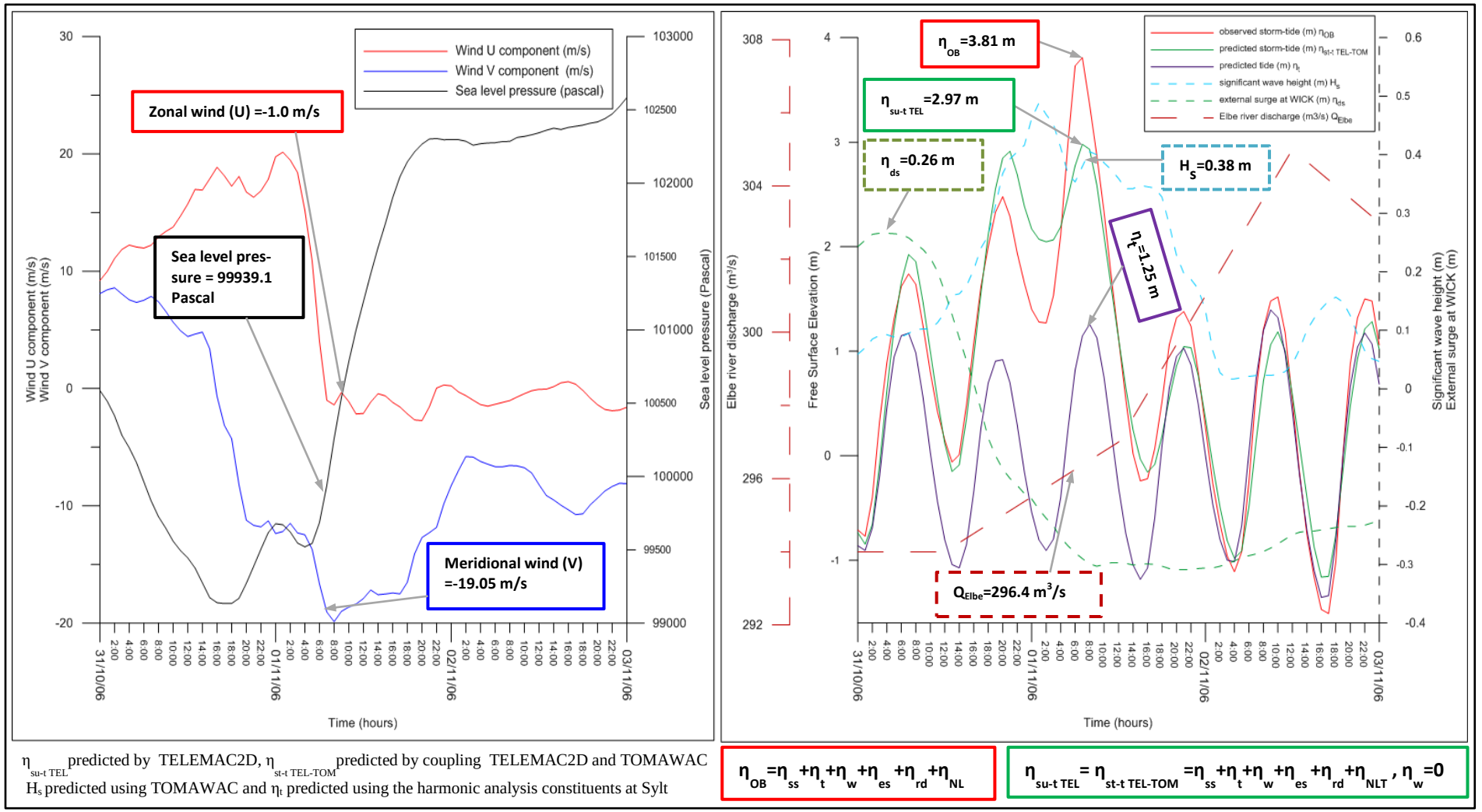

Figure 3.10: Storm characteristics, predicted surge-tide by TELEMAC2D and the extreme of observed water level during the storm of November 2006 at Cuxhaven.

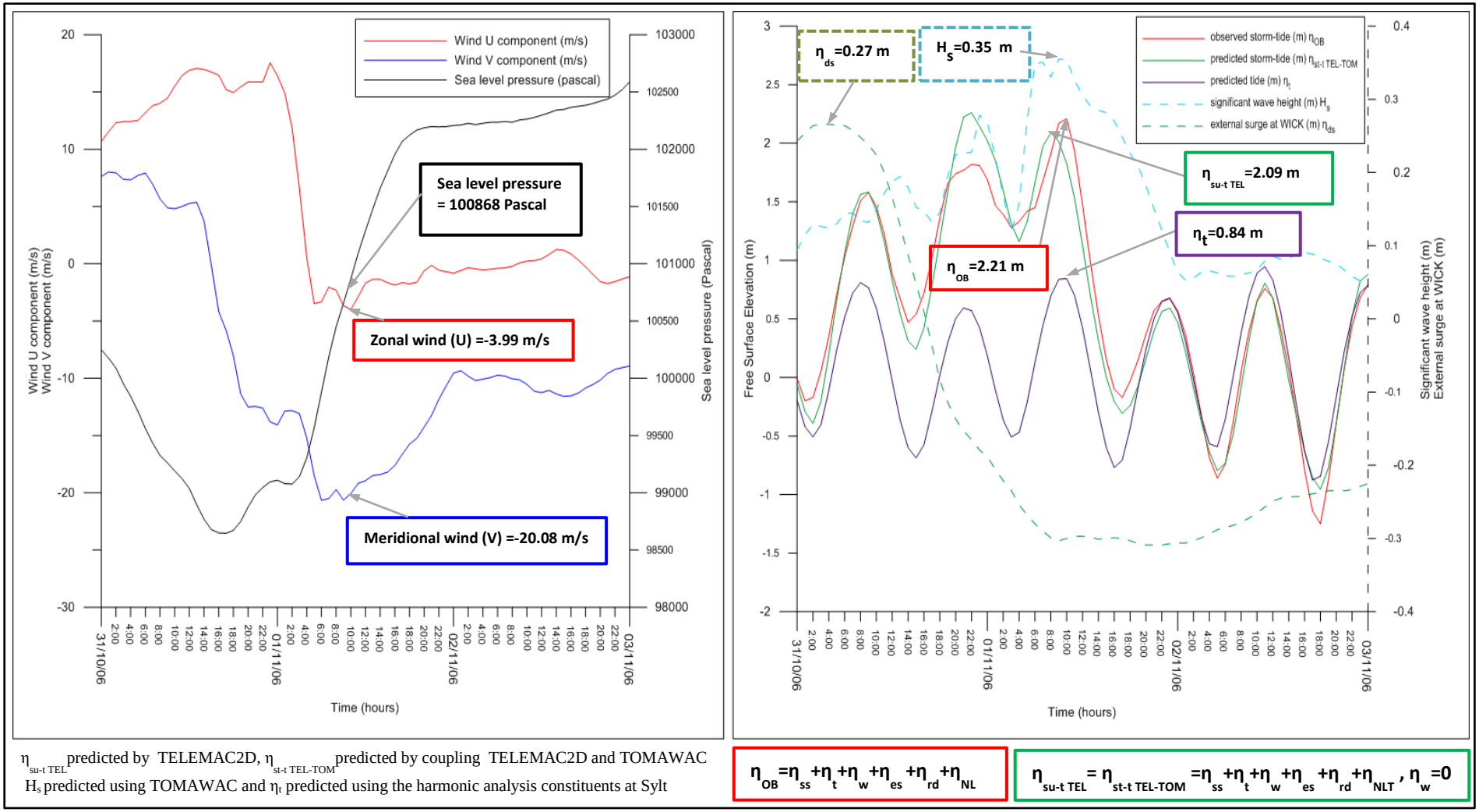

Figure 3.11: Storm characteristics, predicted surge-tide by TELEMAC2D and observed water levels during the storm of November 2006 at Sylt.

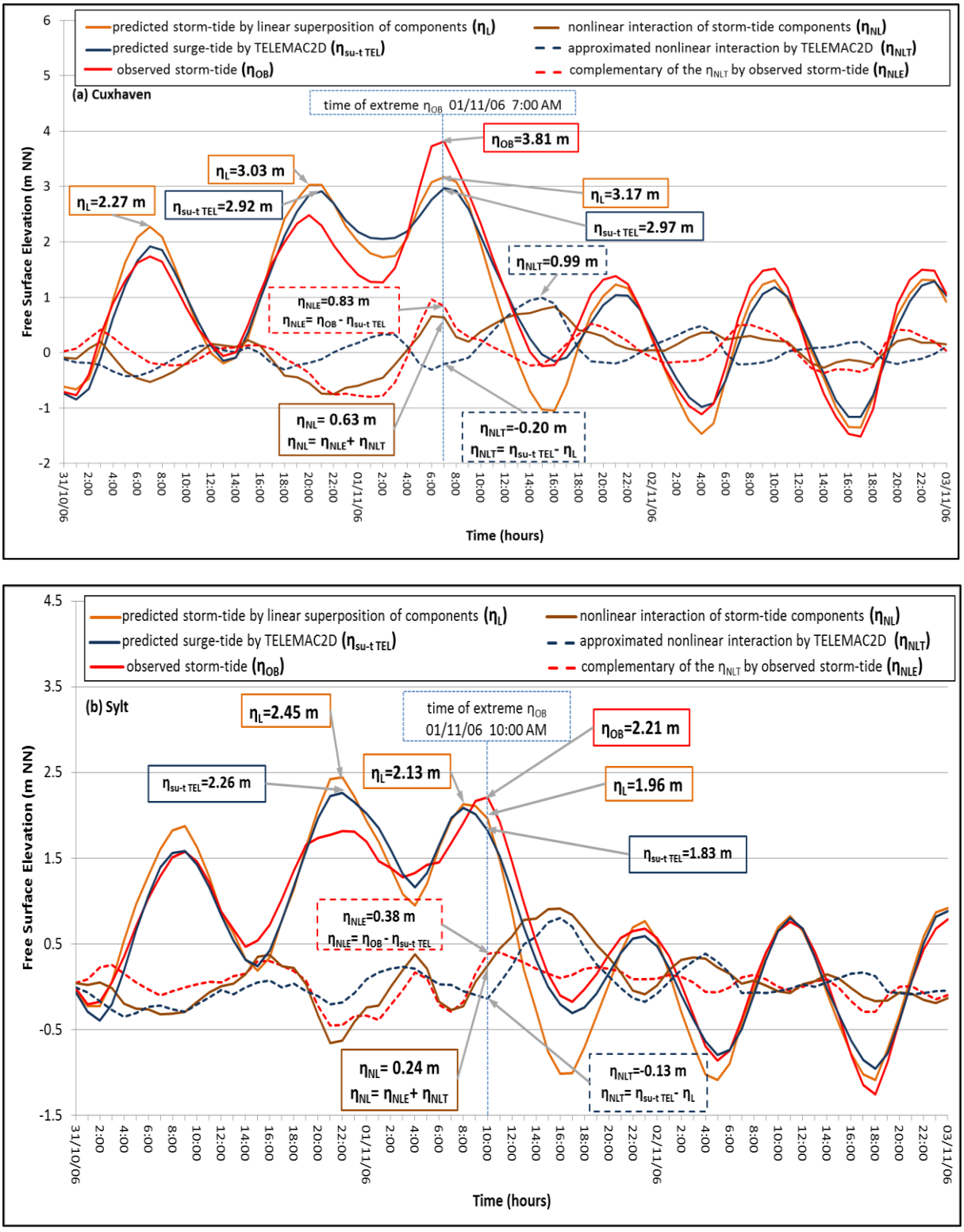

Figure 3.12: Storm-tide prediction by linear superposition η_L and TELEMAC2D $\eta_{su\text{-}t\ TEL}$ along with the observed storm-tide η_{OB} with the effect of nonlinear interaction η_{NL} between extreme storm-tide components during the storm of November 2006 at Cuxhaven (a) and Sylt (b).

3.2.5 Wave propagation for the North Sea using TOMAWAC

In order to study the nearshore wave field in the German Bight and its effect on surge-tide, the non-steady wave propagation over the North Sea model is performed with TOMAWAC. The wave evolution by TOMAWAC includes the deep and shallow water source/sink terms of wave energy, which are described by Eq. (3.12). The setup of geometry mesh, initial conditions and the boundary conditions file for the surge-tide simulation by TELEMAC2D are used by TOMAWAC for the simulation of wave propagation. The significant wave height, the mean period and the mean direction of wave propagation are assessed using the observed data at Sylt in 1998.

a) General Model Settings

The setups of geometry mesh, initial conditions and boundary conditions file for the flow model in the tide case (see section 3.2.3) are used for the wave propagation simulation by TOMAWAC.

- *Boundary conditions*

The boundary conditions, which are prescribed for the surge-tide simulation by TELEMAC2D ($\eta_{su\text{-}t\ TEL}$), are defined inside the boundary condition file during the generation of the bathymetry mesh. This file is used to define the boundary conditions for wave propagation using TOMAWAC, which are shown in Figure 3.13. On the northern open sea boundary, the zero spectrum wave energy is prescribed, since this boundary is shifted away from the shallow part of the North Sea and the swell effect can be generated by wind over the deeper part. So, the influence of wave energy source/sink terms in deep and shallow waters should be taken into account when the waves propagate from the open boundary up to the German coast. On the southern onshore edge of the estuaries the free liquid boundary condition is applied in order to propagate the waves outside the domain without any wave energy entering through it.

- *Wind-driven wave generation (S_{in})*

For wave propagation in the North Sea, the size of the domain and the simulation duration requires the use of wind velocity, which varies in space and time. Therefore, the subroutine PREWINDonly.f is used to convert the interpolated wind velocity components on the computational mesh by the Matlab script "convert.m" to Serafin format (see section 3.2.2(a)). While the temporal interpolation at each time step is performed automatically by TOMAWAC after setting the keyword STATIONARY WIND =false inside the steering file.

The wind input, S_{in}, is based on Janssen's quasi-linear model for wind-wave generation (Janssen, 1989), and implemented like in WAM Cycle 4. This model represents the exponential growth part, while a linear growth model can also be additionally used through setting the keyword LINEAR WAVE GROWTH=1. It must be noted that the dissipated energy when the wind blocks the waves is not considered by TOMAWAC

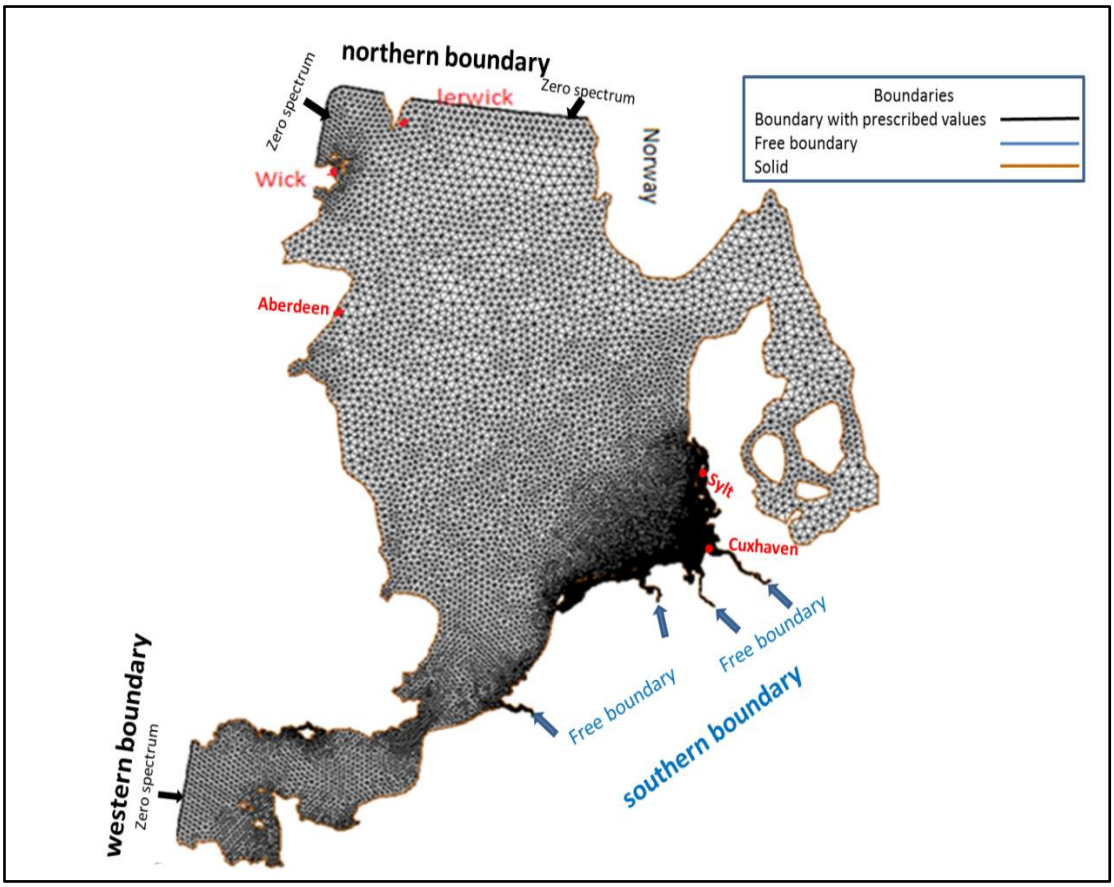

Figure 3.13: Boundary conditions of the North Sea mesh inside TOMAWAC with the prescribed zero spectrum at open-sea boundaries and free liquid boundary in the south.

b) Model options for wave propagation

The simulation of wave propagation in 1998 is carried out over the North Sea mesh. The selected time step Δt should satisfy the courant number criterion, thus Δt is kept constant to 600 seconds so that the maximum courant number remains below 7. The variables defined for graphic print outs are the significant wave height (H_{m0}), the mean wave period (T_{mean}), and the mean wave direction (D_{mean}) as well as the two wave force components (F_x,F_y) contributing to the wave-induced momentum. The printout of the results for all variables is set for every hour. A logarithmic frequency discretization with 25 frequencies is used. The minimum discrete frequency is f_1 = 0.04 Hz and the ratio between two successive frequencies is set to qr = 1.115. The number of discrete directions is set to 16.

The source functions on the right side of Eq. (3.12) represent diverse physical processes in deep and shallow waters in addition to the wave generation by wind. The non-linear energy transfer, S_{nl}, through the four-wave interaction is in deeper water represented by the DIA model proposed by Hasselmann et al. (1985), while the non-linear triad interactions, S_{tr}, in shallow water is modeled using the LTA model proposed by Eldeberky & Battjes (1995). The

source function describing the dissipation due to white capping, S_{ds}, is based on the theory of Komen et al., (1984) and the dissipation model of Janssen, (1991). The rate of dissipation, S_{bf}, due to bottom friction is not taken into account, since the observed wave parameters are outside the surf zone and the computation stops at water depth of 10 m. Depth-induced wave breaking occurs when waves propagate into shallower areas. The formulation of the source term, S_{br} , due to wave breaking is based on the breaking model by Battjes and Janssen (1978).

c) Results from the simulation of wave propagation

The comparison of observed wave parameters with numerical results requires the acquisition of extensive data in order to cover the large domain of spatial and temporal evolutions in the German Bight. Here, field measurements from 1998 are available with a good resolution for significant wave height (H_s), mean wave period (T_m) and mean wave direction (D_m) at Sylt. The data were averaged at regular period of 4 hours without gaps. In order to study the near-shore wave field, the observed parameters at Sylt are compared with the predicted values by TOMAWAC under non-steady wind fields obtained from RCM SN-REMO over the North Sea mesh. Table 3.6 summarizes the model performance statistics for the significant height, the mean period and the direction of the waves. The scatter index (SI) is a standard metric for wave model inter-comparison (Clancy et al., 1986). Lower values of the SI are indications of a better forecast. For significant wave height, SI in the literature ranges between 20% for hindcasts with sophisticated models and high quality wind fields and to 60% for some operational forecasts with less accurate winds (Clancy et al., 1986; Janssen et al., 1984). Regarding the calculated significant wave height in 1998 at Sylt, SI is 48%, which is considered as a good performance due to the use of the RCM SN-REMO wind field with a resolution of 50 km. The best prediction by TOMAWAC is obtained for the mean wave direction, in which the SI error reduces to 5% and the correlation is 0.93. Moreover, the calculated mean wave period well reproduces the observed values, since SI is 19% and the correlation coefficient is 0.82.

Table 3.6: Performance of TOMAWAC for hindcasting the significant height, the mean period and the mean direction of the waves at Sylt over the whole year 1998.

Station / **parameter**	**Sylt**					
	Significant wave height (m)		**Mean wave period (second)**		**Mean wave direction (degree North=0°)**	
	observed	**predicted**	**observed**	**predicted**	**observed**	**predicted**
Mean	1.07	1.25	5.09	4.72	274.4	270.77
RMSE	0	0.52	0	1	0	14.66
Scatter Index= $\frac{\text{RMSE}}{\text{Mean observation}} * 100\%$	0%	48%	0%	19%	0%	5%
Standard deviation σ	0.64	0.74	0.85	0.96	33.9	38.42
Correlation coefficient	1	0.72	1	0.82	1	0.93

Figure 3.14 shows the predicted and observed values of significant wave height, mean wave period and mean wave direction during January 1998 at Sylt. It is noticeable that the significant wave height and the mean wave period are less well-predicted than the mean wave direction, which is due to the coarse resolution of wind field by the RCM SN-REMO. The maximum H_s reaches 4.44 m in January 4, 1998, while the predicted value is only 3.13 m. This affects also the prediction of the mean wave period, which is underestimated at the time of maximum H_s and reaches 6.7 s instead of 8.5s observed in January 4, 1998. The performance might be further enhanced if finer resolution meteorological data of the RCM SN-REMO is available.

d) Coupling of wave propagation and surge-tide simulations

AS both TELEMAC2D and TOMAWAC models are parts of the TELEMAC system, they share the same geometry and boundary conditions files to run the simulations. Therefore, the wave model TOMAWAC can be coupled with the flow model TELEMAC2D. The coupling is applied using the following four keywords inside the steering file of TELEMAC2D:

- COUPLING WITH, to which the value 'TOMAWAC' must be assigned.
- WAVE DRIVEN CURRENT must be set to 1.
- TOMAWAC STEERING FILE, which specifies the name of the TOMAWAC steering file.
- COUPLING PERIOD FOR TOMAWAC, which specifies every how many TELEMAC2D time steps TOMAWAC is called.

In case of direct coupling, TELEMAC2D is the main programme and calls the TOMAWAC subroutine WAC.f, which is the main subroutine of TOMAWAC and solves the governing equation for the generation and propagation of the directional wave spectrum (Benoit, 2011).

TELEMAC2D transfers to TOMAWAC the updated values of flow field and water depths, while TOMAWAC calculates the wave characteristics accordingly to those values and returns to TELEM-AC2D the updated values of the wave driving forces (F_x,F_y) acting on the surge-tide. The effect of waves on the surge-tide at Cuxhaven and Sylt is assessed during the the storms of January 2000, November 2006 (see Figure 3.10 and Figure 3.11) and November 2007 (called Tilo, see Figure 3.15). The surge-tide simulations during these storms over the North Sea area by TELEMAC2D were coupled with the wave simulations by TOMAWAC. The wave setup (η_w) is the difference between the coupled storm-tide results ($\eta_{\text{st-t TEL-TOM}}$) and the simulated surge-tide by TELEMAC2D alone ($\eta_{\text{su-t TEL}}$). It is noticeable that, the wave setup does not exceed 10 cm (Figure 3.15) during the storm of November 2007 (due to the long duration of westerly winds (see Table 4.3) and has no effect in the storms of January 2000 and November 2006. So, the wave setup has approximately no contribution to the water level at both interesting sites, because the source of the momentum flux to the water column is limited to the white capping-induced energy dissipation outside the surf zone with depth greater than 20 m.

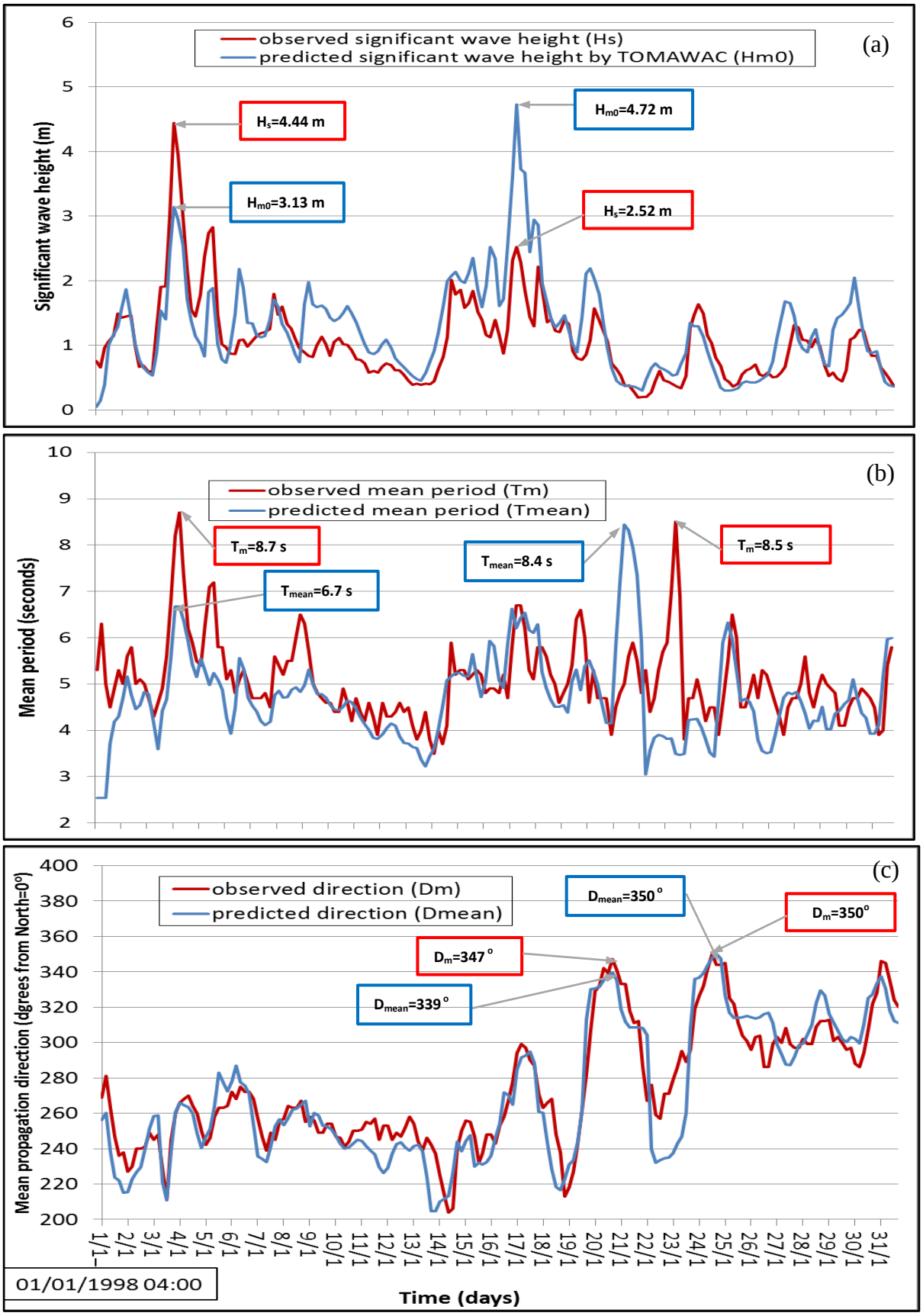

Figure 3.14: prediction of significant wave height (a), mean period (b) and mean propagation direction (c) during January 1998 at Sylt.

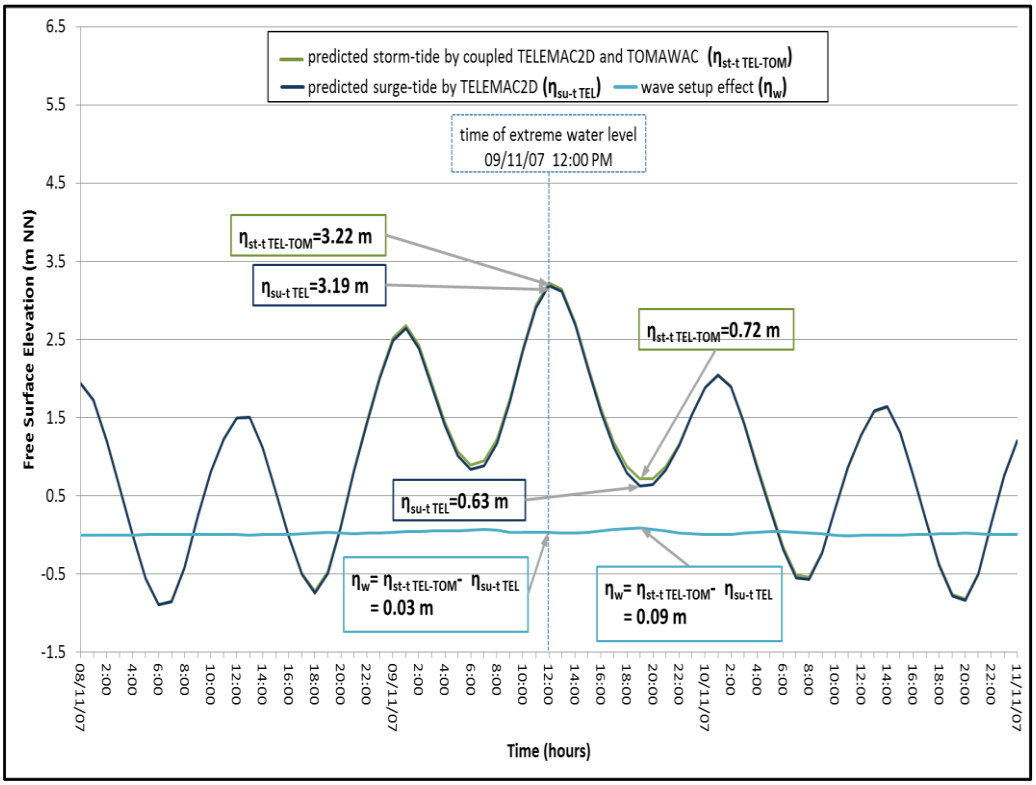

Figure 3.15: Effect of wave setup on the water level during the storm of November 2007 (Tilo) at Cuxhaven.

The tidal oscillation in the North Sea is regular and deterministically predictable. The tidal simulation is performed using TELEMAC2D in order to define the Chezy friction coefficient as a function of the water depth. Therefore, the results of the tidal simulation serves as a basis for the modelling of the surge-tide after defining the friction coefficient value according to water depth in 4 subdomains of the North Sea (see Eq. (3.29)).. The predicted tide from 2006 by TELEMAC2D is validated with the real-tide at Cuxhaven, Sylt and Helgoland. The predicted tide reproduces almost exactly the tide measured at the three aforementioned stations in the German Bight. The correlation coefficient between measured and predicted tide at the three stations reaches 0.99, while the RMSEts ranges from 0.08 m at Cuxhaven (see Figure 3.7) to 0.11 at Helgoland.

The implementation of the surge-tide simulation using TELEMAC2D is carried out taking into account the meteorological and tidal forces in addition to the effects of the Atlantic external surge and the southern rivers discharge at the boundaries (see Figure 3.8). Two external surge NARX models are developed for Wick and Lerwick, which are used to fill the gaps in the observed external surge data between 1970 and 2007. Moreover, these NARX models will also be used to predict the external surge for future surge-tide realization 2070-2100 (see chapter 5). The input deck of the two NARX models consists of the wind and pressure data that are extracted from the regional climate model RCM SN-REMO wind fields and pressure fields (SLP) at Wick and Lerwick. For the NARX model in Lerwick, the lowest RMSE is 0.06 m with a correlation coefficient of 0.88, while an RMSE of 0.09 m and a correlation coeffi-

cient of 0.83 are obtained for the NARX model in Wick. The performance of the two NARX models is relatively good, which might be enhanced if the observed wind and SLP are used in the input deck instead of the predicted by SN-REMO.

The prediction performance of both NARX models can also be enhanced by adding to their input the external surge predicted by the surge-tide model (TELEMAC2D) covering the North Atlantic. On the southern boundary of the North Sea model, the daily fresh water discharges of the four main rivers (Westerschelde, Ems, Weser, and Elbe) are temporally interpolated every 15 minutes in order to achieve a better synchronization with the tidal level data. although the effect of rivers discharge on the water level in the German Bight is almost negligible, especially for small river discharge values, river discharge samples at every hour are more adequate for surge-tide modelling as its contribution increase with smaller distance to tidal border of the river.

The simulated and observed values of the 2006 surge-tide at Cuxhaven and Sylt are comparatively analyzed using three performance parameters (standard deviation σ, Root Mean Square Error RMSE and correlation coefficient (CC) as presented in Table 3.5. The performance parameters at Sylt are better than those at Cuxhaven. The standard deviation of the surge-tide $\eta_{su\text{-}t\ TEL}$ predicted by TELEMAC2D at Sylt with σ =0.69 m, is representative of the observed values η_{OB}, meanwhile the correlation coefficient is approximately 0.96 at both sites. The extreme values of the observed water level η_{OB}at both sites during the storm of November 2006 is larger than the predicted $\eta_{su\text{-}t\ TEL}$ values. The difference is assumed to be due to the approximation of the nonlinear interaction between the components of the surge-tide by TELEMAC2D (η_{NLT}) that may additionally shift the arrival time of the extreme peak of $\eta_{su\text{-}t\ TEL}$.

The combination of tidal and storm surge in interaction with the external surge is required for the evaluation of past (1970-2007) and future (2070-2100) surge-tide events in the North Sea. The simulation time for one year using TELEMAC2D is 8 hours (parallel processing on 8 cores processor of computer "erebos1" kindly made available by BAW), so it takes totally one week for the 30 years (1970 to 2000 or 2070 to 2100). Therefore, TELEMAC2D provides a powerful and computationally efficient tool that can be part of an operational modelling system for storm-tide prediction.

In order to study the nearshore wave field in the German Bight and its possible effect on surge-tide, the modelling of the non-steady wave propagation over the North Sea model is performed with TOMAWAC, which is part of the entire TELEMAC model system. The setup of the input files (the geometry mesh, the initial conditions and the boundary conditions) for the flow model TELEMAC2D in the surge-tide case are also used for the wave model TOMAWAC. The prediction performance for the significant wave height (in 1998) at Sylt is characterized by Scatter Index SI = 48% and CC=0.72) . It is considered as a good performance despite the use of the RCM SN-REMO wind field with resolution of 50 km. The best prediction by TOMAWAC is obtained for the mean wave direction (SI =5% and CC= 0.93) followed by mean wave period (SI =19% and CC= 0.82). The performance might be enhanced if finer resolution meteorological data of the RCM SN-REMO were available (Clancy et al.,

1986; Janssen et al., 1984). The wave setup (η_w) is the difference between the coupled storm-tide results ($\eta_{st\text{-}t\ TEL\text{-}TOM}$) and the simulated surge-tide by TELEMAC2D alone ($\eta_{su\text{-}t\ TEL}$). It is noticeable that, the wave setup does not exceed 10 cm (Figure 3.15) during the storm of November 2007 (due to the long duration of westerly winds (see Table 4.3) and has no effect in the storms of January 2000 and November 2006. So, the wave setup has approximately no contribution to the water level at both interesting sites, because the source of the momentum flux to the water column is limited to the white capping-induced energy dissipation outside the surf zone with depth greater than 20 m.

3.3 Summary and Concluding Remarks

The TELEMAC model system can be used for free surface flow, sedimentology, and waves, it is particularly appropriate for large domain because it uses only one mesh grid with finite element discretization in space (see Figure 3.1). Moreover, TELEMAC can utilize multiprocessor computers to run in parallel version and its code can be modified by users to program particular functions of a simulation. The hydrodynamics and wave propagation over the North Sea are simulated using the selected flow model TELEMAC2D and the wave propagation model TOMAWAC.

TELEMAC2D solves the non-conservative form of the shallow water equations. It considers the propagation of long waves such as surge and tide, including an approximation of the non-linear interaction between them. On the other hand, TOMAWAC solves the wave action density (N) conservation equation (Eq. (3.11)). The application domain of TOMAWAC does not include harbour areas and further cases where the effects of wave reflection and/or wave diffraction cannot be neglected. The source and sink terms of N are classified as linear and non-linear terms. For the latter, Taylor's expansion is applied keeping only the first-order terms.

Surge-tide simulations using TELEMAC2D are carried out taking into account the meteorological and tidal forces in addition to the effects of the external surge from the Atlantic and of the discharge of the southern rivers at the boundaries (see Figure 3.8). The observed external surge is higher at the north-west part than between Scotland and Norway. The most suitable sites for considering the external surge of the North Sea model are Wick and Lerwick. Two external surge NARX models are developed, one for Wick and one for Lerwick, which are used to fill the gaps in the observed external surge data between 1970 and 2007. Moreover, they will also be used in chapter 5 to predict the external surge for future surge-tide realization 2070-2100. The performance of the two NARX models is relatively good (see Table 3.3), since the predicted wind and SLP by SN-REMO are used in the input deck instead of the observed wind and SLP at both sites. Moreover, their performance can be enhanced if the predicted external surge by surge-tide model covering the North Atlantic is added to the input deck.

The combination of tidal and meteorological conditions in interaction with the external surge is required for the evaluation of past (1970-2007) and future (2070-2100) surge-tide events in the North Sea. The simulation time for one year using TELEMAC2D is 8 hours (parallel pro-

cessing on 8 cores processor of computer "erebos1" kindly made available by BAW), so it takes totally one week for the 30 years (1970 to 2000 or 2070 to 2100). Therefore, TELEMAC2D provides a powerful and computationally efficient tool that can be part of an operational model system for storm-tide prediction in the North Sea. The simulated and observed values of the 2006 surge-tide at Cuxhaven and Sylt are compared.

The performance parameters (standard deviation σ, Root Mean Square Error RMSE and correlation coefficient (CC) as presented in Table 3.5. The performance parameters at Sylt are better than those at Cuxhaven. The standard deviation of the surge-tide $\eta_{su\text{-}t\ TEL}$ predicted by TELEMAC2D at Sylt with σ =0.69 m, is representative of the observed values η_{OB}, meanwhile the correlation coefficient is approximately 0.96 at both sites. The extreme values of the observed water level η_{OB} at both sites during the storm of November 2006 are larger than the predicted $\eta_{su\text{-}t\ TEL}$ values. The difference is assumed to be due to the approximation of the non-linear interaction between the components of the surge-tide by TELEMAC2D (η_{NLT}) that may additionally shift the arrival time of the extreme peak of $\eta_{su\text{-}t\ TEL}$. On other hand the observed water level data series contain naturally the relevant information about the nonlinear interaction of extreme storm-tide components at both sites. A pragmatic data-driven approach can learn from the observed water level data. This approach can use artificial neural networks (ANNs) to assess the contributions of the missing non-linear interaction terms to the resulting extreme storm-tide (see chapter 4).

AS both TELEMAC2D and TOMAWAC models are parts of the TELEMAC system, they share the same geometry and boundary conditions files to run the simulations and can be coupled. The wave setup (η_w) is the difference between the coupled storm-tide results ($\eta_{st\text{-}t\ TEL\text{-}TOM}$) and the simulated surge-tide by TELEMAC2D alone ($\eta_{su\text{-}t\ TEL}$). It is noticeable that, the wave setup does not exceed 10 cm (Figure 3.15) during the storm of November 2007 (due to the long duration of westerly winds (see Table 4.3)) and has no effect in the storms of January 2000 and November 2006. So, the wave setup has approximately no contribution to the water level at both interesting sites, because the source of the momentum flux to the water column is limited to the white capping-induced energy dissipation outside the surf zone with depth greater than 20 m. The coupling of TELEMAC2D and TOMAWAC for storm-tide simulation at the two selected sites, Cuxhaven and Sylt, has approximately no difference with surge-tide simulations and the effect of wave setup can be neglected. This reduces the computation time by using TELEMAC2D only instead of coupling TELEMAC2D and TOMAWAC to hindcast the storm-tide observed in the past (1970-2007) (see chapter 4) and to predict future storm-tide (2070-2100) (see chapter 5).

4 Extraction of the nonlinear interaction between the extreme storm-tide components at Cuxhaven and Sylt

A proper physically-based coupling of all components will probably take decades to be implemented in the current operational hydrodynamic models. Because the storm-tide phenomenon is affected by many different factors, it usually has strong nonlinear and nonstationary characteristics. Meanwhile, rather a more pragmatic data-driven approach is required to assess the contributions of these nonlinear interactions to the resulting extreme storm-tide. Making use of Artificial neural networks (ANNs), which are able to approximate implicitly any nonlinear mathematical functions (Hornik, 1993), allow plausible simulations of complex systems behaviour without any preceding knowledge of the internal relations among their components (Haykin, 1999). So, from the nonlinear functionality background of the biological neural networks and its ability to learning, ANNs are being applied to extreme storm-tide prediction, provided that a reasonable amount of good quality observed water level data has been collected. The ANNs models provide two significant advantages due to its ability of overcoming the problem of nonlinear relationships (Tissot et al., 2002):

1. They reduce the requirements of having a large computation grid outside the region of interest,
2. They can easily incorporate information from land-based stations (e.g., information about frontal passages) which may be difficult to incorporate into a finite element model discretized over the water only.

Such a pragmatic approach is proposed, which is based on two types of extreme water level ANNs models: (i) using the Nonlinear Autoregressive with eXogeneous inputs (NARX) neural network model alone (Type-A), (ii) combining the NARX models with hydrodynamic numeric models (flow model TELEMAC2D (Hervouet, 2007; Hervouet & Van Haren, 1994) and wave field model TOMAWAC (Benoit, 2003; Benoit et al., 2001)) (Type-B). Ensembles methods are then used to reduce variance and minimize error especially in extreme storm-tide events. Several ensemble fitting neural network (EFN) models are developed and tested. The approach was applied for two pilot sites in the North Sea (Cuxhaven and Sylt). In this way the nonlinear interactions of the different extreme storm-tide components are considered and correct the substantial errors in both magnitude and timing of the extreme storm-tide peaks. Since the observed water level data series is used during the NARX training process, it contains the relevant information about the nonlinear interaction of extreme storm-tide components. The ensemble models are able to extract the contribution of the nonlinear interaction between the different extreme storm-tide components at both sites by subtracting the results of the hydrodynamic models (linear superposition of storm-tide components) from the ensemble results (hybrid TELEMAC-NARX model).

Since the long-term water level observations in the past at Sylt may be not available, the logical way of this data recovery is to use measurements from the nearest available tide gauge station like Cuxhaven. However, differences in the phase and amplitude of water level between the two tide gauges (due principally to the tides) make it difficult to determine reliable

linear relationships between the two pilot sites. This holds especially for sites separated by distances from tens to hundreds kilometers. So due to the non-linear nature of the relationship, another NARX model is required to supplement hourly water level records at Sylt using observations from Cuxhaven.

4.1 Artificial Neural Networks and backpropagation learning algorithm

Data-driven modeling (DDM) uses algorithms (such as ANNs, fuzzy systems and evolutionary computation) that estimate unknown mapping or dependency (could be until now not fully understood) between system inputs and its outputs based on the available data (Mitchell, 1997). When such a relationship is discovered, it can be used to predict the future system outputs from the known input values (Figure 4.1).

ANNs is a methodology used in building models that are based on data-driven modelling (DDM), which would complement the "knowledge-driven" models (process-based models) describing behaviour of physical systems (Solomatine, 2002).

4.1.1 Physical Structure of biological neuron

Neuron has four general regions: dendrites, synapses, cell body, and axon; each defined by its physical position in the cell as well as its function, the structure of a generic neuron is shown in Figure 4.2.

a) Functionality and information processing of biological neuron

The transmembrane potential is the electrical potential of the cell's interior relative to its surroundings. Inputs from other neurons or specific stimuli cause changes in the neuron's membrane potential that act as signals, transmitting and processing information. Thus, to understand how neurons become excited or inhibited and how they communicate with other cells, we first need to examine how chemical and electrical forces form, maintain, and alter membrane potentials. The important membrane processes that will be examined are the resting potential, graded potential, action potential, synaptic activity, and information processing (Figure 4.3).

- *Resting potential*: a resting cell has ions that unequally distributed between the interior of cells and the fluid that surrounds them. As a result, the inside of a cell is negatively charged relative to the outside. Because the attraction of opposite charges across the plasma membrane is a source of potential energy, this charge difference or voltage, called the resting membrane potential.
- *Graded potential*: A typical stimulus produces a temporary or short-lived, localized change in the resting potential. The effect, which decreases with distance from the stimulus, is called a graded potential. Graded potentials are called "graded" because their magnitude varies directly with stimulus strength. The stronger the stimulus, the more the voltage changes and the farther the current flows.

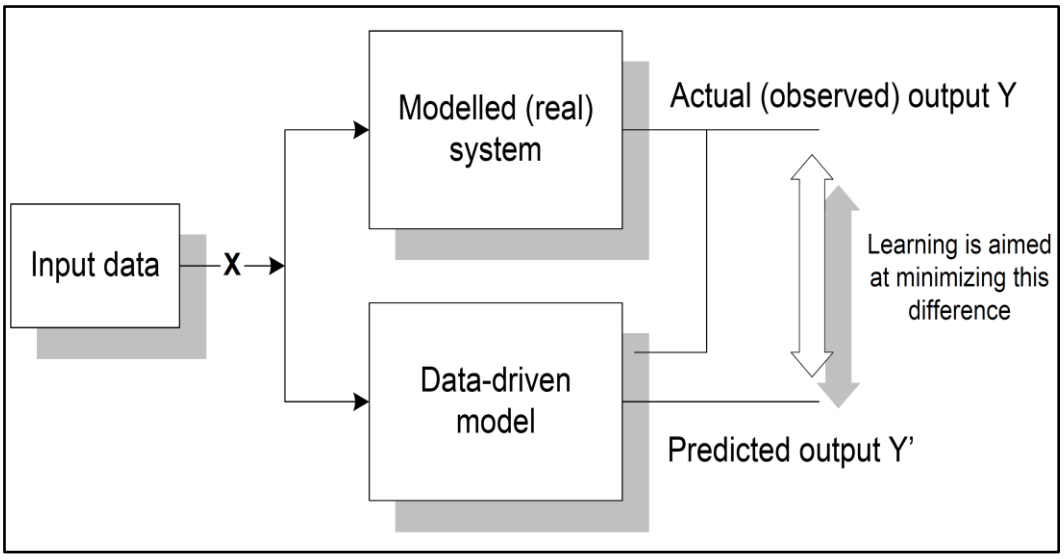

Figure 4.1: Learning process in data-driven modelling (Solomatine, 2002).

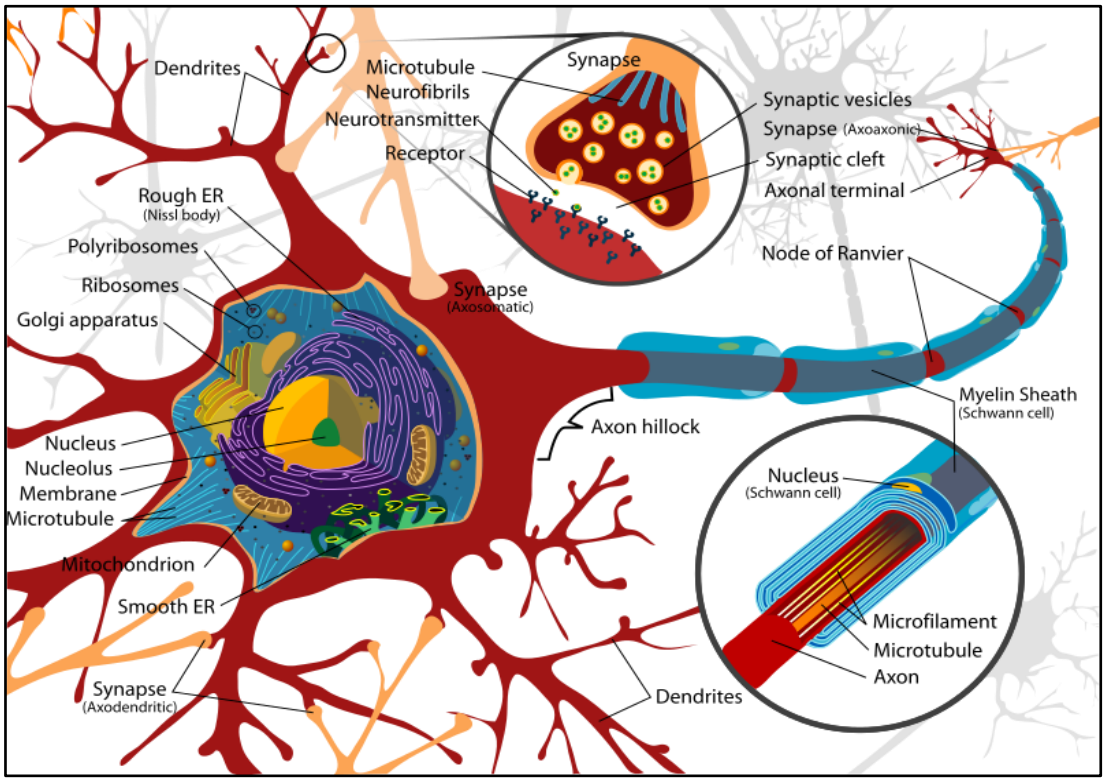

Figure 4.2: Schematic representation of biological neuron ("Complete neuron cell diagram," 2013).

- *Action potential*: If the graded potential is large enough, it triggers an action potential in the membrane of the axon. The principal way neurons send signals over long distances is by generating and propagating action potentials (APs) along the surface

of an axon and does not diminish as it moves away from its source. This impulse travels along the axon to one or more synapses.

- *Postsynaptic potential*: Synaptic activity then produces graded potentials in the plasma membrane of the postsynaptic cell. The presynaptic cell typically releases neurotransmitters. These chemicals bind to receptors on the postsynaptic plasma membrane, changing its permeability and producing graded potentials.
- *Information processing*: When a nerve impulse reaches the axon terminal, it sets into motion a chain of events that triggers neurotransmitter release. The response of the postsynaptic cell ultimately depends on what the stimulated receptors do and what other stimuli are influencing the cell at the same time. The integration of stimuli at the level of the individual cell is the simplest form of information processing in the nervous system.

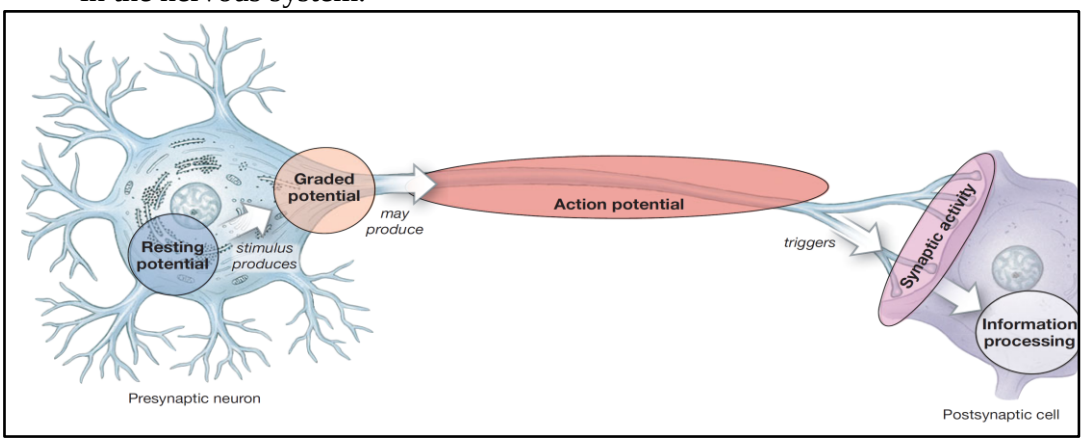

Figure 4.3: An Overview of Neural Activities (Martini et al., 2011).

4.1.2 Mathematical model of artificial neuron

The artificial neuron (AN) is a mathematical representation of the biological one that was introduced before. Since its introduction by (McCulloch & Pitts, 1943), there have been hundreds of different models considered as ANNs. The differences are in the activation function, topology, and learning algorithms.

In principle, each AN receives signals from the environment (system causal variables) or other ANs. In this way, they mimic some biological neurons that are specialized to detect changes in environment from outside the body, or the synapse between any two communicating biological neurons. Thus, if we have a neuron (node) receiving R input signals p_1, p_2,…, p_R, then these form an input vector (p). The modulatory effect of each synapse is encapsulated by simply multiplying the incoming signal with a weight value, where excitatory and inhibitory actions are modelled using positive and negative values of the weight vector (W). This is the analogue of a postsynaptic potential and may be negative or positive, depending on the sign of the weight that represents the action of neurotransmitters on a postsynaptic neuron. Therefore, each node has R weights w_1, w_2,…, w_R and form the R products w_1p_1, w_2p_2,…, w_Rp_R, which is the analogue of graded potential by biological neuron.

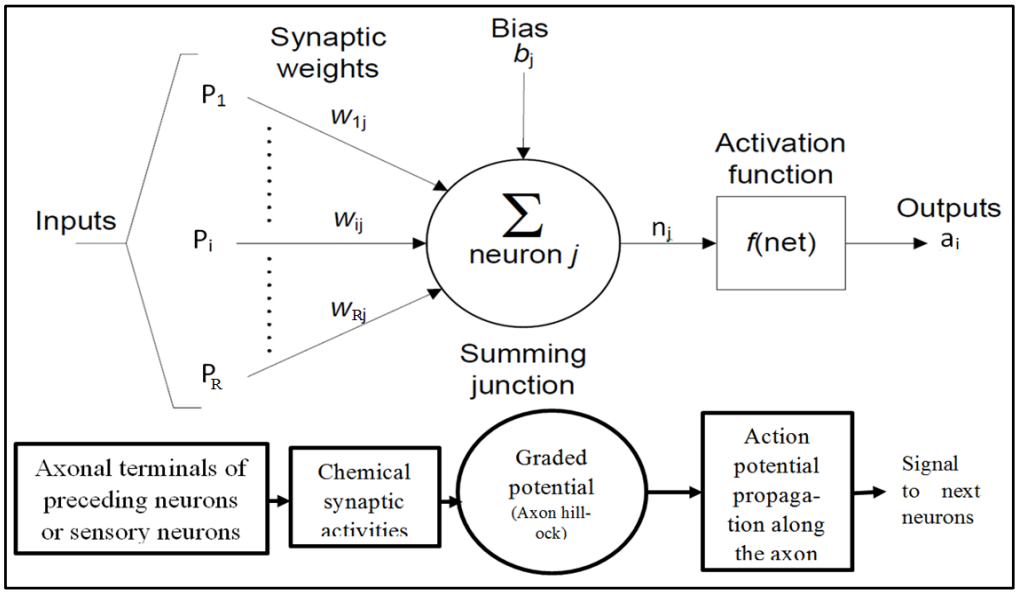

Figure 4.4: An artificial neuron model.

To emulate the generation of action potentials and information processing by biological neuron, we need a threshold value or bias b_j associated with each AN. The bias should now be combined with all weighted input products in a process to emulate the integration of EPSPs and IPSPs, which is taking place at the axon hillock. This will be done by simply adding them together to produce the net (n_j) as follows:

$$n_j = p_1 w_{1j} + p_2 w_{2j} + \cdots + p_R w_{Rj} + b_j \tag{4.1}$$

where w_{ij} represents the connection weight from the $i-th$ AN in the preceding layer to the current layer neuron j.

The firing of an AN and the strength of the exiting signal are controlled by an activation function. The AN collects all incoming signals, and computes a net signal as a function of the respective weights. The net signal serves as input to the activation function which calculates the output signal of the AN (The "all-or-nothing" character of the action potential by biological neuron). The bias of the AN must be exceeded before it can be activated. A constant 1 enters the neuron as an input and is multiplied by a scalar bias b. The following equation defines the operation:

$$a_j = f\left(\sum_{i=1}^{R} p_i w_{ij} + b_j\right) \tag{4.2}$$

The function f is called an activation function. Its functional form determines the response of the AN to the net input signal. The net input to the transfer function f is n, which is the sum of

the bias b and the vector product Wp. The neuron's output (a) is a scalar in this case. If there was more than one neuron, the network output would be a vector. Neurons can use any differentiable transfer function to generate their output such as logsig and tansig functions (Hagan et al., 1996), considering the output value of these function was in the range of [-1,1].

4.1.3 Artificial neural networks architectures

Usually one neuron may not be enough even with many inputs, so two or many neurons working together in parallel in a way so called a layer, also many layers can be attached together to mimic the real neural networks for better performance.

(a) Multiple layers of artificial neurons

A network can have several layers. Each layer has its own weight matrix W, its own bias vector b, a net vector n and an output vector a. Some additional notation is necessary to be introduced to distinguish between the weight matrices, output vectors, etc., for each of these layers. In that case, the number of the layer is appended as a superscript to the names for each of these variables. The use of this layer notation can be appreciated in the three-layer network shown below, and in the equations at the bottom of the Figure 4.5.

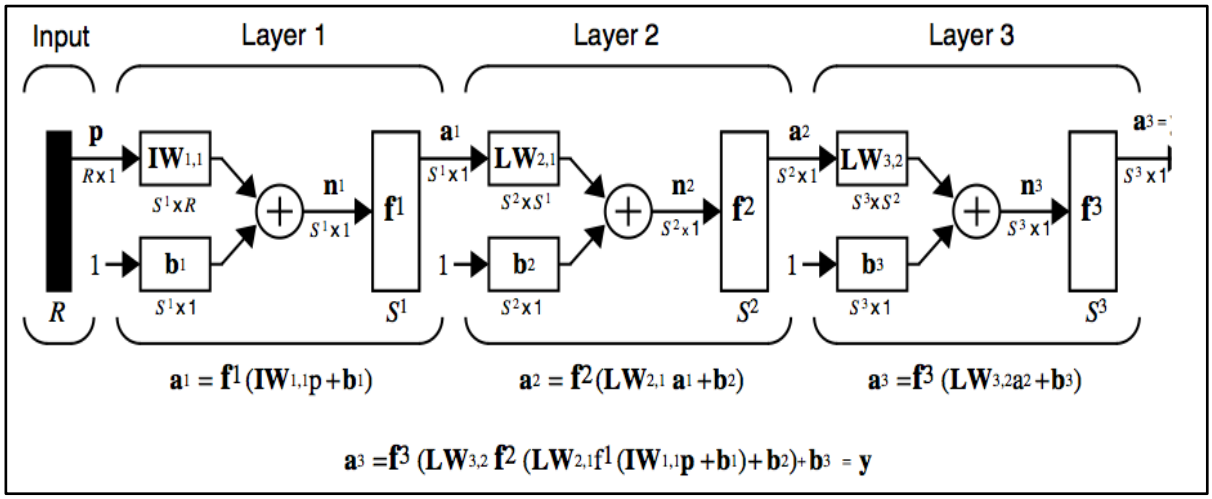

Figure 4.5: Schematic example with three-layer network abbreviated notation (Beale et al., 2013).

The three-layer network shown in Figure 4.5 has R inputs, S^1 neurons in the first layer, S^2 neurons in the second layer, etc. Moreover, in each layer a constant input 1 is fed to the bias for each neuron. Normally, different layers can have different numbers of neurons.

4.1.4 Learning methods

The learning process, also known as training or teaching is carried out according to a learning method. During learning the synaptic weights and biases are adjusted so that the error surface

converges to a minimum. Here comes the learning algorithms to find the best values for W and b from the given data until a certain criterion is achieved.

The training process for an ANN is employed to find optimal weight matrices W and bias vector b in order to generate an output vector $a = (a_1, \ldots, a_j, \ldots, a_q)$ that is as close as possible to the target vector $ta = (t_1, \ldots, t_j, \ldots, t_q)$. So its objective is to minimize a predetermined error function that usually has the form:

$$E = \sum_q \sum_p (t_j - a_j)^2 \tag{4.3}$$

where t_j is a component of the desired output vector ta ,

and a_j is the corresponding ANN output,

p is number of nodes in the output layer and q is number of training patterns.

Each pass through the training data is called epoch and the ANN learns through the overall change in weights accumulated over many epochs. One of the main types of learning is *Supervised learning* (Figure 4.6), where the ANN is provided with a data set consisting of input vectors and a target (desired output) associated with each input vector. This data set is referred to as the training set. The aim of supervised training is then to adjust the weight values such that the error between the generated output y of the neuron and the target output t, is minimized.

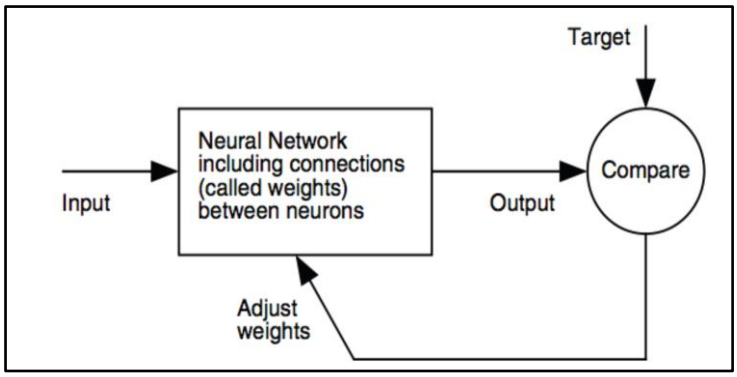

Figure 4.6: Supervised Artificial Neural Network learning process schematic (Beale et al., 2013).

(a) Back-propagation and Levenberg-Marquardt training algorithms

The back-propagation is a type of the supervised learning where the training set (input and target data pairs) is provided to the ANN. The most common ANN architecture used with back-propagation algorithm is the feed-forward multilayer perceptron (MLP).

Standard back-propagation is a gradient descent algorithm, which seeks the weight and bias vectors that minimize the error by starting with an arbitrary random initial vectors, then re-

peatedly modifying it in small steps (i.e. move along the negative of the gradient of the performance function). At each step, these vectors are altered in the direction that produces the steepest descent along the error surface. The steps of the algorithm are presented below:

1. Set initial weights randomly, usually in small range near to zero, e.g. [-0.1,0.1]
2. For each example or pattern in training set
   a. Apply input, P to calculate output a.
   b. Compare the predicted output a with the observed output ta.
   c. Calculate error: e = ta-a
3. Use error to revise weights and biases vectors:$X_{k+1}=X_k+\alpha_s\, g_k$, where α is the learning rate and g_k is the current gradient.
4. Repeat step 2 until convergence (no error changes).

Usual back-propagation training methods like gradient descent and gradient descent with momentum are usually too slow for practical problems. There are high-performance algorithms that can converge from ten to one hundred times faster than other algorithms. All these faster algorithms operate in batch modes and based on other standard optimization techniques, such as conjugate gradient, Quasi-Newton and Levenberg-Marquardt methods.

An alternative algorithm called the Levenberg-Marquardt algorithm proposed by Hagan and Menhaj (1994). This algorithm is a quasi-Newton approach and it has the capability of finding optimal solutions for a variety of problems. It gives much quicker convergence at the cost of more intensive computational requirements. As the quasi-Newton methods, the Levenberg-Marquardt algorithm was designed to approach second-order training speed without having to compute the Hessian matrix (the matrix of the second-order partial derivatives) (Beale et al., 2013).

Error surfaces of dynamic networks like NARX can be more complex than those of static networks like MLP. In function approximation problems, for networks like NARX that contain up to a few hundred weights, the Levenberg-Marquardt algorithm will have the fastest convergence. This advantage is especially noticeable if very accurate training is required. It is specifically designed to minimize sum-of-square error function of the form (Ranganathan, 2004),

$$E = {}^1\!/_2 \sum_q (e_q)^2 = {}^1\!/_2 \, \|e\|^2 \qquad (4.4)$$

Where e_q is the error in the q^{th} exemplar or pattern and e is a vector with element e_q. If the difference between the pervious weight vector w(k)and the new weight vector $w(k+1)$ is small, the error vector can be expanded to first order by means of a Taylor series (Sapna et al., 2013)

$$e(k+1)=e(k)+ {\partial e_q}/{\partial w_i}\,(w(k+1)-w(k)) \tag{4.5}$$

As a consequence, the error function can be expressed as

$$E= {1}/{2}\left\| e(k)+ {\partial e_q}/{\partial w_i}\,(w(k+1)-w(k))\right\|^2 \tag{4.6}$$

Minimizing the error function with respect to the new weight vector, gives

$$w(k+1)=w(k)- (J^T J)^{-1}J^T e(k) \tag{4.7}$$

Where J is the jacobian

$$(J)_{qi}\equiv {\partial e_q}/{\partial w_i} \tag{4.8}$$

Since the Hessian for the sum-of-square error function is

$$(\text{Hessian})_{ij}= {\partial^2 E}/{\partial w_i \partial w_j} = \sum\left\{\left({\partial e_q}/{\partial w_i}\right)\left({\partial e_q}/{\partial w_i}\right)+e_q\, {\partial^2 e_q}/{\partial w_i \partial w_j}\right\} \tag{4.9}$$

Neglecting the second term, then the Hessian matrix can be approximated as Hessian $= J^T J$

Updating of the weights therefore involves the inverse Hessian or an approximation thereof for nonlinear networks. The Hessian is relatively easy to compute, since it is based on first order derivatives with respect to the network weights that are easily accommodated by back-propagation. Although the updating formula could be applied iteratively to minimize the error function, this may result in a large step size, which would invalidated the linear approximation on which the formula is based (Sapna et al., 2013).

In the Levenberg-Marquardt algorithm, the error function is minimized, while the step size is kept small in order to ensure the validity of the linear approximation. This is accomplished by use of a modified error function of the form (Sapna et al., 2013),

$$E = {}^{1}/_{2} \left\| e(k) + {}^{\partial e_q}/_{\partial w_i} (w(k+1)-w(k)) \right\|^2 + \mu \|w(k+1)-w(k)\|^2 \qquad (4.10)$$

where μ is a parameter governing the step size.

Minimizing the modified error with respect to w(k+1) gives,

$$w(k+1)=w(k)- (J^T J+\mu I)^{-1} J^T e(k) \qquad (4.11)$$

very large values of μ amount to standard gradient descent. When the scalar μ is very small, this amounts to the Newton method using the approximated Hessian matrix. Newton's method is faster and more accurate near an error minimum, so the objective is to go to Newton's method as quickly as possible. Thus, μ is decreased after each successful step (that means reduction in performance function) and is increased only when a tentative step would increase the performance function.

4.1.5 Capabilities and limitations of ANN approach

(a) Advantages of the ANN approach

The major advantage of neural networks is that, they are capable of approximating any continuous function, and thus the researcher does not need to have any hypotheses about the underlying physical processes and their modelling (Haykin, 1999). The resulting network developed in the process of "learning" represents a pattern detected in the data (data driven modelling). Thus, in principle, ANN method can also be applied to many research issues in coastal engineering.

(i) Hindcasting: Training with short-term data for long-term predictions.

Theoretically, as long as the collected training data set covers the maximum range of the possible variability in the interested process, a short-term data set can be used to train the developed ANN model for long-term predictions.

(ii) Real-time nowcast

ANN models can be effectively used in real-time forecasting due to the rapid speed in obtain the model output.

(b) Limitations and Potential Solution Approaches of the ANN Approach

(i) Predictions limited to training stations

Normally, The ANN model has to be trained using an observed time series obtained at certain station. It cannot provide predictions at other stations where the model is not trained. So, we need to collect data for model training at every station where we expect to obtain long-term model predictions. Moreover, we may not have enough field observations at every station. This might represent the major limitation of the ANN models in comparison with process based models. However, the combine of ANNs models with the process based models reduce the required amount of training data to be collected from single or several stations.

(ii) Training algorithm

A back-propagation network based on the standard gradient-descent training method sometimes suffers from slow convergence to the presence of one or more local minima. There are several optimization methods which can be used to improve the convergence speed and the performance of network training. All these faster algorithms operate in batch modes and based on other standard optimization techniques, such as conjugate gradient, Quasi-Newton and Levenberg-Marquardt methods.

(iii) Overfitting

In general, overfitting is one of the problems that may occur during the training of a neural network. Since the network has memorized the training pattern it cannot generalize to new data. In this case the error for a training series is very small but the developed network results into large error for new data series.

The first approach for improving network generalization is to use an adequate-size network, which is just large enough to provide an adequate fit. The larger a network is, the more complex the functions that the network can create which may cause overfitting. If we use a small enough network, it will not have enough power to overfit the data.

The second method for improving generalization is called early stopping. In this technique, the validation series was used to improve the generalization. The validation error is monitored during the training process. The errors on the validation and training series usually decrease during the initial phase of training and as soon as the network begins to overfit the data, the validation error increases for a number of iterations (here six iterations), the training is stopped.

(iv) Data Ranges for Network Training

In general, an ANN is trained using data within a specific range. Then, in applying a validated ANN model in forecasting simulations, the results are expected to be good if the data are given within the same range, which is similar to the interpolation of a regression function. If the data are out of the range, which is similar to the extrapolation of a regression function, model simulations sometime may not be good.

To resolve this weakness, we can analyze the long-term historic data, and use a data set that reflects the maximum range to cover the extreme weather and storm surge conditions. As a result, data to be used in any ANN model simulations will fall within the range of the training data set so that good simulation results can be obtained.

Artificial Neural Networks (ANNs) are systems based on the operation of biological neural networks (BNNs), in other words, are a mathematical abstraction (an emulation) of BNNs. Both BNNs and ANNs are network systems consist basically from "neurons". ANNs are a type of nonlinear processing systems that are ideally suited for a wide range of complex systems behaviour, especially those where there is no physical knowledge of the internal relation known for nonlinear behaviour completion. ANNs can be trained to solve certain problems using a teaching method (like back-propagation algorithm) and samples data. A drawback of back-propagation algorithm is that it needs a long learning time and is affected by local minima. While it gives good results, its convergence to optimal network tends to be rather slow. An alternative algorithm called the Levenberg-Marquardt algorithm proposed by Hagan and Menhaj (1994), which gives much quicker convergence as the quasi-Newton methods. In this way, identically constructed ANN can be used to perform different tasks depending on the training received. With proper training, ANNs are capable of generalization, the ability to recognize similarities among different input patterns, especially patterns that are new or have been corrupted by noise.

4.2 Development of the NARX models to predict extreme storm surges at Cuxhaven and Sylt

Using the hourly meteorological forcing between 1970 and 2007 generated by the Regional Climate Model (RCM) SN-REMO, along with the observed water level data from 1997 to 2007 for Cuxhaven and from 1999 to 2007 for Sylt, two types of extreme water level ANNs models called NARX (Nonlinear AutoRegressive eXogenous inputs) were developed: (i) NARX neural network model to predict the extreme storm-tide (Type-A), (ii) NARX neural network model to nonlinearly correct the numerical storm-tide results from TELEMAC2D (Type-B).

The construction of each NARX model type is performed in two phases (see Table 4.1), due to the large number of neural architectural parameters (e.g. the number of hidden layers and number of hidden neurons in each layer) that can be modified. The first phase deals with the determination of the optimum number of input variables time series lags that should be included as input, also the optimum architectural parameters and best training algorithm using STATISTICA Automated Neural Networks (SANN) in STATISTICA package version 10 from Statsoft Inc.. In the second phase, the final NARX model type is developed using Matlab neural networks toolbox for further structural parameters configuration and modifications that are based on the optimum structure obtained by SANN.

The use of ensembles methods can significantly reduce variance and minimize error especially in extreme storm-tide events. The ensemble forecasting method averages results from the best NARX models. Several different ensemble fitting neural network (EFN) models are developed and tested, varying the architectural parameters used for each ensemble.

Finally, the two types of NARX models and their ensemble prediction results are validated in terms of correlation coefficient (CC), root mean square of error (RMSE) and standard devia-

tion (σ) using observed water level data, in order to determine the models with the best prediction performance for water levels at the two locations between 1991 and 2007.

4.2.1 Input variables selection and preparation for the developed NARX models

The ANN models in the learning phase capture the nonlinear nature between extreme water level components using a moderate time span (approximately 5 years) of the observed water levels at Cuxhaven and Sylt. A subset of the observed water level data at Cuxhaven and Sylt for learning and validating the models should be selected such that it does not contain gaps and/or a substantial amount of improbable observed values. This criterion is fulfilled for Cuxhaven data between 1997 and 2007, while for Sylt between 2000 and 2007. The observed water level data for each year of the above selected periods are recorded with time interval between 10 minutes and 1 hour, which are temporally interpolated in order to be synchronized with the available meteorological data every hour.

Table 4.2 shows the input and output data for the two developed NARX models at Cuxhaven and Sylt. The input deck of the two NARX models types consists of the astronomical tidal forecasts, significant wave height produced by TOMAWAC numerical wave model, the two wind speeds components in east-west direction (wind U component or zonal component) and in south-north direction (wind V component or meridional component), external surge from Wick station, and sea level pressure for Cuxhaven and Sylt in addition to the Elbe river discharge (in case of Cuxhaven only).

For Cuxhaven and Sylt, the wind and pressure setups are presented to the developed NARX models in input deck as the sea level pressure and the two wind speed components data (in east-west direction (wind U component or zonal component) and in south-north direction (wind V component or meridional component)). For the two pilot sites, Figure 4.7 and Figure 4.8 show the descriptive statistics for these three meteorological factors. They exhibit almost the same statistical magnitude of the data mean, median and statistical distribution behaviour. Only the wind meridional component at Sylt was slightly stronger than at Cuxhaven because of the higher wind data frequency in the ranges of 10 to 30 m/s and -10 to -30 m/s for Sylt. These three meteorological factors were generated using the RCM SN-REMO, which interpolated in space and time to the interested TELEMAC2D North Sea modeled area including Cuxhaven and Sylt (Tayel & Oumeraci, 2012b).

The study of 73 external surges which occurred from 1971 to 1995, showed that the residual contribution of the external surge in Cuxhaven without the wind effects may amount 10 cm to 109 cm (Gönnert & Thumm, 2010). In order to take this component into account, the observed external surges data at Wick between 1969 and 2007 were downloaded from the British Oceanographic Data Centre (BODC) website http://www.bodc.ac.uk/, but these data contain gaps and improbable values. So an external surge NARX model was used to fill the gaps in the observed external surge (Tayel & Oumeraci, 2012b).

The seiche component for the storm surge in the North Sea once occurred in December 1954. Two storm surges “twin” occurred during the period of 21-24 of December. The period be-

tween the maxima of the two storms (about 35 hours) was such as to cause almost complete resonance for the North Sea (Weenink, 1956). Normally, the storms of the North Sea have wind variations at time scales shorter than the resonance period in order to complicate the response. At Cuxhaven and Sylt, the seiche is triggered mainly by tides and/or storm surges long waves. So, seiche is introduced through the surge-tide simulation results by TELEMAC2D, which are based on the bathymetry and geometry of the North Sea area of 2006, to the developed NARX models.

The effect of waves on the surge-tide at Cuxhaven and Sylt is shown during the the storms of January 2000, November 2006 (see Figure 3.10 and Figure 3.11) and November 2007 (called Tilo, see Figure 3.15) by coupling TELEMAC2D and TOMAWAC (see section 3.2.5). The wave setup has no effect at both sites, since they are outside of the surf zone with depth greater than 20 m. Therefore, the coupling of TELEMAC2D and TOMAWAC is not required for the North Sea model to include the wave setup effect (η_w) at both sites in order to reduce computation time. Nevertheless, the significant wave heights (H_s) were calculated by using the meteorological forces of the RCM SN-REMO over the North Sea area and extracted for Cuxhaven and Sylt as input for the two NARX types.

The daily fresh water discharges of the Elbe River at Geesthacht from 1960 to 2007 are supplied by Federal Waterways Engineering and Research Institute (BAW), which are hourly interpolated in order to be synchronized with the other NARX input variables data.

Coriolis force is a result of the earth rotation, and causes wind-driven currents in the Northern Hemisphere to be deflected to the right in a rotating frame of reference. This apparent force affects all oceanic and atmospheric movement in coordinates that rotate with the earth. In a basin with the dimensions of the North Sea, the rotation of the earth affects the tides and other components. The importance of the earth's rotation can be estimated with the Rossby deformation radius (Pedlosky, 1982). The Rossby radius for the North Sea is about 270 km making necessary to take into account the inertia effects of Coriolis force. Hence, during the surge-tide simulations by TELEMAC2D, which build the input to the developed NARX models, the keyword CORIOLIS is set to true.

The observed external surges data at Wick, which is one of the NARX models inputs, is calculated as the difference between the actually observed water level and the predicted astronomical tide. It includes implicitly the effect of sea level rise over the deep northern part of the North Sea. Furthermore, it is added linearly to tides in the north-western boundary during surge-tide simulations by TELEMAC2D (Figure 3.8), which is included in NARX input variables.

Table 4.1: Development phases 1 and 2 for NARX models Type A and Type B at Cuxhaven and Sylt.

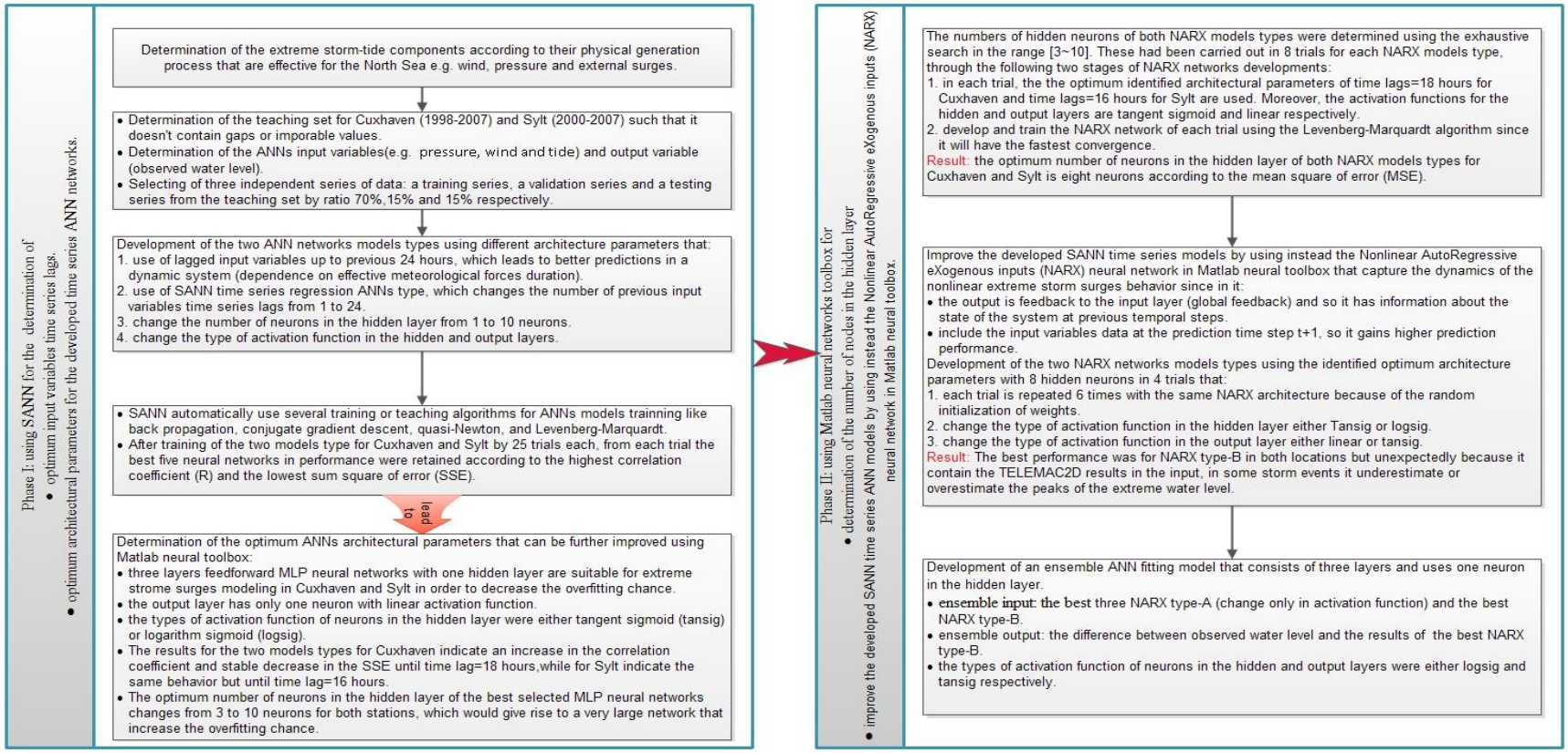

SANN: STATISTICA Automated Neural Networks, which used to automatically train and try the various combinations of architectural parameters for ANNs development.
NARX Type-A: NARX neural network models to predict the extreme storm-tide without the inclusion of numerical surge-tide results from TELEMAC2D in input.
NARX Type-B: NARX neural network models to nonlinearly correct the numerical surge-tide results from TELEMAC2D

Table 4.2: Input and output for the developed NARX models Type A and Type B at Cuxhaven and Sylt.

Description	**Cuxhaven (Type-A and Type-B)**	**Sylt (Type-A and Type-B)**
Input	• Time series of wind U component. • Time series of wind V component. • Time series of sea level pressure. • Time series of observed water level. • Time series of Elbe River discharge. • Time series of external surge at Wick. • Astronomical tidal prediction time series. • TOMAWAC Significant wave height (H_s) results time series. • TELEMAC2D surge-tide results time series (for Type-B only).	• Time series of wind U component. • Time series of wind V component. • Time series of sea level pressure. • Time series of observed water level. • Time series of external surge at Wick. • Astronomical tidal prediction time series. • TOMAWAC Significant wave height (H_s) results time series. • TELEMAC2D surge-tide results time series (for Type-B only).
output	Time series prediction of extreme water level every hour	Time series prediction of extreme water level every hour
Training period	1998 to 2005	2000 to 2005
Prediction period	1991 to 2007	1991 to 2007

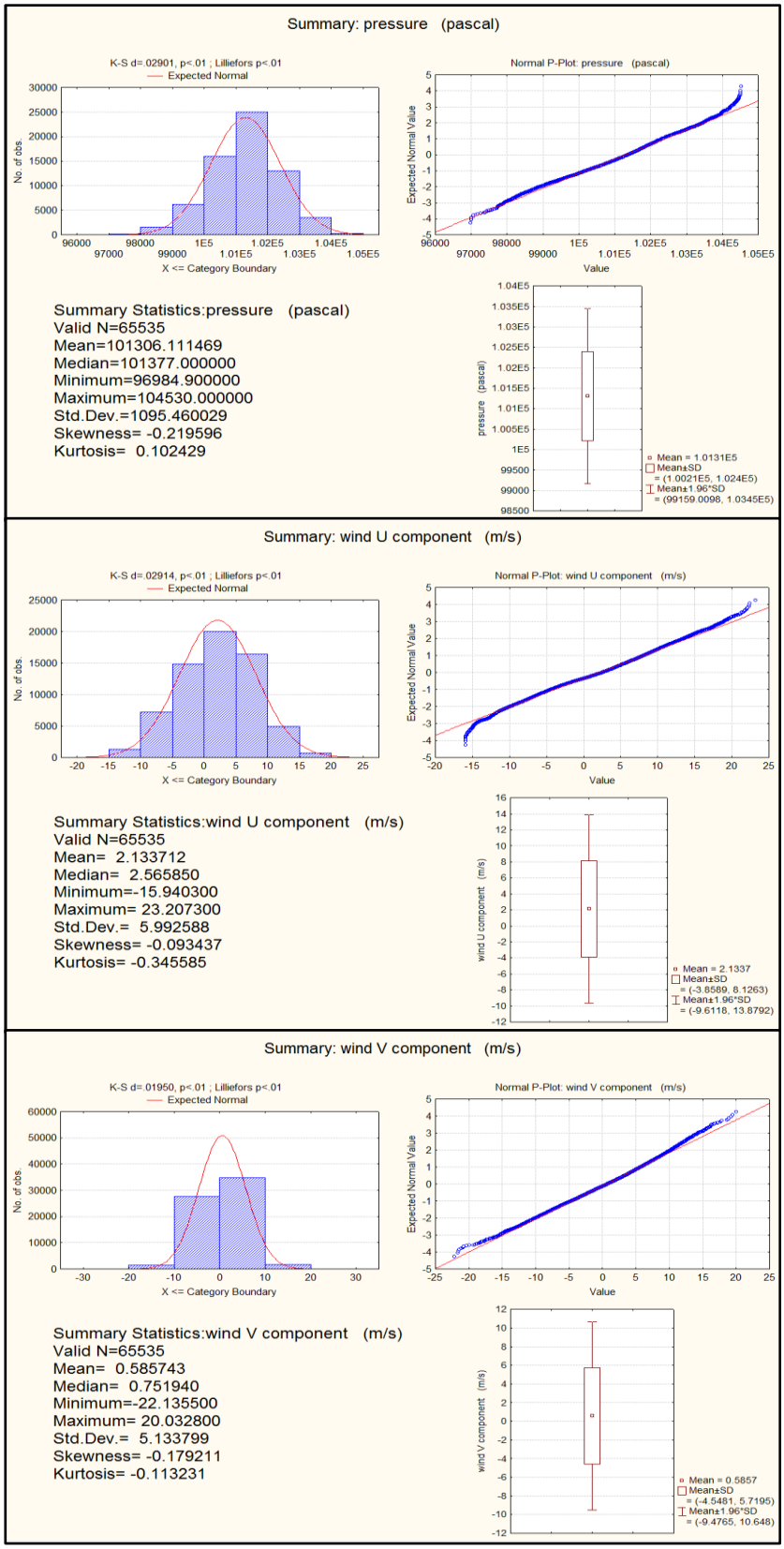

Figure 4.7: Descriptive statistics of the main meteorological factors at Cuxhaven between 1998 and 2007.

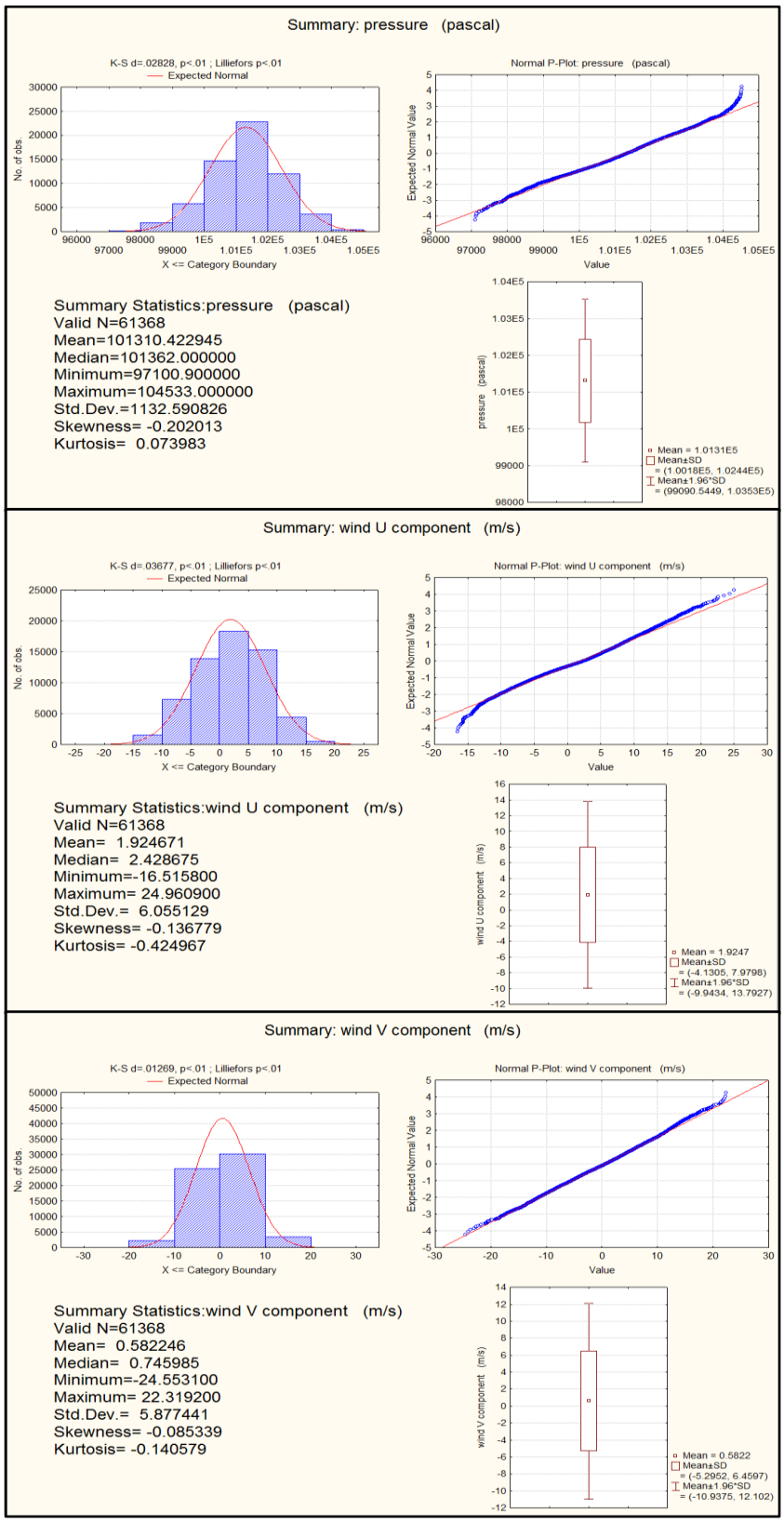

Figure 4.8: Descriptive statistics of the main meteorological factors at Sylt between 2000 and 2007.

4.2.2 The nonlinear nature of observed extreme storm-tide at Cuxhaven and Sylt

In order to examine the effects of storm events on the nonlinear nature of the observed extreme water level inside the German bight, three storm events were selected, namely, the storms of January 2000, November 2006 and November 2007 (called Tilo). These storms were selected owing to their historical significance and the amount of destruction caused (Munich Re, 2012). Table 4.3 shows the main characteristics of the selected storm events and the extreme observed water levels (η_{OB}) generated by the input variables in Table 4.2. These storms were typical low-pressure areas (less than 100000 Pascal) moving from west to east across the central North Sea as shown by mean wind directions (Table 4.3), causing strong onshore winds combined with a strong surge. The mean wind speeds during these selected storms ranged between 16.1 and 20.4 m/s, and the mean wind directions were between 284.3^o and 333.9^o. During the storms of January 2000 and November 2006, the meteorological characteristics at Cuxhaven differ slightly from those at Sylt. In contrast, the mean wind speed and duration during the storm of November 2007 at Cuxhaven are 16.1 m/s and 29 hours respectively, differ from those at Sylt of 19 m/s and 24 hours respectively. It is noticeable that, as the duration is getting shorter, the mean wind speed is getting higher. The longest northwesterly wind happened during the 2007 storm event at Cuxhaven of 29 hours but its mean wind speed is the lowest with 16.1 m/s. Furthermore, the shortest duration occurred during the January 2000 storm event at Sylt of 10 hours but its mean wind speed is the highest with 20.4 m/s. The January 2000 and November 2006 storms occurred in conjunction with a neap tide, as opposed to a spring tide for November 2007. The tidal range of the spring tide at Cuxhaven is 3.0 m, which is about the double of its value at Sylt with 1.7 m. This occurrs due to the difference in latitude and morphology of the two sites. Moreover, the observed external surges at Wick have an effect on the extreme water level during the storm of January 2000 with maximum of 0.76 m, while it is much less important during the other two storms. Since the external surges propagate from Wick to Cuxhaven and Sylt, its effect on the two sites occurs after the time of its maximum at Wick (Figure 4.9 and Figure 4.10). The effects of wave setup and river discharge on the water level during these storms are almost negligible (see tion 4.2.13.2.5) especially with the small wave heights (H_s < 1 m) and small river discharge (Q < 600 m^3/s) (Table 4.3). The predicted storm-tide by TELEMAC2D ($\eta_{st\text{-}t\ TEL\text{-}TOM}$) at Cuxhaven and Sylt during these three storms serve as input to the ANNs models. The comparison between the extreme of $\eta_{st\text{-}t\ TEL\text{-}TOM}$ and the observed storm-tide (η_{OB}) is explained in sections 4.3.2 and 4.3.3. It is noticeable that, the heights of η_{OB} peaks always overestimate those calculated by $\eta_{st\text{-}t\ TEL\text{-}TOM}$ during these three storms at Cuxhaven and Sylt. This is due to the approximation of the nonlinear interaction between the components by TELEMAC2D (η_{NLT}) that lead additionally to the shift in the arrival time of $\eta_{st\text{-}t\ TEL\text{-}TOM}$ (see Figure 4.9 and Figure 4.10). moreover, the overestimation of sea level pressure in certain storms leads to the underestimation of the predicted storm-tide such as in storm of November 2007. The highest extreme η_{OB} occurs during the 2007 storm event at Cuxhaven with 4.42 m, while it was 3.19 m for $\eta_{st\text{-}t\ TEL\text{-}TOM}$.

Figure 4.9 and Figure 4.10 show the temporal variations of the input variables (Table 4.2) for Cuxhaven and Sylt respectively during the storm of January 2000. The two wind speed components and sea level pressure are the interpolated values at Cuxhaven and Sylt which are extracted from the RCM SN-REMO. Furthermore, the Elbe river discharge at Neu Darchau and the external surges at Wick were extracted from the recorded measurements. The tides at the selected sites were calculated using the harmonic analysis of the observed water level. Only the significant wave height (H_s) and the $\eta_{st\text{-}t\ TEL\text{-}TOM}$ were simulated by the wave propagation model TOMAWAC and the hydrodynamic model TELEMAC2D respectively under the effect of the meteorological force of SN-REMO. The observed storm-tide at the two pilot sites η_{OB} contains all of the components and implicitly their nonlinear interaction (η_{NL}). The highest η_{OB} peaks during the storm of January 2000 at Cuxhaven and Sylt, which reach 3.86 m and 3.02 m respectively, overestimate those calculated by $\eta_{st\text{-}t\ TEL\text{-}TOM}$ of 2.97 m and 3.02 m respectively. Moreover, the η_{NLT} , which approximates the nonlinear interaction, shifts in the arrival time of $\eta_{st\text{-}t\ TEL\text{-}TOM}$ peak by -9 hours at Sylt (see Figure 4.10).

Table 4.3: Characteristics of the selected storm events and the extreme of observed storm-tide (η_{OB}) at Cuxhaven and Sylt.

Station / input variables	Cuxhaven			Sylt		
	January 2000	**November 2006**	**November 2007**	**January 2000**	**November 2006**	**November 2007**
sea level pressure (Pascal)	98675.3	99441.6	99848.6	98197.6	99455	99723.2
mean wind speed (m/s)	18.4	17.8	16.1	20.4	16.9	19
mean wind direction North =0°	284.3	298.1	319.8	294.5	333.9	329.6
duration of mean wind speed (hours)	10	22	29	10	23	24
Tidal range (m)	2.4	2.6	3.0	1.5	1.6	1.7
maximum external surge at Wick (m)	0.76	0.26	0.40	0.76	0.26	0.40
significant wave height H_s (m)	0.32	0.38	0.41	0.20	0.35	0.24
Elbe river discharge (m^3/s)	577.3	296.4	524	-	-	-
time for $\eta_{st\text{-}t\ TEL\text{-}TOM}$	30/1/2000 7:00 AM	1/11/2006 7:00 AM	9/11/2007 12:00 PM	30/1/2000 6:00 AM	1/11/2006 8:00 AM	9/11/2007 1:00 PM
Height of $\eta_{st\text{-}t\ TEL\text{-}TOM}$ (m)	3.24	2.97	3.19	2.58	2.09	2.30
time for highest η_{OB} peak	30/1/2000 6:00 AM	1/11/2006 7:00 AM	9/11/2007 12:00 PM	30/1/2000 7:00 AM	1/11/2006 10:00 AM	9/11/2007 1:00 PM
highest η_{OB} peak (m)	3.86	3.81	4.42	3.02	2.21	2.65

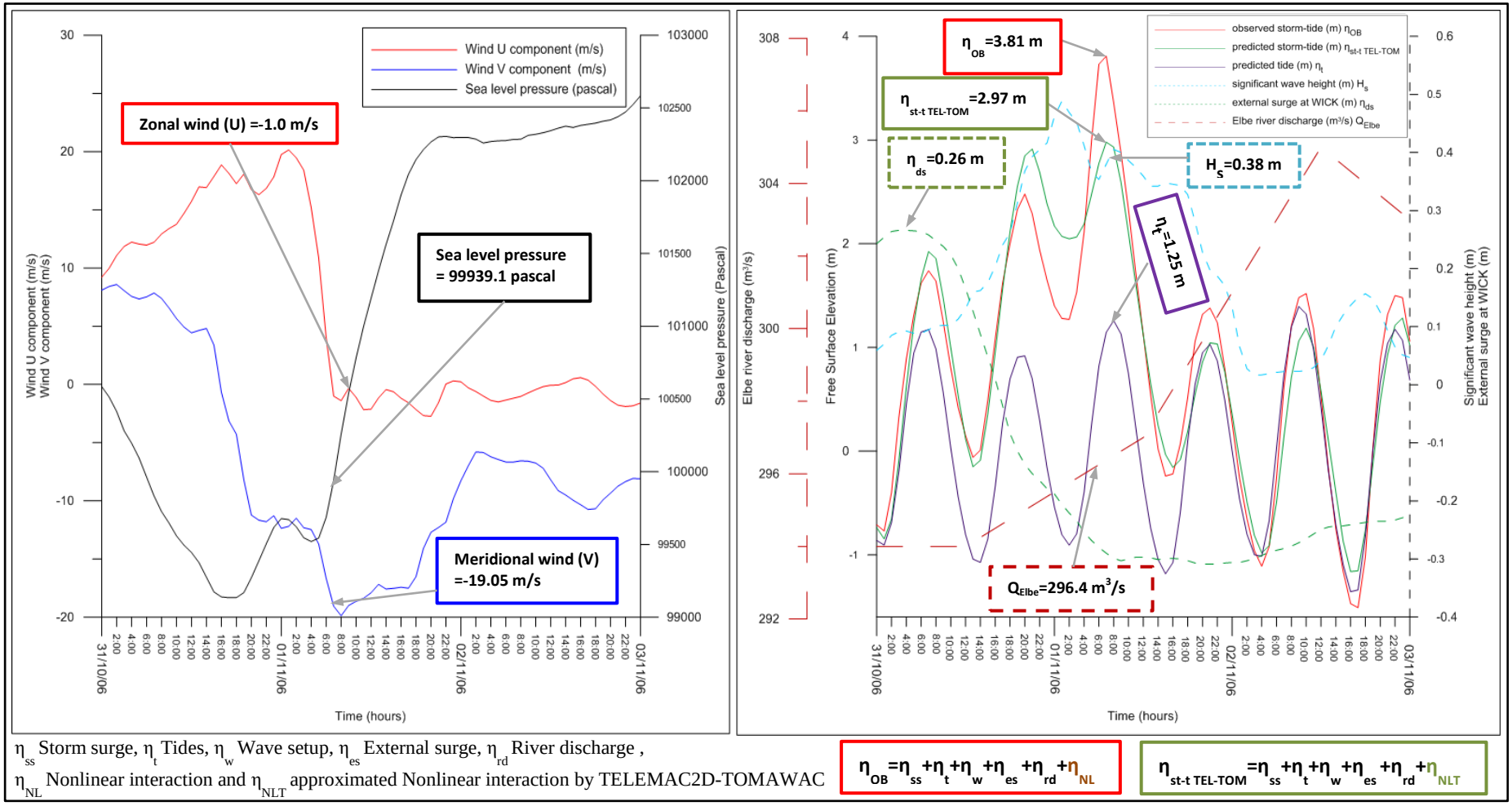

η_{ss} Storm surge, η_t Tides, η_w Wave setup, η_{es} External surge, η_{rd} River discharge ,
η_{NL} Nonlinear interaction and η_{NLT} approximated Nonlinear interaction by TELEMAC2D-TOMAWAC

$\eta_{OB}=\eta_{ss}+\eta_t+\eta_w+\eta_{es}+\eta_{rd}+\eta_{NL}$

$\eta_{st\text{-}t\ TEL\text{-}TOM}=\eta_{ss}+\eta_t+\eta_w+\eta_{es}+\eta_{rd}+\eta_{NLT}$

Figure 4.9: Storm characteristics, ANN models input variables and the extreme of observed storm-tide during the storm of January 2000 at Cuxhaven.

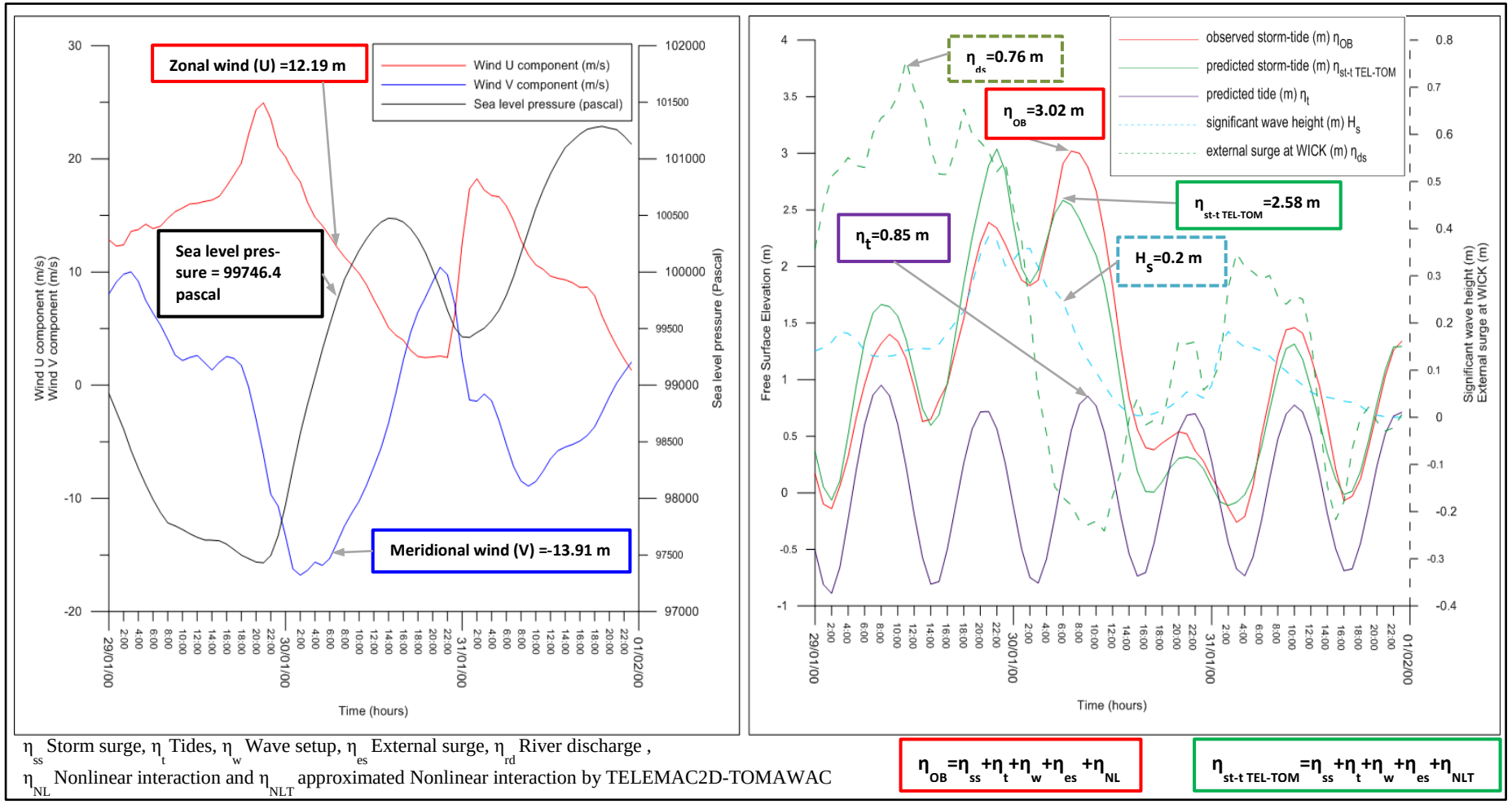

Figure 4.10: Storm characteristics, ANN models input variables and the extreme of observed storm-tide during the storm of January 2000 at Sylt.

4.2.3 Identification of ANNs optimum parameters using SANN

In any neural network model development, the first step is to design a specific network architecture. The architecture of a network describes how many layers a network has, the number of neurons in each layer, each layer's activation function, and how the layers are linked to each other. Finding an optimal ANN architecture still remains an open problem of investigation and depends on the application domain (Noorzaei et al., 2007). The size and structure of the network needs to match the nature and complexity of the investigated phenomenon. In general, because the latter is obviously not known well at this early stage, this task is not easy and requires a lot of trial and error (Alliance & Huang, 2007). Therefore, Statistica Automated Neural Networks (SANN) was used to automatically test the various combinations of architectural parameters, in addition to obtain the optimum input variables time series lags that should be included. The final NARX model is refined and developed using Matlab neural networks toolbox as the second phase for further architectural parameters configuration based on the optimum architecture obtained by SANN. The different ANNs models using SANN are developed through the following three stages:

Stage 1- Data Selection and ANNs models construction by SANN

The general approach of learning begins with selecting three independent series of data among the available data series: a training series, a validation series and a testing series. The training series should contain most of the extreme events (Jayawardena & Fernando, 2001). Two ANN model types were developed using SANN for Cuxhaven and Sylt. Both types were learned using the same observed water level data and input deck. Exceptionally, type-B models have included in input additionally the predicted hourly surge-tide results from TELEMAC2D. Moreover, since the distance between Sylt and the main four rivers in the southern of the North Sea is more than 100 km, the Elbe river discharge input data is not included for both ANN model types of Sylt. Figure 4.11 show the input and output variables along with the modified structural parameters for the designed ANNs by SANN at Cuxhaven. The span periods of the used learning data for Cuxhaven and Sylt were from 1998 to 2005 and from 2000 to 2005 respectively. Therefore the above selected learning data sets for Cuxhaven and Sylt are divided randomly in three series as the training series, the validation series and test series, which represent respectively 70%, 15% and 15% of the data.

SANN provides time series (regression) analysis type, which considers that the target (dependent) variables are continuous in nature, and may involve lagged (over time) predictions. Therefore, it is used for both ANN types with input variables time series lags from 1 to 24 and it can be represented as

$$y(t+1) = f[u_m(t), u_m(t-1), \dots, u_m(t-d_u+1)], \quad m = 1,2,\dots, input\ variables\ number \tag{4.12}$$

where u_m(t)∈ℜ and y(t)∈ℜ denote, respectively, the (m) input variables and the output variable of the model at discrete time step t, while d_u≥1 is the input-memory orders. The nonlinear mapping f(.) is generally unknown and can be represented, for example, by a standard Multilayer Perceptron (MLP) network.

Regression type series is usually concerned with predicting one or more continuous variables using a set of inputs at the same time step, so it considered only as the inclusion of zero lags of the input variables time series as follow

$$y(t+1) = f[u_m(t+1)], \qquad m = 1,2,\dots, input\ variables\ number \qquad (4.13)$$

For Cuxhaven and Sylt, only the regression and time series regression types are used in the development of ANN types. The input variables (u_m) for both ANN models type, which are developed by SANN, did not include the previous observed water level series as input.

Stage 2- Model training

SANN automatically use several training or teaching algorithms (back propagation, conjugate gradient descent, quasi-Newton, and Levenberg-Marquardt) to update the weights and biases in order to minimize the prediction error made by the network. From an initially random configuration of weights and thresholds (i.e., a random point on the error surface), the training algorithms incrementally seek for the global minimum. For Cuxhaven and Sylt, the optimum architecture of the two models types using SANN was determined by teaching many MLP networks that have different architectural parameters. For each model type, 25 trials have been carried out. In such way the time lags of input variables were changed from 0 to 24. In each trail several MLP networks were trained by varying (i) the number of neurons in the hidden layer from 1 to 10 neurons, (ii) the type of activation function (identity, logistic, tangent sigmoid, exponential and sine functions) in the hidden and output layers.

Stage 3- Determination of the optimum ANN architectural parameters

In each trial for the two ANN model types A and B at Cuxhaven and Sylt, only the best network based on the test set performance was selected. The results of the two models types for Cuxhaven indicate an increase in the correlation coefficient and stable decrease in Sum Square of Error (SSE) until d_u=18 hours, while for Sylt the same behaviour is observed but only until d_u=16 hours.

The optimum number of neurons in the hidden layer for the best selected MLP neural network changes from 3 to 10 neurons for both stations, which would give possibility to increase the over fitting chance. So, the exact number of neurons in the hidden layer will be determined in the second phase with the Matlab neural toolbox (Beale et al., 2013), which provides further architectural parameters configuration and efficient time series neural networks types more than SANN. Moreover, the candidate types of activation function of neurons in the hidden layer were either tangent sigmoid (tansig) or logarithm sigmoid (logsig). While the output layer has only one neuron with linear activation function.

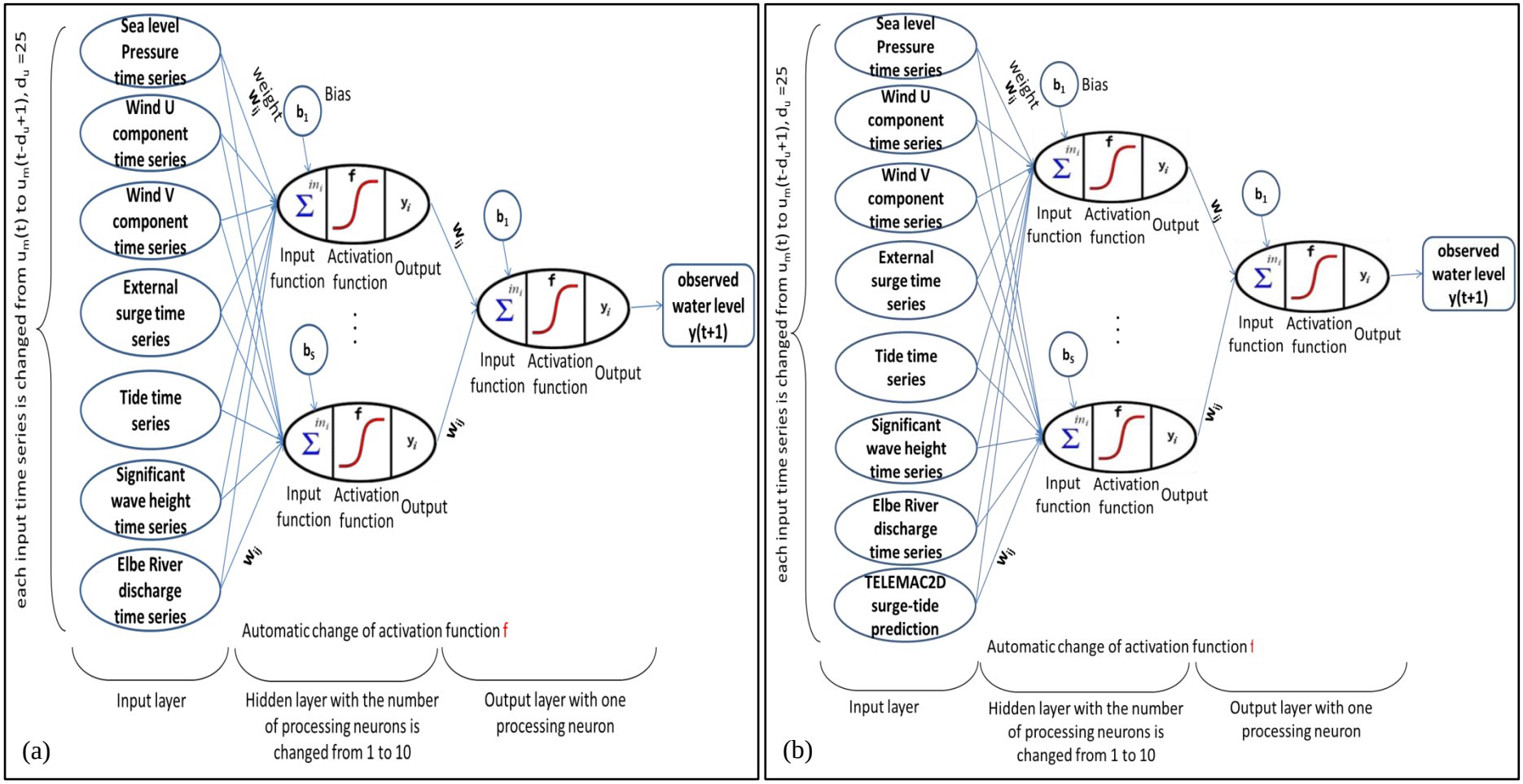

Figure 4.11: Change of the architectural parameters of Type-A (a) and Type-B (b) ANNs models for Cuxhaven (in case of Sylt without Elbe discharge input variable) (see Eq. (4.12) and (4.13)).

4.2.4 Determination of the optimal number of neurons in the hidden layer of NARX models by Matlab neural networks toolbox

The optimum MLP neural networks architecture developed using SANN consists of three feed forward layers i.e. with only one hidden layer, but the optimum number of neurons in this layer changes in the range from 3 to 10. If this number of neurons is not large enough, it will not capture the underlying behavior of the data. On the other hand, if it is larger than the underlying behaviour of nonlinear interaction between the storm-tide components, it may increase the over fitting chance and large computational time required for learning. In most cases, the selection of the optimal number of nodes (neurons) in the hidden layer is a trial-and-error procedure (Jayawardena & Fernando, 2001). The numbers of hidden neurons of both NARX models types were selected using the exhaustive search in the range from 3 to 10. These have been carried out in 8 trials for each NARX model type, through the following two steps:

Step 1-NARX Models formulation

The NARX neural network is a recurrent neural network model with feedback only from the output neurons. It has exogenous and endogenous time delayed inputs, which can be mathematically represented as follows (Menezes Jr & Barreto, 2008):

$$y(t+1) = f\big[y(t), y(t-1), \dots, y\big(t-d_y+1\big); u_m(t+1), u_m(t), \dots, u_m(t-d_u+1)\big], \quad m = 1,2, \dots, input\ variables\ number \tag{4.14}$$

where $d_u \geq 1$ and $d_y \geq 1$, $d_u \geq d_y$, are the input-memory and output-memory orders. The next value of the dependent output signal y(t) is regressed on previous values of the output signal and previous values of an independent (this means exogenous) input signals. The resulting connection architecture is becoming a NARX recurrent neural network, as shown in Figure 4.12.

For the determination of the number of hidden nodes, several NARX neural networks are developed using the optimum identified architectural parameters by SANN (see section 4.2.3). The two taped delay lines in each NARX network consists of d_u=18 hours for Cuxhaven and d_u=16 hours for Sylt. Furthermore, the selected activation functions for the hidden and output layers were respectively tansig and linear, as shown in Figure 4.13.

Step 2- NARX Models training and results

For Cuxhaven and Sylt, the number of hidden neurons for both NARX models types is determined using the exhaustive search in the range from 3 to 10. These had been carried out in 8 trials for each NARX models type using the built-in matlab Levenberg-Marquardt algorithm. In each trial, the number of the hidden layer neurons is increased by one then repeated 30

times because of the random weight initialization. The performance of these NARX models is "validated" according to the Mean Square Error (MSE) over the entire training, validation and test series.

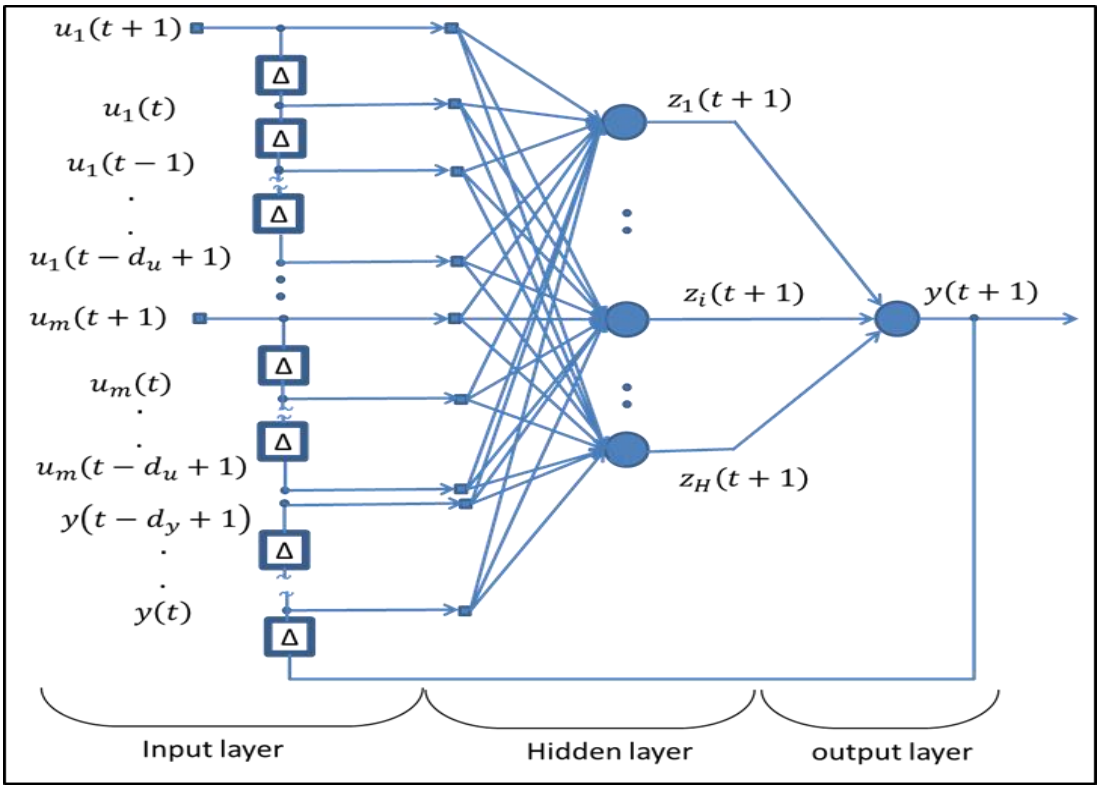

Figure 4.12: Schematic representation of a NARX neural network, the boxed "Δ" represents a delay.

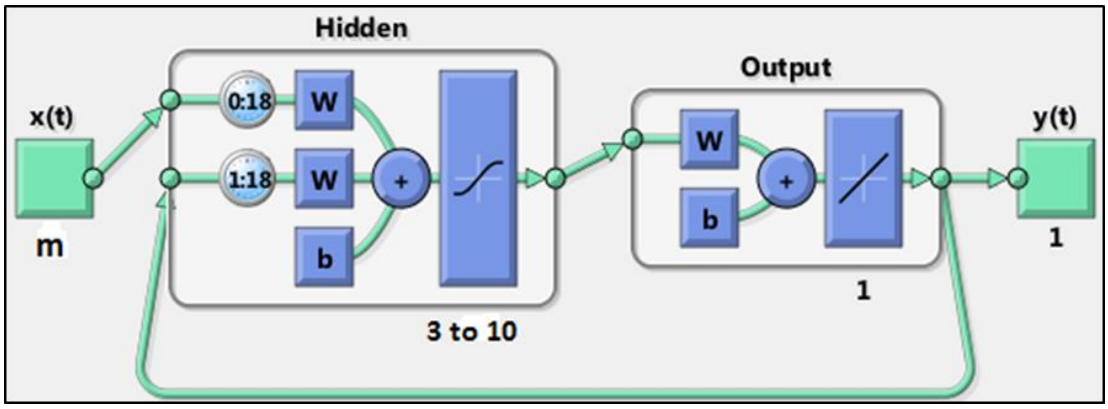

Figure 4.13: NARX architecture for determination of the number of hidden neurons with m input variables (see Figure 4.11), tansig and linear activation functions in the hidden and output layers respectively (screenshot from neural toolbox in MATLAB 2013b).

The MSE in each trial is characterized by a stable decrease (better performance) as the number of neurons in the hidden layer increases. This stable decrease of the MSE will change if the hidden neurons number leads to the over fitting problem. The lowest MSE for the two NARX models types is obtained with 8 neurons in the hidden layer based on its highest per-

formance. The lowest MSE over all the repetitions for NARX model Type-B at Cuxhaven, which is 0.022 m, is lower than its counterpart of NARX model Type-A with 0.029 m. which indicates a higher performance of NARX Type-B than NARX Type-A due to the inclusion of the predicted surge-tide by TELEMAC2D in its input variables. This was also confirmed for Sylt, since the lowest MSE over all the repetitions for NARX model Type-B, which is 0.014 m, is lower than its counterpart of NARX model Type-A with 0.020 m.

4.2.5 Implementation of the NARX models for Cuxhaven and Sylt

The SANN's time series analysis type generates a static feed forward MLP and all the dynamic information that could be learned from the past memories of the output (feedback) path is discarded. Hence, this simplified formulation, as shown in Eq. (4.12) eliminates a considerable portion of the representational capabilities as a dynamic neural network. In order to capture the dynamics of the nonlinear extreme storm-tide behaviour and to obtain a dynamic neural network model, there are two elements that can be used simultaneously: memory lines and feedback. So, for improving the accuracy and predictability of the developed SANN time series models, the NARX neural network is used instead and implemented by Matlab neural networks toolbox. The output feedbacks to the input layer (global feedback) in NARX networks.

For developing the final NARX models types, the optimum architectural parameters of the number of hidden layer neurons with 8 neurons, the input variables time lags with d_u=18 hours for Cuxhaven and d_u=16 hours for Sylt are used. Only the type of activation function is changed for hidden and output layers. The transfer functions tansig or logsig are possible in the hidden layer, while for the output layer tansig and linear functions are the most appropriate.

The development of each NARX model type has been implemented in four trials using the built-in matlab Levenberg-Marquardt algorithm. In each trial, the type of activation function is changed either for hidden or output layers then repeated 30 times because of the random weight initialization. These NARX models prediction results were "validated" in terms of correlation coefficient (CC), Root Mean Square of Error (RMSE), mean and standard deviation (σ) using the observed water level from 1998 to 2007 for Cuxhaven and from 2000 to 2007 for Sylt.

Table 4.4 and Table 4.5 list the best "validation" results of each NARX models type for Cuxhaven and Sylt, respectively. It is obvious from these tables that NARX Type-B models at both sites (Cuxhaven and Sylt) perform better (lower RMSE and higher correlation for Type B) than NARX Type-A models. Moreover, the tansig and linear activation functions in the hidden and output layers, respectively, provide the best performance for each NARX model type. For NARX Type-B models in Cuxhaven, the lowest RMSE is 0.153 m with correlation of 0.99. The best NARX Type-B model in Sylt has an RMSE of 0.124 m and correlation of 0.98.

Figure 4.14 shows the temporal variations of the best results for each NARX models type with the observed water level (η_{OB}) and the predicted storm-tide by coupled TELEMAC2D-TOMAWAC ($\eta_{st\text{-}t\ TEL\text{-}TOM}$) at Cuxhaven and Sylt during the storm of January 2000. NARX Type-B models show a relatively good performance during this storm. Moreover, the time of the highest peak of the storm-tide predicted by both NARX models types (η_A by NARX Type-A model and η_B by NARX Type-B model) occurred at the time of η_{OB} highest peak of the actually observed water level. This provides an indication of the nonlinear capability of both NARX models types to correct the predicted time of the numerically predicted water level $\eta_{st\text{-}t\ TEL\text{-}TOM}$. The later has at both sites two maximum peaks of about the same height during the storms of January 2000. Therefore, the highest peak of $\eta_{st\text{-}t\ TEL\text{-}TOM}$ at Sylt during the storm of January 2000 occurs 9 hours before the time of η_{OB} highest peak. This is due to the approximation of the nonlinear interaction between the components by TELEMAC2D-TOMAWAC, while both NARX models types learn from the observed storm-tide.

Table 4.4: Standard deviation (σ), Root Mean Square Error (RMSE) and correlation coefficient (CC) results of NARX models under change of the activation function in the hidden and output layers for Cuxhaven from 1998 to 2007.

hidden layer activation function	output layer activation function	mean	σ	RMSE	CC
observed	**observed**	0.153 m	1.108 m	0 m	1
Tansig	**linear**	0.154 m	1.106 m	0.160 m	0.989
Tansig	**Tansig**	0.146 m	1.109 m	0.165 m	0.988
Logsig	**linear**	0.141 m	1.099 m	0.164 m	0.988
Logsig	**Tansig**	0.172 m	1.117 m	0.173 m	0.987

(a) Type-A models without inclusion of the predicted surge-tide by TELEMAC2D in the input variables.

hidden layer activation function	output layer activation function	mean	σ	RMSE	CC
observed	**observed**	0.153 m	1.108 m	0 m	1
Tansig	**linear**	0.147 m	1.101 m	0.153 m	0.990
Tansig	**Tansig**	0.158 m	1.097 m	0.158 m	0.989
Logsig	**linear**	0.139 m	1.099 m	0.155 m	0.990
Logsig	**Tansig**	0.144 m	1.101 m	0.159 m	0.989

(b) Type-B models that include the predicted surge-tide by TELEMAC2D in the input variables.

Table 4.5: Standard deviation (σ), Root Mean Square Error (RMSE) and correlation coefficient (CC) results of NARX models under change of the activation function in the hidden and output layers for Sylt from 2000 to 2007.

hidden layer activation function	output layer activation function	mean	σ	RMSE	CC
observed	**observed**	0.057 m	0.705 m	0 m	1
Tansig	**linear**	0.056 m	0.706 m	0.132 m	0.982
Tansig	**Tansig**	0.059 m	0.707 m	0.135 m	0.981
Logsig	**linear**	0.057 m	0.705 m	0.132 m	0.982
Logsig	**Tansig**	0.069 m	0.702 m	0.134 m	0.981

(a) Type-A models without inclusion of predicted surge-tide by TELEMAC2D in the input variables.

hidden layer activation function	output layer activation function	mean	σ	RMSE	CC
observed	**observed**	0.057 m	0.705 m	0 m	1
Tansig	**linear**	0.056 m	0.698 m	0.124 m	0.984
Tansig	**Tansig**	0.066 m	0.694 m	0.125 m	0.98
Logsig	**linear**	0.067 m	0.697 m	0.124 m	0.984
Logsig	**Tansig**	0.061 m	0.691 m	0.125 m	0.983

(b) Type-B models that include the predicted surge-tide by TELEMAC2D in the input variables.

4.2.6 Improvement of NARX models for Cuxhaven and Sylt using ensemble methods

The NARX Type-B models give higher weights to the $\eta_{\text{su-t TEL}}$ input variable during training, since its data value was the nearest to the target variable η_{OB}. This, in some individual extreme storm events (see Figure 4.14(b)), may lead to either underestimate the maximum peaks of water level (e.g. storm of December 1999 at Cuxhaven) or to overestimate it (e.g. storm of January 2000 at Sylt). In order to overcome this problem especially in extreme storm-tide events, an ensemble has been developed, which averages results from the best NARX models.

The input deck of the ensemble fitting neural network (EFN) models (Figure 4.15) consists essentially of four different storm-tide prediction results from the best three NARX Type-A models and the best NARX Type-B model (see Table 4.4 and Table 4.5). In addition, the input deck contains the time lagged meteorological forces (sea level pressure, zonal and meridional wind speed components) for Cuxhaven or Sylt. The output of the EFN models is the difference between the observed storm-tide (η_{OB}) and the predicted storm-tide by NARX Type-B (η_B) either at Cuxhaven or Sylt. So, the developed EFN networks are trained in a way that

makes the developed EFN models learn more nonlinear interaction terms "if possible" without changing the long term time series prediction performance gained from the results of both NARX Types A and B.

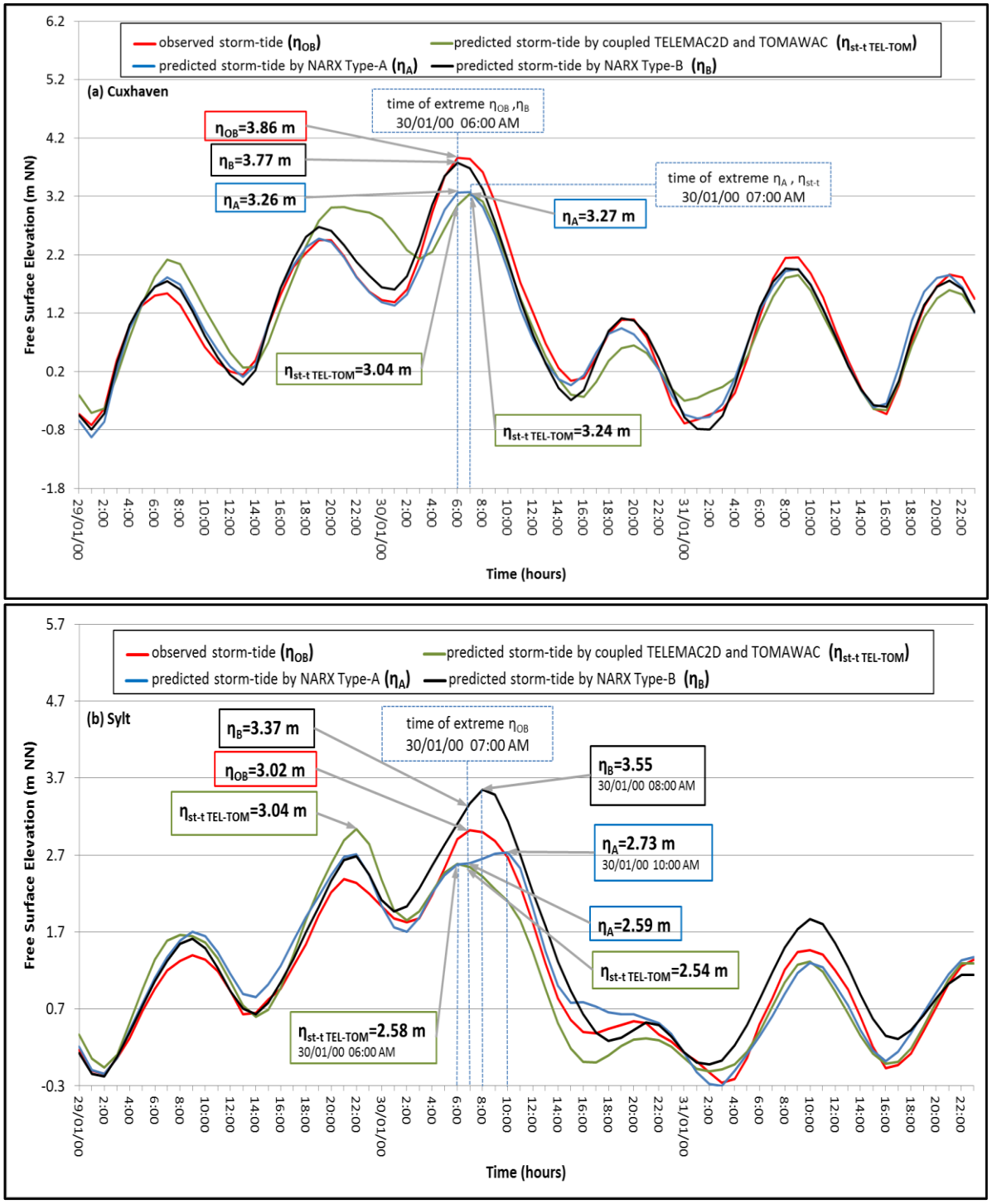

Figure 4.14: Results of NARX model types A and B during the storm of January 2000 at Cuxhaven (a) and Sylt (b).

The optimum architectural parameters (Figure 4.15) are: one neuron in the hidden and output layers with the time lags of meteorological input variables d_u=18 hours for Cuxhaven and d_u=16 hours for Sylt. Only the activation function type is changed for the hidden and output layers. The transfer functions tansig or logsig are possible in the hidden layer, while for the output layer tansig, logsig and linear functions are more appropriate candidates. The development of EFN models has been implemented in six trials using the built-in matlab Levenberg-Marquardt algorithm. In each trial, the activation function type is changed either for the hidden or output layers, and then repeated 30 times because of the random weight initialization.

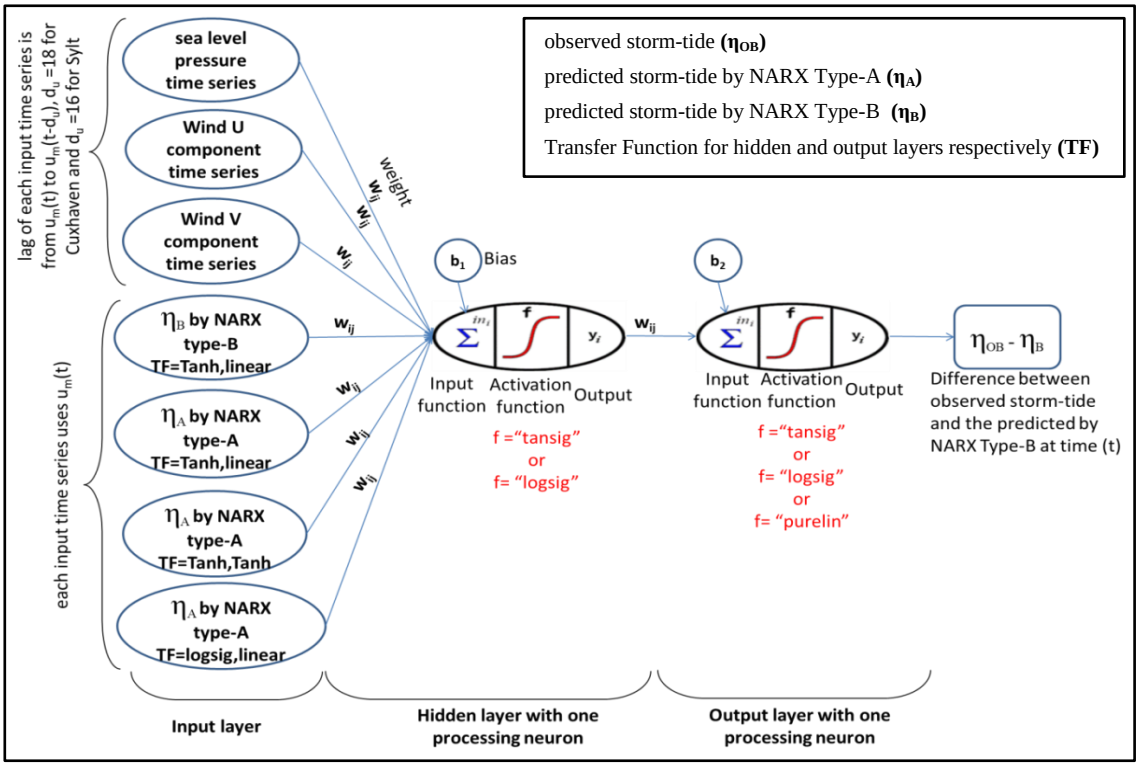

Figure 4.15: Input and output variables of the Ensemble Fitting Network (EFN) for Cuxhaven and Sylt with one neuron in the hidden and output layers.

Using the observed water level during storms from 1998 to 2007 for Cuxhaven and from 2000 to 2007 for Sylt, the EFN model prediction results (η_{EFN}) were "validated" in terms of correlation coefficient (CC), RMSE and σ. The results show that the logsig and tansig activation functions in the hidden and output layers respectively give the best performance (lowest RMSE and highest correlation) for Cuxhaven and Sylt. For the EFN models in Cuxhaven, the lowest RMSE is 0.148 m with a correlation of 0.99. The best EFN model for Sylt has an RMSE of 0.124 m and a correlation of 0.98.

The validation results of best η_{EFN} are close in value to its counterparts from the best NARX Type-B results at both sites Cuxhaven and Sylt (see Table 4.4 and Table 4.5). So, the long term prediction performance gained with the results of NARX model Type-B is inherited inside the η_{EFN} as shown in Figure 4.16. During the storm of January 2000 at Sylt and in De-

cember 1999 at Cuxhaven (Figure 4.16), the height and occurrence time of η_{EFN} highest peak are approximately the same as those of the actually observed water level η_{OB}.

The inter-comparison of the actually observed water level (η_{OB},), the numerically predicted water level ($\eta_{su\text{-}t\ TEL}$) and the ensemble results (η_{EFN}) is graphically summarized by meaningfully making use of the Taylor diagram approach (Taylor, 2001) as shown in Figure 4.17. The η_{OB} data from 1998 to 2007 for Cuxhaven and from 2000 to 2007 for Sylt are used for this comparison. The position of each label on the Taylor diagram is determined by the values of the correlation coefficient (CC), root mean square of error (RMSE) and standard deviation (σ). In the Taylor diagrams, these statistical parameters are normalized by dividing both the RMSE and the σ of the compared results by the standard deviation of the observations ($\sigma_{observed}$). The key issue in the Taylor diagram approach (Taylor, 2001) is to recognize the relationship between the four statistical parameters of interest (here RMSE, σ_{result}, $\sigma_{observed}$ and CC):

$$(\mathrm{RMSE})^2 = (\sigma_{\mathrm{result}})^2 + (\sigma_{\mathrm{observed}})^2 + 2 * \sigma_{\mathrm{result}} * \sigma_{\mathrm{observed}} * \mathrm{CC} \qquad (4.15)$$

The η_{EFN} results have a correlation of 0.99, 0.98 and a normalized RMSE of 0.13 m, 0.17m at Cuxhaven and Sylt, respectively. Moreover, the EFN models perform better during the individual extreme storm events than NARX model Type B as depicted in Figure 4.16 during the storms of December 1999 at Cuxhaven and January 2000 at Sylt .The ensemble models (η_{EFN}) predict correctly the occurrence time of the η_{OB} highest peak during the storm of December 1999 at Cuxhaven, while the occurrence time of η_B highest peak predicted by NARX model type B is delayed by one hour. Moreover, the η_{EFN} highest peak resulting from the ensemble model reaches 3.84 m, which is better predicted than by NARX model type B with η_B peak of only 1.9 m. However, there is still a difference of 0.66 m between η_{EFN} and η_{OB} during the storm of December 1999 (called Anatol) at Cuxhaven, which is mainly due to the overestimation of the predicted sea level pressure by the climate model SN-REMO as compared to the observed pressure. The observed core pressure of Anatol on 3rd of December is 953 hPa (Nilsson et al., 2005), while the predicted by SN-REMO reaches 986 hPa. It decreases the water level by one centimeter for each hPa increase in pressure, which reaches 33 cm. Moreover, this increase in sea level pressure results in a reduction of predicted wind speed than the observed during the storm, which reaches up to 5 m/s (Nilsson et al., 2005) and decrease further the predicted water level. Hence, this leads to the shift down of η_{EFN} curve even at the trough, which occurs before the highest peak (see Figure 4.16(a)). During the storm of January 2000 at Sylt, the η_{EFN} highest peak is exactly the same as the η_{OB} highest peak with 3.02 m, while the η_B maximum highest peak predicted by NARX model type B is overestimated.

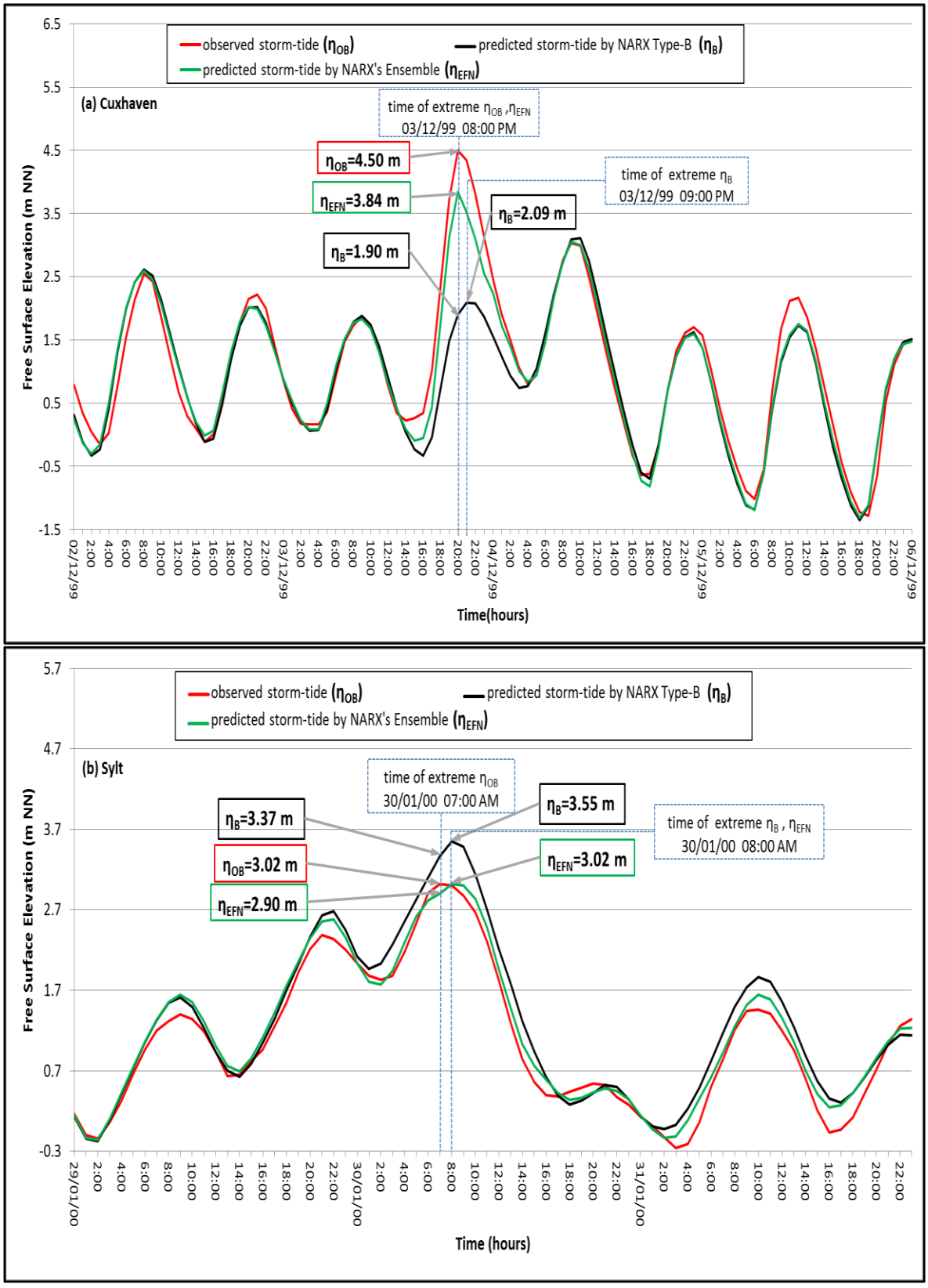

Figure 4.16: Results of NARX ensemble models and NARX Type-B models at Cuxhaven during the storm of December 1999 (a) and at Sylt during the storms of January 2000 (b).

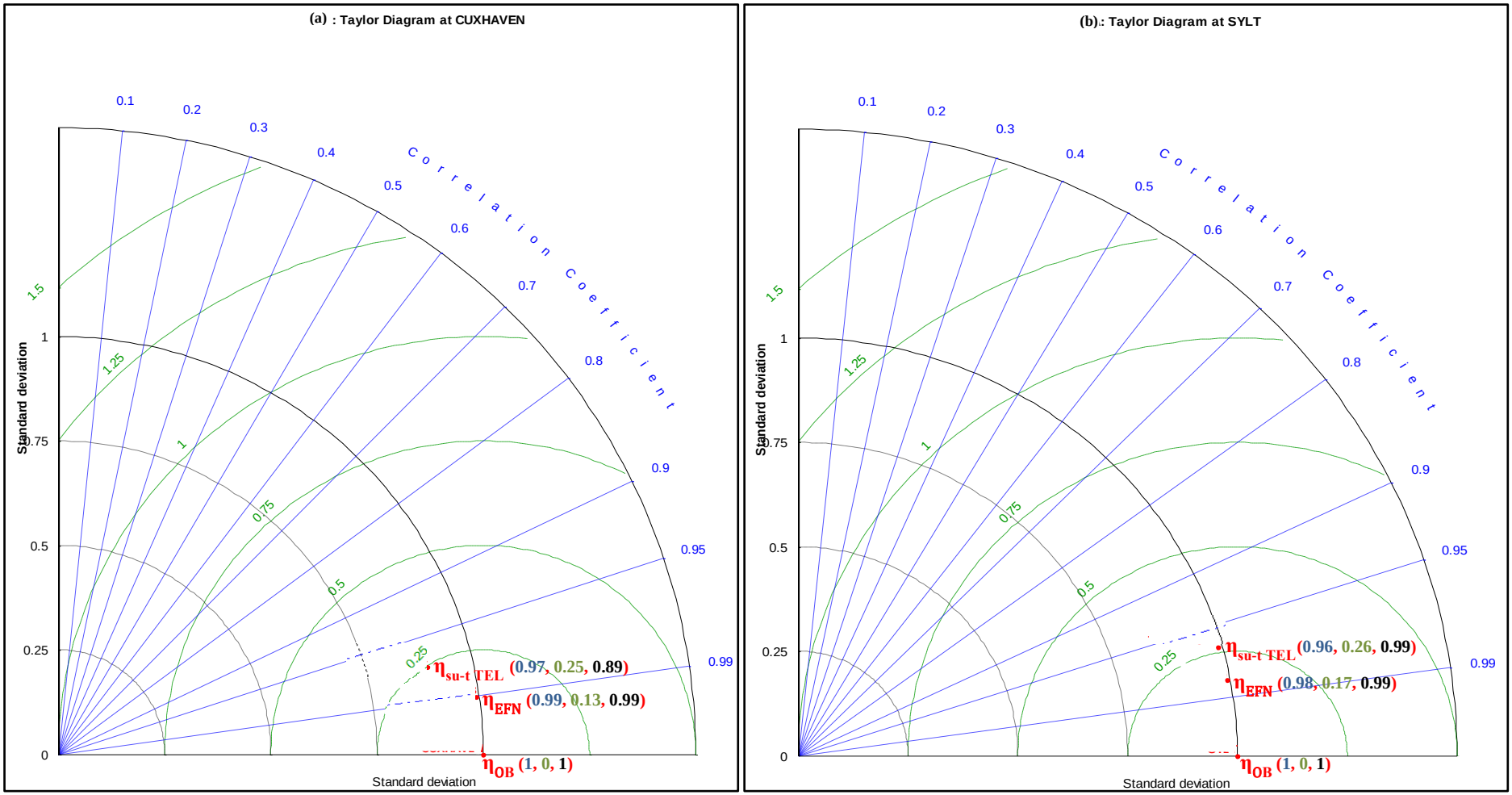

Figure 4.17: Taylor diagrams of the observed storm-tide (η_{OB}), the predicted surge-tide ($\eta_{su\text{-}t\ TEL}$) by TELEMAC2D and the predicted storm-tide (η_{EFN}) by NARX Ensemble models at Cuxhaven (a) and Sylt (b) based on the correlation coefficient (CC), normalized root mean square error (RMSE) and normalized standard deviation (σ).

Two types of extreme water level models were developed for Cuxhaven (Elbe Estuary) and Sylt (Open coast) in the North Sea, Germany which are (i) artificial neural models (Nonlinear Autoregressive with eXogeneous inputs (NARX)) (Type-A) and (ii) Combination of the NARX models with the hydrodynamic models (Type-B). The input deck of the two NARX models types consists of the astronomical tidal forecasts, significant wave height produced by TOMAWAC numerical wave model, the two wind speed components, external surge from Wick station, and sea level pressure for Cuxhaven and Sylt in addition to Elbe river discharge (in case of Cuxhaven only). Afterward an ensemble of both NARX model types has been developed using the ensemble fitting neural network (EFN) in order to reduce variance and minimize error especially for extreme events. This hybrid modelling approach considers the nonlinear interaction of the different extreme storm-tide components, so that the substantial errors in both magnitude and timing of the peak extreme storm-tide water level can be corrected.

The inter-comparison of the actually observed water level (η_{OB},), the numerically predicted water level ($\eta_{su\text{-}t\ TEL}$) and the ensemble results (η_{EFN}) is graphically summarized by meaningfully making use of the Taylor diagram approach (Taylor, 2001). The η_{EFN} results have a correlation of 0.99, 0.98 and a normalized RMSE of 0.13 m, 0.17m at Cuxhaven and Sylt, respectively. Moreover, the EFN models perform better during the individual extreme storm events than NARX model Type B.

4.3 Evaluation of the effect of nonlinear interactions between extreme storm-tide components

The used hydrodynamic model "TELEMAC2D" (version 6.2 in parallel processing mode) solves the non-conservative form of the shallow water equations, written with h (depth) and u, v (flow velocity components) as the unknowns (Hervouet, 2007). It considers the propagation of long waves such as surge and tide, including the non-linear interaction between them. The numerical solution of these equations is based upon the fractional step method with two steps: (i) Advection and (ii) Propagation, diffusion and source terms (representing the wind, Coriolis force, bottom friction, a source or sink of momentum within the domain). The method of characteristics has been applied to solve the advection of velocities u and v. The propagation, diffusion and source terms are solved by the finite element method, where an implicit time discretization allows the elimination of the non-linearity in the equations. In that case, the nonlinear terms are approximated linearly in time. Variation in the formulations and space discretization transform the continuous equations into a linear discrete system, which is solved using an iterative procedure based on the conjugate gradient method (Hervouet & Van Haren, 1994). This treatment of the nonlinear terms can lead to either underestimated or overestimated water level peaks during extreme storms and to incorrect prediction of their occurrence times.

4.3.1 Overall approach

A proper prediction based on the complete understanding of the processes underlying the nonlinear interactions may require several decades to be implemented in the current operational hydrodynamic models. Therefore, the data-driven modeling using ANN methodology is used for complementing the nonlinear interaction terms by learning from the observed water levels. Through a combined use of the developed NARX ensemble and a state of the art hydrodynamic model such as "TELEMAC2D", it is possible to extract the nonlinear interaction between the different extreme storm-tide components as summarized in the following nine steps (Figure 4.18):

1. Prescribe the forcing responsible for the generation of all extreme storm-tide components to the North Sea mesh in TELEMAC2D (Figure 3.8) as "inputs" along with their boundary conditions (e.g. sea level pressure, meridional and zonal wind speed components represent the forcing factors for storm surge component).
2. Evaluate each component of the extreme storm-tide $\eta_{st\text{-}t}$ (as defined in Figure 2.15) independently using the North Sea mesh in TELEMAC2D (Figure 3.8). So, the boundary conditions of each component are prescribed separately for the North Sea model area.
3. The components obtained from step 2 are linearly superposed in order to predict the linear surge-tide for Cuxhaven or Sylt (η_L); i.e. the nonlinear interaction between the components is not considered. The linear surge-tide does not include the wave setup effect (η_w), since it has almost no contribution to the observed storm-tide at Cuxhaven and Sylt (see section 4.2.1).
4. Drive the North Sea mesh in TELEMAC2D using the boundary conditions of all components, which are prescribed simultaneously in order to predict the surge-tide ($\eta_{su\text{-}t\ TEL}$).
5. Calculate the difference between $\eta_{su\text{-}t\ TEL}$ predicted in step 4 and η_L predicted in step 3 in order to extract the nonlinear interaction between the components as approximated in TELEMAC2D (η_{NLT}).
6. Calculate the difference between the observed storm-tide (η_{OB}) and the approximated surge-tide by TELEMAC2D ($\eta_{su\text{-}t\ TEL}$), which are assumed to represent the complementary nonlinear interaction (η_{NLE}): so $\eta_{NLE} = \eta_{OB} - \eta_{su\text{-}t\ TEL}$.
7. Train and develop the NARX ensemble models using the η_{NLE} calculated in step 6, which is not considered by TELEMAC2D.
8. Predict the complementary nonlinear interaction η_{NLE} using the developed NARX ensemble models for Cuxhaven and Sylt from 1991 to 2007.
9. Linearly add the approximated nonlinear interaction η_{NLT} by TELEMAC2D of step 5 and its complementary η_{NLE} by NARX ensemble models of step 8 in order to get the total nonlinear interaction (η_{NL}): $\eta_{NL} = \eta_{NLT} + \eta_{NLE}$.

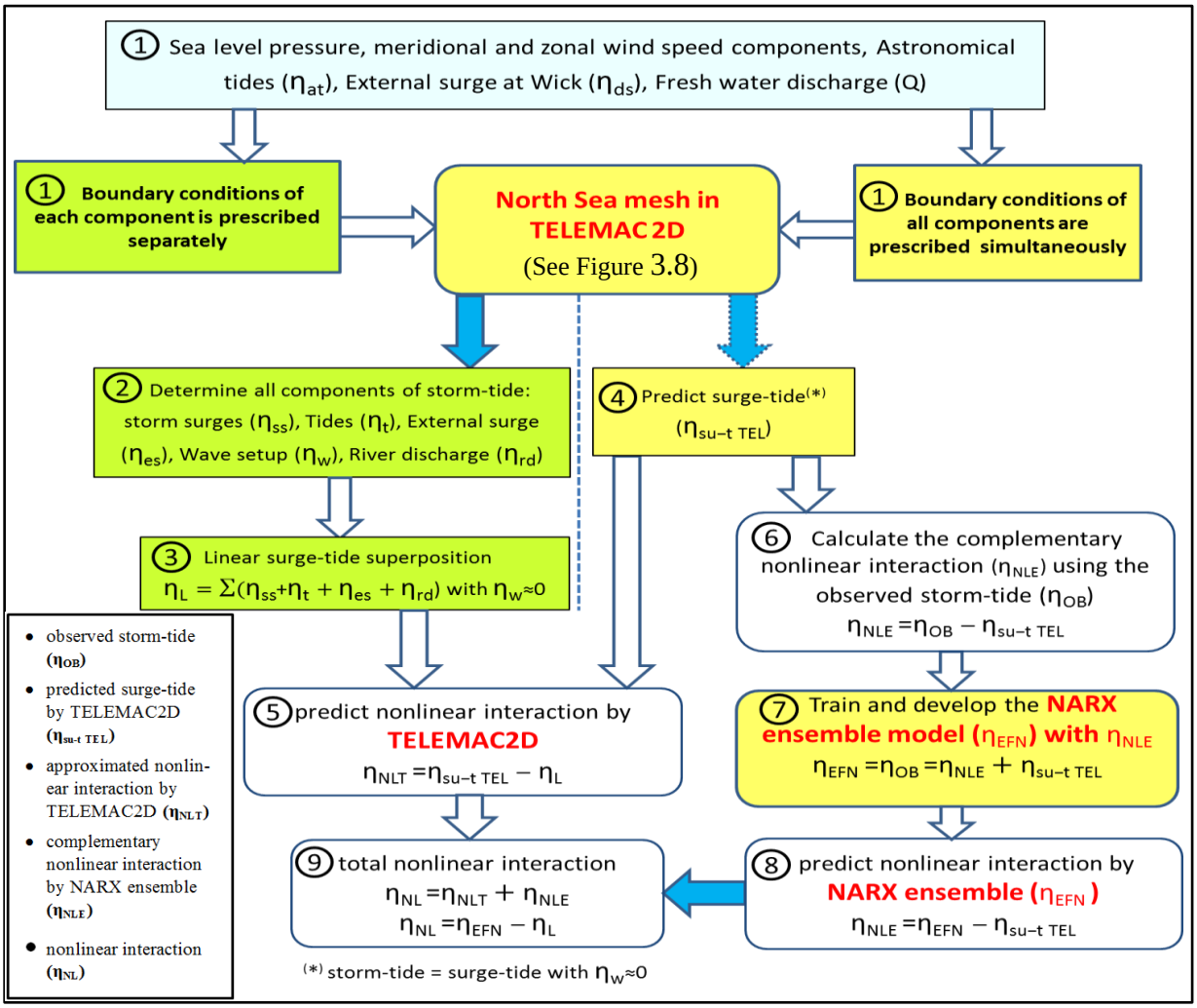

Figure 4.18: Extraction of the component η_{NL} resulting from the nonlinear interactions between the different extreme surge components for Cuxhaven and Sylt.

4.3.2 Extraction of the nonlinear interaction approximated by the numerical model in the $\eta_{su\text{-}t\ TEL}$ results (steps 1 to 5 in Figure 4.18)

(a) Procedure

For the extraction of the approximated nonlinear interaction effect (η_{NLT}) considered in the predicted surge-tide by TELEMAC2D ($\eta_{su\text{-}t\ TEL}$), the linear superposition of the extreme surge-tide components (η_L) should be subtracted from the $\eta_{su\text{-}t\ TEL}$: $\eta_{NLT} = \eta_{su\text{-}t\ TEL} - \eta_L$. The η_L consists of the linear addition of tide (η_L), storm surge (η_{ss}), external surge (η_{es}) and rivers discharge (η_{rd}) effects, which are simulated independently from each other by TELEMAC2D over the North Sea area (Figure 3.8). The calculated η_{NL} is based on the assumption that the individual storm-tide components are simulated with enough accuracy. This assumption is validated as the predicted tide reproduces almost exactly the tide measured in the German Bight. The correlation coefficient between measured and predicted tide reaches 0.99, while

the RMSE is less than 0.11 m (see section 3.2.3). Nevertheless, the uncertainty due to storm surge and external surge components may require further accuracy sensitivity analysis. The effect of wave setup (η_w) on the extreme storm-tide depends on the location of the selected site (inside or outside the surf zone). Both sites are outside of the surf zone and the effect of wave setup on the η_L and $\eta_{su\text{-}t\ TEL}$ can thus be neglected (see section 4.2.1).

For the surge-tide $\eta_{su\text{-}t\ TEL}$ simulations by TELEMAC2D, the boundary conditions of the North Sea hydrodynamic model are prescribed using all of the extreme storm surges components between 1991 and 2007 (Tayel & Oumeraci, 2012b). These boundary conditions are shown in Figure 3.8, on the northern open sea boundary (Northern border: Scotland-Norway), the tidal water level on each node and the external surge either from Wick or Lerwick stations are linearly added. On the western boundary (West border: France-England) only the tidal water level is prescribed at each node. So, the influence of the shallow water can be taken into account when the tidal wave plus external surge propagate from the open boundary up to the German coast. On the southern onshore edge of the estuaries the fresh water discharge of the adjacent rivers / estuaries are prescribed at each river section. In the linear superposition surge-tide η_L simulations, the boundary conditions for each component are prescribed separately in order to evaluate its effect during storms. For example, only the tidal water level on each node of the Northern and West borders are prescribed for evaluating the tidal effect, while the meteorological forces only drive the model for evaluating the storm surge effect without prescribing any of the open-sea or river discharge boundary conditions.

(b) Results

During the storms of January 2000, November 2006 and November 2007, the temporal variations of the predicted linear superposition η_L with the contribution of each component at Cuxhaven and Sylt are predicted. At the times of the observed extreme water level η_{OB} ($(\eta_{OB})_{max}$) during these three storms, the highest η_L peaks at Cuxhaven reach 3.22 m, 3.17 m and 3.31 m for the storms in January 2000, November 2006 and November 2007, respectively, which are higher than their counterparts at Sylt of 2.52 m, 1.96 m and 2.44 m, respectively. Since the contribution of storm surge (η_{ss}) and tide (η_t) at Sylt are lower than those at Cuxhaven due to the difference in geographical locations of the two sites. The storm surge, tide and external surge components have the largest contribution to the η_L at both sites, while the effect of rivers discharge and wave setup are almost negligible. Figure 4.19 shows the contribution of each extreme storm-tide component during the storm of January 2000 at Cuxhaven and Sylt. The highest contribution is from storm surge effect with maximum of 3.00 m and 2.28 m at Cuxhaven and Sylt, respectively. The tide effect is less than the storm surge at the time of $(\eta_{OB})_{max}$ in both sites; it reaches 1.00 m and 0.56 m at Cuxhaven and Sylt, respectively. Only during the storm of January 2000, the external surge has positive effect on η_L in Cuxhaven and Sylt at the times of $(\eta_{OB})_{max}$ by 0.34 m and 0.26 m, respectively. In contrast during the storms of November 2006 and 2007 in both sites, the external surge has negative effect on η_L ranging from -0.05 m to -0.13 m at the times of $(\eta_{OB})_{max}$.

For Cuxhaven and Sylt during the storms of January 2000, November 2006 and November 2007, the heights of η_L peaks overestimate always the $\eta_{su\text{-}t\ TEL}$ peaks that include the nonlinear interaction η_{NLT} approximated by the numerical model TELEMAC2D. At the times of $(\eta_{OB})_{max}$ during these three storms, the predicted $\eta_{su\text{-}t\ TEL}$ reach 3.04 m, 2.97 m and 3.19 m respectively at Cuxhaven, which are lower than the predicted η_L of 3.22 m, 3.17 m and 3.31 m, respectively for the storms in January 2000, November 2006 and November 2007.

Figure 4.20 shows the temporal variations of the predicted linear superposition η_L and surge-tide $\eta_{su\text{-}t\ TEL}$ by TELEMAC2D in addition to the approximated nonlinear interaction (η_{NLT}) at Cuxhaven and Sylt during the storm of January 2000. The extreme linearly predicted water level η_L ($(\eta_L)_{max}$) and the extreme predicted surge-tide $\eta_{su\text{-}t\ TEL}((\eta_{su\text{-}t\ TEL})_{max})$ at Cuxhaven reach 3.37 m and 3.24 m respectively, while they were 3.28 m and 3.04 m at Sylt respectively. At both sites, the occurrence times of $(\eta_L)_{max}$ and $(\eta_{su\text{-}t\ TEL})_{max}$ during this storm are exactly the same. Moreover, the $(\eta_{su\text{-}t\ TEL})_{max}$ at Sylt during the storms of January 2000 and November 2006 occur before the $(\eta_{OB})_{max}$ by 9 hours. Since the highest storm surge peak at Sylt during these storms are synchronized approximately with high tide (see Figure 4.19(b)). Furthermore, the maximum positive external surge of 0.5m (Figure 4.19(b)) at Sylt occurred at the time of storm surge peak during the storm of January 2000.

4.3.3 Extraction of the complementary terms for the nonlinear interaction using the predicted η_{EFN} results (steps 6 to 8 in Figure 4.18)

(a) procedure

The predicted storm-tide by NARX ensemble (η_{EFN}) includes the complementary terms (η_{NLE}) for the approximated nonlinear interaction by TELEMAC2D (η_{NLT}). The complementary terms (η_{NLE}) are basically the linear addition of (see section 4.2)

(i) Difference between the predicted storm-tide by NARX Type-B model (η_B) and the predicted surge-tide by TELEMAC2D ($\eta_{su\text{-}t\ TEL}$).

(ii) Difference between the predicted storm-tide by NARX ensemble (η_{EFN}) and the predicted storm-tide by NARX Type-B model (η_B).

So, the predicted η_{NLE} is obtained by direct subtraction of the predicted $\eta_{su\text{-}t\ TEL}$ from η_{EFN} (i.e. $\eta_{NLE} = \eta_{EFN} - \eta_{su\text{-}t\ TEL}$). Since the developed NARX ensemble is trained based on the observed water level (η_{OB}), so the predicted storm-tide by η_{EFN} and η_{OB} are considered as equivalent (see step 7 in Figure 4.18).

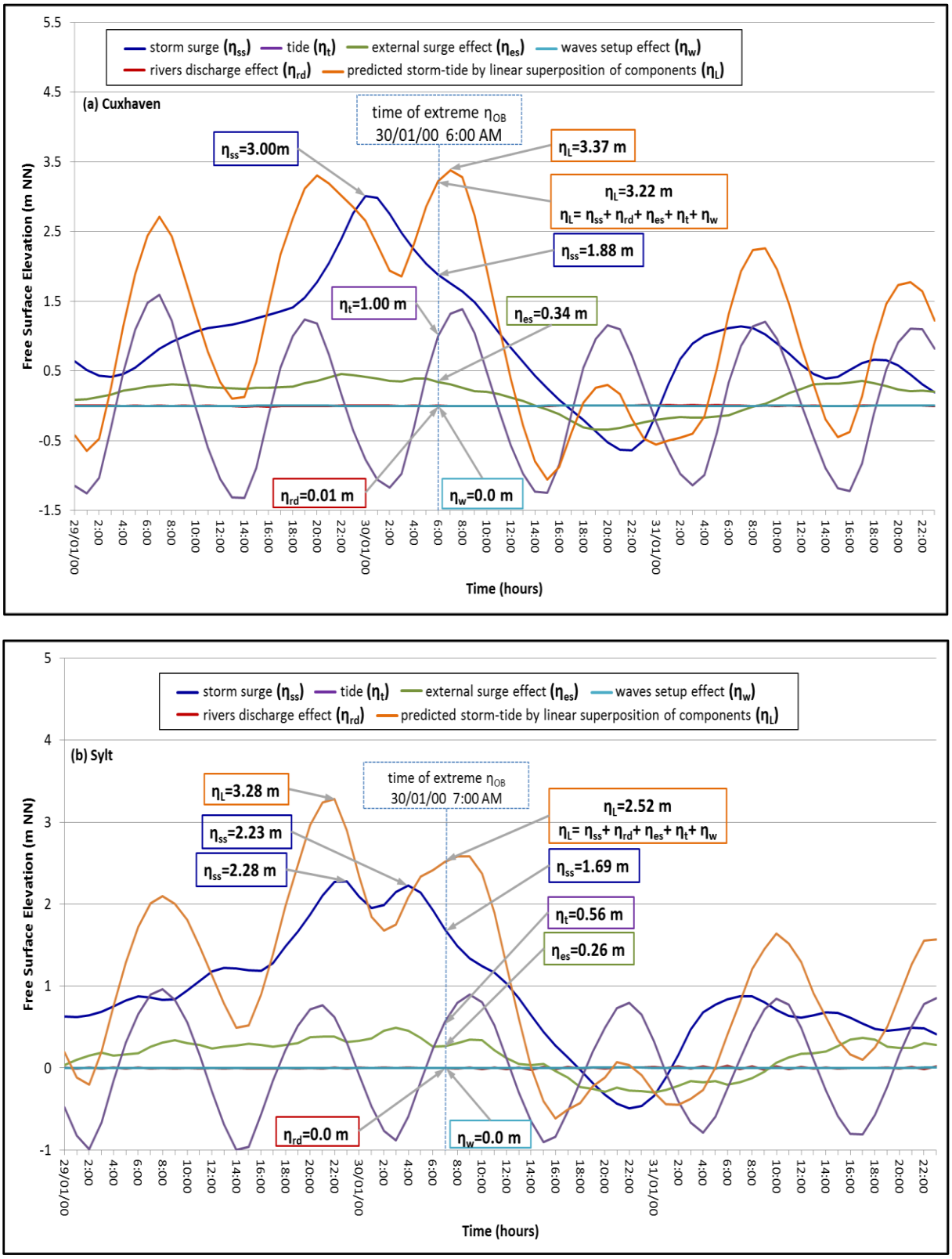

Figure 4.19: Storm-tide prediction by linear superposition η_L and contribution of each extreme storm-tide component during the storm of January 2000 at Cuxhaven (a) and Sylt (b).

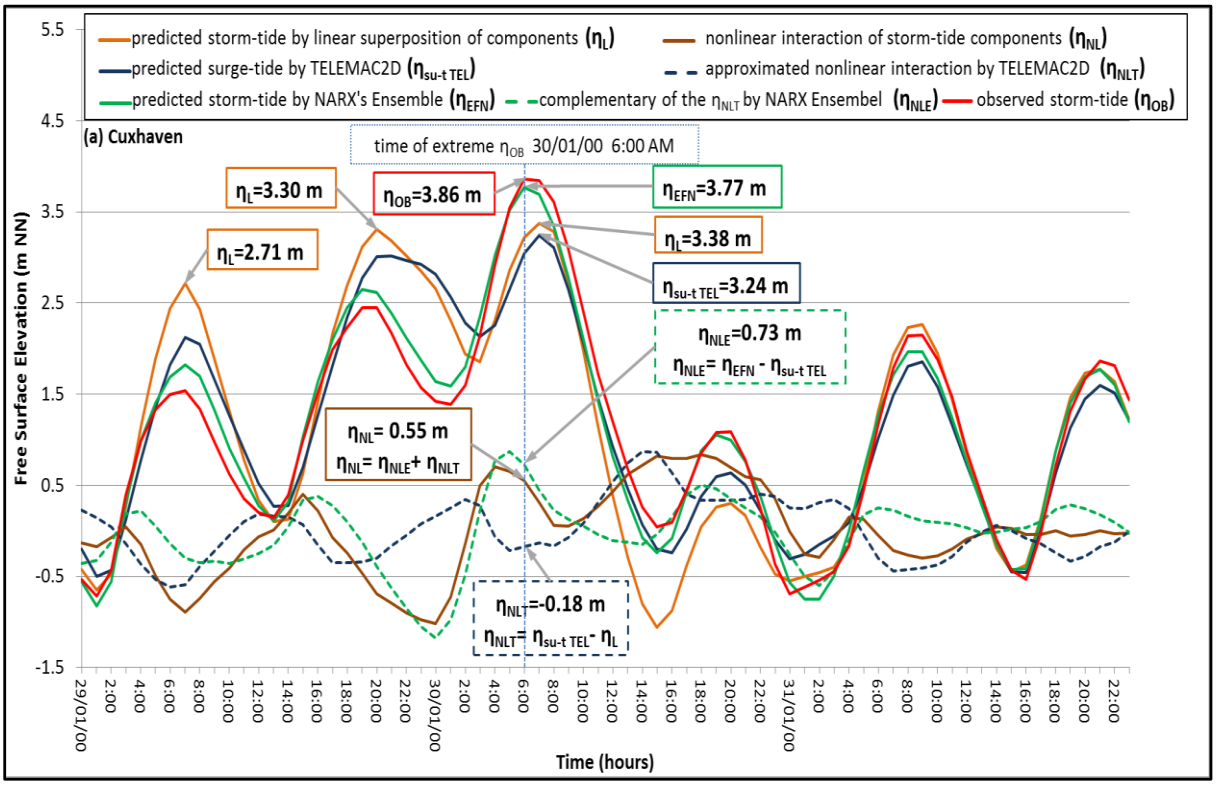

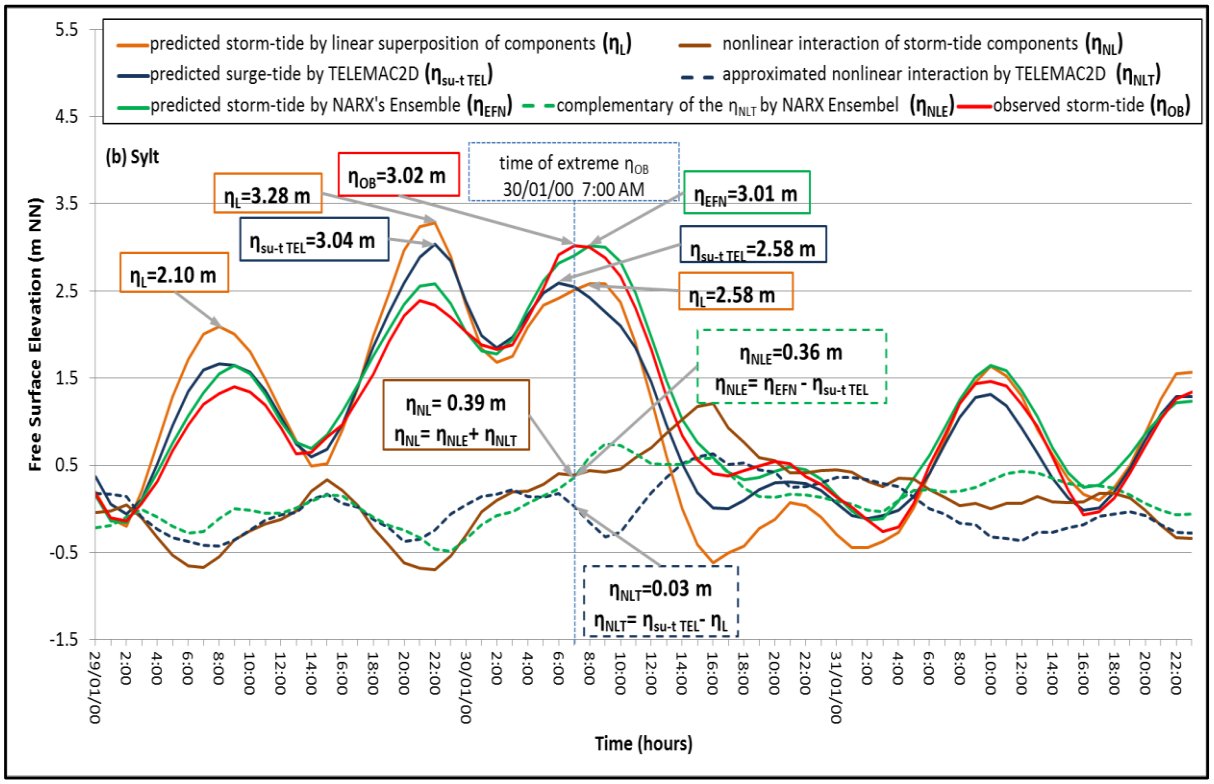

Figure 4.20: Storm-tide prediction by linear superposition η_L, TELEMAC2D $\eta_{su\text{-}t\ TEL}$ and NARX ensemble η_{EFN} with the effect of nonlinear interaction η_{NL} between extreme storm-tide components during the storm of January 2000 at Cuxhaven (a) and Sylt (b).

(b) Results

The temporal variations of η_{EFN} with the complementary terms (η_{NLE}) at Cuxhaven and Sylt are predicted for the storms of January 2000, November 2006 and November 2007. The η_{EFN} peaks, which occur directly before the times of $(\eta_{OB})_{max}$ at both sites, are always overestimated by the predicted $\eta_{su\text{-}t\ TEL}$ peaks and η_L peaks. This is due to the strong reduction of η_{EFN} peaks by η_{NLE} and η_{NLT}. At Cuxhaven during these three storms, the effect of η_{NLE} causes a reduction of the η_L peaks, which occurs directly before the times of $(\eta_{OB})_{max}$, by -0.12 m, -0.36 m and -0.14 m in addition to the reduction of η_{NLT} by -0.34 m, -0.18 m and -0.34 m respectively for the storms of January 2000, November 2006 and November 2007. In contrast, at the times of $(\eta_{OB})_{max}$ in Cuxhaven and Sylt, The η_{NLE} results in the overestimation or underestimation of the η_{EFN} peaks when compared with the $\eta_{su\text{-}t\ TEL}$ and η_L peaks (Table 4.6) according to the following two conditions:

(i) If the η_L and $\eta_{su\text{-}t\ TEL}$ peaks, which occur directly before the time of extreme η_{EFN} ($(\eta_{EFN})_{max}$), are < 3.00 m and < 2.50 m respectively, then their following peaks would overestimate the peak of η_{EFN} at the time of $(\eta_{EFN})_{max}$. Since the peaks of η_{EFN}, η_L and $\eta_{su\text{-}t\ TEL}$, which occur before the times of peak $(\eta_{EFN})_{max}$, do not increase the mean water level (MWL) during the storm significantly. Therefore, the following peaks of η_{EFN}, η_L and $\eta_{su\text{-}t\ TEL}$will propagate under a pronounced shoaling effect that increase their heights simultaneously. For example, the η_{NLE} decreases $(\eta_{su\text{-}t\ TEL})_{max}$ by -0.08 m and -0.11 m respectively during the storms of November 2006 (see Figure 4.21(b)) and November 2007 at Sylt. Moreover, the η_{NLT} causes a decrease of $(\eta_L)_{max}$ by -0.04 m and -0.14 m respectively, which is added to the η_{NLE} decrease and support it.

(ii) If the η_L and $\eta_{su\text{-}t\ TEL}$ peaks, which occur directly before the time of $(\eta_{EFN})_{max}$, are ≥ 3.00 m and ≥ 2.50 m respectively, then their following peaks would underestimate the peak of η_{EFN} at the time of $(\eta_{EFN})_{max}$. Since only the peaks of η_L and $\eta_{su\text{-}t\ TEL}$, which occur before the times of $(\eta_{EFN})_{max}$, increase the MWL during the storm to a limit by which their following peaks will propagate under no shoaling effect. Therefore, the following peaks of η_L and $\eta_{su\text{-}t\ TEL}$will propagate in deeper water with less pronounced shoaling, which decrease their heights simultaneously. In contrast, the peak of η_{EFN} propagates under strong shoaling effect that increases its height, as their counterparts in condition (i). For example, during the storms of January 2000 (Figure 4.20(a)), November 2006 (Figure 4.21(a)) and November 2007 at Cuxhaven, the η_{NLE} increases $(\eta_{su\text{-}t\ TEL})_{max}$ by 0.53 m, 0.21 m and 0.29 m respectively. However, the η_{NLT} decreases $(\eta_L)_{max}$ by -0.14 m, -0.20 m and -0.12 m respectively for the storms of January 2000, November 2006 and November 2007.

Bottom stress (Eq. (3.9)) and wind surface stress (see Eq. (3.30) and (3.31)) consider the reciprocal of the water depth h. These equations indicate that increases in h yield reduced influ-

ences of surface and bottom stresses on total water levels (Arns et al., 2015). Arns et al. (2015) indicates that taking atmospheric forcing into account partly compensates tidal high water increases by surge reduction due to increases in the water depth. Moreover, the high water levels are shifted towards an earlier occurrence, and this is also mainly a result from water depth increases causing reduced shallow water effects and friction.

During these three storms, the times of $(\eta_L)_{max}$ and $(\eta_{su\text{-}t\ TEL})_{max}$ are shifted with the same amount of time from the time of $(\eta_{OB})_{max}$ at both site. Therefore, only the complementary nonlinear terms η_{NLE} can be considered as the main factor to shift the times of $(\eta_{EFN})_{max}$. During the storm of November 2006 at Sylt (see Figure 4.21(b)), the times of η_L and $\eta_{su\text{-}t\ TEL}$ peaks occurred two hours before the time of $(\eta_{OB})_{max}$ and $(\eta_{EFN})_{max}$.

4.3.4 Nonlinear interaction between all storm-tide components (step 9 in Figure 4.18)

(a) procedure

Since the predicted storm-tide by η_{EFN} and η_{OB} are considered as equivalent (see step 7 in Figure 4.18), the nonlinear interaction between all storm-tide components at Cuxhaven and Sylt (η_{NL}) is the difference between the predicted storm-tide by NARX ensemble (η_{EFN}) and the linear storm-tide (η_L): ($\eta_{NL} = \eta_{EFN} - \eta_L$). So, the η_{NL} obtained in step 9 in Figure 4.18 can be considered as equivalent to the linear superposition of the nonlinear interaction η_{NLT} approximated in step 5 by TELEMAC2D and the complementary nonlinear terms η_{NLE} predicted by NARX ensemble (EFN) trained in step 7 by the results of step 6: $\eta_{NL} = \eta_{NLT} + \eta_{NLE}$

(b) Results

At Cuxhaven during the storms of January 2000, November 2006 and November 2007 (Table 4.6), the inclusion of the total nonlinear interaction η_{NL} in the predicted η_{EFN} leads to overestimate the result $(\eta_L)_{max}$ obtained from linear superposition in Step 3 by 0.39 m, 0.01 m and 0.17 m respectively. Moreover, the time of arrival for $(\eta_{EFN})_{max}$ during the storm of November 2006 at Cuxhaven is delayed by one hour (Figure 4.21(a)). Since the increase effect by η_{NLE}, which is mainly from the storm-tide wave shoaling, results in the slowing down and increasing height of $(\eta_{EFN})_{max}$. In contrast, at Sylt during the storms of November 2006 (Figure 4.21(b)) and November 2007, the inclusion of the η_{NL} in the predicted η_{EFN} leads to underestimate the $(\eta_L)_{max}$ by -0.12 m and -0.25 m respectively, since the reduction induced by η_{NLE} is supported by the reduction of η_{NLT}.

The proposed hybrid approach is applied in Figure 4.22 and Figure 4.23 to analyze comparatively the extreme effect of nonlinear interaction by all extreme storm-tide components during the period between 1991 and 2007. The results in Figure 4.22 (highest effect) and Figure 4.23 (lowest effeect) for Cuxhaven and Sylt are summarized in the following three stages:

Stage 1- Predict the highest and lowest possible storm-tide from 1991 to 2007 ($(\eta_{EFN})_{max}$ and $(\eta_{EFN})_{min}$, respectively) (steps 1 to 9 in Figure 4.18), which occur at times t_{max} and t_{min}, respectively, using the developed NARX ensemble model. This also includes the nonlinear interaction component η_{NL} at times t_{max} and t_{min} (step 9 Figure 4.18).

Table 4.6: Effect of the nonlinear interaction (η_{NL}) on the heights of predicted storm-tide peaks (m) and their time of arrival (hours) at Cuxhaven and Sylt during the storms of January 2000, November 2006 and November 2007.

sites / parameter	Cuxhaven			Sylt		
	January 2000	**November 2006**	**November 2007**	**January 2000**	**November 2006**	**November 2007**
observed storm-tide highest peak $(\eta_{OB})_{max}$ (m)	3.86	3.81	4.42	3.02	2.21	2.65
time of $(\eta_{OB})_{max}$	1/30/2000 6:00 AM	11/1/2006 7:00 AM	11/9/2007 12:00 PM	1/30/2000 7:00 AM	11/1/2006 10:00 AM	11/9/2007 1:00 PM
linear superposed storm-tide η_L (m)	3.38	3.17	3.31	2.58	2.13	2.44
time shift for η_L peak at time of $(\eta_{OB})_{max}$ (hours)	+1	+0	+0	+1	-2	+0
suge-tide by TE-LEMAC2D $\eta_{su\text{-}t\ TEL}$ (m)	3.24	2.97	3.19	2.58	2.09	2.30
time shift for $\eta_{su\text{-}t\ TEL}$ peak at time of $(\eta_{OB})_{max}$ (hours)	+1	+0	+0	-1	-2	+0
storm-tide by NARX ensemble η_{EFN} (m)	3.77	3.18	3.48	3.01	2.01	2.19
time shift for η_{EFN} peak at time of $(\eta_{OB})_{max}$ (hours)	+0	+1	+0	+1	+0	+1
approximated nonlinear interaction η_{NLT}	-0.14	-0.20	-0.12	0.00	-0.04	-0.14
complementary nonlinear interaction η_{NLE}	0.53	0.21	0.29	0.03	-0.08	-0.11
nonlinear interaction $\eta_{NL} = \eta_{NLT} + \eta_{NLE}$	0.39	0.01	0.17	0.03	-0.12	-0.25

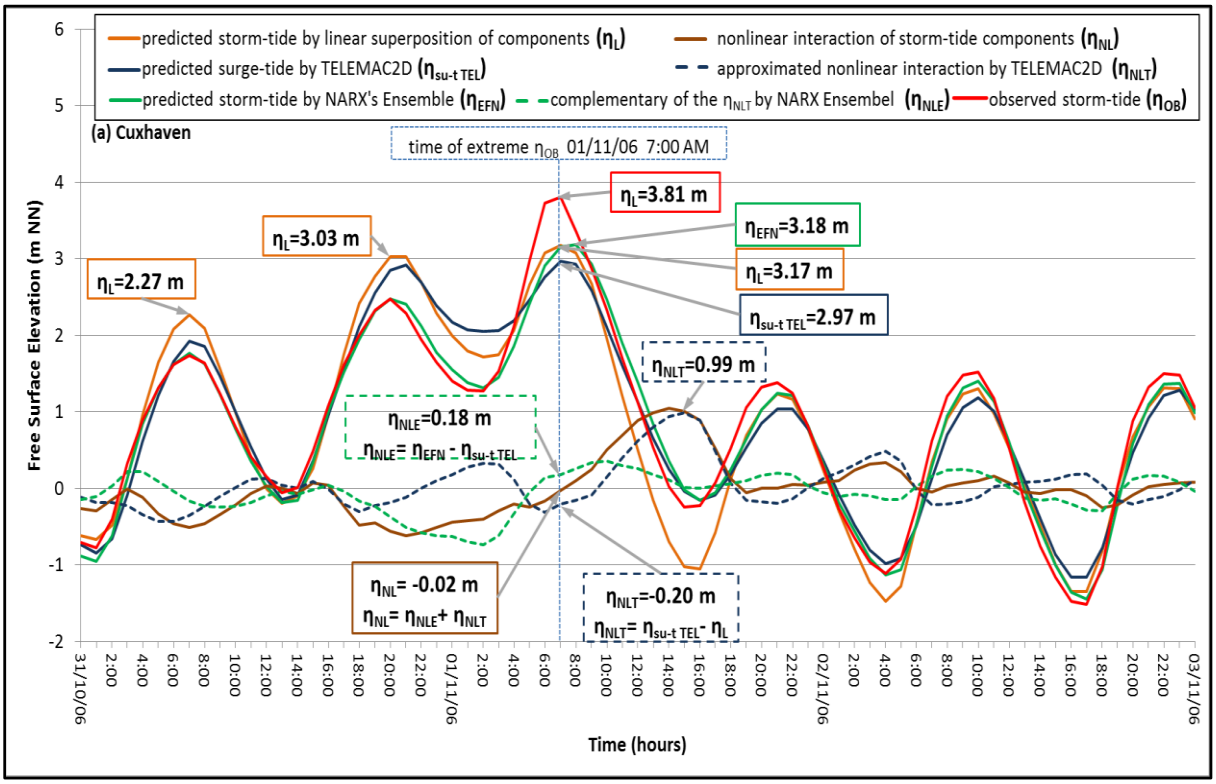

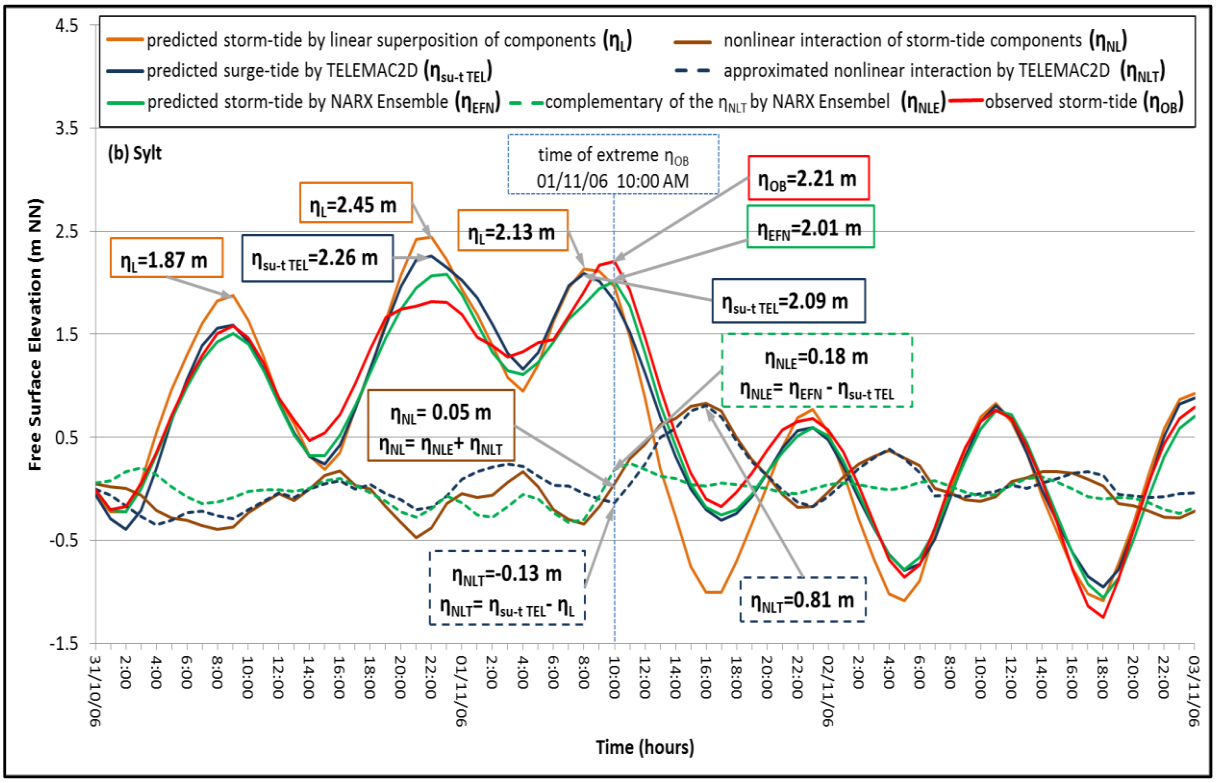

Figure 4.21: Storm-tide prediction by linear superposition η_L, TELEMAC2D $\eta_{su\text{-}t\ TEL}$ and NARX ensemble η_{EFN} with the effect of nonlinear interaction η_{NL} between extreme storm-tide components during the storm of November 2006 at Cuxhaven (a) and Sylt (b).

Stage 2- Evaluate the effect of each extreme storm-tide component depicted in Figure 2.15 and their nonlinear interaction on $(\eta_{EFN})_{max}$ and $(\eta_{EFN})_{min}$ at times t_{max} and t_{min}, respectively, as follows:

2.1. Using TELEMAC2D (steps 1 and 2 in Figure 4.18), predict each storm-tide component independently at times t_{max} and t_{min} (occurrence time of the peak $(\eta_{EFN})_{max}$ or trough $(\eta_{EFN})_{min}$, respectively, predicted in Stage 1).

2.2. Apply the proposed hybrid approach in Figure 4.18 to evaluate the effect of nonlinear interaction (η_{NL}) between the components predicted in sub-stage 2.1 at times t_{max} and t_{min} (steps 3 to 9 in Figure 4.18).

Stage 3- Evaluate the highest and lowest physical limit of storm-tide from 1991 to 2007 as follows:

3.1. Evaluate each storm-tide component independently, which occurred over the entire period from 1991 to 2007 using TELEMAC2D (steps 1 and 2 in Figure 4.18).The coupling between TELEMAC2D and TOMAWAC is used to predict the wave setup component for years 2000, 2006 and 2007 only.

3.2. Apply the proposed hybrid approach in Figure 4.18 to predict the nonlinear interaction (η_{NL}) between the components obtained from sub-stage 3.1, which occurred over the entire period from 1991 to 2007.

3.3. Extract the highest peak and lowest trough of each storm-tide component evaluated in sub-stage 3.1 in addition to the highest peak and lowest trough of their nonlinear interaction ($(\eta_{NL})_{max}$ and $(\eta_{NL})_{min}$, respectively) predicted in sub-stage 3.2, independently of their occurrence in time over the entire period 1991-2007; i.e. the extracted peaks or troughs do no not necessarily occur at the same time.

3.4. Superpose linearly the extracted highest peaks ($(\eta_{all})_{max}$) or lowest troughs ($(\eta_{all})_{min}$) from sub-stage 3.3, which might be considered to represent the highest or lowest physical limit of extreme storm-tide over the entire considered time period, respectively, though it is very improbable that the peaks or troughs of superposed storm-tide components will occur at the same times.

The linear superposition $(\eta_{all})_{max}$ is always higher than the highest possible storm-tide $(\eta_{EFN})_{max}$ (see Figure 4.22) at both sites over the entire time period 1991-2007. Since the maximum of each component and nonlinear interaction occur independently at different times. The $(\eta_{all})_{max}$ and $(\eta_{EFN})_{max}$ at Cuxhaven, which are respectively 7.21 m and 4.00 m, are higher

than their respective counterparts at Sylt of 5.66 m and 3.2 m. However, the percentages of $(\eta_{NL})_{max}$ and external surges maximum $((\eta_{es})_{max})$ at Cuxhaven, which are respectively 21% and 9.5%, are lower than their respective counterparts at Sylt of 25.80% and 10.97%. Since the storm surges and tide at Cuxhaven are higher than their counterparts at Sylt, which leads to deeper water depth at Cuxhaven with less pronounced shoaling effect. Furthermore, the effect of nonlinear interaction η_{NL} on $(\eta_{EFN})_{max}$ at Cuxhaven results in a reduction of water level by 4%. In contrast, the η_{NL} at Sylt results in increase of water level by 18.6%.

The highest observed water level between 1991 and 2004 occurred in the storm Anatol on 3 December 1999. It reaches 4.5 m at Cuxhaven, while it is 3.61 m at Sylt (Jensen & Mudersbach, 2008; Jensen et al., 2006). These values are higher than the $(\eta_{EFN})_{max}$ at Cuxhaven and Sylt (1991-2007) calculated in this study, which are 4.00 m and 3.2 m, respectively. This might be due to the overestimation of sea level pressure by the RCM SN-REMO during extreme storm event Anatol (see section 4.2.6).

The linear superposition $(\eta_{all})_{min}$ is always lower than the lowest possible storm-tide $(\eta_{EFN})_{min}$ (see Figure 4.23) at both sites over the entire time period 1991-2007. The $(\eta_{all})_{min}$ and $(\eta_{EFN})_{min}$ at Cuxhaven, which are respectively -5.04 m and -2.97 m, are lower than their respective counterparts at Sylt of -4.26 m and -2.51 m. However, the percentages of $(\eta_{NL})_{min}$ and external surge minimum $((\eta_{es})_{min})$ at Cuxhaven, which are respectively 23.65% and 10%, are lower than their respective counterparts at Sylt of 25.52% and 10.55%. This is similar to the $(\eta_{NL})_{max}$ and $(\eta_{es})_{max}$ behaviours at both sites. Furthermore, the effect of nonlinear interaction η_{NL} on $(\eta_{EFN})_{min}$ at Cuxhaven and Sylt results in a reduction of water level by 9% and 13%, respectively.

Figure 4.22 shows that the relative contribution of wave setup $((\eta_{w})_{max})$ is negligibly small with maximum values up to 1.2% at both pilot sites. Moreover, the contribution of river discharge maximum $((\eta_{rd})_{max})$ at Sylt and Cuxhaven is not more than 1% and also without any noticeable effect. Similarly as depicted in Figure 4.23, the contribution of river discharge minimum $((\eta_{rd})_{min})$ at both sites is not more than 1% and also the relative contribution of wave setup minimum $((\eta_{w})_{min})$ is 0.2%.

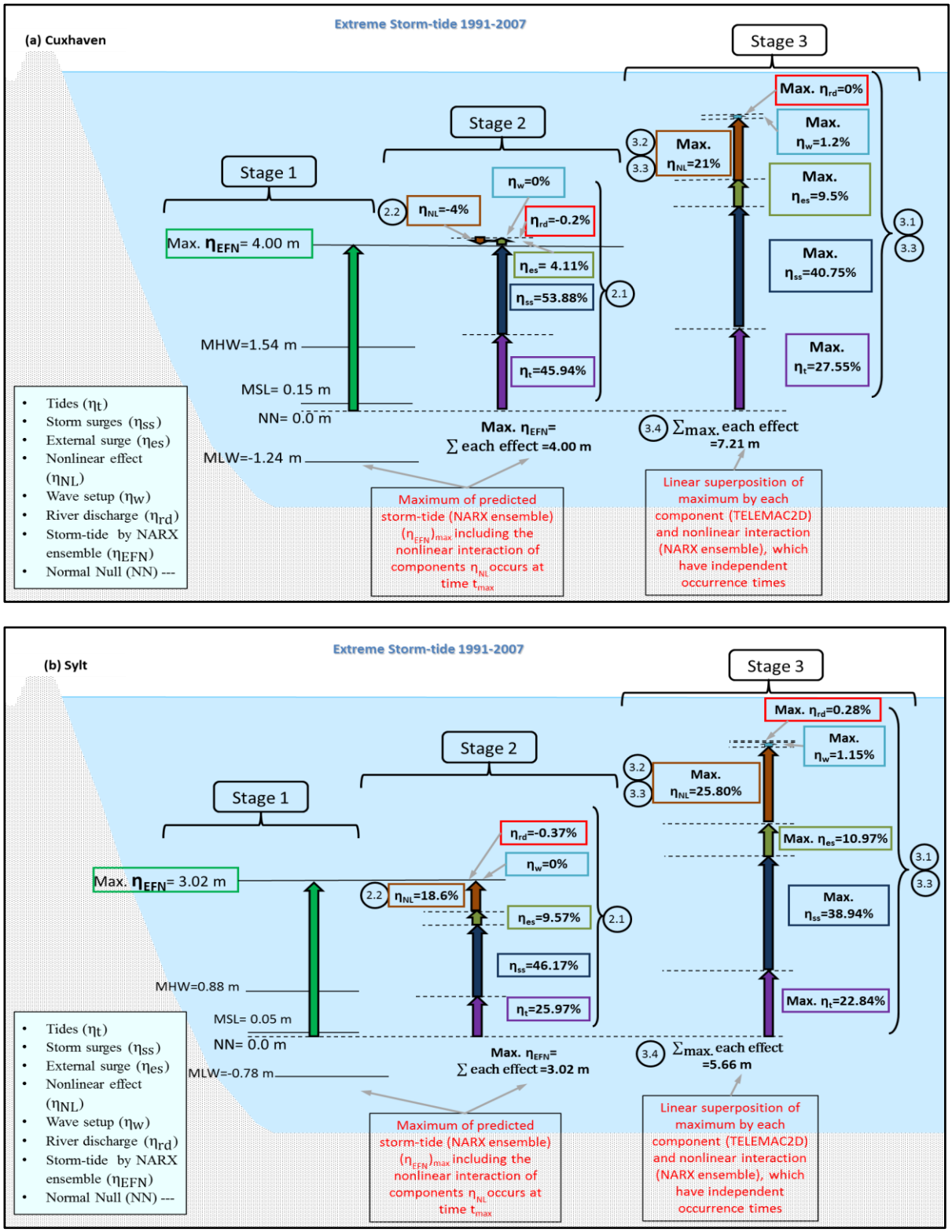

Figure 4.22: Maximum combination of the components in Figure 2.15 along with the nonlinear interaction between them (η_{NL}) and the predicted storm-tide by NARX ensemble (η_{EFN}) at Cuxhaven (a) and Sylt (b) during the period from 1991 to 2007.

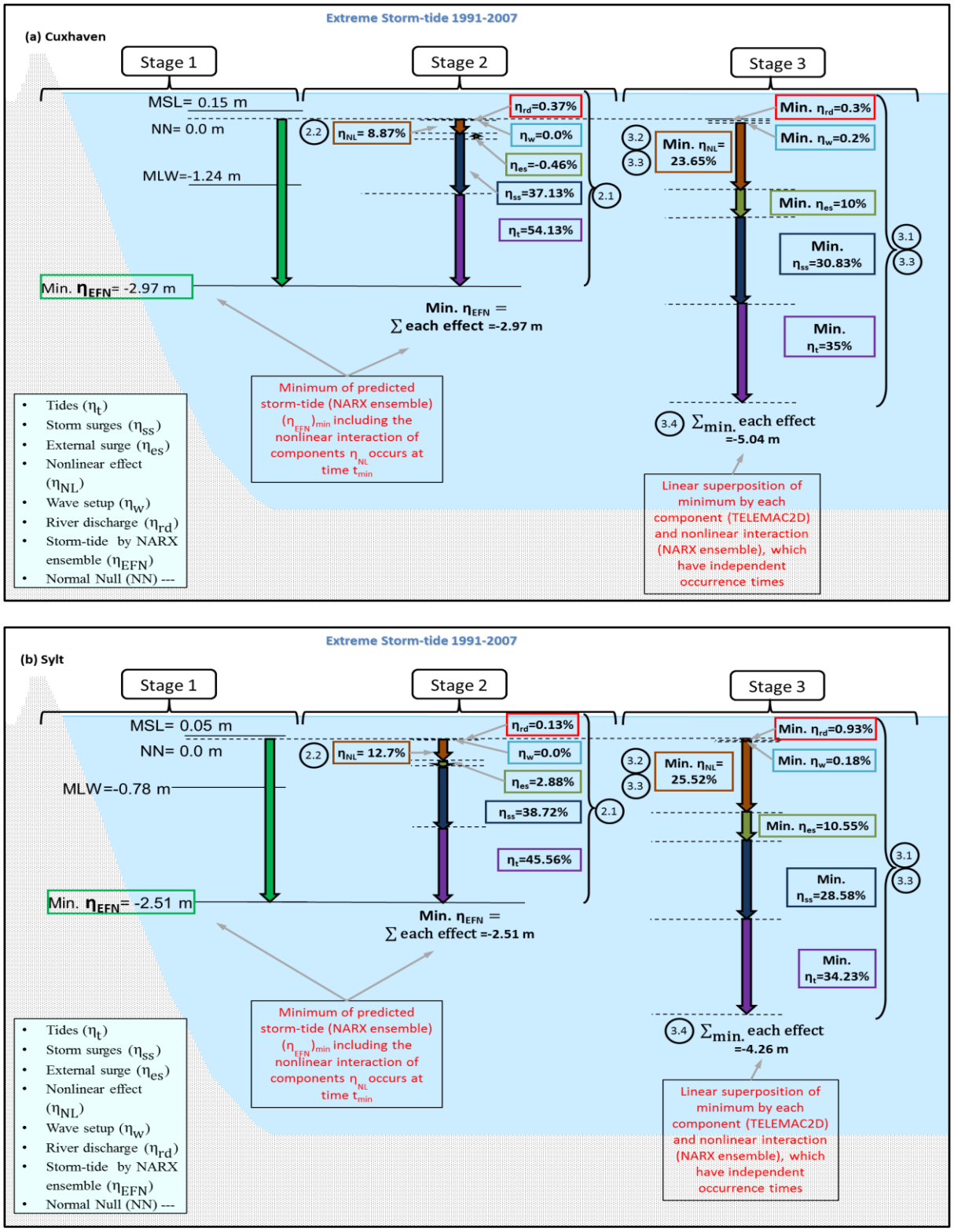

Figure 4.23: Minimum combination of the components in Figure 2.15 along with the nonlinear interaction between them (η_{NL}) and the predicted storm-tide by NARX ensemble (η_{EFN}) at Cuxhaven (a) and Sylt (b) during the period from 1991 to 2007.

The account for nonlinear interaction by NARX ensemble models may result either in the reduction or increase of the highest water level during storms when compared with the linear superposition of extreme storm-tide components according to the following two situations at both sites (Cuxhaven and Sylt):

(i) If the η_L peak resulting from linear superposition, which occurs directly before the time of $(\eta_{EFN})_{max}$ resulting from the NARX ensemble model, is less than 3 m, then its following peak would overestimate the peak of η_{EFN} at the time of $(\eta_{EFN})_{max}$. Since the peaks of η_{EFN} and η_L, which occur before the time of $(\eta_{EFN})_{max}$, do not increase significantly the mean water level (MWL) during the storm. Therefore, the following peaks of η_{EFN} and η_L will propagate under more pronounced shoaling effect that increases their heights simultaneously.

(ii) If the η_L peak, which occurs directly before the time of $(\eta_{EFN})_{max}$, is larger than 3.00 m, then its following peak would underestimate the peak of η_{EFN} at the time of $(\eta_{EFN})_{max}$. Since only the peak of η_L, which occurs before the time of $(\eta_{EFN})_{max}$, increases the MWL during the storm to a limit by which its following peak will propagate under less pronounced shoaling effect.

The highest peak of each components predicted series by TELEMAC2D and the nonlinear interaction (η_{NL}) predicted by the NARX ensemble over the entire time period 1991-2007 at Cuxhaven and Sylt are added together linearly ($(\eta_{all})_{max}$). The result is assumed to represent the highest physical limit of extreme storm-tide over the entire considered time period, though it is very improbable that the peaks of superposed storm-tide components will occur at the same times. The peak obtained through linear superposition $(\eta_{all})_{max}$ at Cuxhaven, which reaches 7.21 m , is higher than its counterpart at Sylt of 5.66 m. The maximum effect of the nonlinear interaction $(\eta_{NL})_{max}$ at Cuxhaven, which reaches 21%, is lower than its counterpart of 25.80% at Sylt. Since the storm surges and tide at Cuxhaven are higher than their counterparts at Sylt, thus resulting in higher water level with less pronounced shoaling effect.

4.4 The use of Relational NARX model to fill data gaps in observed water level from a remote data site

The recorded near shore water level at Sylt is of great importance in applications such as ocean engineering and safe navigation. Unfortunately, there are gaps in this record at Sylt, which are existed due to the lack of tide-gauge in the past time, failures in the measuring tide-gauge due to strong storms or when it is upgraded. Such gaps introduce difficulties and uncertainties to the sea level analysis and prediction. For instance, missing data may cause the estimate of mean sea level to be biased. The traditional ways to fill such gaps depend on its size. For example, the small gaps (of the order of minutes to tens of minutes) that occur in relatively frequent sea-level measurements can be easily fixed using linear interpolation. Moreover, the small and larger gaps can be restored using harmonic analysis. However, the former does not account for any physics governing the sea-level variations, while the latter does not con-

sider any meteorological and external forces, but only the tide generated by the Sun's and Moon's gravitational attractions.

Another logical way for missing data recovery is to use the observed data set from the nearest available tide-gauge station, which is Cuxhaven. However, differences in the phase and amplitude of sea level between the two gauges (principally due to the tide and storm surge) make it difficult to determine a reliable linear relationship between them. Especially, tide and storm surge in shallow-water areas like the North Sea have nonlinear interaction nature. Moreover, the two gauges are separated by a distance of more than one hundred kilometers. So, due to the nonlinear nature of the relationship in space and time, a NARX model is developed to retrieve missing data at Sylt using observed water level from Cuxhaven. The dynamics of nonlinear relationship behaviour are captured by the use of the memory line, and feedback in the NARX model. The memory line applied through the input time series lags of d_u=18 hours for Cuxhaven, while the feedback used the output time series lags of d_u=16 hours for Sylt. Finally, the relational NARX model results were validated in terms of correlation coefficient (CC) and root mean square of error (RMSE) using the observed water level at Sylt from 2000 to 2007.

The development of Relational NARX model, which acquire the nonlinear relationship between the recovered site (e.g. Sylt) and Source site (e.g. Cuxhaven), is accomplished in three stages as depicted in Figure 4.24. Stage-1 determines the requirements of both sites in order to get the highest performance by the Relational NARX model. While stage-2 deals with the determination of the input and output variables time series lags that should be included as input, also the optimum architectural parameters for the Relational NARX model. In stage-3, the validation of Relational NARX model results is performed in order to choose the optimum Relational NARX model that gives the highest performance.

4.4.1 Requirements for missing data retrieval from a remote data source site (stage-1 in Figure 4.24)

The recovered site (like Sylt) and source site (Cuxhaven), which have nonlinear relationship between them, are affected by the same storm-tide components and should fulfill the following six requirements:

1. Geographical location of both sites (recovered and source sites) must be in the covered area by same storms. So, they are either affected simultaneously by same storms or not. Cuxhaven and Sylt are located in the southeastern part of the North Sea (the German Bight), which has shallow depth with an average of 22m.
2. The statistical distributions and properties of meteorological forces (sea level pressure, zonal and meridional wind speed components) for the two sites are approximately similar. Cuxhaven and Sylt exhibit almost the same statistical magnitude of the data mean, median and statistical distribution behaviour (Figure 4.7 and Figure 4.8). So that the meteorological generation forces for storm surge and wave effect at both sites are similar.

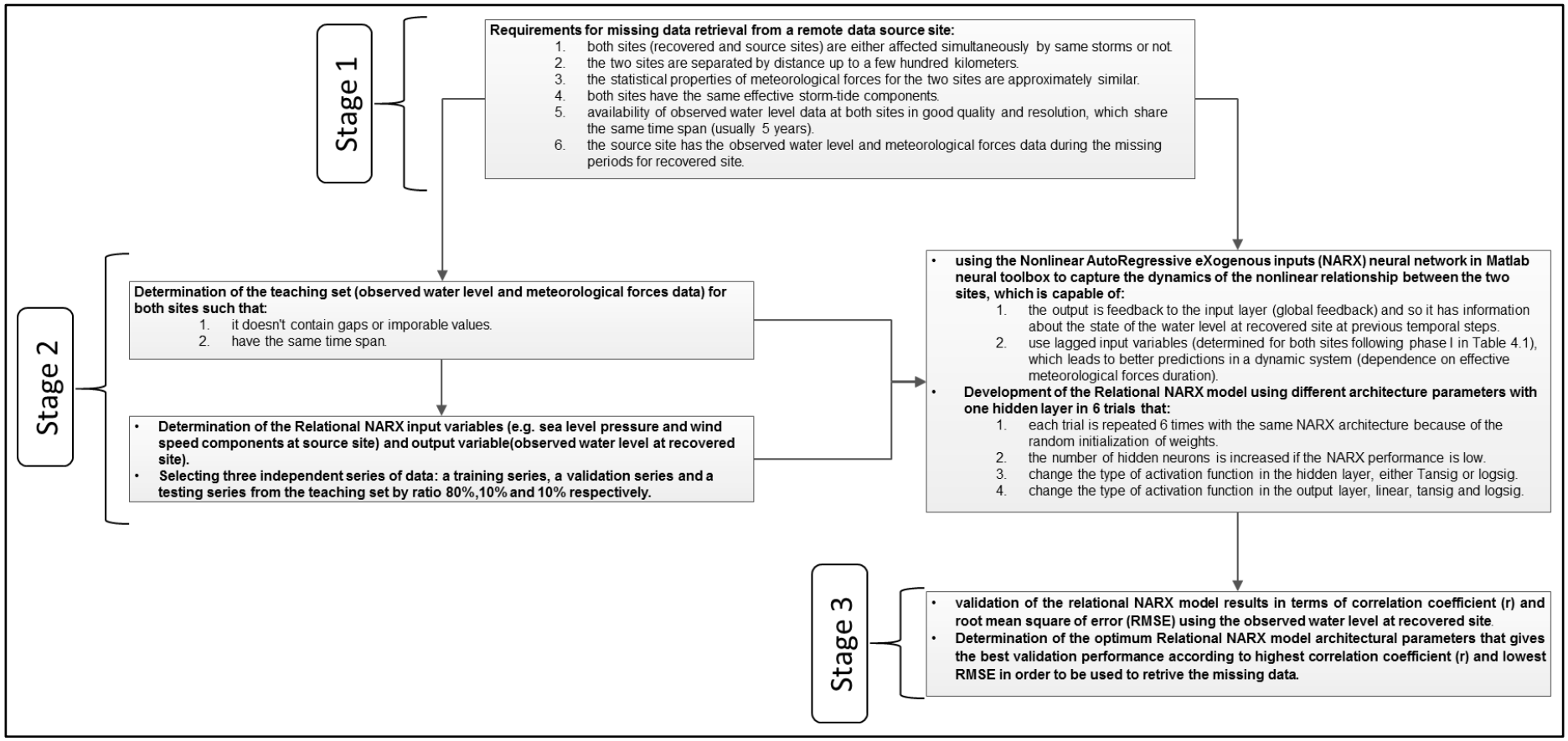

Figure 4.24: Development of Relational NARX model for observed water level data retrieval from a remote data source site.

3. The two sites are separated by distance up to a few hundred kilometers. The distance between Cuxhaven and Sylt is not more than 200 kilometers.
4. Differences in the phase and amplitude of water level between the two sites are principally due to the tide and storm surge. Hence, both sites are affected by the same effective storm-tide components. Moreover, if the recovered site has strong river discharge effect, it should be included as input variable to the developed NARX network. Sylt is an open coast site to the North Sea, while Cuxhaven is in Elbe estuary mouth and dominated by Nothe sea tides and storm surge with negligible effect of Elbe river discharge (section 4.3.4(b)).
5. The source site has the observed water level and meteorological forces during the missing period for recovered site. The sea level records of Cuxhaven tide gauges are sustained for the period from 1840 to present, which is one of the long records in the North Sea area.
6. Availability of the observed water level data at both sites in order to train the developed Relational NARX model that
    a. Share the same span of time (usually for 5 years),
    b. In good quality (it doesn't contain gaps or improbable values) and resolution (at least every one hour).

    Observed water level data at Cuxhaven and Sylt between 2000 and 2007 are recorded with time interval between 10 minutes and 1 hour, which are temporally interpolated in order to be synchronized with the available meteorological data every hour.

4.4.2 Data input selection and Relational NARX model formulation (stage-2 in Figure 4.24)

A subset of the observed water level and the meteorological forces data at Cuxhaven and Sylt should be selected, which have the same span of time, in order to learn and validate the relational NARX model. This criterion is fulfilled for Cuxhaven and Sylt data between 2000 and 2007. The data from 2000 to 2005 at Cuxhaven and Sylt was dedicated for learning process of the relational NARX model, which constitutes 52608 learning samples, while the data of years 2006 and 2007 are used for validation of the model. These learning sets for Cuxhaven and Sylt are divided randomly in three series: (i) the training series (80% of the data), (ii) the validation series (10% of the data) and (iii) test series (10% of the data).

The input deck for the relational NARX model consists of the time lagged meteorological forces (sea level pressure, zonal and meridional wind components) and observed water level at Cuxhaven (Figure 4.25). The output is the predicted storm-tide at Sylt as shown in Figure 4.25. Moreover, the optimum architecture consists of three feedforward layers using one neuron in the hidden and output layers in addition to a feedback connection from the output to input layer. The time lag of input variables is d_u=18 hours for Cuxhaven, while the time lag of output variable is d_y=16 hours for observed water level at Sylt (see section 4.2.3). Only the activation functions are changed for hidden and output layers. The activation functions tansig or logsig are possible in the hidden layer, while in the output layer tansig, logsig and

linear functions are the best candidates. This Relational NARX model can be mathematically represented as,

$$y(t) = f\left[y(t-1), \dots, y\left(t-d_y\right); u_m(t), \dots, u_m(t-d_u)\right], with\ \ m = 1,2, \dots, input\ variables\ number \tag{4.16}$$

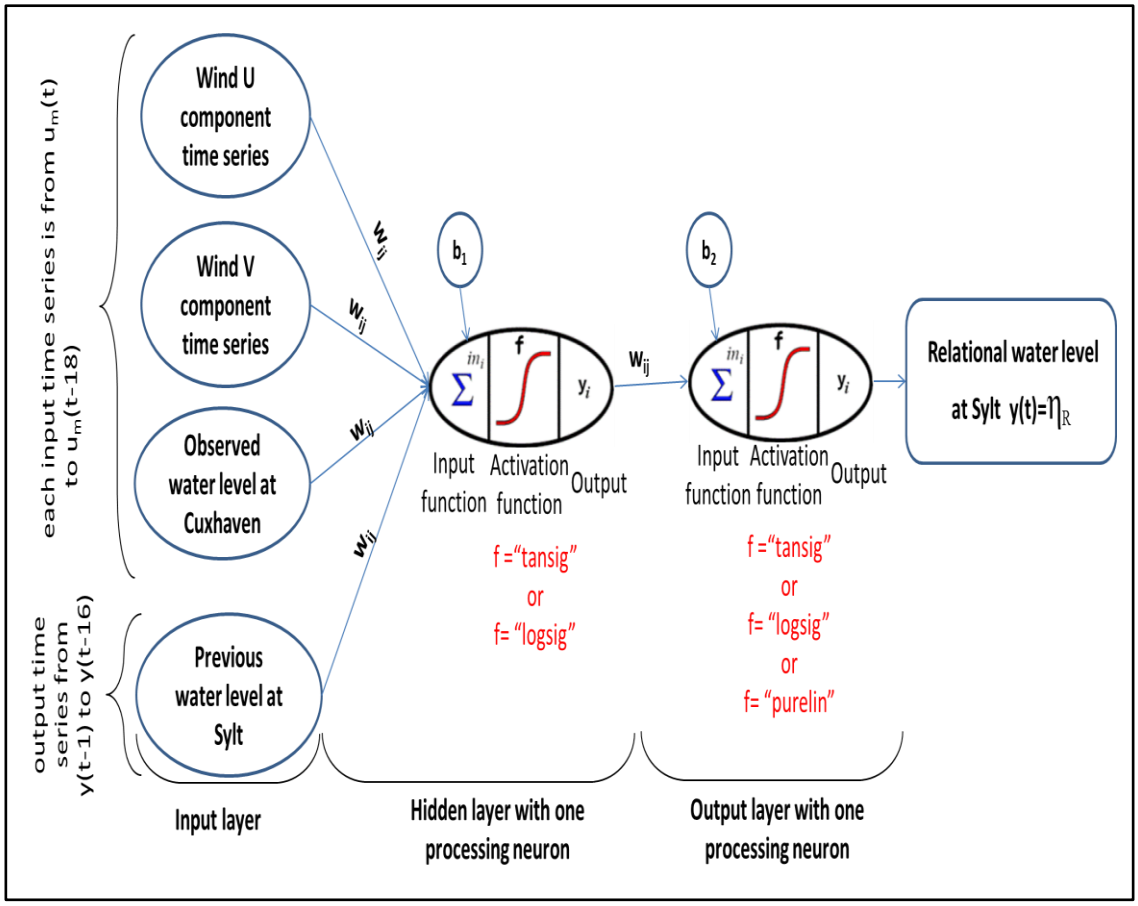

Figure 4.25: Inputs and output for the relational NARX model at Sylt using the meteorological forces and observed water level at Cuxhaven as input.

The development of Relational NARX model had been implemented in 6 trials using the built-in matlab Levenberg-Marquardt algorithm (see section 4.1.4). In each trial, the activation function is changed either for hidden or output layers then repeated 30 times because of the random weight initialization. Moreover, the hidden layer with one neuron has good performance during the Relational NARX model training.

Figure 4.26 shows as example of the relational NARX model architecture using matlab toolbox, which consists of three feedforward layers using the tansig and linear activation functions for the hidden and output layers, respectively.

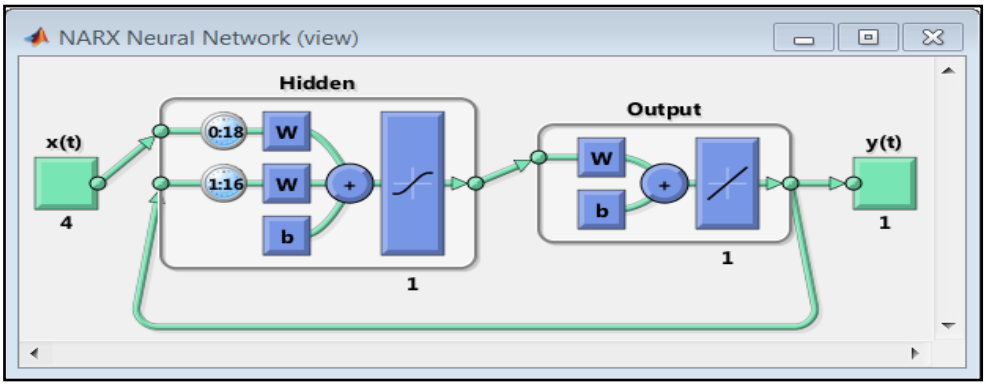

Figure 4.26: Relational NARX architecture for Sylt with 4 external input variables (the three meteorological forces and observed water level at Cuxhaven), one feedback variable (the previous observed water level at Sylt) and the activation functions of the hidden and output layers are tangent sigmoid and linear respectively.

4.4.3 Validation and results of the Relational NARX model for Sylt (stage-3 in Figure 4.24)

Using the observed water level from 2000 to 2007 at Sylt, the prediction results of developed Relational NARX models were validated in terms of correlation coefficient (CC), RMSE and σ. Table 4.7 lists the best validation result of each trial for Relational NARX models. It is obvious from this table that the tansig and purelin activation functions in the hidden and output layers, respectively, give the best performance with RMSE and correlation of 0.078 m and 0.99, respectively (lowest RMSE and highest correlation). The best Relational NARX model has mean and σ of 0.066 m and 0.669 m, respectively, which represent the observed water level mean and σ of 0.057 m and 0.705 m respectively. Moreover, using the logsig as an activation function in the hidden and/or output layers leads to degradation of the performance, since their Relational NARX models have the highest RMSE and lowest r. The highest RMSE is 0.43 m, when the logsig function is used in the hidden and output layers. The lowest r is 0.81, when the logsig function is used in output layer.

Figure 4.27 shows Taylor diagram for Sylt between the observed water level (η_{OB}), the predicted $\eta_{su-t\,TEL}$ by TELEMAC2D, the predicted storm-tide (η_R) by the best Relational NARX model and η_{EFN} by NARX ensemble. The η_R result has the best performance according to the highest r of 0.99 along with the lowest normalized RMSE of 0.11 m.

Figure 4.28 shows the temporal variations of the predicted storm-tide by the Relational NARX model (η_R), NARX ensemble (η_{EFN}) in addition to the observed water level at Sylt (η_{OB}) during the storms of November 2006 and November 2007. The highest η_R peaks reach 2.43 m and 2.79 m during the storms of November 2006 and November 2007, respectively, and they slightly overestimate the highest η_{OB} peaks of 2.21 m and 2.65 m respectively. This occurs due to the inclusion of the meteorological forces at Cuxhaven as input to the Relational NARX model as shown in Figure 4.25, which differ slightly than the meteorological force at Sylt (see Table 4.3). In contrast during the storm of January 2000, the highest η_R peak reach-

es 3.02 m and slightly underestimates the highest η_{OB} peak of 2.77 m. Since the sea level pressures during these three storms at Cuxhaven are higher than those at Sylt (see Table 4.3) with the maximum difference in pressure happen during the storm of January 2000. Moreover, the time of highest η_R peak coincide with the times of highest η_{OB} peak during the storms of January 2000 and November 2007, while it occurs 2 hours before η_{OB} peak during the storm of November 2006.

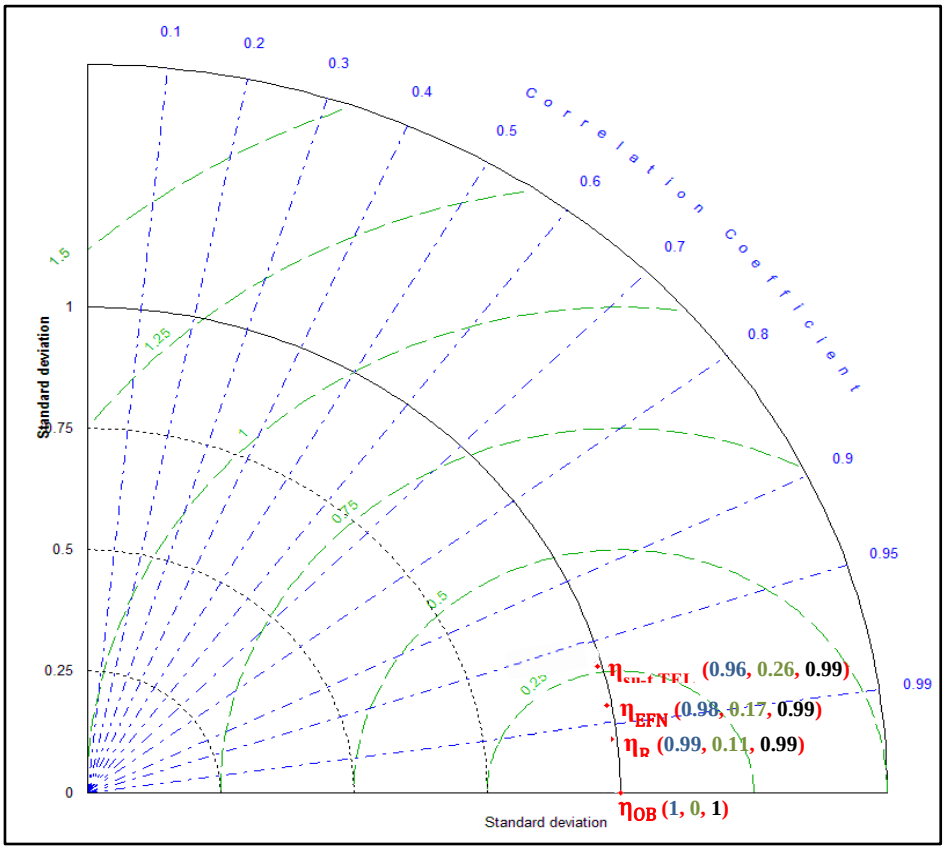

Figure 4.27: Taylor diagram of the observed water level (η_{OB}), the predicted surge-tide ($\eta_{su-t\,TEL}$) by TELEMAC2D, the predicted storm-tide (η_R) by the Relational NARX model and η_{EFN} by NARX ensemble at Sylt based on the normalised correlation coefficient (CC), normalised root mean square error (RMSE) and normalised standard deviation (σ).

Table 4.7: Standard deviation (σ), Root Mean Square Error (RMSE) and correlation coefficient (CC) Validation results (m) of the relational NARX models for Sylt from 2000 to 2007.

hidden layer activation function	output layer activation function	mean	σ	RMSE	CC
observed	**observed**	0.057 m	0.705 m	0	1
Tansig	**linear**	0.066 m	0.699 m	0.078 m	0.993 m
Tansig	**Tansig**	0.059 m	0.701 m	0.128 m	0.983 m
Tansig	**Logsig**	0.818 m	0.451 m	0.431 m	0.811 m
Logsig	**linear**	0.066 m	0.699 m	0.078 m	0.993 m
Logsig	**Tansig**	0.061 m	0.701 m	0.128 m	0.983 m
Logsig	**Logsig**	0.779 m	0.434 m	0.433 m	0.816 m

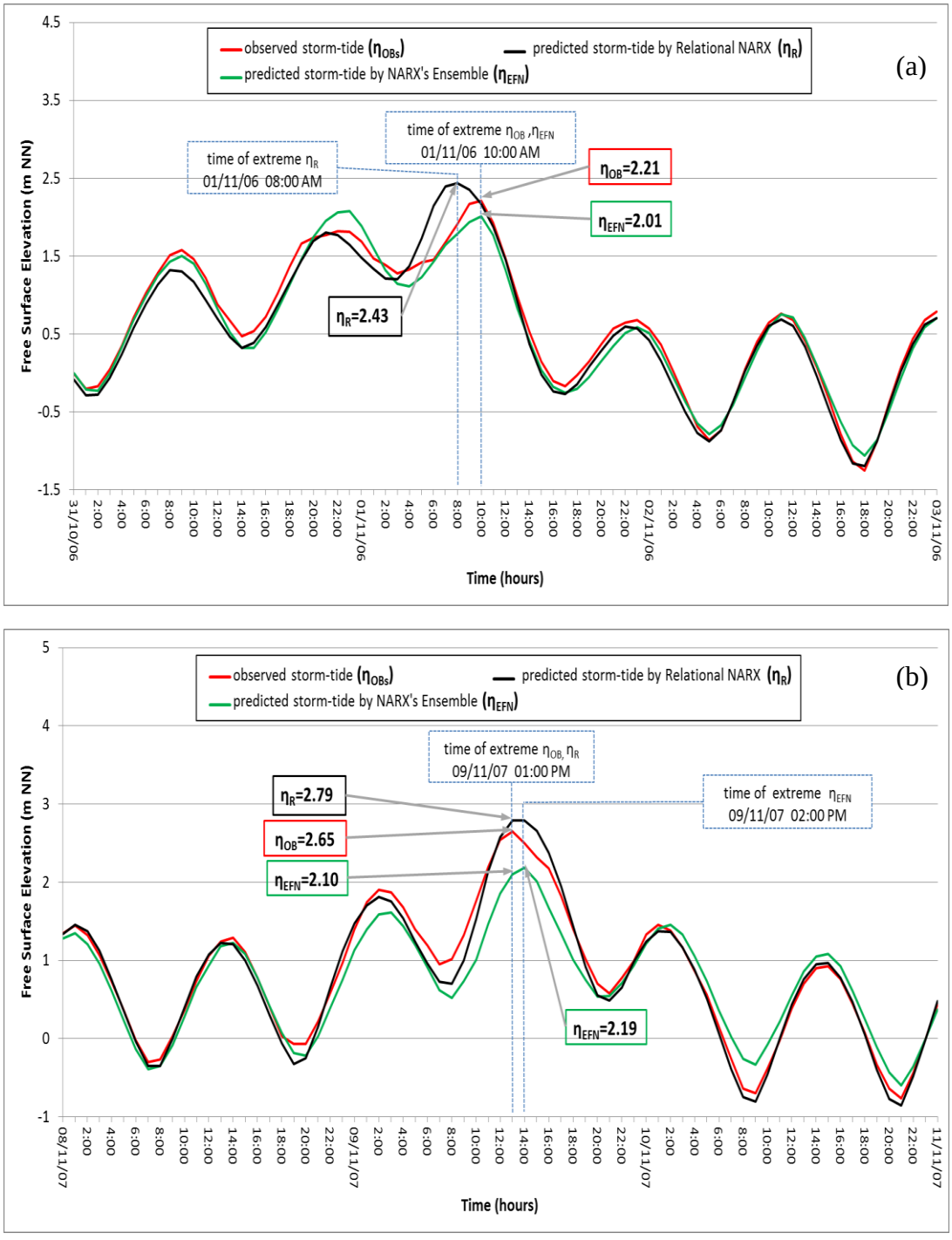

Figure 4.28: Results of Relational NARX model during the storms of November 2006 (a) and November 2007 (b) at Sylt.

Relational NARX model is developed to retrieve missing data at Sylt using observed water level from Cuxhaven. The dynamics of this nonlinear relationship behaviour are captured by the use of the memory line, and feedback in the NARX model. The memory line applied through the input time series lags of 18 hours for Cuxhaven, while the feedback used the output time series lags of 16 hours for Sylt. The tansig and purelin activation functions in the

hidden and output layers of the Relational NARX model, respectively, give the best performance with RMSE and correlation of 0.078 m and 0.99, respectively (lowest RMSE and highest correlation). The prediction by Relational NARX model (η_R) has beter performance than η_{EFN} by NARX ensemble, since it has the lowest normalized RMSE of 0.11 m. The highest η_R peaks reach 2.43 m and 2.79 m during the storms of November 2006 and November 2007, respectively, and they slightly overestimate the highest η_{OB} peaks of 2.21 m and 2.65 m respectively.

4.5 Summary and Concluding Remarks

Combining the strengths of ANN methodology with those of numerical modelling (TELEMAC2D and TOMAWAC) provides a powerful and computationally efficient operational model system for storm-tide prediction as exemplarily shown in Cuxhaven and Sylt. It can also be applied for reconstructing the missing data using sequential time series predictions by NARX ensemble, which reduces the amount of training data (usually five years show very good performance). Another advantage of the hybrid model system is its capability to account for nonlinear interaction between the extreme storm-tide components, so the substantial errors in both magnitude and timing of the results predicted by numerical modelling can be corrected. Two types of NARX models and their ensemble were developed and validated using the observed water level between 1999 and 2007 at Cuxhaven and Sylt. For Cuxhaven's NARX ensemble model, the lowest RMSE is 0.148 m with a correlation of 0.99. The NARX ensemble model in Sylt has an RMSE of 0.123 m and a correlation of 0.98.

The account for nonlinear interaction by hybrid models may result either in the reduction or increase of the highest water level during storms when compared with the linear superposition of extreme storm-tide components according to the following two situations at both sites (Cuxhaven and Sylt):

(i) If the peak obtained by linear superposition η_L, which occur directly before the time of extreme η_{EFN} ($(\eta_{EFN})_{max}$), is < 3.00 m, then its following peak would overestimate the peak of η_{EFN} at the time of $(\eta_{EFN})_{max}$. Since the peaks of η_{EFN} and η_L, which occur before the times of peak $(\eta_{EFN})_{max}$, do not increase the mean water level (MWL) during the storm significantly. Therefore, the following peaks of η_{EFN}, η_L and $\eta_{su\text{-}t\ TEL}$ will propagate under a pronounced shoaling effect that increases their heights.

(ii) If the peak of η_L, which occur directly before the time of $(\eta_{EFN})_{max}$, are ≥ 3.00 m, then its following peaks would underestimate the peak of η_{EFN} at the time of $(\eta_{EFN})_{max}$. Since only the peak of η_L , which occurs before the times of $(\eta_{EFN})_{max}$, increases the MWL during the storm to a limit by which their following peak will propagate without shoaling effect. In contrast, the peak of η_{EFN} propagates under strong shoaling effect that increases its height.

The highest physical limit of extreme storm-tide (1991-2007) at Cuxhaven and Sylt ($(\eta_{all})_{max}$) are calculated including the maximum of nonlinear interaction ($(\eta_{NL})_{max}$). The peak of $(\eta_{all})_{max}$ at Cuxhaven, which reaches 7.21 m , is higher than its counterpart at Sylt of 5.66 m. The maximum effect of $(\eta_{NL})_{max}$ at Cuxhaven, which reaches 21%, is lower than its counterpart of 25.80% at Sylt. Since the storm surges and tide at Cuxhaven have higher contribution to water level than their counterparts at Sylt, thus resulting in less pronounced shoaling effect. Therefore, the consideration of $(\eta_{NL})_{max}$ would be relevant for the safety of many coastal facilities, which depends on the magnitude of highest physical limit of extreme storm-tide $(\eta_{all})_{max}$.

The recorded near shore water level at Sylt is of great importance but there are gaps in it. The Relational NARX model is developed to retrieve the missing data at Sylt using observed water level from Cuxhaven (2000-2007). Especially, the two sites are separated by a distance of more than one hundred kilometers, and both sites are affected by the same storms and storm-tide components. The prediction by Relational NARX model (η_R) has better performance than the predicted storm-tide by NARX ensemble (η_{EFN}), it has the lowest normalized RMSE of 0.11 m. since it includes the observed water level at Cuxhaven in the input deck.

5 Extreme storm-tide in the 21st century under the projected climatic change for the German Bight

Extreme storm-tide along the North Sea coasts presents the most important threat for coastal infrastructure and human safety. Especially with the increasing use of coastal regions for settlement and as industrial areas, which have already a high population density and valuable assets, the costs of extreme storm-tide damage can be very high. As one of the impacts of climate change, extreme storm-tide threat might increase mainly due to the change in wind climate. Moreover, sea level rise induced by climate change also significantly contributes to extreme storm-tide that will threat the North Sea coasts. Therefore, the objectives of this chapter are (i) to assess the changes in extreme surge-tide conditions induced by possible future climate change projection (e.g. between 2070 and 2100) over the North Sea, and (ii) to estimate the extreme effects of this projection and sea level rise on storm-tide at two pilot sites in the German Bight (Cuxhaven and Sylt).

To achieve objective (i) the first step is to assess extreme surge-tide under the current climate conditions using the 20th century meteorological forces between 1970 and 2000 (called hereafter"control simulation"). In a second step, possible future storm-tide climate based on the IPCC emission scenario (SRES A1B, between 2070 and 2100) is investigated using the hydrodynamic model TELEMAC2D for the North Sea (called hereafter "future climate change simulation").

To achieve objective (ii) the hybrid modelling approach described in section 4.3 is then used to account for the contribution of nonlinear interactions between the different storm-tide components at Cuxhaven and Sylt (Figure 5.1). As global circulation models (GCMs) show systematic errors (bias) in their simulations between the hindcast and control surge predictions (1960-1990) (Woth, 2006), the difference between the mean of future (2070-2100) and control (1970-2000) simulations at both sites will represent the response of applied emission scenario (A1B).

The German Bight is shallow with an average water depth of 22 m. So the time scale of morphological evolution becomes larger and its effect smaller as the water is getting deeper i.e. more than 10 m (Woth, 2006; Gaslikova et al., 2013). In both control and future simulations, the future changes in today's bathymetry were not taken into account, since at both sites (Cuxhaven and Sylt) the water depth is greater than 20 m. Moreover, the expected sea level rise can be linearly superimposed on the predicted storm-tide as the water depth is larger than 10 m (Lowe & Gregory, 2005; Woth, 2006; Sterl et al., 2009; Howard et al., 2010; Gaslikova et al., 2013).

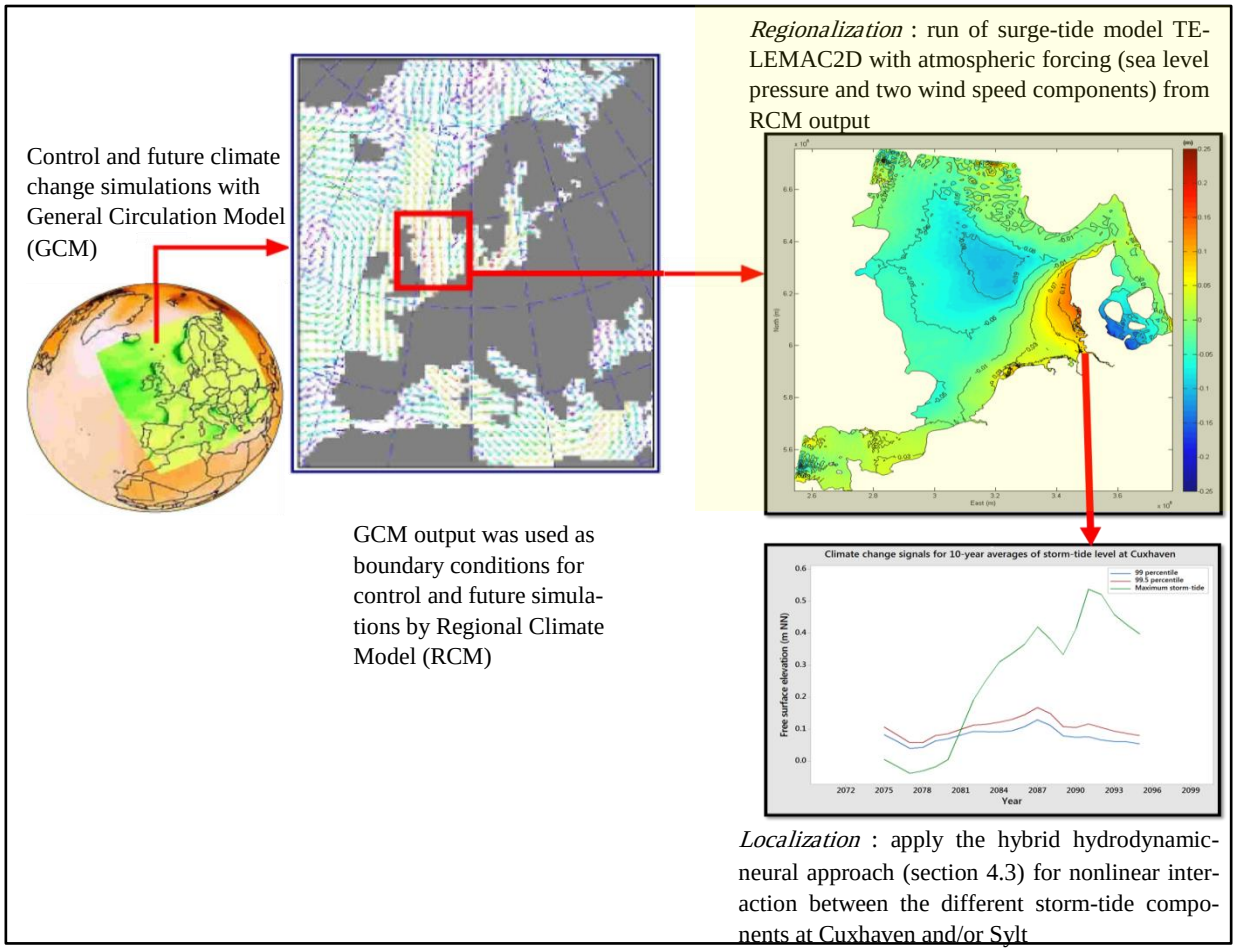

Figure 5.1: Methodology to derive climate change signals for regional (North Sea) and local (Cuxhaven and Sylt) storm-tide climate (modified from (Woth, 2006)).

5.1 Assessment of changes in extreme surge-tide conditions induced by possible future climate change projection (between 2070 and 2100) over the North Sea

In reaction to anthropogenic climate change, IPCC aims to document the knowledge about climate change on global and regional scales. Vulnerable zones were identified in five assessment reports by IPCC and the possible changes, which are based on a range of different scenarios, were analyzed. As described in the IPCC Forth Assessment Report (AR4), the North Sea coasts might be adversely affected by the changing climate. These coasts are densely populated and have highly industrialized areas, which are currently below or slightly above today's mean sea level. Therefore, the majority of North Sea coasts encompass coastal low lands and are highly vulnerable to storms with their extreme water levels and associated waves. The potential changes in surge-tide climate are investigated over the North Sea area in order to identify the highly flood-prone coastal low lands.

The future climate change, which is conditional upon assumed projection of future GHG emissions ("Scenario"), is based on a cascade of numerical climate models (Figure 5.1). General Circulation Models (GCMs) were used to simulate future climate conditions globally, while Regional Climate models (RCMs) were applied to "dynamically downscale" these global conditions to a finer grid covering western Europe including the North Sea area.

Both control and future simulations of surge-tide are based on regionalized meteorological conditions with the regional climate model CLM (Lautenschlager et al., 2009), which is forced on the boundary by output of the general circulation model ECHAM5/MPIOM (Roeckner, 2003). Woth (2006) finds that only the CLM wind and pressure fields lead to extreme storm surges of a magnitude comparable to those obtained in the hindcast, while other RCMs meteorological results underestimate it. Therefore, the hourly Near-surface wind speed components (10 m) and 3-hourly mean Sea Level Pressure (SLP) fields from the CLM regionalizations (18 km x 18 km resolution) were used to simulate surge-tide over the North Sea by TELEMAC2D. Today's or reference surge-tide conditions are represented by ''control simulation'' (1970–2000), which is tested statistically using real present-day climate ''hindcast simulation''. Possible future conditions in case of global warming are represented by ''climate realization'' (2070–2100).The analysis of future climate change effect on the water levels by focussing on extreme values (annual 99.5 percentile and maximum surge-tide) and with special emphasis on the German Bight is performed in the following two stages:

- Stage 1: Simulation of the hindcast and control surge-tide climate between 1970 & 2000
- Stage 2: Simulation of future surge-tide climate (2070-2100) for the North Sea

5.1.1 Control and hindcast surge-tide simulations for the North Sea using TELEMAC2D (Stage 1)

In this section, the simulation of the hindcast and control surge-tide climate between 1970 and 2000 is performed according to the steps shown in Figure 5.2 and described below:

1. Prescribe the meteorological forces which are the main responsible factors for the generation of surge-tide, to the North Sea model in TELEMAC2D (Figure 3.8) as "inputs" for control or hindcast simulations (e.g. sea level pressure, meridional and zonal wind speed components).
2. Prescribe the boundary conditions of the North Sea hydrodynamic model in TELEMAC2D using all extreme surge-tide components (Figure 2.15) between 1970 and 2000 (astronomical tides at northern and western open boundaries (η_{at}), external surge from Wick or Lerwick linearly added to tides on the northern boundary (η_{ds}) and fresh water discharge (η_{Q}) from the main southern rivers (see Figure 3.8).
3. Drive the North Sea model in TELEMAC2D using boundary conditions of all components in step 2, which are prescribed simultaneously in order to predict the surge-tide

either under meteorological control conditions $(\eta_{\text{su-t TEL}})_{C20\_2}$ or hindcast conditions $(\eta_{\text{su-t TEL}})_{H20}$.

4. Calculate the annual percentiles of surge-tide at Cuxhaven and Sylt over 1970–2000 from the hindcast and control simulations.
5. Test how close the surge-tide statistics from the control simulation is to real present-day surge-tide conditions (hindcast simulation) at Cuxhaven and Sylt.
6. Calculate the annual upper percentiles of hindcast simulation (99.5 percentile ($P^{xn}_{H20}(99.5)$) and maximum surge-tide ($P^{xn}_{H20}(100)$)) for years n from 1970 to 2000 at every mesh point *x* in the North Sea model (Figure 3.8).
7. Calculate the confidence intervals for the mean of $P^{xn}_{H20}(99.5)$ and $P^{xn}_{H20}(100)$ over 1970-2000 ($CI^x(99.5)$ and $CI^x(100)$) at every mesh point *x* with a statistical significance level of 95% using student's *t* test.

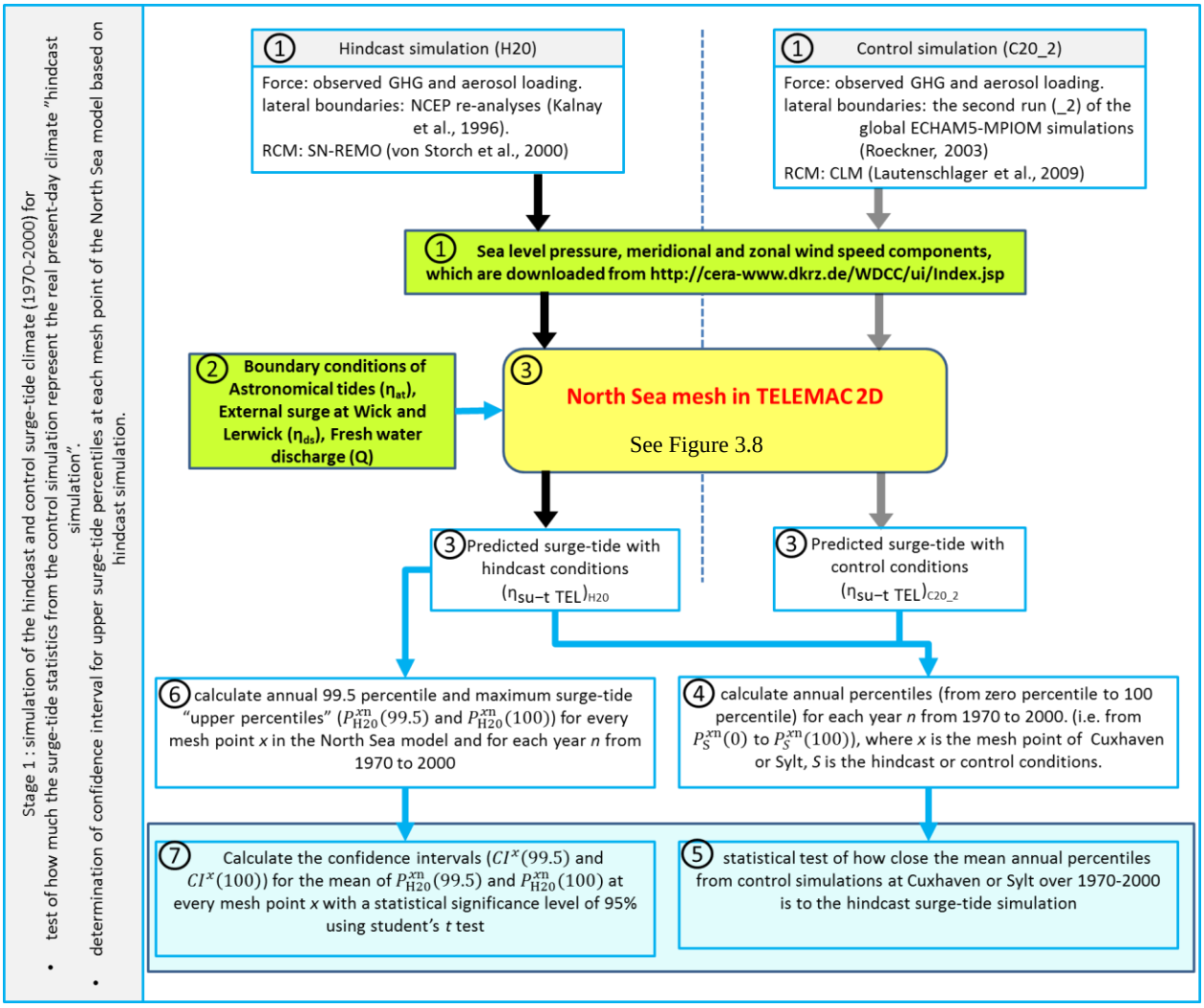

Figure 5.2: simulation of the hindcast and control surge-tide climate between 1970 and 2000.

(a) Meteorological data preparation and application for the North Sea model (1970-2000) in TELEMAC2D (step 1 in Figure 5.2)

The regular tidal movements in the North Sea are continuously modified to a greater extent by the effect of meteorological forces (essentially wind and pressure). The hydrodynamic model TELEMAC2D requires the 10 m height wind and sea level pressure (SLP) fields as meteorological forces for the control or hindcast surge-tide simulations (1970-2000). If the meteorological forces are sufficiently accurate, surge-tide and their statistics can be satisfactorily modelled with TELEMAC2D, especially if the focus is on long-term statistics rather than on single events. Therefore, the hourly zonal and meridional wind speed components along with the 3-hourly SLP fields from the CLM regionalization (0.165^o x 0.165^o horizontal resolution) is used as the control climate (C20_2). The RCM CLM is forced on boundaries by the second run of global ECHAM5-MPIOM simulation (1.8^o x 1.8^o horizontal resolution). So the underscore 2 is related to the initial conditions for the global simulation (Figure 5.2, step 1). The selection of initial condition 2 for the GCM is related to the selection of future initial condition as described in section 5.1.2(a). In contrast, the hourly wind speed components and SLP fields for hindcast simulation were regionalized with SN-REMO (0.5^o x 0.5^o horizontal resolution), which is driven with atmospheric NCEP re-analyses as global conditions. The hindcast conditions describe the actual weather in 1970-2000. Control conditions describe a random sequence of weather events that shares with the hindcast only the same statistics but not the details at any time. The difference between control and hindcast meteorological conditions is summarized in Table 5.1.

The regionalized meteorological data of hindcast conditions are provided by Helmholtz-Zentrum Geesthacht (HZG) in netcdf format for each month between 1958 and 2007, while the control condition data is downloaded from the WDCC - World Data Center for Climate-http://www.dkrz.de/daten/wdcc/ under CERA “Climate and Environmental Retrieval and Archive”. The RCMs SN-REMO and CLM are set up for running on a rotated grids with North Poles located at (-170^o longitude, 32.5^o latitude) and (-162^o longitude, 39.25^o latitude) respectively, which differ from the geographical North Pole (0^o longitude, 90^o latitude). So, the hindcast and control meteorological conditions are rotated back to geographical coordinate system with the North Pole of (0^o longitude, 90^o latitude). These re-rotated meteorological conditions are transformed afterward to “3-degree Gauss-Kruger zone 3” coordinate system, which is used by the North Sea hydrodynamic model in TELEMAC2D (Figure 3.8).

In order to use the hindcast and control datasets over the North Sea mesh in TELEMAC2D, each dataset is interpolated (Figure 5.3):

(i) in space over the computation grid (Figure 3.8) and stored in TELEMAC2D serafin format file for each year between 1970 and 2000 (Tayel & Oumeraci, 2012b),
(ii) in time during the surge-tide simulation at the internal computation time step by TELEMAC2D.

Therefore, after the interpolation in space of the hourly wind speed components and SLP fields, a linear temporal interpolation is performed at each computational time step inside TELEMAC2D by the modified subroutine METEO.f (Tayel & Oumeraci, 2012b).

Table 5.1: Regional climate models for the generation of meteorological driving forces fields for the North Sea model in TELEMAC2D.

Model / **Parameter**	**SN-REMO**	**CLM**
Forcing	Observed GHG and aerosol loading during 20th century. hindcast (1960-2007)	• Observed GHG and aerosol loading during 20th century. control (1960-2000) • IPCC climate change scenario A1B during 21th century. future (2070-2100)
Future scenarios	No	A1B_2 (2070-2100)
GCM	NCEP Reanalysis	second run of global climate model ECHAM5/MPIOM (Roeckner, 2003)
RCM	SN-REMO (von Storch et al., 2000) from HZG	CLM (Lautenschlager et al., 2009) from Deutscher Wetterdienst, (DWD)
RCM coverage region	10.3^{o} W to 70.73^{o} E and 29.6^{o} N to 67.8^{o} N	10.7^{o} W to 36.9^{o} E and 34.5^{o} N to 69.9^{o} N
Spatial resolution	0.5° x 0.5° (50 km x 50 km)	0.165° x 0.165° (ca. 18 km x 18 km)
Temporal resolution	Every one hour.	Every one hour for 10 m wind. every 3-hours for sea level pressure
number of grid points in (longitude, latitude)	(81,91)	(241,255)
position of north pole (longitude, latitude)	(-170^{o},32.5^{o})	(-162.0^{o},39.25^{o})
regionalized meteorological results	Near-surface wind and pressure fields over Western Europe and adjacent seas including the North Sea area.	Near-surface wind and pressure fields over Western Europe and adjacent seas including the North Sea area.

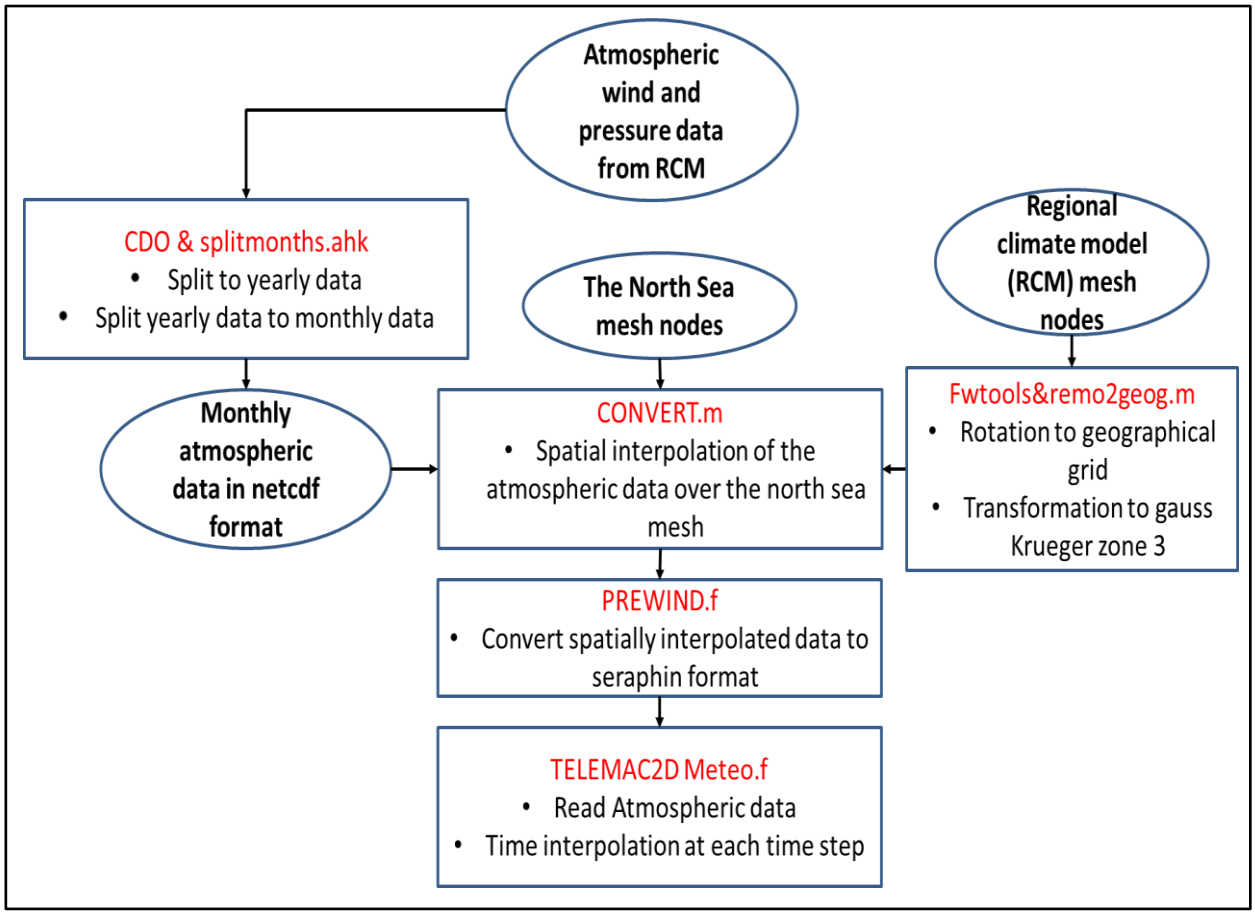

Figure 5.3: Interpolation scheme of meteorological data for the North Sea model, where the developed codes (except Climate Data Operator (CDO), remo2geog.m and Fwtools are free software) are in red and their functions are in black (Tayel & Oumeraci, 2012b).

Figure 5.4 shows the statistics of extremes in sea level pressure and near surface wind as obtained in the atmospheric SN-REMO hindcast. These extremes are described as the 29-years mean of 1st percentile for SLP and as the 99th percentile for 10-m wind speed (Woth, 2006). In the hindcast, a gradient of sea level pressure from 970 hPa (North-West) to 982 hPa (South-East) of the North Sea area is found. Meanwhile, wind speeds between 17 and 20 m/s are produced, increasing from South to North (Woth, 2006).

The CLM control simulation shows an overestimation of the sea level pressure (Figure 5.5 (a)) relative to the SN_REMO hindcast (Figure 5.4(a)). This overestimation increases from North to South with the smallest difference of about 0.5 hPa occurring in the northern part and the largest difference of about 4.5 hPa in the southern part of the computational domain (Woth, 2006). Accordingly, the extreme near-surface wind speed is slightly overestimated. The 99th percentile of wind speed is about 0.5 m/s higher in the southern and south-western parts of the analysed domain, while it increases to about 1.5 m/s in the north-eastern part (Woth, 2006).

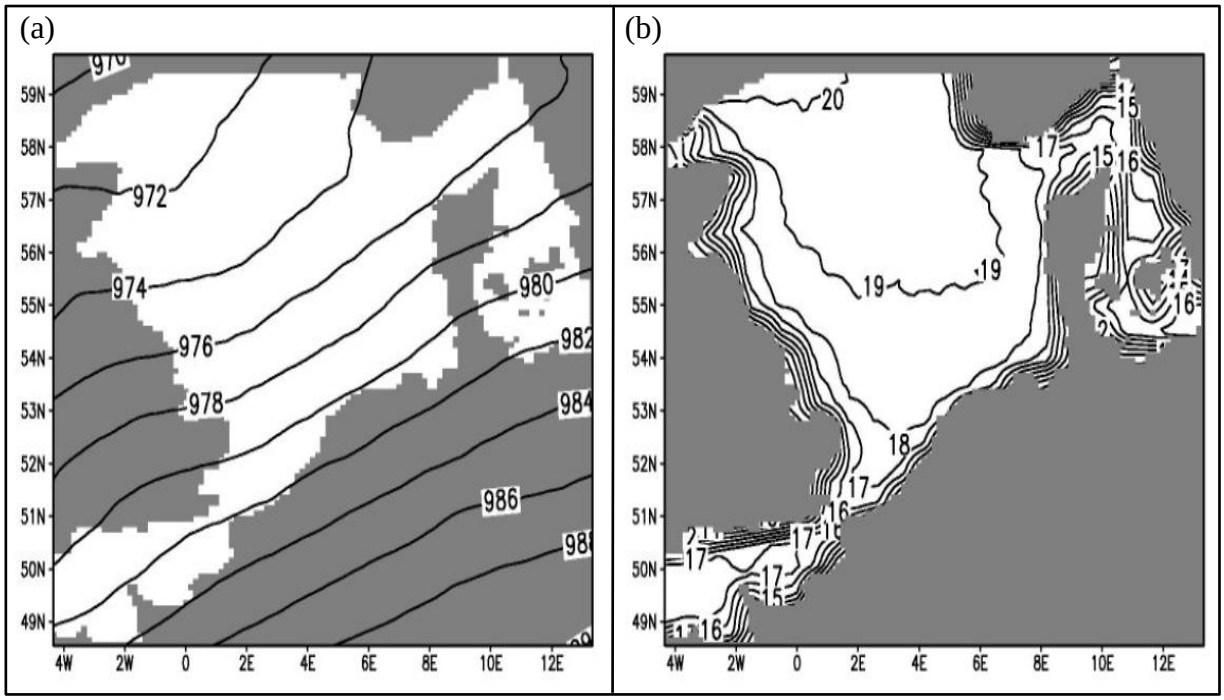

Figure 5.4: Inter-annual mean of the 1st percentile sea level pressure (SLP) (a) and of the 99th percentile 10-m wind speed (b) derived from SN_REMO, hindcast, 1961 – 1990. Units: hPa (SLP) and m/s (wind speed) (Woth, 2006).

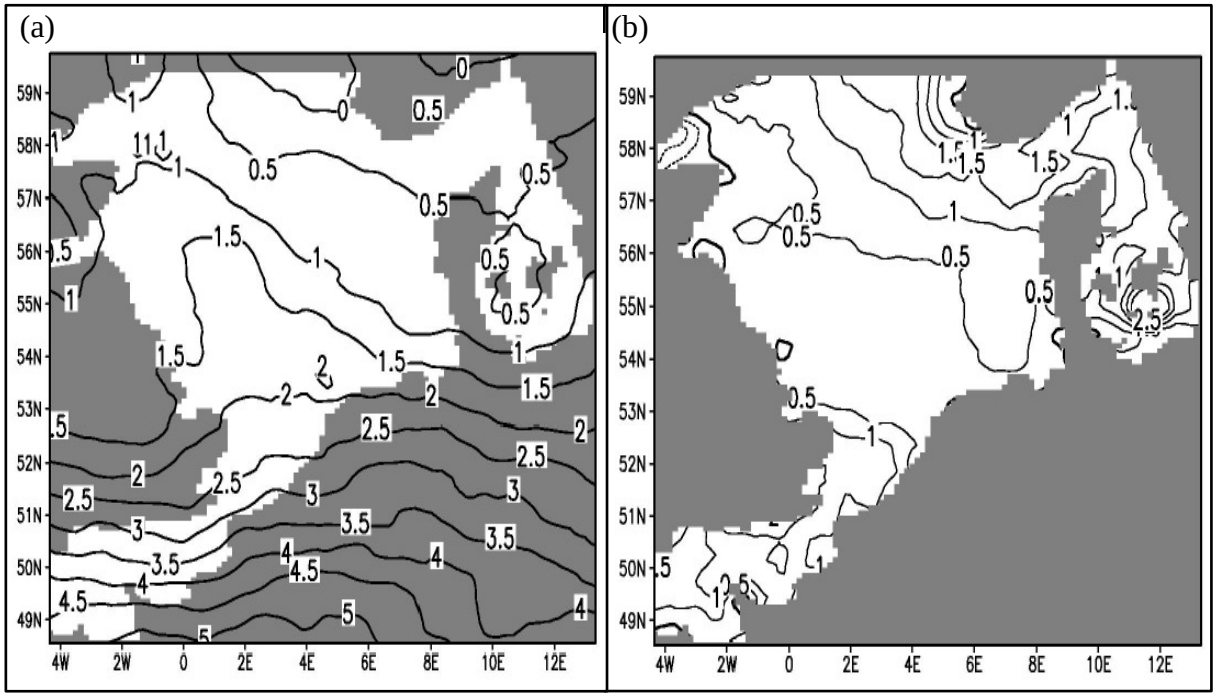

Figure 5.5: Biases of inter-annual mean of the 1st percentile sea level pressure (SLP) (a) as well as of the 99th percentile 10-m wind speed (b) derived from CLM, control condition, 1961 – 1990 relative to the SN_REMO hindcast (Figure 5.4). Units: hPa (SLP) and m/s (wind speed) (Woth, 2006).

(b) Boundary conditions for the North Sea mesh in TELEMAC2D (step 2 in Figure 5.2)

Coastlines adapt to the forcing induced by stochastic events such as waves and storm surges, which are superimposed nonlinearly on the periodic components and processes of the astronomical tides. In fact, the tidal motion in a shelf sea is not usually the direct action of the tidal attractive forces on Earth by the two planets moon and sun. Therefore in the North Sea, the observed tides are a co-oscillating response to the tides generated in the North Atlantic Ocean (Banner, 2011). These co-oscillating tides are expressed by waves which enter and exit the North Sea through the northern open boundary with the North Atlantic Ocean. However, minor tides may also enter and exit the North Sea area through the Dover Strait in the south and the Skagerrak in the east. Therefore, the predicted water level at each node of the northern and western open-sea boundaries (78 nodes) for the North Sea model (Figure 3.8) is used, which is predicted by BSH model for year 2006 and provided by BAW. For these nodes, the harmonic tidal constituents were calculated based on the year 2006 using "Tidal Analysis Toolbox" (Pawlowicz et al., 2002) in order to predict the boundary tidal level for control and hindcast surge-tide simulations between 1970 and 2000.

The prediction of steering forces at the lateral boundaries using the harmonic tide analysis alone does not account for the longer aperiodic water level changes induced by external surges. The influence of Atlantic external surges, which propagate to the North Sea as a long wave in counter clockwise direction (Figure 2.6), but independently of the tidal phase and any periodic regularity, is important for the accurate calculation of water elevations in the North Sea. The observed external surge for the North Sea is higher at the north-west boundary than at the north boundary between Scotland and Norway (Figure 3.8). In order to take this phenomenon into account for the North Sea model in TELEMAC2D, the external surge at Wick (north-west boundary) or Lerwick (north boundary) can be added linearly to the tidal level at each node of the northern open sea boundary (see Figure 3.8). The observed external surges data at Wick and Lerwick between 1969 and 2007, which were used in both control and hindcast surge-tide simulations, was downloaded from the British Oceanographic Data Centre (BODC) website http://www.bodc.ac.uk/. The downloaded data for each year of the above selected period (1969-2007) is recorded with time interval between 15 minutes and 1 hour, which is temporally interpolated in order to be synchronized with the predicted tide at the northern boundary nodes every 15 minutes. Moreover, the observed external surge for Wick contains data gaps and improbable values mostly in the years 1970, 1971 and 1985, while it is the case for Lerwick in the years 1999 and 2000. Since the time interpolation of gaps for the two locations will generate constant external surge values, which are not appropriate for the northern open boundary of the North Sea model. So two external surge NARX models were developed and used to fill the gaps in observed external surge for Wick and Lerwick, which are used for the prediction of external surge in the future simulation between 2070 and 2100 (Tayel & Oumeraci, 2012b).

The effect of river discharge on water levels during storms is almost negligible at Cuxhaven and Sylt especially for smaller discharges ($Q<600\ m^3/s$). The maximum contribution of river

discharge ($(\eta_{rd})_{max}$) at Cuxhaven is not more than 1% Q=3620 m^3/s and without any noticeable effect on surge-tide simulations (see section 4.3.4). Therefore, surge-tide simulations in the North Sea could be calculated without being affected by errors in river discharge predictions. The daily fresh water discharges from the four main rivers in southern of the North Sea area (Westerschelde, Ems, Weser, and Elbe) over 1960-2007 are provided by BAW, which are temporally interpolated every 15 minutes in order to be synchronized with tidal and external surges data in the boundary file for each year between 1970 and 2000.

(c) Processing hindcast and control surge-tide simulations results (steps 3 to 7 in Figure 5.2)

The objectives of the investigations are hindcast and control surge-tide simulations over the North Sea, i.e., the wind and pressure related water-levels under hindcast and control metrological forces. Thus, each simulation was performed using the same model boundary setup, i.e., forced by the same water-level variations at the lateral boundaries representing the global astronomical tidal dynamics, the same external surges from Atlantic Ocean and the same main rivers discharges. The boundaries are located sufficiently far away from the area of interest (southeastern of the North Sea: German Bight) to allow the generation of realistic meteorological-induced surges and the consideration of tide-surge interactions in the interior (see Figure 3.8). Since most of the damages expected in the coastal zone are due to near-shore shallow water effects, which are resolved to a practically sufficient approximation in TELEMAC2D. For the simulations presented here, Gauss-Krüger 3 coordinates with changing spatial resolution from 26 km in the northern Dogger Bank to 80 m in the German estuaries were used. The resulting surge-tides of these simulations include the interactions of storm surges with the tides by TELEMAC2D for control conditions ($(\eta_{su\text{-}t\ TEL})_{C20\_2}$) and hindcast conditions ($(\eta_{su\text{-}t\ TEL})_{H20}$). The state-variables (free surface elevation, vertically averaged velocity and water depth) are stored for all “wet” grid points of the model domain every hour. The first 10 days of each simulation was discarded to account for potential spin-up effects.

Basically, the purpose is to examine the similarity of the control simulation, which is supposed to be representative for the period 1970-2000, with the hindcast simulation as follows:

1. Extract from the hindcast and control surge-tide simulations over the North Sea the annual percentiles of surge-tide (from zero percentile to 100 percentile) for two sites in the German Bight (Cuxhaven and Sylt).
2. Calculate the 30-years average of each extracted percentile
3. Compare the statistics of averaged surge-tide percentiles obtained from the hindcast with the control simulations statistics at both sites (Cuxhaven and Sylt).

Figure 5.6 shows the comparison of the mean annual percentiles for predicted surge-tide (1970–2000), which are obtained from the hindcast and control simulations for both sites (Cuxhaven in the Elbe estuary and Sylt in the open-coast of North Sea). These sites represent quite well the conditions in the larger areas around them. It can be seen that the percentiles from the control and hindcast simulations are very close to each other when the entire period

is considered. Therefore, the control simulation statistics are generally in good agreement with the hindcast at each site, which is represented by the linear correlation of more than 0.99. There is a tendency to a slight underestimation for surge-tide extremes by the control simulation in each site. This is due to the overestimation of the sea level pressure by control meteorological conditions relative to the SN_REMO hindcast (see Figure 5.5 (a)). It should be noted that the underestimation of some extreme events is not a unique shortcoming of the statistical model but also present in numerical models (Dangendorf et al., 2014; Wahl et al., 2010; Weisse & Plüß, 2006). Dangendorf et al. (2014) suggested that the temporal and spatial resolution of the model meteorological forcing is the most likely responsible for the deviations in the highest percentiles. Figure 5.6 indicates that the inter-annual variability of each surge-tide percentiles from the hindcast is close to its counterpart in the control simulations for both sites. For example, the variance of the annual 99.5 percentiles for both control simulations lie within 0.5 cm around the hindcasted variance in each site.

This analysis demonstrates that the *control climate*, which will be used as *a reference for future climate change impacts*, is in agreement with the results from the hindcast simulations and has thus a resemblance with the real climate effect on surge-tide.

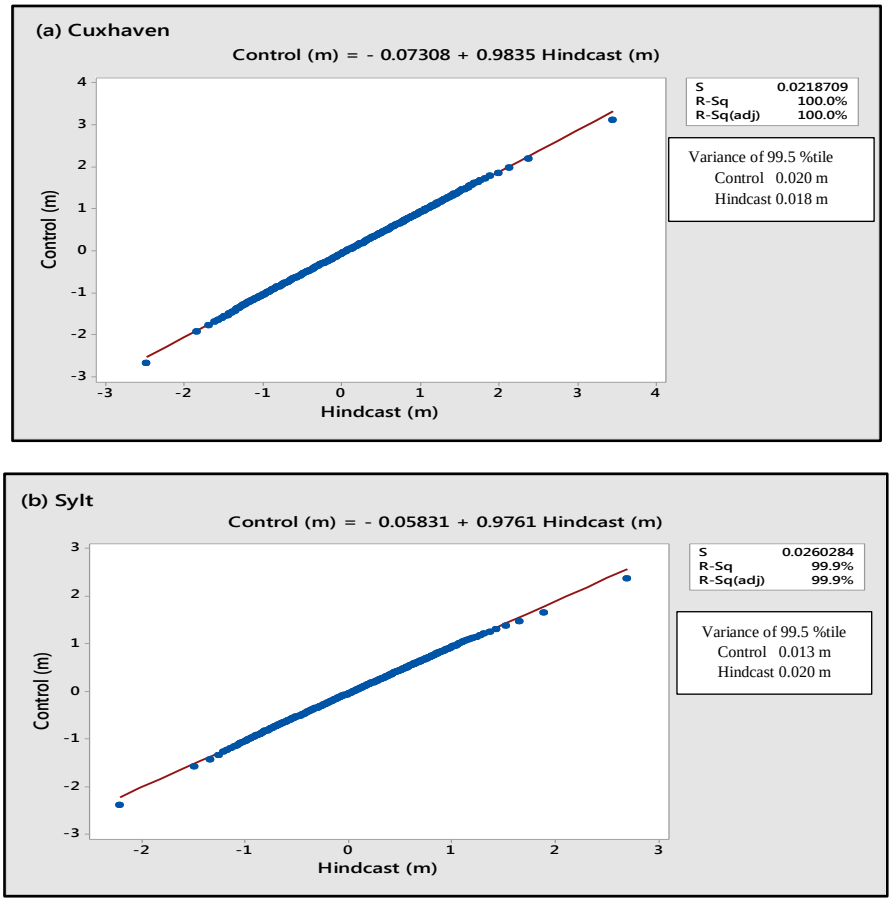

Figure 5.6: Mean annual percentiles of surge-tide (from zero percentile to 100 percentile) in meters at Cuxhaven (a) and Sylt (b) over 1970–2000 from the hindcast ($(\eta_{su\text{-}t\ TEL})_{H20}$) and control simulations ($(\eta_{su\text{-}t\ TEL})_{C20\_2}$) by TELEMAC2D.

Hindcast and control simulations are analysed spatially over the North Sea for the time period between 1970 and 2000. Since extreme surge-tide conditions have the largest implications for many sectors, such as coastal structures and infrastructures, offshore platforms and other facilities or shipping, the analysis is limited to extreme events. In that way, the annual upper percentiles (99.5 percentile ($P_S^{xn}(99.5)$) and maximum surge-tide ($P_S^{xn}(100)$) is considered, where *S* is either hindcast or control simulation (($\eta_{\text{su-t TEL}})_{H20}$ or $(\eta_{\text{su-t TEL}})_{C20\_2}$, respectively) for n years from 1970 to 2000 at each grid point *x* (see Figure 3.8). The averages of upper percentiles are considered to be a relatively robust measure for changes in the statistics of extreme events. So these percentiles were averaged over a 30-year time period from 1970 to 2000 for hindcast and control simulations (for 99.5 percentile ($P_S^x(99.5)$ and maximum surge-tide ($P_S^x(100)$, respectively). Figure 5.7 presents the inter-annual means of 99.5th and 100th percentiles from North Sea surge-tide under the hindcast meteorological condition ($P_{H20}^x(99.5)$ and $P_{H20}^x(100)$, respectively) along with their confidence intervals ($CI^x(99.5)$ and $CI^x(100)$, respectively) using Student's *t* test under a statistical significance level of 95%. It is noticeable that $P_{H20}^x(99.5)$ and $P_{H20}^x(100)$ along with their confidence intervals are affected mainly by the large-scale tidal amphidromic system of the North Sea. In the German Bight, the $P_{H20}^x(99.5)$ (see Figure 5.7(b)) increases from 0.6 m near the middle amphidromic point to 2.4 m close to the landward border of the Elbe estuary, while $P_{H20}^x(100)$ (see Figure 5.7(e)) increases from 1.2 m to 3.6 m. in the southern part of North Sea, where another amphidromic system stretching from the Wash to Dover, The $P_{H20}^x(99.5)$ (see Figure 5.7(b)) increases from 1.2 m to 4.0 m close to the landward border of Wash or Dover, while $P_{H20}^x(100)$ (see Figure 5.7(e)) increases from 1.8 m to 4.5 m. Confidence intervals $CI^x(99.5)$ and $CI^x(100)$ represent the range of natural variability by surge-tide climate. The lower and upper values of $CI^x(99.5)$ (Figure 5.7(a) and (c)) and $CI^x(100)$ (Figure 5.7(d) and (f)) are close to $P_{H20}^x(99.5)$ and $P_{H20}^x(100)$, respectively and reflect the increasing effect on surge-tide with larger distances from the tidal amphidromic points locations.

The bias signals of the control simulations for upper percentiles ($\Delta_{C20\_2}^x(99.5)$ and $\Delta_{C20\_2}^x(100)$) are defined as the difference between the mean values $P_{C20\_2}^x(99.5)$ or $P_{C20\_2}^x(100)$ in the control simulation (C20_2) and the corresponding mean values $P_{H20}^x(99.5)$ or $P_{H20}^x(100)$ from the hindcast simulation (H20) i.e.:

$$\Delta_{C20\_2}^x(99.5) = P_{C20\_2}^x(99.5) - P_{H20}^x(99.5) \tag{5.1}$$

$$\Delta_{C20\_2}^x(100) = P_{C20\_2}^x(100) - P_{H20}^x(100) \tag{5.2}$$

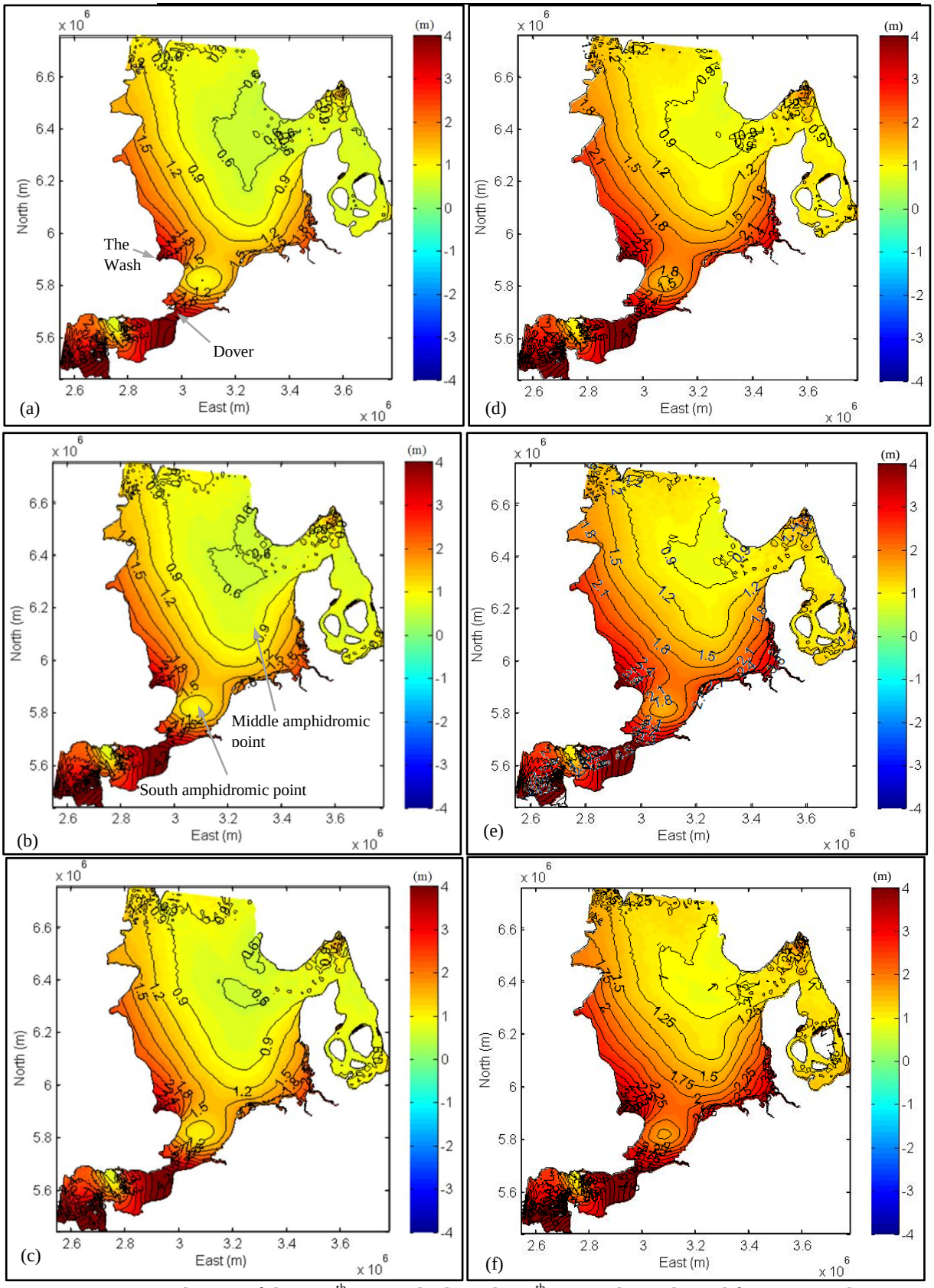

Figure 5.7: Inter-annual mean of the 99.5th percentile (b) and 100th percentile (e) derived from surge-tide in meters under SN_REMO hindcast, 1970 – 2000, along with their confidence intervals on a 95% level based on a Student's *t* test. Lower and upper values of the 99.5th percentile confidence interval are in (a) and (c), respectively, while for the 100th percentile are in (d) and (f), respectively.

Generally, there is a gradual decrease in the bias signal of the control simulation for the upper percentiles from the middle of North Sea toward the Elbe estuary. For $\Delta^{x}_{C20\_2}(99.5)$ and $\Delta^{x}_{C20\_2}(100)$, the maximum decrease in the mean difference of surge-tide occurs in the south-eastern North Sea (see Figure 5.8), which reach -0.14 m and -027 m, respectively. These correspond to about 6% and 7.5% decrease, respectively for $\Delta^{x}_{C20\_2}(99.5)$ and $\Delta^{x}_{C20\_2}(100)$, in comparison to the maximum hindcast simulation values. Moreover, $\Delta^{x}_{C20\_2}(99.5)$ and $\Delta^{x}_{C20\_2}(100)$ are approximately zero in the middle of the upper North Sea region. This corresponds to the general pattern of the sea level pressure overestimation by the regional climate model CLM, which increases from the northern to the southern North Sea.

An extreme surge-tide event is defined for a period covering one or more hourly intervals during which the 99.5th percentile is exceeded. The average duration and number of such extreme events in the hindcast and control simulations are also determined over the North Sea (1970-2000). In fact, both characteristics are important parameters in the context of design, constructions and operation of marine structures and other facilities. Figure 5.9 shows the inter-annual means of the duration and frequency for extreme events under the hindcast meteorological conditions ($d^{x}_{H20}(\geq 99.5)$ and $f^{x}_{H20}(\geq 99.5)$, respectively) along with their confidence intervals ($CI^{x}_{d}(\geq 99.5)$ and $CI^{x}_{f}(\geq 99.5)$, respectively) using Student's *t* test with statistical significance level of 95 %. Since $P^{x}_{\mathrm{H20}}(99.5)$ and $P^{x}_{\mathrm{H20}}(100)$ over the North Sea are affected mainly by the large-scale tidal amphidromic system of the North Sea, duration $d^{x}_{H20}(\geq 99.5)$ and frequency $f^{x}_{H20}(\geq 99.5)$ of the extreme events and their confidence intervals are also affected. In the German Bight, duration $d^{x}_{H20}(\geq 99.5)$ decreases from 9 hour near the middle amphidromic point to 3 hour close to the landward border of the Elbe estuary (see Figure 5.9 (b)), while frequency $f^{x}_{H20}(\geq 99.5)$ increases from 5 event/year to 13.4 event/year (see Figure 5.9 (e)). In the southern part of the North Sea, where another amphidromic system stretching from the Wash to Dover, duration $d^{x}_{H20}(\geq 99.5)$ decreases from 6 hour to 2.4 hour close to the landward border of the Wash or Dover (see Figure 5.9(b)). In contrast, mean frequency $f^{x}_{H20}(\geq 99.5)$ increases from 8 event/year to 12.8 event/year close to the deep water border of Wash or Dover and then decreases to approximately 5 event/year toward their landward borders (see Figure 5.9 (e)). This corresponds to the general pattern of the storm surge height distribution for the North Sea, which has its maximum in the German Bight (Woth, 2006; Gaslikova et al., 2013) and affected mainly by tides.

Confidence intervals $CI^{x}_{d}(\geq 99.5)$ and $CI^{x}_{f}(\geq 99.5)$ represent the range of natural variability for the duration and frequency of extreme surge-tide events, respectively. The lower and upper values of $CI^{x}_{d}(\geq 99.5)$ (Figure 5.9 (a) and (c)) and $CI^{x}_{f}(\geq 99.5)$ (Figure 5.9 (d) and (f)) are close to $d^{x}_{H20}(\geq 99.5)$ and $f^{x}_{H20}(\geq 99.5)$, respectively, furthermore their behaviour as a function of the distance from the location of tidal amphidromic points is similar.

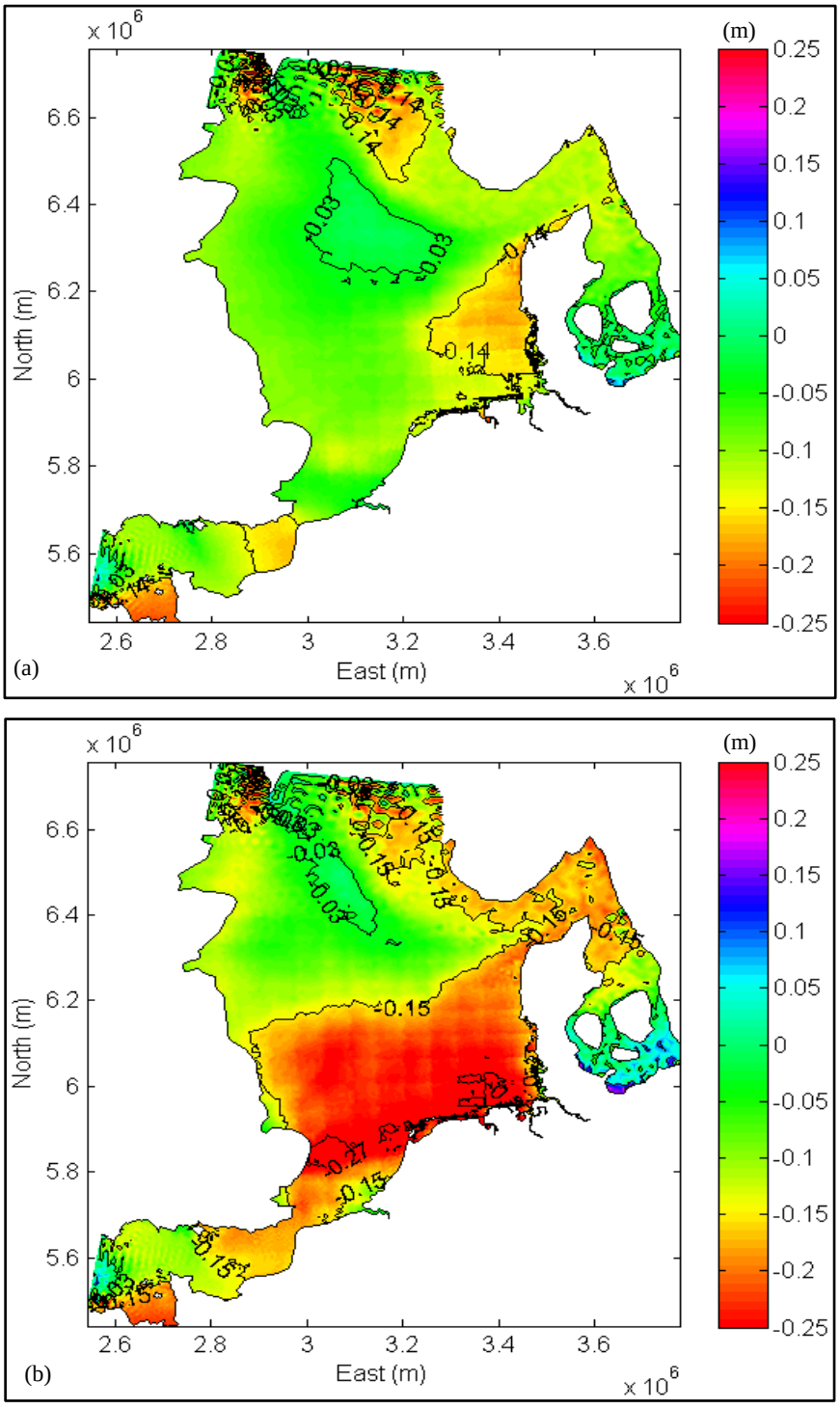

Figure 5.8: Control bias signals for 30-year surge-tide averages (1970-2000) of annual 99.5 percentile (a) and 100 percentile (b) over the North Sea in meters.

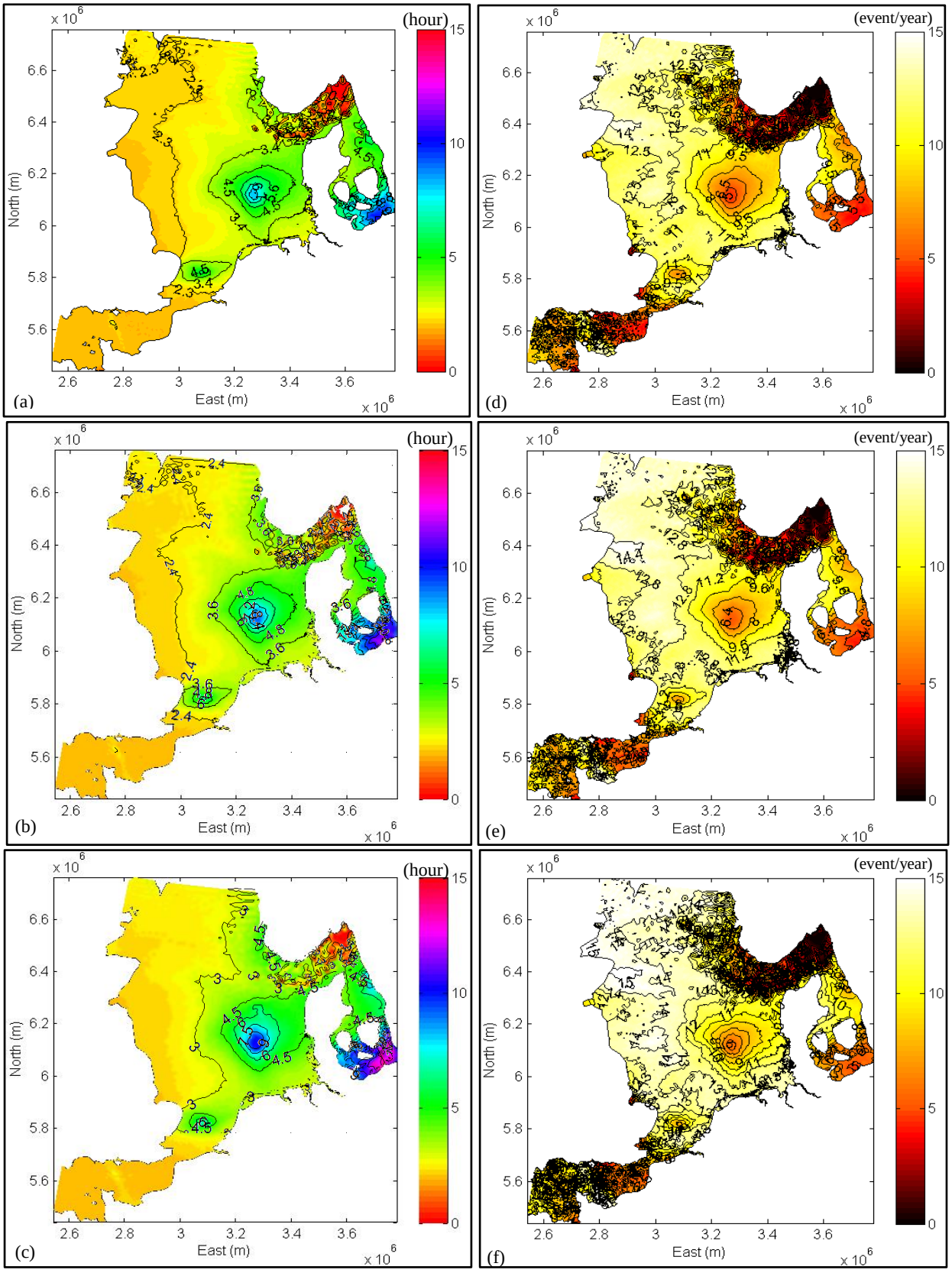

Figure 5.9: Annual mean duration of extreme events "surge-tide with percentiles above 99.5% tile" (b) and mean number of these events (e) for the hindcast (1970-2000), along with their confidence intervals on a 95% level by Student's *t* test. Lower and upper values of the extreme events duration are in (a) and (c), respectively, while for their frequency are in (d) and (f), respectively.

The bias signal of the mean duration and frequency for extreme surge-tide events ($\Delta d^{x}_{C20\_2}(\geq 99.5)$ or $\Delta f^{x}_{C20\_2}(\geq 99.5)$, respectively) is defined as the difference between the mean value ($d^{x}_{C20\_2}(\geq 99.5)$ or $f^{x}_{C20\_2}(\geq 99.5)$,respectively) in the control simulation (C20_2) and the corresponding mean value ($d^{x}_{H20}(\geq 99.5)$ or $f^{x}_{H20}(\geq 99.5)$, respectively) from the hindcast simulation (H20) i.e.:

$$\Delta d^{x}_{C20\_2}(\geq 99.5) = d^{x}_{C20\_2}(\geq 99.5) - d^{x}_{H20}(\geq 99.5) \tag{5.3}$$

$$\Delta f^{x}_{C20\_2}(\geq 99.5) = f^{x}_{C20\_2}(\geq 99.5) - f^{x}_{H20}(\geq 99.5) \tag{5.4}$$

Generally in the control surge-tide simulations, the annual-mean duration and frequency of extreme events compare well with the hindcast simulations over the North Sea. Annual-mean duration $\Delta d^{x}_{C20\_2}(\geq 99.5)$ decreases to one hour only around the middle amphidromic point in the German Bight, while it remains approximately constant in the rest of the North Sea in the hindcast simulations (Figure 5.10 (a)). Moreover, the change in the number of extreme events $\Delta f^{x}_{C20\_2}(\geq 99.5)$ increases to 1.61 event/year in the area around the middle amphidromic point with no or very slight changes in the rest of the North Sea area (Figure 5.10 (b)).

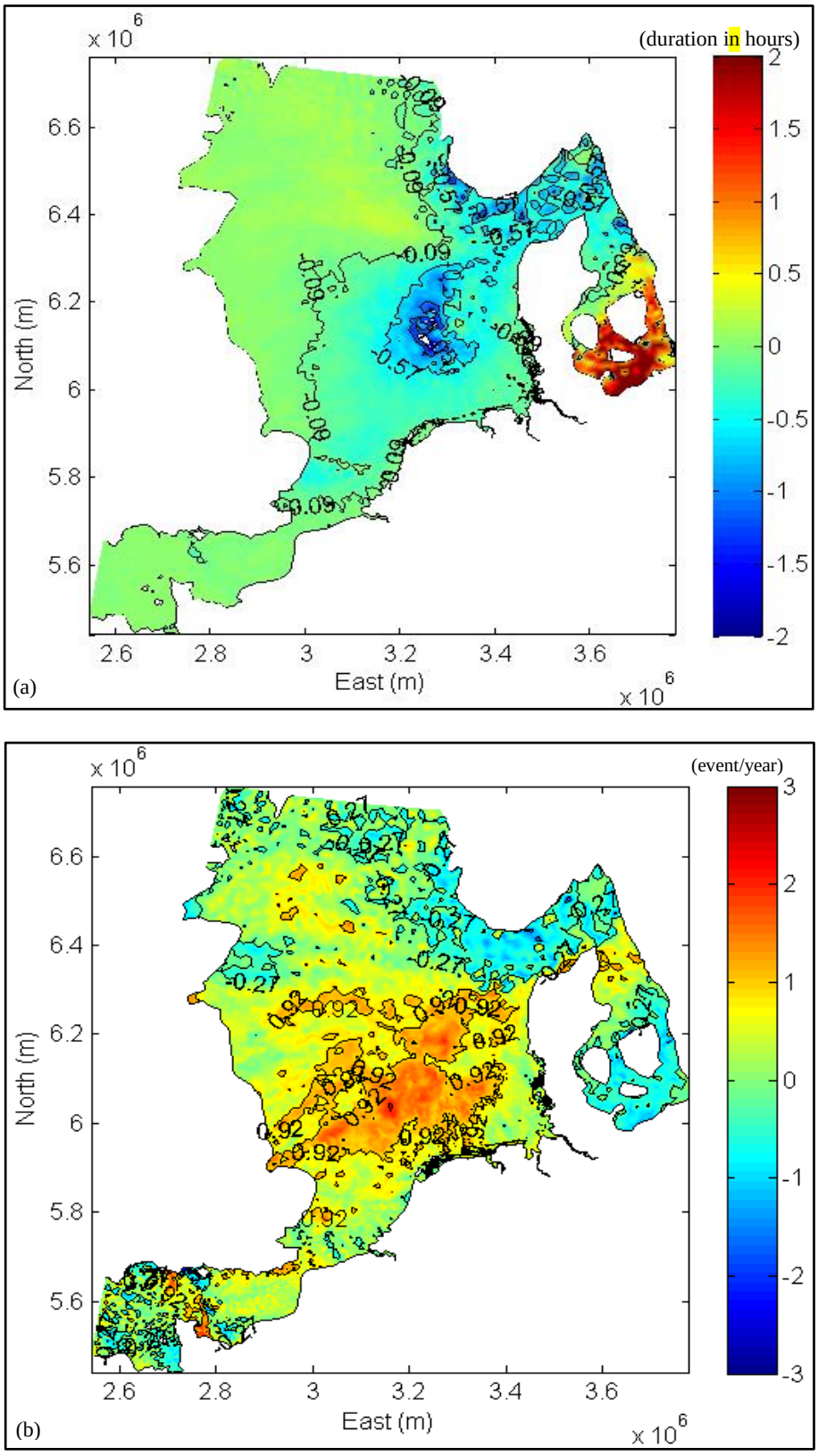

Figure 5.10: Control bias signals of the duration (a) and frequency (b) for extreme surge-tide events as the difference between their annual means in the control simulation (C20_2; 1970-2000) and the corresponding mean values from the hindcast simulation (H20; 1970-2000).

The results from the control simulations of the surge-tides over the North Sea are statistically in agreement with those from the hindcast simulations in 1970-2000 and have thus a resemblance with the real climate. The bias signal of the control simulations for upper percentiles ($\Delta^{x}_{C20\_2}(99.5)$ and $\Delta^{x}_{C20\_2}(100)$) gradually decreases from the middle part of the North Sea toward the Elbe estuary. The $\Delta^{x}_{C20\_2}(99.5)$ and $\Delta^{x}_{C20\_2}(100)$ show a maximum decrease of about 6% and 7.5%, respectively in comparison with the maximum values obtained from the hindcast simulations in the southeastern of North Sea. Moreover, the annual-mean duration and frequency of extreme events in the control simulations compare well with the hindcast over the North Sea. Since the systematic errors (bias) appear in the control simulations of the present storm-tide conditions, the difference between the future and control simulations will represent the response of future emission scenario. So the results of this statistical analysis demonstrates that the control climate by the RCM CLM can be used as an adequate reference for future climate change impacts.

5.1.2 Future surge-tide simulation for the North Sea using TELEMAC2D (Stage 2)

In this section, the simulation of future surge-tide climate (2070-2100) for the North Sea is performed according to the steps shown in Figure 5.2 and described below:

1. Prescribe the meteorological forces regionalized by CLM model, which are the main responsible factors for the generation of surge-tide, to the North Sea model in TELEMAC2D (Figure 3.8) as "inputs" for future simulation under A1B scenario (e.g. sea level pressure, meridional and zonal wind speed components).
2. Use the average fresh water discharge of the main four rivers in southern North Sea as boundary conditions for fresh water discharge (Q) under future conditions (2070-2100).
3. Predict the external surge at Wick or Lerwick (η_{ds}) under future conditions (2070-2100) using the developed time series prediction by NARX models that are used to fill the missing data in 1970 - 2007.
4. Predict the astronomical tide for each mesh point in northern and western boundaries of the North Sea model (Figure 3.8).
5. Drive the North Sea model in TELEMAC2D using the boundary conditions of all components, which are prescribed simultaneously in order to predict the surge-tide under future meteorological conditions $(\eta_{\text{su-t TEL}})_{\text{A1B\_2}}$.
6. Calculate the annual upper percentiles of control (predicted in stage 1, step 3) and future simulations (99.5 percentile ($P^{x\text{n}}_{S}(99.5)$) and maximum surge-tide ($P^{x\text{n}}_{S}(100)$), where S is either control simulation $(\eta_{\text{su-t TEL}})_{\text{C20\_2}}$ for years n from 1970 to 2000 or future simulation $(\eta_{\text{su-t TEL}})_{\text{A1B\_2}}$ between 2070 and 2100) at every mesh point *x* in the North Sea model (Figure 3.8).
7. Calculate the mean of $P^{x\text{n}}_{S}(99.5)$ and $P^{x\text{n}}_{S}(100)$ in step 6 either over 1970-2000 for control condition ($P^{x}_{C20\_2}(99.5)$ and $P^{x}_{C20\_2}(100)$) or over 2070-2100 for future condition ($P^{x}_{A1B\_2}(99.5)$ and $P^{x}_{A1B\_2}(100)$) at every mesh point *x*.

8. Calculate the climate change signals ($\Delta^x(99.5)$ and $\Delta^x(100)$) as the difference between the mean value $P^x_{A1B\_2}(99.5)$ or $P^x_{A1B\_2}(100)$ in the climate change simulation (A1B_2) and the corresponding mean value $P^x_{C20\_2}(99.5)$ or $P^x_{C20\_2}(100)$ from the control simulation (C20_2) i.e.:

$$\Delta^x(99.5) = P^x_{A1B\_2}(99.5) - P^x_{C20\_2}(99.5) \tag{5.5}$$

$$\Delta^x(100) = P^x_{A1B\_2}(100) - P^x_{C20\_2}(100) \tag{5.6}$$

9. Compare the climate change signals $\Delta^x(99.5)$ and $\Delta^x(100)$ with the corresponding confidence intervals $CI^x(99.5)$ and $CI^x(100)$ (calculated in stage 1, step 7) to identify the significant changes in future surge-tide climate for every mesh point *x* in the North Sea model.

(a) Meteorological data preparation and application for the North Sea model (2070-2100) in TELEMAC2D (step 1 in Figure 5.11)

The surface wind is considered as the main forcing factor for surge-tide in the North Sea. The changes in extreme wind conditions due to climate change help to explain future changes in the extreme storm-tide events. The effects of climate change depend on the selected scenario among the "future climate scenarios" proposed by IPPC (Houghton, 1996; Houghton et al., 1992, 2001). Employing scenarios requires the construction of a series of possible, mutually exclusive but internally consistent futures, which describe different developments of the dynamics conditional upon a number of key assumptions (Woth, 2006). These futures are not equally probable but they are all possible, and should be plausible and logical (von Storch & GKSS, 2005). These 'storylines' are translated into different amounts of climatically relevant greenhouse gas emissions (GHG) and aerosols loadings until the end of 21st century (see Box 5.1). Afterward, the GHG and aerosols loadings are specified externally to the GCMs in order to compute several decades of weather, typically using a 6-hourly output interval. The GCM outputs were dynamically downscaled using the RCMs to a finer grid covering Western Europe including the North Sea area (see Figure 5.1). Moreover, these emissions could lead to different rates of sea level rise depending on the thermal expansion of ocean and continental ice sheet melting in response to the increase of global temperature. Table 5.2 summarizes the different scenarios along with their induced global temperature increases and sea level rises according to IPCC Assessment Report AR4 of 2007.

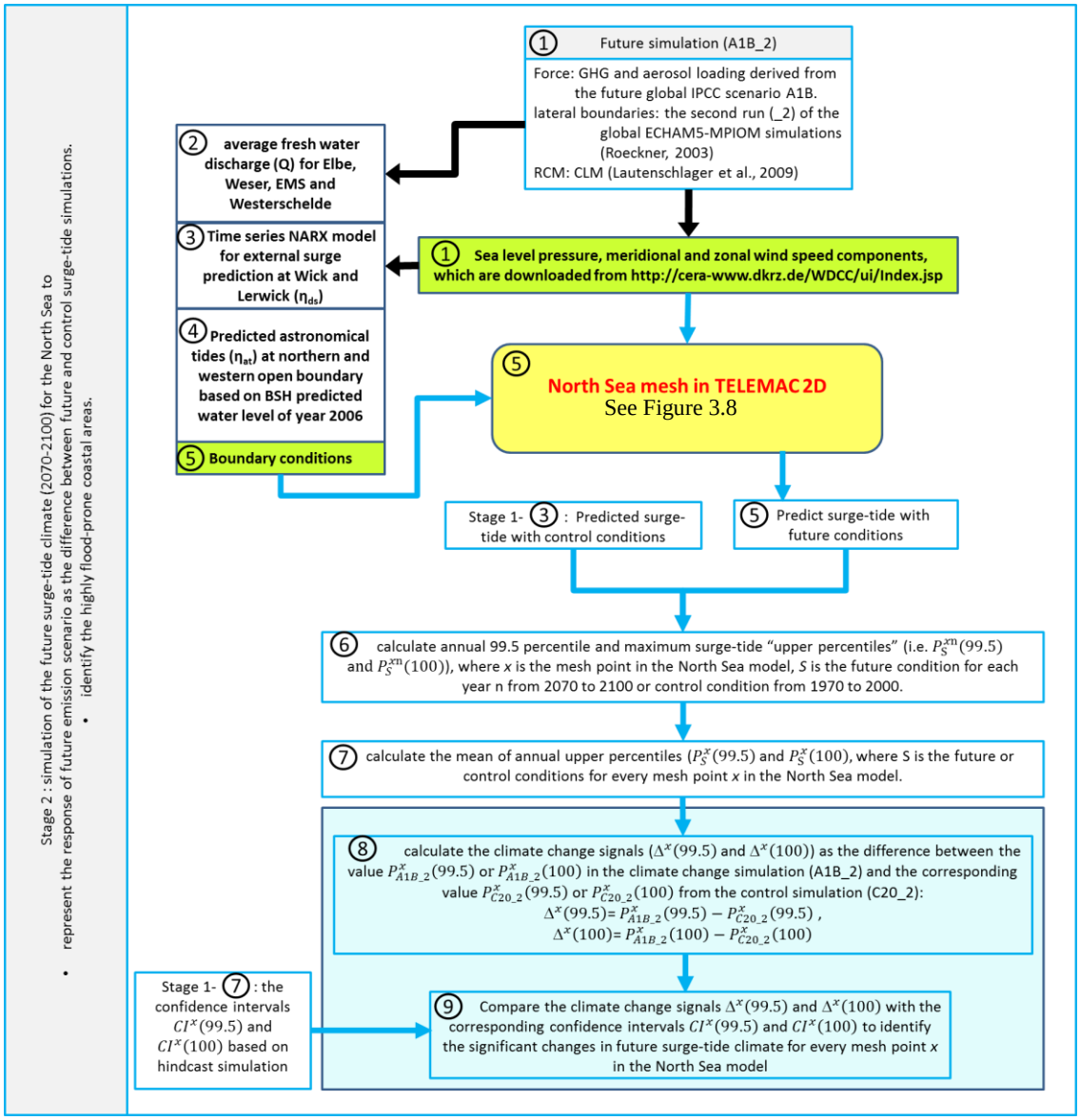

Figure 5.11: simulation of the future surge-tide change signals (2070-2100) for the North Sea based on control and hindcast results from stage 1(Figure 5.2).

Table 5.2: Emissions scenarios with their increase in global temperature and projected sea level rise in 2100 according to PCC Assessment Report AR4 of 2007 (Chini, 2012).

Scenario name	Emissions scenario	Global temperature increase (C), with likely range in 2100	Sea level rise in 2100 (m)
A1F1	high	4.0 (2.4 – 6.4)	0.26 – 0.59
A2	Medium high	3.4 (2.0 – 5.4)	0.23 – 0.51
A1B	medium	2.8 (1.7 – 4.4)	0.21 – 0.48
B2	Low medium	2.4 (1.4 – 3.8)	0.20 – 0.43
B1	low	1.8 (1.1 – 2.9)	0.18 – 0.38

THE EMISSION SCENARIOS OF THE IPCC SPECIAL REPORT ON EMISSION SCENARIOS (SRES)

A1. The A1 storyline and scenario family describes a future world of very rapid economic growth, global population that peaks in mid-century and declines thereafter, and the rapid introduction of new and more efficient technologies. Major underlying themes are convergence among regions, capacity building and increased cultural and social interactions, with a substantial reduction in regional differences in per capita income. The A1 scenario family develops into three groups that describe alternative directions of technological change in the energy system. The three A1 groups are distinguished by their technological emphasis: fossil-intensive (A1FI), non-fossil energy sources (A1T) or a balance across all sources (A1B) (where balanced is defined as not relying too heavily on one particular energy source, on the assumption that similar improvement rates apply to all energy supply and end use technologies).

A2. The A2 storyline and scenario family describes a very heterogeneous world. The underlying theme is self-reliance and preservation of local identities. Fertility patterns across regions converge very slowly, which results in continuously increasing population. Economic development is primarily regionally oriented and per capita economic growth and technological change more fragmented and slower than other storylines.

B1. The B1 storyline and scenario family describes a convergent world with the same global population, that peaks in mid-century and declines thereafter, as in the A1 storyline, but with rapid change in economic structures toward a service and information economy, with reductions in material intensity and the introduction of clean and resource-efficient technologies. The emphasis is on global solutions to economic, social and environmental sustainability, including improved equity, but without additional climate initiatives.

B2. The B2 storyline and scenario family describes a world in which the emphasis is on local solutions to economic, social and environmental sustainability. It is a world with continuously increasing global population, at a rate lower than A2, intermediate levels of economic development, and less rapid and more diverse technological change than in the B1 and A1 storylines. While the scenario is also oriented towards environmental protection and social equity, it focuses on local and regional levels.

An illustrative scenario was chosen for each of the six scenario groups A1B, A1FI, A1T, A2, B1 and B2. All should be considered equally sound.

The SRES scenarios do not include additional climate initiatives, which means that no scenarios are included that explicitly assume implementation of the United Nations Framework Convention on Climate Change or the emissions targets of the Kyoto Protocol.

Box 5.1: Summary of emissions scenarios proposed in the IPCC Special Report on Emission Scenarios (Meehl et al., 2007).

In this study, only one emission scenario has been selected due to the long simulation time of the North Sea model that will be required for the generation of surge-tide by TELEMAC2D and wave propagation by TOMAWAC under all scenarios. The selected scenario should represent the ensemble mean of all scenarios and preserve a good skillful-scale, i.e. the scale at which atmospheric features are described reasonably well by a climate model. The skillful-scale should be larger than the actual grid cell resolution of a climate model (Pielke, 1991; von Storch, 1995).

Recently, the investigation of storm surge potential changes (trends) under several scenarios for the North Sea over the last 30-year of 21th century have been conducted. (Gaslikova et al., 2013) analysed the 99 percentile of the annual 10 m height wind speed for storm surge chang-

es under two climate change scenarios. They used the 99 percentile of wind speed, since the latter reaches about 18 m/s that is above eight Beaufort (17.2 m/s), which is a storm benchmark. The climate change conditions were A1B_1, A1B_2, B1_1 and B1_2, i.e. two IPCC emission scenarios (SRES A1B and B1) under two initial conditions for the GCM (1 and 2). For this purpose, the hourly wind and 3-hourly SLP fields from the COSMO-CLM regionalizations (0.165^o x 0.165^o horizontal resolution) forced at the boundary by the global ECHAM5-MPIOM simulations (1.8^o x 1.8^o horizontal resolution) for the two control climates C20_1 and C20_2 (1961-2000) and for the four future climate projections A1B_1, A1B_2, B1_1 and B1_2 (2001-2100) were used. The differences between the four climate projections for 30-year period (2071-2100) and the corresponding control climate (1961-1990) for the mean annual 99 percentile show an increase for most parts of the North Sea (see Figure 5.12). On a 95 %-level, these changes are only statistically significant (based on a Student's t test) above roughly 0.4 m/s. The maximum changes of all projections (except B1_2) occur in the southern North Sea including the German Bight. All projections show a decrease (not statistically significant) in the mean annual 99 percentile in the northern and northeastern North Sea. Moreover, a general view of the four climate change realisations is shown through the differences of the ensemble mean for the annual 99 percentile between the 30-year period 2071–2100 and the control period 1961–1990 (see Figure 5.13). These differences show an increase of wind speeds up to 0.3 m/s in the southern North Sea and the German Bight (Gaslikova et al., 2013). Note that due to the larger sample size of the ensemble mean compared to the single realizations, already changes larger than 0.2 m/s are statistically significant on a 95 %-level (Gaslikova et al., 2013).

From Figure 5.12 and Figure 5.13, the changes of the mean 99 percentile wind speed regionalized by the ECHAM5-MPIOM/CLM models under A1B_2 realization has the most resemblance to the characteristics shown by the ensemble mean. Under the A1B_2 and ensemble mean future realizations, the changes in mean annual 99 percentile wind speed of 0.2 m/s cover approximately the same distributions for the middle and southern parts of the North Sea including the German Bight, while both realizations reflect a decrease of -0.2 m/s in the northeastern North Sea. On the other hand, the changes in mean annual 99 percentile wind speed under A1B_1 and B1_1 realizations, which reach 0.6 m/s and 0.4 m/s, respectively, are stronger than those shown by the ensemble mean in the middle and southern parts of the North Sea. While there are no changes under B1_2 realization due to climate change in most parts of the North Sea.

Therefore, the future realization with A1B_2 is used in this study to show the impact of climate change projections on surge-tide and waves over the North Sea area. So the same preparation procedure is also adopted in the control conditions (see section 5.1.1(a)), since the configuration of the used meteorological models is exactly like in the control simulations (1970-2000). The regionalized meteorological data of future conditions under A1B_2 realization is downloaded from the WDCC website http://www.dkrz.de/daten/wdcc/. The future meteorological conditions (the wind at 10m elevation above MSL and SLP fields) between 2070 and 2100 are rotated back to geographical coordinate system with North Pole (0^o longitude, 90^o latitude). These re-rotated meteorological conditions are transformed afterward to the "3-

degree Gauss-Kruger zone 3" coordinate system, which is used by the North Sea hydrodynamic model in TELEMAC2D (Figure 3.8). Thereafter, the same interpolation scheme of control conditions is applied (see Figure 5.3). The transformed future meteorological conditions are interpolated in space over the North Sea computation grid (Figure 3.8). Accordingly, a linear temporal interpolation is performed at each computational time step inside TELEMAC2D by the modified subroutine METEO.f (Tayel & Oumeraci, 2012b).

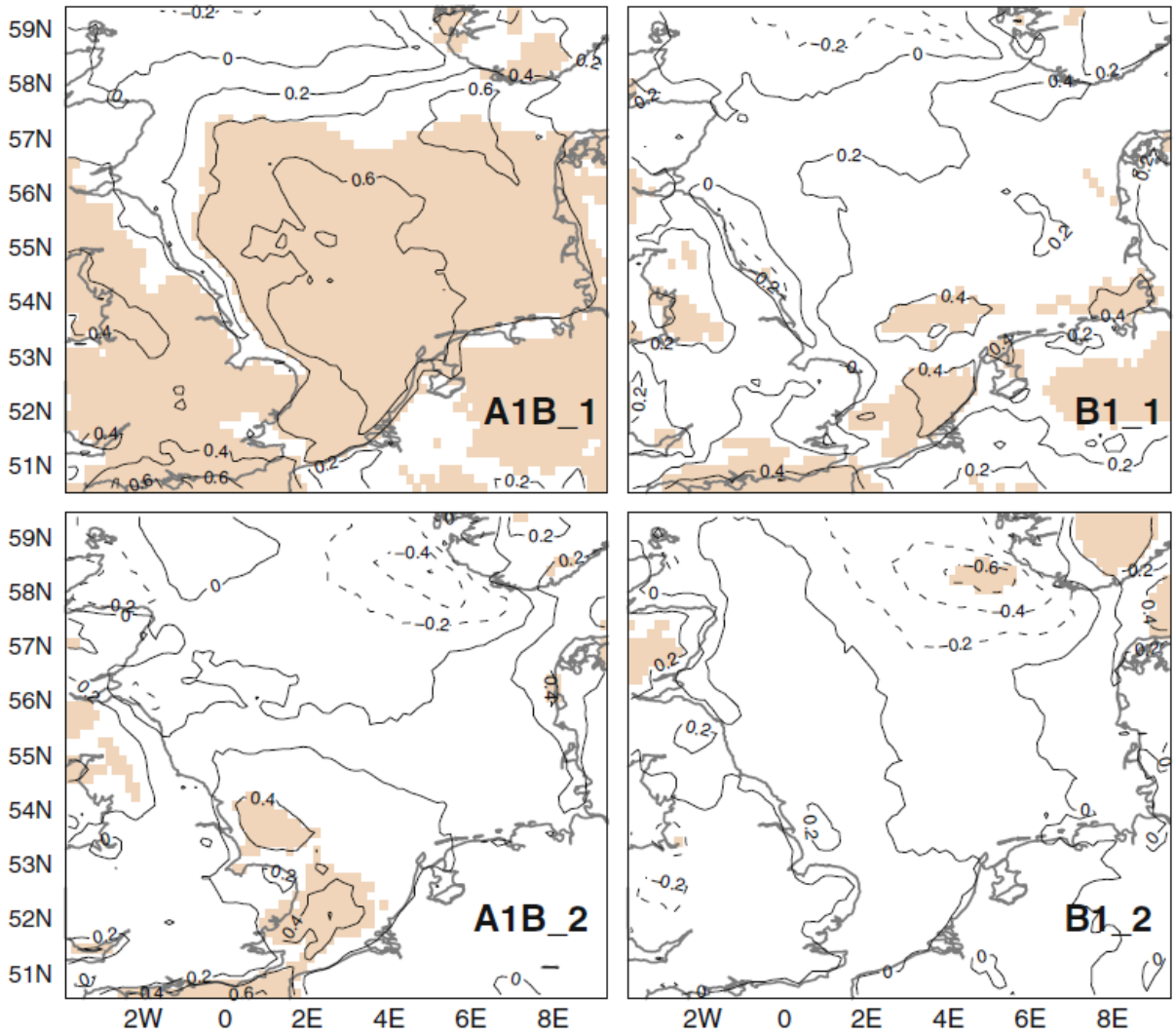

Figure 5.12: Climate change signals for 30-year averages of annual 99 percentile wind speed in meters per second for A1B_1 (upper left), B1_1 (upper right), A1B_2 (lower left) and B1_2 (lower right). Shaded areas show significant differences on a 95% level based on a Student's t test (Gaslikova et al., 2013).

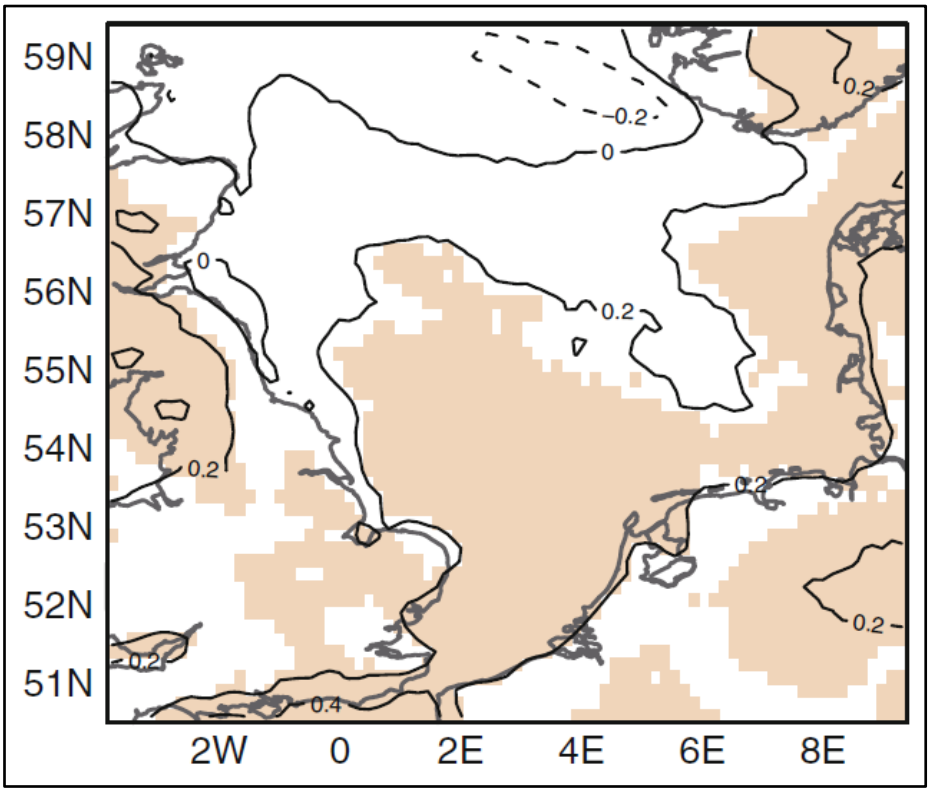

Figure 5.13: Climate change signal for 30-year averages of annual 99 percentile wind speed in meters per second for the ensemble mean (the mean of the four climate projections A1B_1, A1B_2, B1_1 and B1_2). Shaded areas show significant differences on a 95% level based on a Student's t test (Gaslikova et al., 2013).

Figure 5.14 displays climate change signals of the annual 99 percentile wind speed as deviations of future mean (A1B_2, 2070-2100) from the control mean (C20_2, 1970-2000) for Cuxhaven and for Sylt. The 10-year running averages of annual 99 percentile wind speed are calculated for the future meteorological conditions, since the annual values of each 10 years in (2070-2100) follow a normal distribution (normality test with Anderson-Darling with P-value>0.05). These signals show a strong increase up to ca. 2087 followed by a decrease up to 2095, which vary spatially between the two sites (Cuxhaven and Sylt). For the two sites in the German Bight, the maximum value is reached in 2087 with 0.50 m/s for Cuxhaven and 0.21 m/s for Sylt, while the minimum value occurs in 2077 with -0.20 m/s for Cuxhaven and -0.41 m/s for Sylt. Moreover, there are similarities between the two sites in the patterns of the temporal change in the annual 99 percentile signals. Nevertheless, the climate change signals at Cuxhaven, which are all positive from 2080 to 2095, are stronger than those of Sylt that only positive between 2086 and 2088.

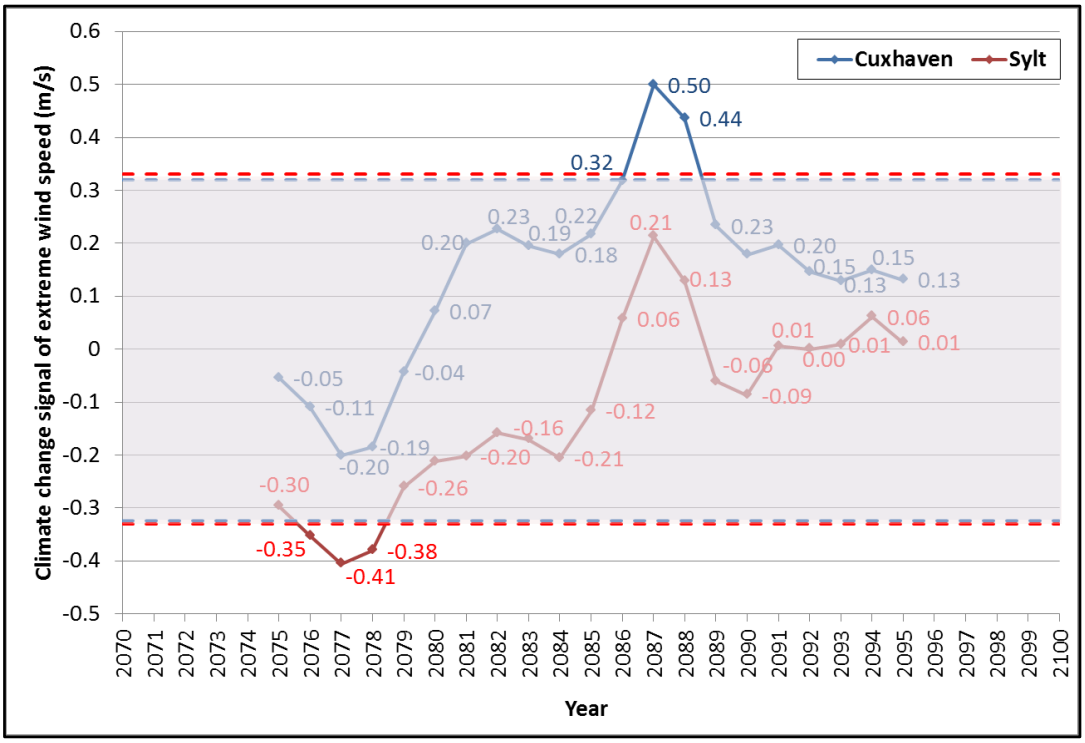

Figure 5.14: Time series of climate change signals for 10-year running averages of annual 99 percentile wind speed in meters per second for the A1B_2 climate (2070-2100) relative to the mean of control climate (1970-2000) at Cuxhaven and Sylt. Shaded areas between blue or red dashed lines correspond to the 95 % confidence interval for the hindcast mean based on bootstrapping at Cuxhaven or Sylt, respectively.

In addition to the effect of the changes in wind speed on surge-tide levels in coastal areas, the effects of the frequency of strong winds and wind direction are also considerable. For Cuxhaven and Sylt, the wind directions were divided into 30° sectors from 15°-45° to 345°-15° (where 0°=360° is the north) and the frequency of strong wind speeds (≥17.2 m/s) coming from a particular sector has been calculated. The mean changes in wind direction are illustrated by Figure 5.15 for Cuxhaven and Sylt for two 30-year time intervals in 1970-2000 and in 2070-2100, showing a direct comparison of the frequency distributions of strong wind speeds between these two time intervals at Cuxhaven (Figure 5.15a) and Sylt (Figure 5.15b). At both sites, there is a general increase in frequency of strong south-westerly to north-westerly winds and a slight decrease of northerly and/or easterly winds. Moreover, the northerly and/or easterly winds at Cuxhaven have approximately no effect compared to westerly winds, while they have very weak effect the frequency of strong wind speeds at Sylt.

The changes in frequency distributions for wind speeds greater than 17.2 m/s between control (C20_2) and future (A1B_2) simulations show whether and how the dominant strong wind directions could change due to climate change, thus resulting in different impacts on the different coastal sites of the North Sea.

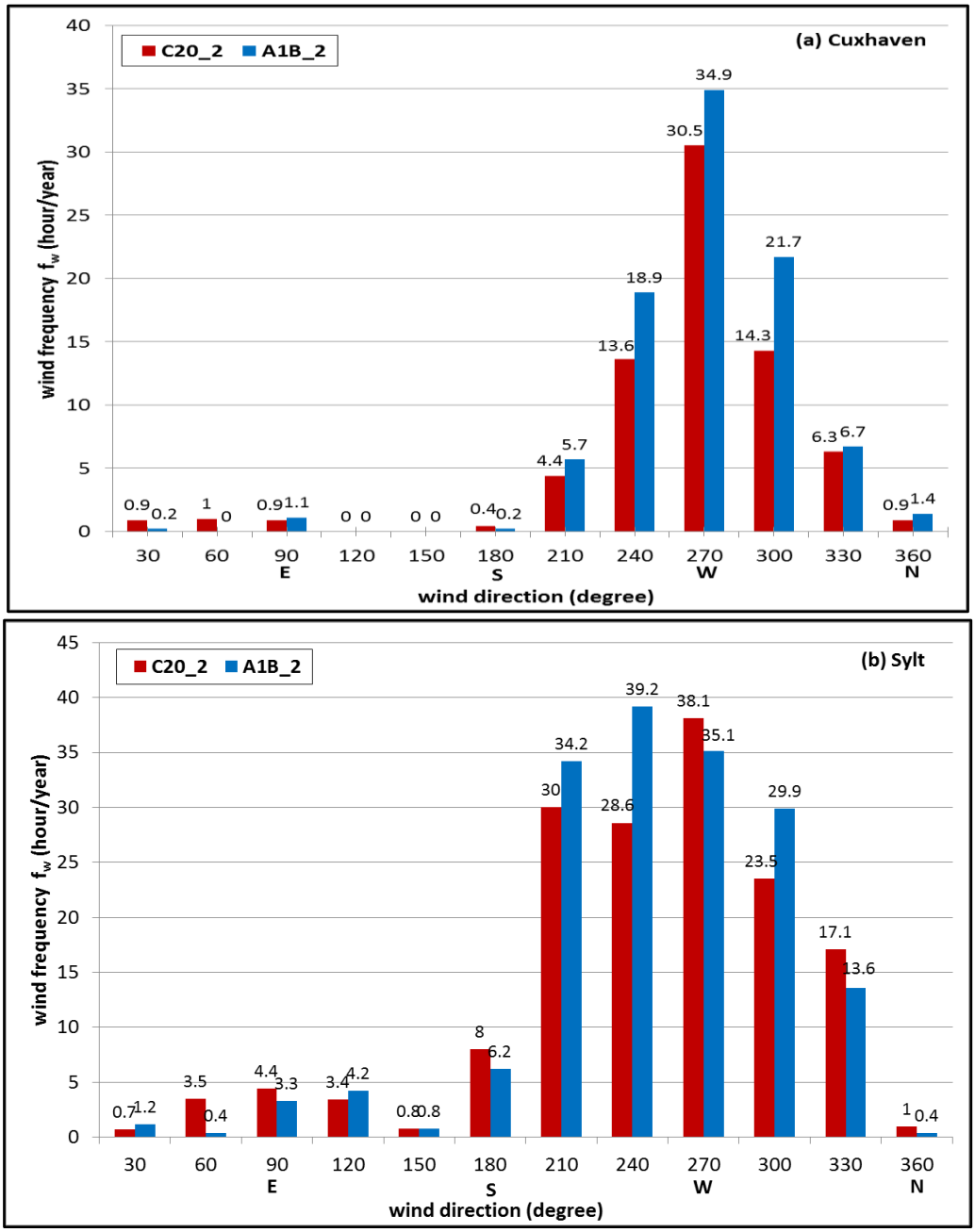

Figure 5.15: Frequency distribution of wind directions for wind speeds greater than 17.2 m/s for two 30-year time intervals corresponding to two realizations (C20_2: 1970-2000; A1B_2: 2070-2100) for Cuxhaven (a) and Sylt (b). Angles 90°, 180°, 270° and 0°=360° correspond to E(ast), S(outh), W(est) and N(orth), respectively.

Figure 5.16 shows the temporal variations of the differences in strong winds frequencies between the last 30 years of the 21st century (2070-2100) and the last 30 years of the 20st century (1970-2000), which represents the reference control climate for Cuxhaven ($\Delta f\_w_{A1B\_2}^{Cuxhaven}$) and Sylt ($\Delta f\_w_{A1B\_2}^{Sylt}$). The 10-year running averages of the annual frequencies for strong westerly winds (165°-345°) are calculated for the future meteorological conditions. The annu-

al frequencies of each decade in 2070-2100 follow a normal distribution (normality test with Anderson-Darling P-value>0.05). At both sites, the frequency of strong winds generally increases for the last 30 years of the 21st century. Moreover, there are similarities in the patterns of the changes of the frequency signals between the two sites, while the frequency signals are close to each other from 2086 to 2100. The frequency signals reach a maximum value in 2087 with 35.35 hour/year in Cuxhaven and 38.10 hour/year in Sylt, while the minimum value occurs in 2077 with -5.20 hour/year in Cuxhaven and -18.95 hour/year in Sylt.

The severity of a storm-tide depends primarily on the wind speed, wind direction and duration. An extreme wind event at Cuxhaven or Sylt is defined as a period covering one or more hourly intervals with wind speed reaching or exceeding the annual 99th percentile. Figure 5.17 shows the temporal changes in durations for extreme wind events ($d\_w_S^x(\geq 99)$), where S describes the meteorological conditions under hindcast and control simulations (1991-2000). The annual durations of each decade under hindcast and control periods generally follow a normal distribution (normality test with Anderson-Darling P-value>0.05). The mean duration of these events in the hindcast simulations at Sylt within ca. 6.15-7.5 hours is relatively shorter than those at Cuxhaven within 6.13-7.93 hours (Figure 5.17 (a)). Moreover, the annual duration of extreme events at both sites increases by approximately 1.5 hour from 1995. Though this part is generally well reproduced in the control simulations, at both sites the annual duration of extreme wind events is slightly underestimated in the period 1992-1996 and then slightly overestimated until 2000 (Figure 5.17 (b)). The bias signal of extreme events duration under control simulations, which is the difference (bias) between the annual duration of extreme wind events duration under control conditions from the hindcast mean (1991-2000). At Cuxhaven it lies in the 95 % confidence interval for the hindcast with zero mean based on bootstrapping, while it experiences a significant change for Sylt only in 1995, 1999 and 2000.

The temporal characteristics of the duration and those of the frequency of extreme wind events are important parameters for the design, constructions and operations of marine structures and facilities in the context of climate change. Figure 5.18(a) shows the climate change signals for 10-year running averages at Cuxhaven and Sylt as a difference of the wind duration between future conditions (A1B_2) and its mean under control conditions (C20_2). The climate change signals at both sites are not significant and are within the range of the natural variability in the results of the hindcast simulations. The duration at Cuxhaven increases under future conditions; the highest increase occurs in 2085 and 2092 with 0.67 hour and then decreases until 2095. While the duration at Sylt increases only in the period 2092-2095 with the highest value of 0.7 hour in 2095 (Figure 5.18(a)).

Figure 5.18(b) shows that for both sites the climate change signals of the frequency for extreme wind events have an inverse relation with the duration signals in Figure 5.18(a). The climate change signals of extreme wind frequency at Cuxhaven and Sylt are not significant. The highest frequency at Cuxhaven reaches a maximum value of 1 event/year in 2080, while for Sylt only 0.66 event/year is reached in 2082.

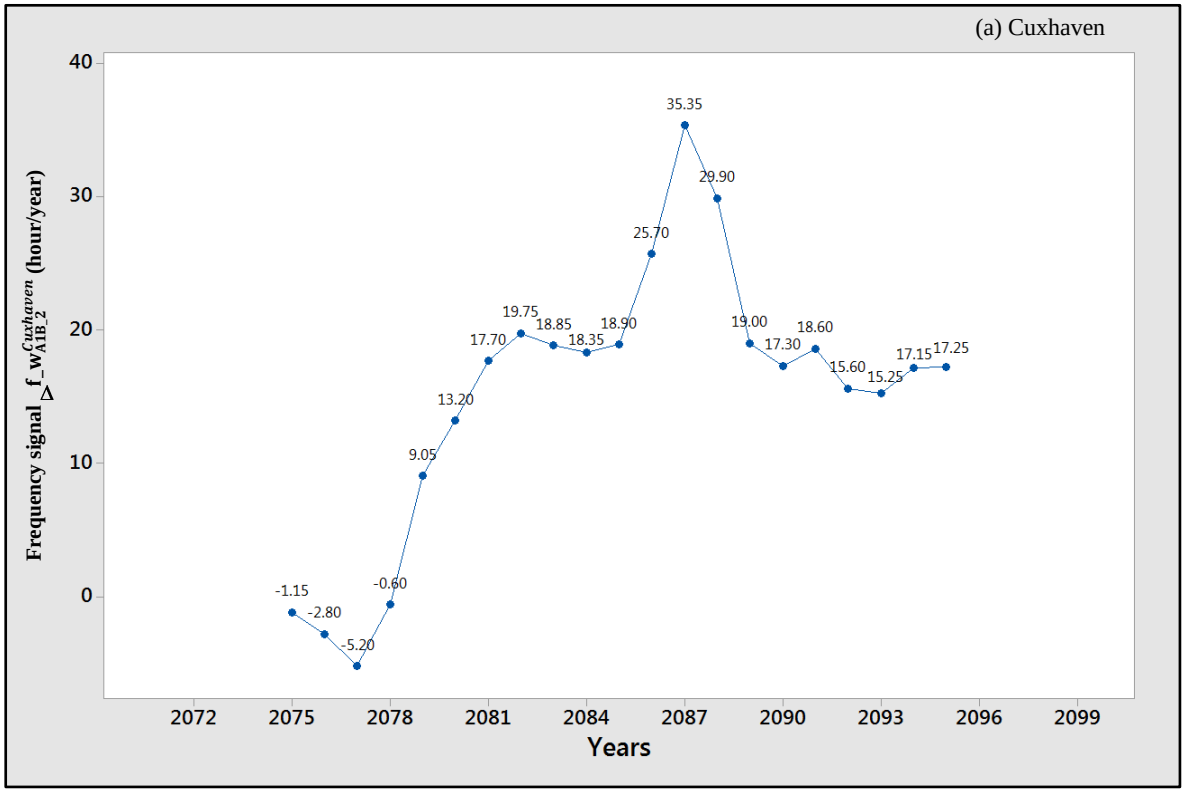

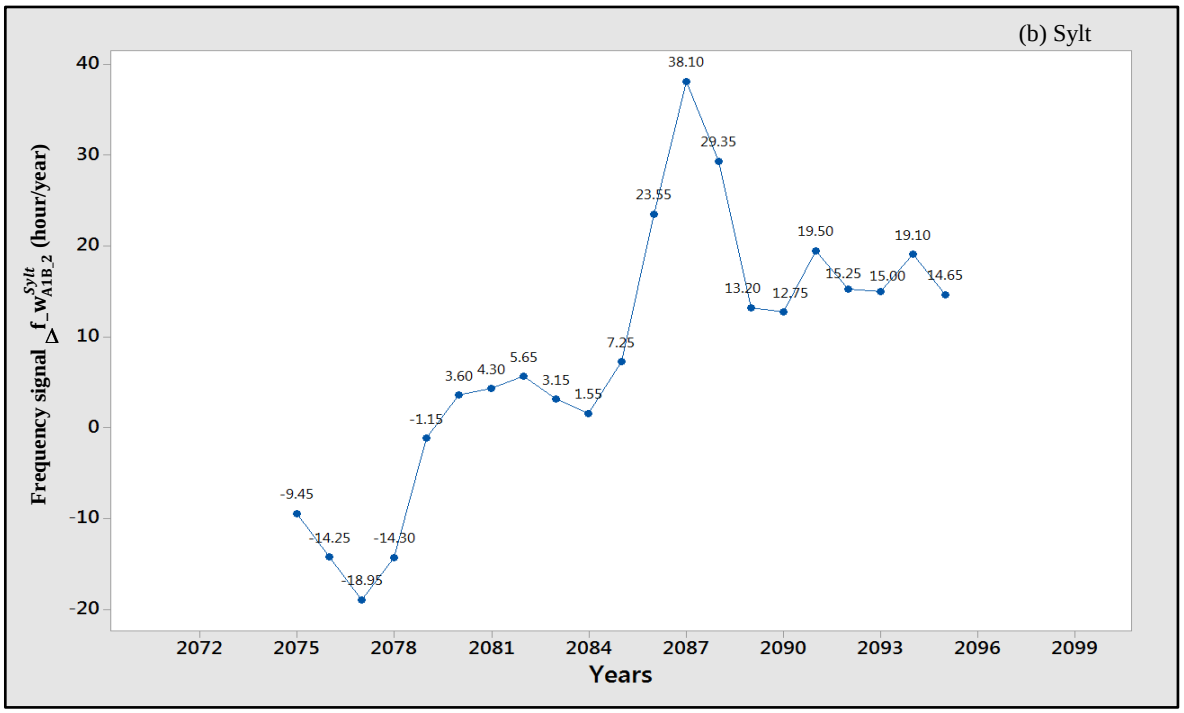

Figure 5.16: Temporal variations of the differences in frequencies for the strong westerly winds (165°-345° and ≥17.2 m/s) between the 10-year running averages of annual frequencies in the end of 21st century (2070-2100) and the average of control annual frequencies in the last 30 years of the 20st century (1970-2000) at Cuxhaven (a) and Sylt (b).

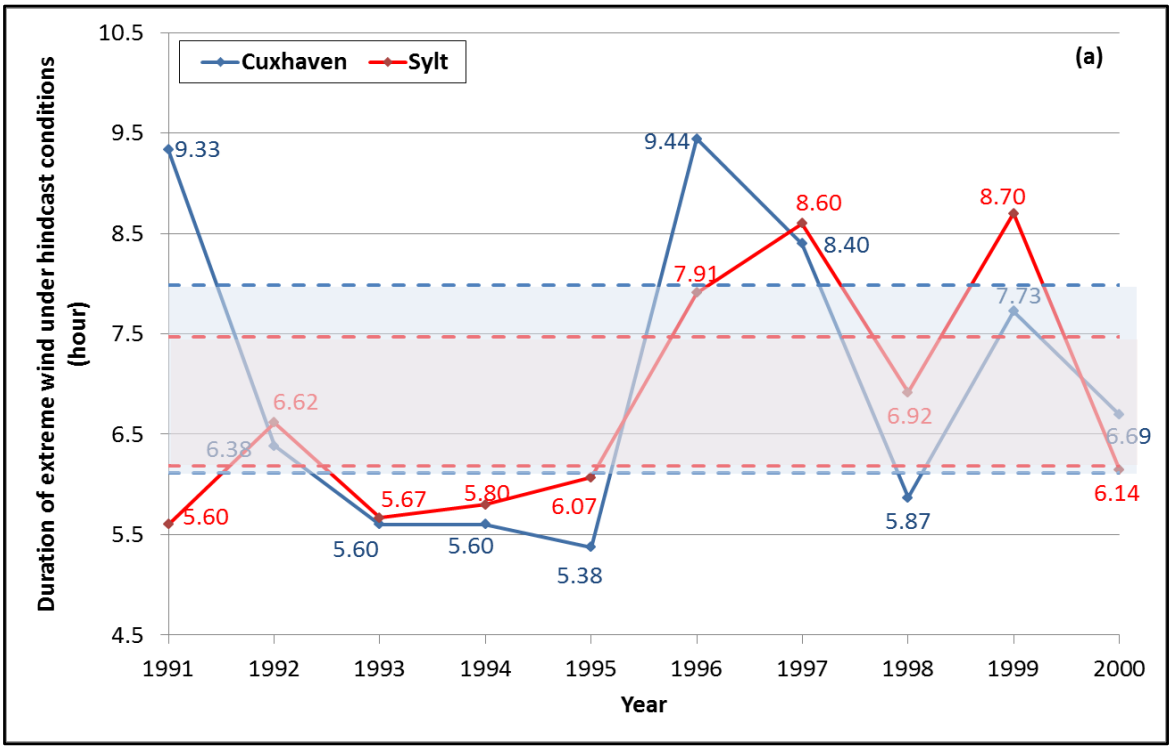

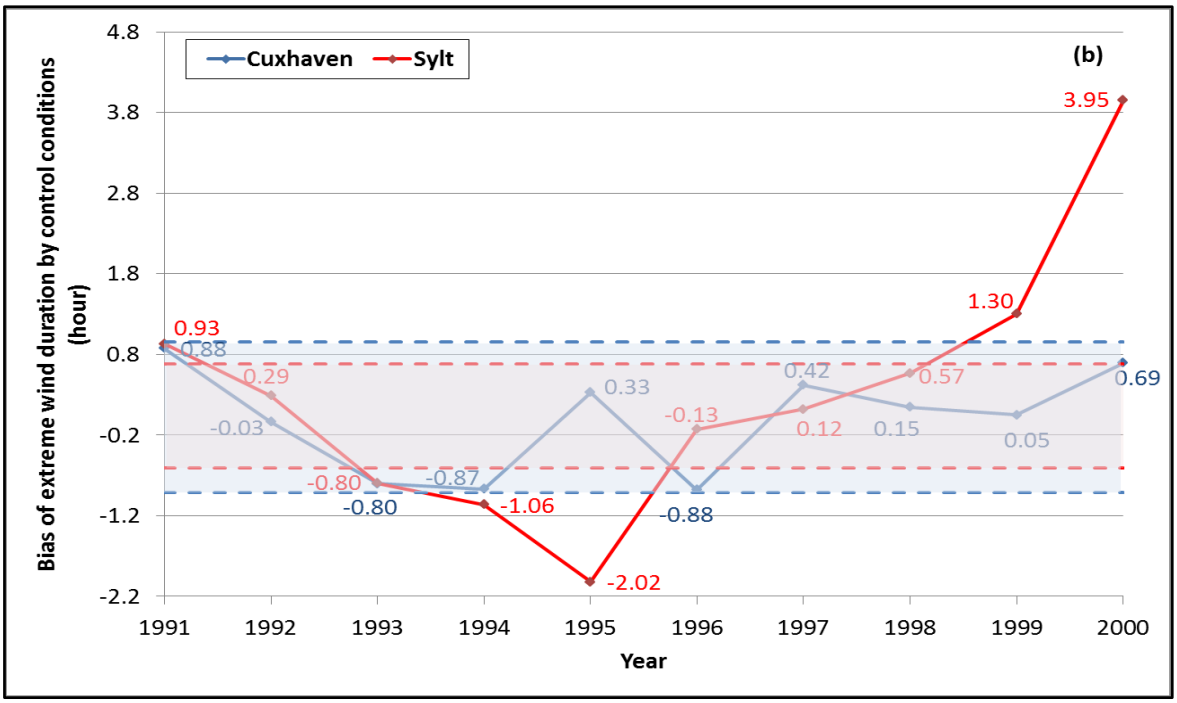

Figure 5.17: Time series of extreme wind duration (wind speed > annual 99% percentile) at Cuxhaven and Sylt under hindcast meteorological conditions 1991-2000 (a) with bias signal under control conditions 1991-2000 as deviations compared to hindcast mean (b). Shaded areas between blue or red dashed lines correspond to the 95 % confidence interval for the hindcast mean based on bootstrapping at Cuxhaven or Sylt, respectively.

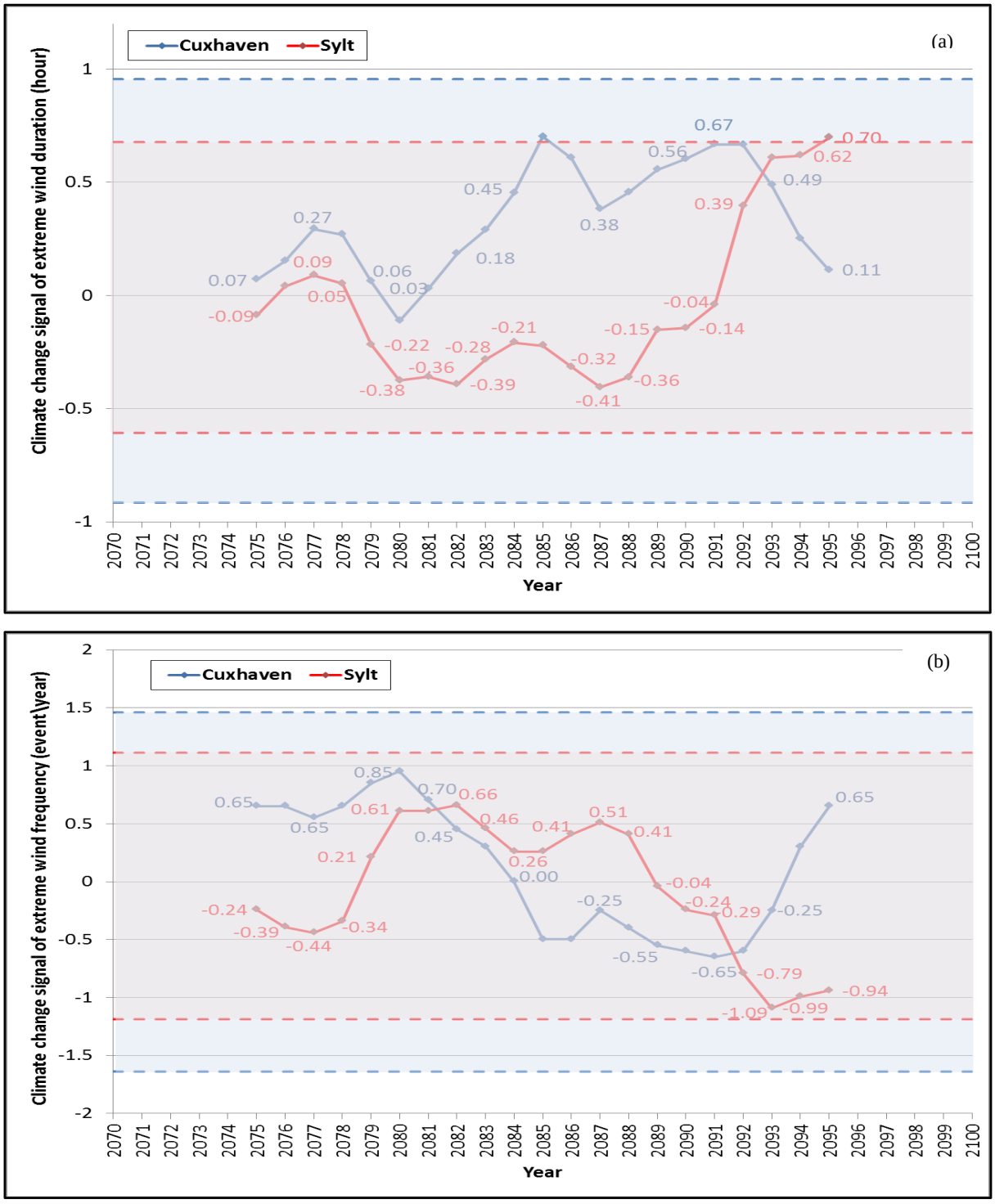

Figure 5.18: Climate change signals for 10-year running averages of extreme wind (wind speed > annual 99% percentile) duration (a) and frequency (b) under future realization 2070-2100 as deviations compared to control mean at Cuxhaven and Sylt. Shaded areas between blue or red dashed lines correspond to the 95 % confidence interval for the hindcast mean based on bootstrapping at Cuxhaven or Sylt, respectively.

(b) Preparation of boundary conditions for the North Sea mesh in TELEMAC2D between 2070 and 2100 (step 2 to 4 in Figure 5.11**)**

Tide in the North Sea constitutes one of the main effective components for extreme storm-tide generation. The maximum tide effect in the time period 1991-2007 reaches 27.5% from the $(\eta_{all})_{max}$ at Cuxhaven and 22.84% from the $(\eta_{all})_{max}$ at Sylt (see Figure 4.22). Therefore, the tidal level at each node of the northern and western open-sea boundaries for the North Sea model (Figure 3.8) between 2070 and 2100 are predicted based on the harmonic tidal constituents of 2006. These tidal constituents were analyzed using the "Tidal Analysis Toolbox" for control and hindcast surge-tide simulations (see section 5.1.1(b)).

Storm surge in the North Sea is expected to have its highest increase due to climate change (2070-2100) in the German Bight (Woth, 2006; Gaslikova et al., 2013). The influence of Atlantic external surges is important for the accurate prediction of surge-tide in the future simulations (2070-2100) under A1B_2 meteorological conditions. Therefore, the external surges in the future simulations are predicted using the two developed NARX models for Wick and Lerwick (Tayel & Oumeraci, 2012b). The external surge at Wick (north-west boundary) or Lerwick (north boundary) is added linearly to the tidal level at each node of the northern open sea boundary (see Figure 3.8) for the future realization of surge-tide.

The maximum contribution of river discharge ($(\eta_{rd})_{max}$) at Sylt and Cuxhaven is not more than 1% and without any noticeable effect on the results of the hindcast surge-tide simulations (see section 4.3.4). Especially the effect of river discharge is approximately zero during low discharge values. Therefore, future surge-tide simulations in the North Sea could be predicted without being affected noticeably by uncertainties in the prediction of river discharges ($Q<3620$ m^3/s). The two main rivers in southern of the North Sea area are Weser and Elbe with larger river discharges than Ems and Westerschelde (see Figure 3.8). The Elbe has a long-term average discharge of 856 m^3/s, while the Weser is 327 m^3/s in 1970-2000. These two average values of the southern rivers discharges are used as boundary conditions in the future surge-tide simulations.

(c) Processing future surge-tide simulations (steps 5 to 9 in Figure 5.11**)**

In the prospect of changing surge-tide statistics due to anthropogenic climate change, these changes are anlysed for the North Sea based on numerical modelling using TELEMAC2D. The analysis is carried out by using a 30-year atmospheric regional simulation which may represent the present-day reference ("control conditions") and possible future-enhanced greenhouse gas conditions ("future conditions"). Because of the deviations between hindcast and control simulations (see section 5.1.1(c)) in the meteorological conditions as well as the surge-tide simulations, the differences between future scenario and control climate projections are interpreted as a relative shift from present-day reference statistics in response to the applied emission scenario. By doing so, it is assumed that the systematic errors (bias) generated by control and scenario simulations are equal, since they are generated by the same GCMs/RCMs in both simulations. This assumption is inherent in all climate change studies

and represents the best possible option so far (Woth, 2006; Gaslikova et al., 2013).The research strategy is to compare surge-tide predictions under meteorological simulations of regional model CLM driven by the global control (C20_2) and climate change (A1B_2) simulations. Both control and future conditions, which are representative for 1970-2000 and 2070-2100, respectively, were based on the observed GHG and aerosol loading during 20th century and on the IPCC A1B SRES scenario, respectively (see Table 5.1). Thus, the future surge-tide simulation, which is predicted over the North Sea model (see Figure 3.8) by TELEMAC2D, is forced simultaneously on the lateral boundaries (see section 5.1.2(b)) with the predicted astronomical tidal dynamics (northern and western boundaries), predicted external surges at Wick and Lerwick (northern boundary) and average rivers discharges (southern boundary). For the future simulation presented here, the same mesh configuration of hindcast and control simulations is used (see section 5.1.1(c)). The resulting surge-tide of future simulations include the interactions of storm surges with the tides by TELEMAC2D under future conditions ($(\eta_{\text{su-t TEL}})_{\text{A1B\_2}}$). The state-variables (free surface elevation, water depth and depth averaged velocity) are stored every hour for all "wet" grid points of the model domain. The first 10 days simulation was discarded to account for potential spin-up effect.

Basically, the climate change signal for surge-tide heights are examined as the difference between future simulation under A1B_2 realization (2070-2100) and control simulation, which is supposed to be representative for the period 1970-2000. This is performed in the following nine steps:

1. Extract the annual upper percentiles of control simulation under C20_2 realization, which are predicted in stage 1, step 3 (Figure 5.2), (99.5 percentile ($P^{x\text{n}}_{\text{C20\_2}}(99.5)$) and maximum surge-tide ($P^{x\text{n}}_{\text{C20\_2}}(100)$), for n years from 1970 to 2000 at every mesh point *x* in the North Sea model (Figure 3.8).
2. Drive the North Sea model in TELEMAC2D to predict the surge-tide under future meteorological condition $(\eta_{\text{su-t TEL}})_{\text{A1B\_2}}$.
3. Extract the annual upper percentiles of future simulation under A1B_2 realization (99.5 percentile ($P^{x\text{n}}_{\text{A1B\_2}}(99.5)$) and maximum surge-tide ($P^{x\text{n}}_{\text{A1B\_2}}(100)$), for n years from 2070 to 2100 at every mesh point *x* in the North Sea model (Figure 3.8).
4. Calculate the mean of annual upper percentiles either over 1970-2000 for control simulation ($P^{x}_{C20\_2}(99.5)$ and $P^{x}_{C20\_2}(100)$) or over 2070-2100 for future simulation ($P^{x}_{A1B\_2}(99.5)$ and $P^{x}_{A1B\_2}(100)$) at every mesh point *x*.
5. Calculate the climate change signals for upper percentiles ($\Delta^{x}(99.5)$ and $\Delta^{x}(100)$) as the difference between the mean of future simulation and the corresponding mean of control simulation according to Eq. (5.5) and (5.6), respectively.
6. Compare the climate change signals $\Delta^{\text{x}}(99.5)$ and $\Delta^{\text{x}}(100)$ with the corresponding confidence intervals $\text{CI}^{\text{x}}(99.5)$ and $\text{CI}^{\text{x}}(100)$ (calculated in stage 1, step 7 (Figure 5.2)) to identify the significant changes in future surge-tide climate for every mesh point *x* in the North Sea model.

7. Extract the average duration and number of extreme surge-tide events in future simulation (2070-2100), which have a period covering one or more hourly intervals and exceeding the 99.5th percentile, over the North Sea ($d^x_{A1B\_2}(\geq 99.5)$ and $f^x_{A1B\_2}(\geq 99.5)$, respectively).
8. Calculate the climate change signal of the mean duration or frequency for extreme surge-tide events ($\Delta d^x_{A1B\_2}(\geq 99.5)$ or $\Delta f^x_{A1B\_2}(\geq 99.5)$,respectively), which is defined as the difference between the mean value $d^x_{A1B\_2}(\geq 99.5)$ or $f^x_{A1B\_2}(\geq 99.5)$,respectively, in the future simulation (A1B_2) and the corresponding mean value $d^x_{C20\_2}(\geq 99.5)$ or $f^x_{C20\_2}(\geq 99.5)$,respectively, in the control simulation (C20_2) i.e.:

$$\Delta d^x_{A1B\_2}(\geq 99.5) = d^x_{A1B\_2}(\geq 99.5) - d^x_{C20\_2}(\geq 99.5) \quad (5.7)$$

$$\Delta f^x_{A1B\_2}(\geq 99.5) = f^x_{A1B\_2}(\geq 99.5) - f^x_{C20\_2}(\geq 99.5) \quad (5.8)$$

9. Compare the climate change signals $\Delta d^x_{A1B\_2}(\geq 99.5)$ and $\Delta f^x_{A1B\_2}(\geq 99.5)$ with the corresponding confidence intervals $CI^x_d(\geq 99.5)$ and $CI^x_f(\geq 99.5)$, respectively, which are based on hindcast simulation (see section 5.1.1(c)), in order to identify the significant changes in future surge-tide climate for every mesh point *x* in the North Sea model.

The climate change signals for upper percentiles of surge-tide $\Delta^x(99.5)$ and $\Delta^x(100)$ are presented in Figure 5.19(a) and Figure 5.20(a), respectively. The result of future climate realization is shown as the difference between mean annual 99.5 or 100 percentiles for surge-tide under the future (2070-2100) and the reference (1970-2000) climate. Generally, there is a gradual increase in the climate change signals of future simulation for the upper percentiles from the middle of North Sea toward the Elbe estuary at the end of the 21st century. The maximum increase in surge-tide extremes occurs in the German Bight. For $\Delta^x(99.5)$ and $\Delta^x(100)$, the maximum increase reaches values of 0.16 m and 0.23 m, respectively, which are about 6.4% and 6.6% increase as compared to the maximum reference (control) simulation values. The lowest decrease of surge-tide extremes are generally found in the middle of North Sea and along the UK east coast. The decrease of $\Delta^x(99.5)$ ranges from -0.04 m to -0.07 along the UK east coast and from -0.07 m to -0.15 in the middle of the North Sea. This corresponds to the general pattern of the storm surge height distribution, since the lowest storm surge extremes are generally found along the UK coast and then it increase eastward along the 10-m depth line with highest values obtained in the German Bight (Woth, 2006). Furthermore, it can be seen that the increase of surge-tide extremes is more pronounced for the eastern German Bight (North Frisian Islands coasts) and the Danish coasts than for the southern German Bight (East Frisian Islands coasts) and the Netherlands coasts. For $\Delta^x(99.5)$, the increase ranges from 0.12 m to 0.16 m in the North Frisian Islands, while it ranges from 0.08 m to 0.11 m in the East Frisian Islands. The results are consistent with the 99.5th storm surge percentile

studied by Woth (2006) within the German Bight along the 10-m bathymetry line, in which it is increased significantly in all scenario simulations (A2 scenario regionalized with 4 different RCMs) by 20–30 cm with highest values in the North Frisian coast. This can be related to the increasing of westerly winds during storms and their increased duration and frequency in the future climate realization (Figure 5.15 and Figure 5.16). The increase of westerly winds frequency during the second half of 21st century in the North Frisian Islands reaches values from 4 to 38 hour/year, while it ranges from 9 to 35 hour/year in the East Frisian Islands. Meanwhile, the duration of extreme wind events in the North Frisian Islands have positive increase in the period 2092-2095 with highest increase occurs in 2095 of 0.7 hour, while it decreases in the East Frisian Islands.

The climate change signals for the upper percentiles of surge-tide are tested to examine whether the signals merely reflect natural variations or are rather related to the effect of a changing climate. Therefore, a series of null hypotheses (Eq. (5.9)) is tested for each mesh point *x* in the North Sea model (Figure 4.37).

$$H_o: P^x_{A1B\_2}(99.5) = P^x_{C20\_2}(99.5) \;\; for\; 99.5\; percentile$$
$$H_o: P^x_{A1B\_2}(100) = P^x_{C20\_2}(100) \;\; for\; 100\; percentile \tag{5.9}$$

For this purpose, the 95% confidence interval is determined based on the Student *t* distribution for the upper percentiles from the hindcast simulation 1970-2000 (see Figure 5.7). Therefore, for each mesh point *x*, it is tested whether the climate change signals ($\Delta^x(99.5)$ and $\Delta^x(100)$) lie in the confidence intervals ($CI^x(99.5)$ and $CI^x(100)$ with zero mean, respectively) or not (reject the null hypothesis). In the latter case, the signals will not reflect natural variations and they are related to the changing forcing by future meteorological conditions. The major and only statistically significant (95 %-level) signals $\Delta^x(99.5)$ and $\Delta^x(100)$ are shown in Figure 5.19(b) and Figure 5.20(b), respectively. The $\Delta^x(99.5)$ signal is only statistically significant (based on a Student's *t* test, 95 %-level) for values more than 0.05 m or less than -0.04 m, while the $\Delta^x(100)$ signal is more than 0.08 m or less than -0.07 m. Therefore, it can be seen that the increase of the surge-tide extremes due to climate change is significant for the German Bight and Netherlands coasts. The decrease is significant for the middle of the North Sea and along the UK east coast.

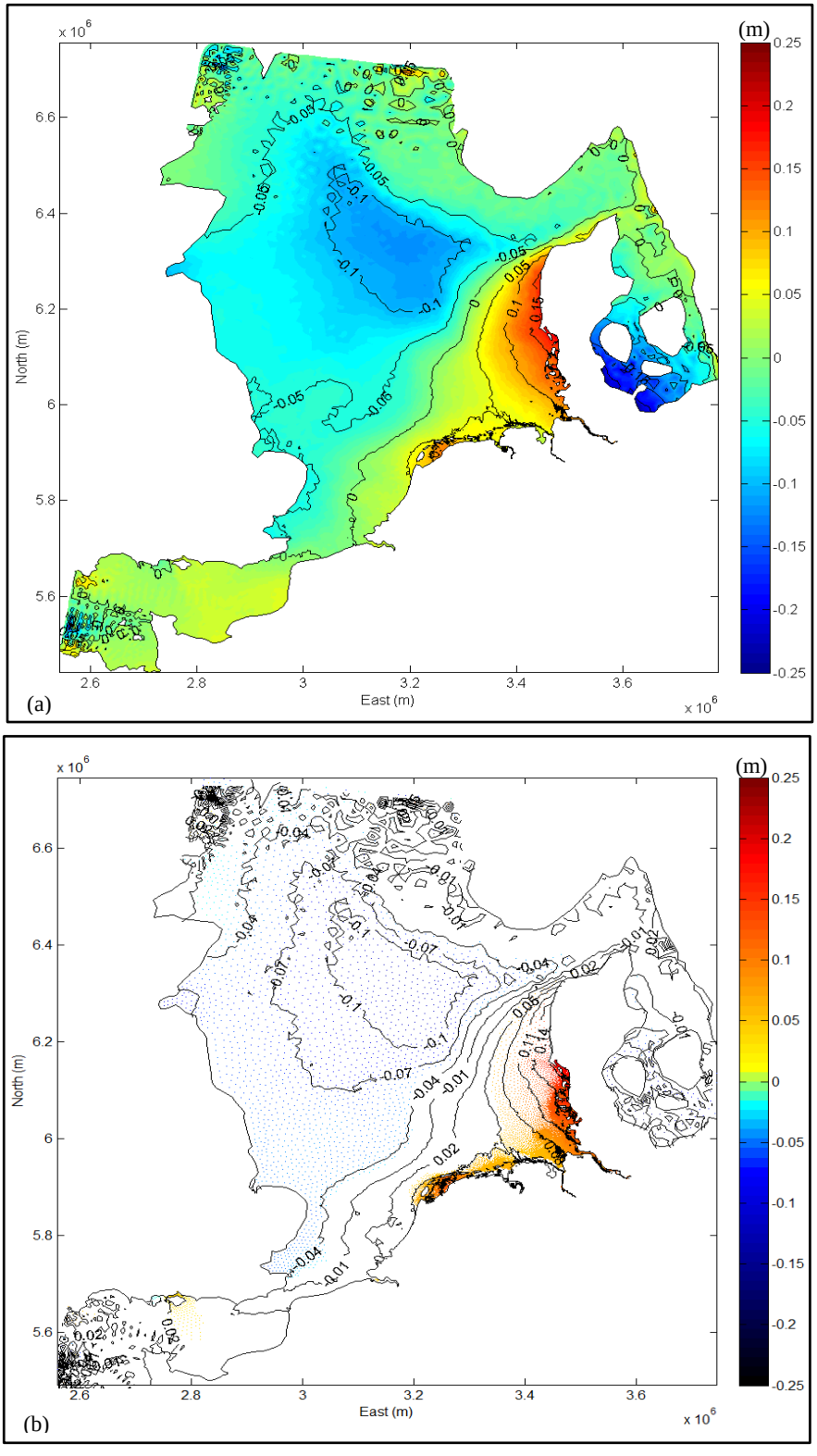

Figure 5.19: Climate change signal of the 99.5 percentile surge-tide ($\Delta^x(99.5)$) in meter as the difference between the 30-year mean of annual values in the future simulation (A1B_2; 2070-2100) and the corresponding mean value in the control simulation (C20_2; 1970-2000) (a). Shaded areas show significant differences on a 95% level based on a Student's *t* test (b).

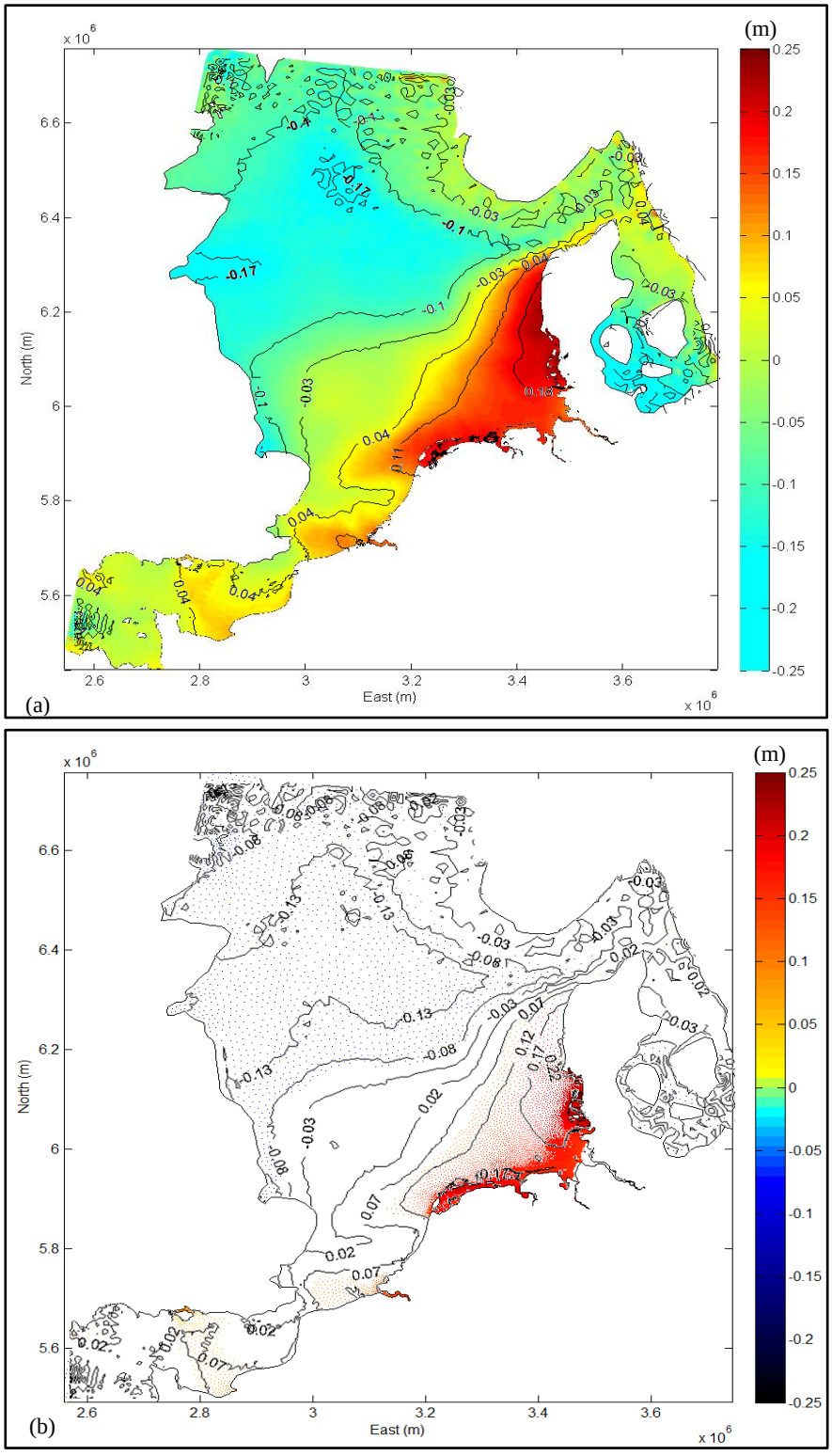

Figure 5.20: Climate change signal of the maximum surge-tide ($\Delta^x(100)$) in meter as the difference between the 30-year mean of annual values in the future simulation (A1B_2; 2070-2100) and the corresponding mean value in the control simulation (C20_2; 1970-2000) (a). Shaded areas show significant differences on a 95% level based on a Student's *t* test (b).

Climate change signals for the mean duration and frequency of extreme surge-tide events over the North Sea ($\Delta d^x_{A1B\_2}(\geq 99.5)$ and $\Delta f^x_{A1B\_2}(\geq 99.5)$, respectively) along with their statistically significant (95 %-level) values are presented in Figure 5.21 and Figure 5.22, respectively. Therefore, a series of null hypotheses (Eq. (5.10)) is tested for each mesh point *x* in the North Sea model to determine whether $\Delta d^x_{A1B\_2}(\geq 99.5)$ and $\Delta f^x_{A1B\_2}(\geq 99.5)$ lie in their natural confidence intervals ($CI^x_d(\geq 99.5)$ and $CI^x_f(\geq 99.5)$ with zero mean, respectively) or not (reject the null hypothesis).

$$H_o: d^x_{A1B\_2}(\geq 99.5) = d^x_{C20\_2}(\geq 99.5) \;\; for\ extreme\ events\ duration$$
$$H_o: f^x_{A1B\_2}(\geq 99.5) = f^x_{C20\_2}(\geq 99.5) \;\; for\ extreme\ events\ frequency \quad (5.10)$$

The mean duration of extreme surge-tide events increases due to climate change along the continental Southern North Sea coast up to the west coast of Denmark (significantly different from zero at the 95% confidence level), while it decreases along the UK east coast and in the middle of North Sea. The $\Delta d^x_{A1B\_2}(\geq 99.5)$ is only statistically significant for values of more than 0.20 hour or less than -0.10 hour (see Figure 5.21(b)). The highest increase of $\Delta d^x_{A1B\_2}(\geq 99.5)$ occurs around the middle amphidromic point in the German Bight with a value of about 1.2 hour, which reflects the strong effect of tide interaction with storm surge. The mean frequency of extreme surge-tide events (Figure 5.22(b)) shows a statistically significant decrease due to climate change along the east coast of UK through southern North Sea coast up to west coast of Denmark, while the changes in the middle and northern North Sea are not significantly different from zero. Despite of that the mean number of extreme storm surge eveis nts increased by about two event/year along the continental Southern North Sea coast up to about Esbjerg in the period 2071-2100 compared to 1961-1990 (Woth, 2006), while the frequency of extreme surge-tide is decreased. This is due to the interaction of tide and external surge with internal storm surge. The $\Delta f^x_{A1B\_2}(\geq 99.5)$ is only statistically significant above a value of 1.3 events/year or less than -0.4 event/year (see Figure 5.22(b)).

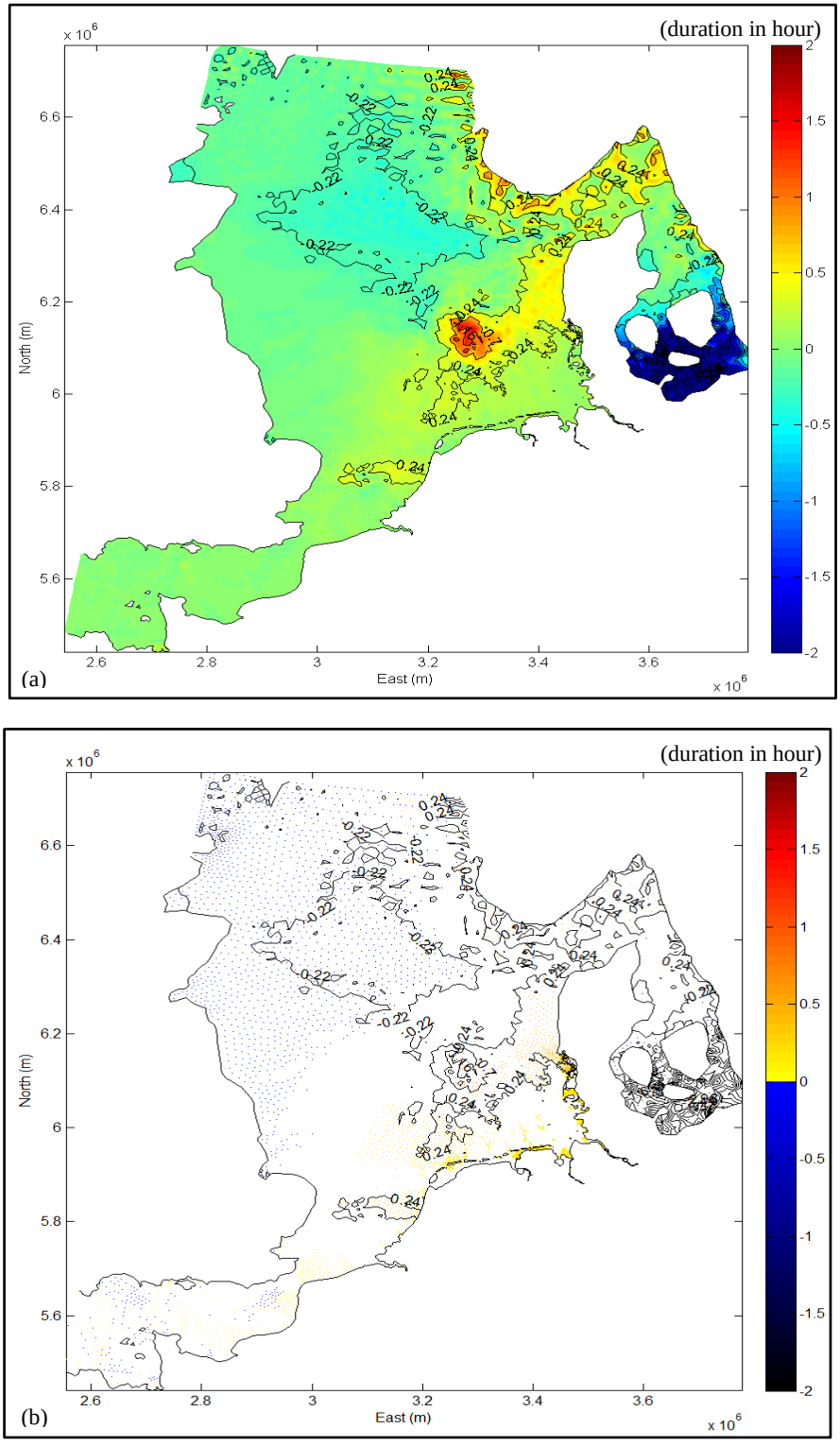

Figure 5.21: Climate change signal of the duration for extreme surge-tide events ($\Delta d^{x}_{A1B\_2}(\geq 99.5)$) as the difference between the 30-year mean of annual extreme events duration in the future simulation (A1B_2; 2070-2100) and the corresponding mean value in the control simulation (C20_2; 1970-2000) (a). Shaded areas show significant differences on a 95% level based on a Student's *t* test (b).

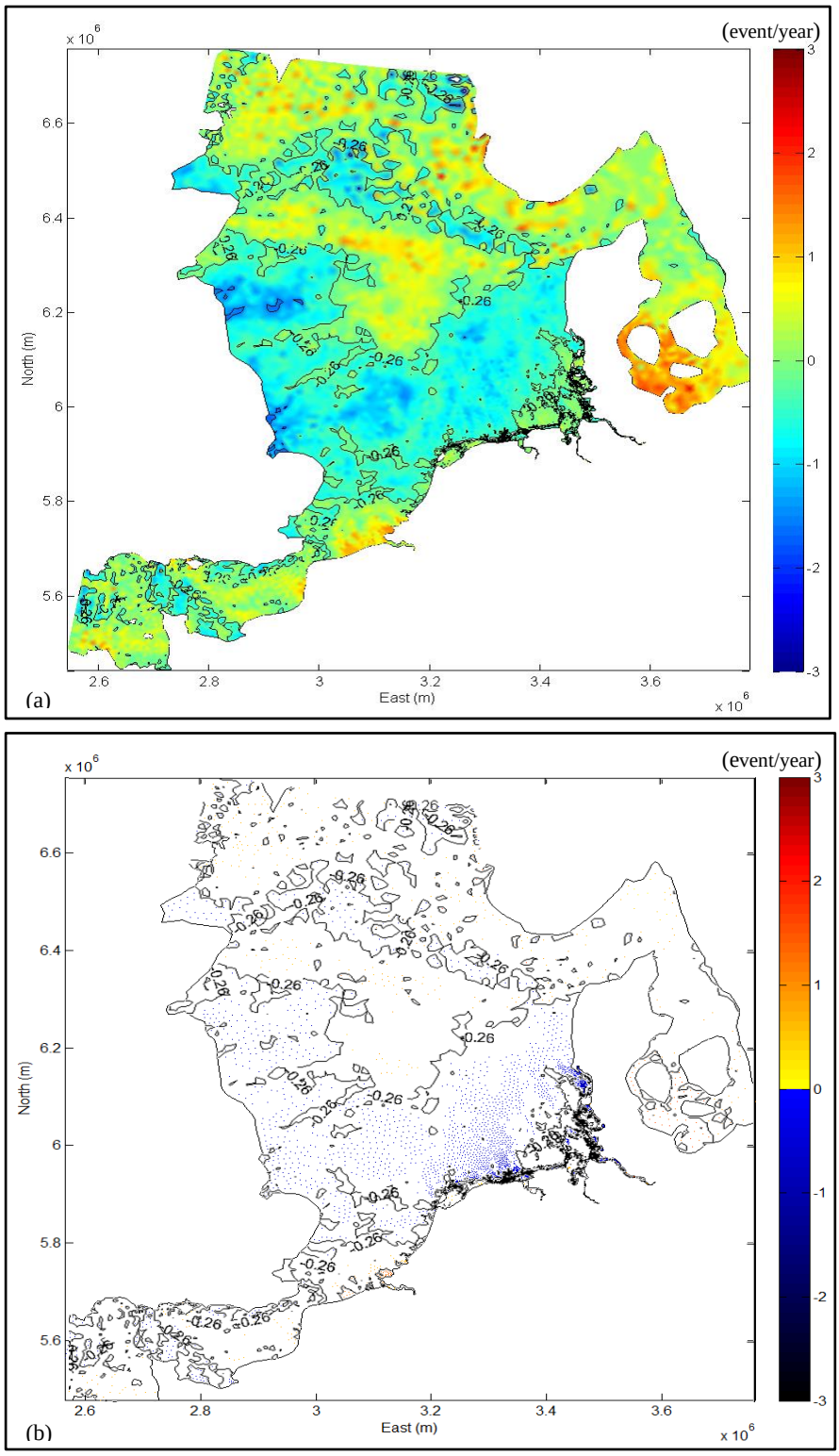

Figure 5.22: Climate change signal of the frequency for extreme surge-tide events ($\Delta f^{x}_{A1B\_2}(\geq 99.5)$) as the difference between the 30-year mean of annual extreme events frequency in the future simulation (A1B_2; 2070-2100) and the corresponding mean value in the control simulation (C20_2; 1970-2000) (a). Shaded areas show significant differences on a 95% level based on a Student's *t* test (b).

The changes of the mean 99 percentile wind speed regionalized by the ECHAM5-MPIOM/CLM models under the A1B scenario represent the ensemble mean of all other future scenarios and preserve a good processes representation scale. Therefore, the change in surge-tide statistics over the North Sea due to anthropogenic climate change is carried out by using 30-year atmospheric regional simulation representing possible future-enhanced greenhouse gas conditions under the A1B scenario ("future conditions"). The climate change signals for upper percentiles of surge-tide $\Delta^x(99.5)$ and $\Delta^x(100)$ have gradual increase from the middle of the North Sea toward the Elbe estuary at the end of 21st century. The maximum increase in the surge-tide extremes of the North Sea occurs in the German Bight. For $\Delta^x(99.5)$ and $\Delta^x(100)$, the maximum increase reaches values of 0.16 m and 0.23 m, respectively, which respectively corresponds to an increase of ca. 6.4% and 6.6% as compared to the maximum reference (control) simulation values. The $\Delta^x(99.5)$ is only statistically significant (based on a Student's *t* test, 95 %-level) for values more than 0.05 m or less than -0.04 m, while the $\Delta^x(100)$ is above 0.08 m or less than -0.07 m. Therefore, the increase of surge-tide extremes due to climate change is significant for the German Bight and Netherlands coasts, while the decrease is significant for the middle of the North Sea and along the UK east coast. The decrease of $\Delta^x(99.5)$ ranges from -0.04 m to -0.07 along the UK east coast and from -0.07 m to -0.15 in the middle of the North Sea. Furthermore, it can be seen that the increase of surge-tide extremes is more pronounced for the eastern German Bight (North Frisian Islands) and the Danish coasts than for the southern German Bight (East Frisian Islands) and the Netherlands coasts. For $\Delta^x(99.5)$, the increase ranges from 0.12 m to 0.16 m in the North Frisian Islands, while it ranges from 0.08 m to 0.11 m in the East Frisian Islands. The results are consistent with the 99.5th storm surge percentile studied by Woth (2006) within the German Bight along the 10-m bathymetry line, in which it is increased significantly in all scenario simulations (A2 scenario regionalized with 4 different RCMs) by 20–30 cm with highest values in the North Frisian coast. This can be related to the increase of westerly winds frequency during storms (Figure 5.15 and Figure 5.16), and their increased duration (Figure 5.18) in the future climate realization. The temporal characteristics of the duration and those of the frequency of extreme wind events in the context of climate change in the North and East Frisian coasts require the increase of security limits for the design, constructions and operations of marine structures and facilities.

The mean duration of extreme surge-tide events increases due to climate change along the continental Southern North Sea coast up to the west coast of Denmark (significantly different from zero at the 95%-level), while it decreases along the UK east coast and in the middle of the North Sea. The $\Delta d^x_{A1B\_2}(\geq 99.5)$ is only statistically significant for values of more than 0.20 hour or less than -0.10 hour. The mean frequency of extreme surge-tide shows statistically significant decrease due to climate change along the continental western North Sea coast through the southern coast up to west coast of Denmark, while changes are not significantly different from zero in the middle and northern North Sea. In general, the surge-tide climate change signals toward the end of the twenty-first century (2070–2100) are comparable to those from storm surge (under A2 scenario) over the North Sea except for frequency of extreme events, which are studied by (Woth, 2006). This is due to the interaction of tide and

external surge with internal storm surge. A stand-alone increase in the frequency of extreme events would be less relevant for many coastal facilities, but an increase in duration and magnitude of extreme events could stretch their security limits.

In this study, the effect of one emission scenario (A1B) regionalized by the ECHAM5-MPIOM/CLM models on surge-tide over the North Sea was examined. The use of different emission scenarios and/or global circulation models may have a larger effect on changes of surge-tide statistics. There might be a considerable variability in the response of the extra tropical atmospheric circulation in dependence on the used GCM and in dependence on the chosen greenhouse gas emission scenario. Dealing with such uncertainties will represent a major challenge for climate impact studies in the future.

5.2 Future storm-tide prediction for Cuxhaven and Sylt using the new hybrid modelling approach

The prediction of future surge-tides under A1B_2 realization (see section 5.1.2) provided the spatial distributions of the climate change signals over the North Sea, together with the signs of the changes. These signals have the highest increase of surge-tide in the German Bight coasts for 2070-2100 compared with 1970-2000. The coastal zones of the German Bight are facing a significant potential increase in storm-tide statistics due to anthropogenic climate change which may differ from the northern to the western locations of the North Sea. Therefore, a localization of storm-tide projections (see Figure 5.1) at specific coastal sites is required. Natural storm-tides adapt to the constituents induced by stochastic events such as storm surges, external surges and wave-set up, which are superimposed nonlinearly on the periodic phenomena of tides (see Figure 4.20). So the increase in storm-tide due to climate change for the two pilot sites in the German Bight (Cuxhaven and Sylt) will be assessed using the new hybrid modelling approach which combines hydrodynamic modelling (TELEMAC2D) and Artificial Neural Networks (NARX) (see section 4.2.6 and Figure 4.15), The capability of this hybrid approach to consider the nonlinear nature of extreme storm-tide was demonstrated in section 4.3. Moreover, the rising of the mean sea level is of major concerns in the context of a changing climate, which can linearly superimposed on the predicted storm-tide as the water depth is more than 10 m at both considered pilot sites, Cuxhaven and Sylt.

The main objective of Section 5.2 is to analyse the climate change signals for extreme storm-tide events at Cuxhaven and Sylt. These signals represent the difference between future storm-tide simulation under A1B_2 realization (2070-2100) and control simulation 1991-2000 in addition to the mean sea level rise, The analysis is performed in the following eight steps (see Figure 5.23):

1. Extract the hourly predicted surge-tide and significant wave height timed series at Cuxhaven and Sylt under hindcast (1991-2000), control (1991-2000) and future (2070-2100) meteorological conditions.
2. Prescribe the responsible forcing for the generation of all extreme storm-tide components at each site (sea level pressure, meridional and zonal wind speed components,

predicted tides, predicted external surge at Wick and mean Elbe river discharge) along with surge-tide and significant wave height time series as "inputs" to the developed Ensemble fitting Networks (EFN) (see section 4.2.6 and Figure 4.15) in order to predict the storm-tide under hindcast, control and future meteorological conditions.

3. Calculate the annual percentiles of storm-tide (from zero to 100 percentiles) at Cuxhaven and Sylt over 1991–2000 from the hindcast and control simulations in order to test how close is the storm-tide statistics from the control simulation is to the hindcast storm-tide at each site.
4. Calculate the confidence intervals for the hindcast upper percentiles over 1991-2000 (($\mathrm{CIs}^{x}(99.5)$ and $\mathrm{CIs}^{x}(100)$), where x is either Cuxhaven or Sylt with a statistical significance level of 95% using bootstrapping.
5. Calculate the mean of annual upper percentiles either over 1991-2000 for control storm-tide simulation ($\mathrm{Ps}^{x}_{\mathrm{C20\_2}}(99.5)$ and $\mathrm{Ps}^{x}_{\mathrm{C20\_2}}(100)$), where x is either Cuxhaven or Sylt) or over 2070-2100 for future simulation ($\mathrm{Ps}^{x}_{\mathrm{A1B\_2}}(99.5)$ and $\mathrm{Ps}^{x}_{\mathrm{A1B\_2}}(100)$).
6. Calculate the climate change signals for upper percentiles ($\Delta s^{x}(99.5)$ and $\Delta s^{x}(100)$), where x is either Cuxhaven or Sylt) as the difference between the mean of future simulation and the corresponding mean of control simulation according to Eq. (5.11) and (5.12), respectively.

$$\Delta s^{x}(99.5) = Ps^{x}_{A1B\_2}(99.5) - Ps^{x}_{C20\_2}(99.5) \tag{5.11}$$

$$\Delta s^{x}(100) = Ps^{x}_{A1B\_2}(100) - Ps^{x}_{C20\_2}(100) \tag{5.12}$$

7. Compare the climate change signals $\Delta s^{x}(99.5)$ and $\Delta s^{x}(100)$ with the corresponding confidence intervals $\mathrm{CIs}^{x}(99.5)$ and $\mathrm{CIs}^{x}(100)$ in step 4 to identify the significant changes in future storm-tide climate at each site.
8. Estimate the extreme effects of future climate change and sea level rise on storm-tide at Cuxhaven and Sylt.

(a) Meteorological data preparation and application for the hybrid model (2070-2100) (steps 1 and 2 in Figure 5.23)

The input deck of the developed hybrid models at Cuxhaven and Sylt (Figure 4.15) consists essentially of four different storm-tide prediction results from the best three NARX Type-A models and the best NARX Type-B model (see Table 4.4 and Table 4.5) at the time of prediction. In addition, the input deck contains the time lagged meteorological forces (sea level pressure (SLP), zonal and meridional wind speed components) for Cuxhaven (time lag=18 hours) or Sylt (time lag=16 hours).

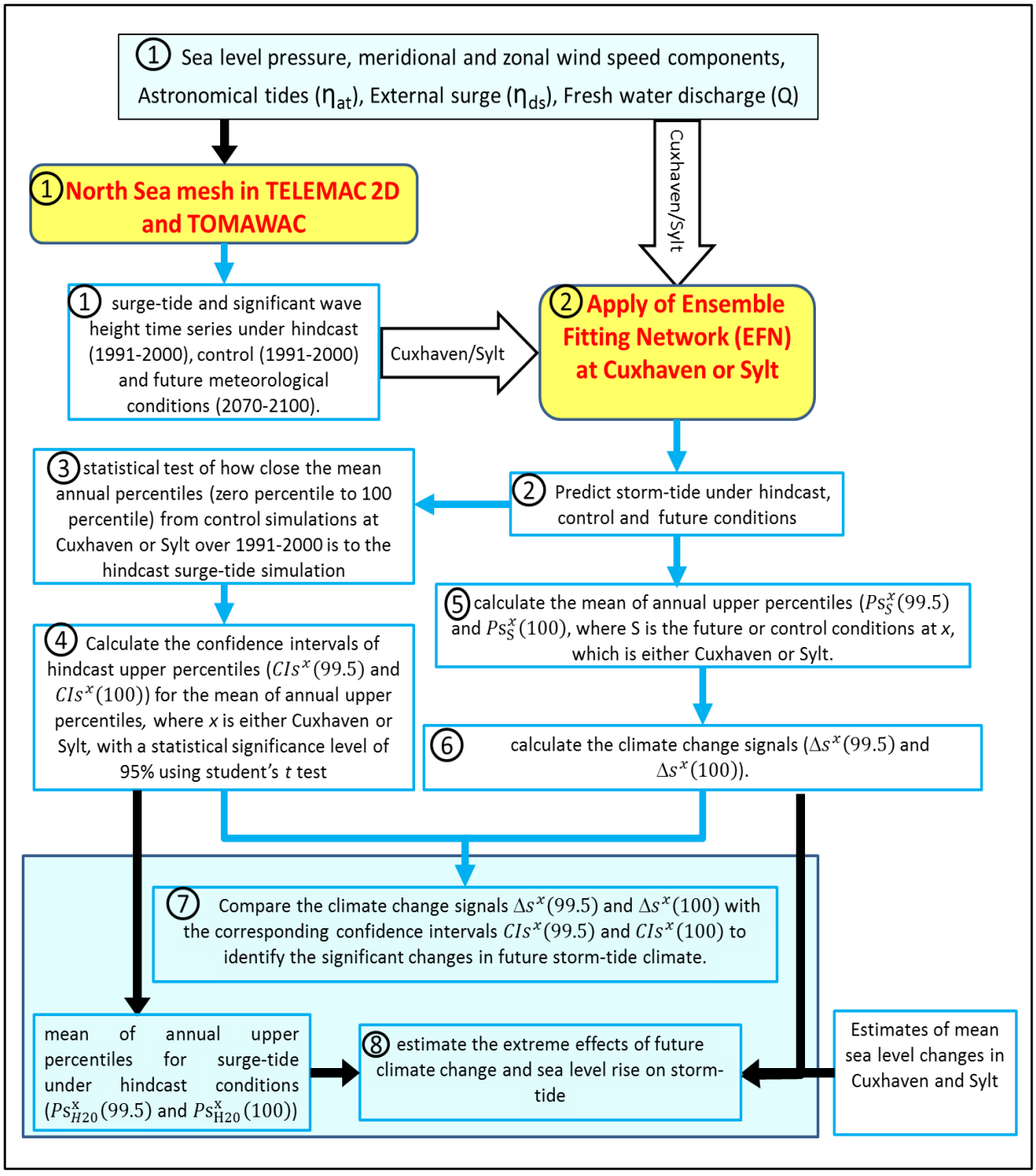

Figure 5.23: Prediction of the future storm-tide change signals (2070-2100) for Cuxhaven and Sylt relative to control simulation (1991-2000).

The input deck for the hybrid models is prepared in the following two steps:

1. The hourly wind speed components and SLP data at Cuxhaven and Sylt for hindcast and control simulations of storm-tide (1991-2000) are extracted from the metrological forces fields over the North Sea prepared in section 5.1.1(a), while they are extracted

for future simulation (2070-2100) from the metrological forces fields over the North Sea prepared in section 5.1.1(a).

2. Prediction of the storm-tide by the best three NARX Type-A models and the best NARX Type-B model. The input deck of the two NARX models types (see Table 4.2) consists of the metrological forces in step 1 at both sites in addition to the hourly predicted surge-tide, tide, external surge at wick, Elbe mean discharge (856 m^3/s for Cuxhaven only) and significant wave height timed series at Cuxhaven and Sylt, which are extracted from surge-tide simulations under hindcast, control (in section 5.1.1(a,c)) and future (in section 5.1.1(a,c)) meteorological conditions.

(b) Processing hindcast, control and future storm-tide results at Cuxhaven and Sylt (steps 3 to 7 in Figure 5.23)

The annual upper percentiles of storm-tide ($Ps_S^{xn}(99.5)$ and $Ps_S^{xn}(100)$, where *x* is either Cuxhaven or Sylt under *S* the hindcast (H20), control (C20_2) and Future (A1B_2) conditions) have been averaged using 10-year time slices (where *n* are 1991-2000 (H20 and C20_2) and 2070-2100(A1B_2)). The upper percentiles time series of ($Ps_{H20}^{xn}(99.5)$ and $Ps_{H20}^{xn}(100)$ under hindcast conditions (see Figure 5.24(a) and Figure 5.25(a)) confirm the higher levels of storm-tide at Cuxhaven than Sylt shown before (see Figure 4.22). The mean of $Ps_{H20}^{xn}(99.5)$ and $Ps_{H20}^{xn}(100)$ at Cuxhaven (step 4 in Figure 5.23), which is about 2.26 m to 2.46 m and 3.27m to 3.72 m, respectively, are higher than those at Sylt of 1.69 to 1.88 m and 2.4 to 2.90 m, respectively. Moreover, the $Ps_{H20}^{xn}(100)$ at Sylt has its highest increase in year 1999 of 3.17 m, which follows the highest duration of extreme wind events by 8.70 hours (see Figure 5.17). It also has to be pointed out that the highest $Ps_{H20}^{xn}(100)$ at Cuxhaven occurs in year 1999 with 4.0 m due to moderate duration and frequency of extreme wind events. Figure 5.24(b) and Figure 5.25(b) display the control bias signals at Cuxhaven and Sylt, respectively, as the annual difference of control storm-tide from the hindcast mean. Under the control climate at both sites, the $Ps_{C20\_2}^{xn}(99.5)$ and $Ps_{C20\_2}^{xn}(100)$ are generally underestimated except in year 1997. Moreover, the bias signals are significantly different than $CIs^x(99.5)$ and $CIs^x(100)$ under the hindcast conditions, which is mainly due to systematic errors of global climate models in their meteorological results of the present climate. So future storm-tide statistics is subtracted from control mean assuming that these runs are producing the same biases and the statistically significant differences are interpreted as the response of the applied emission scenario realization (A1B_2).

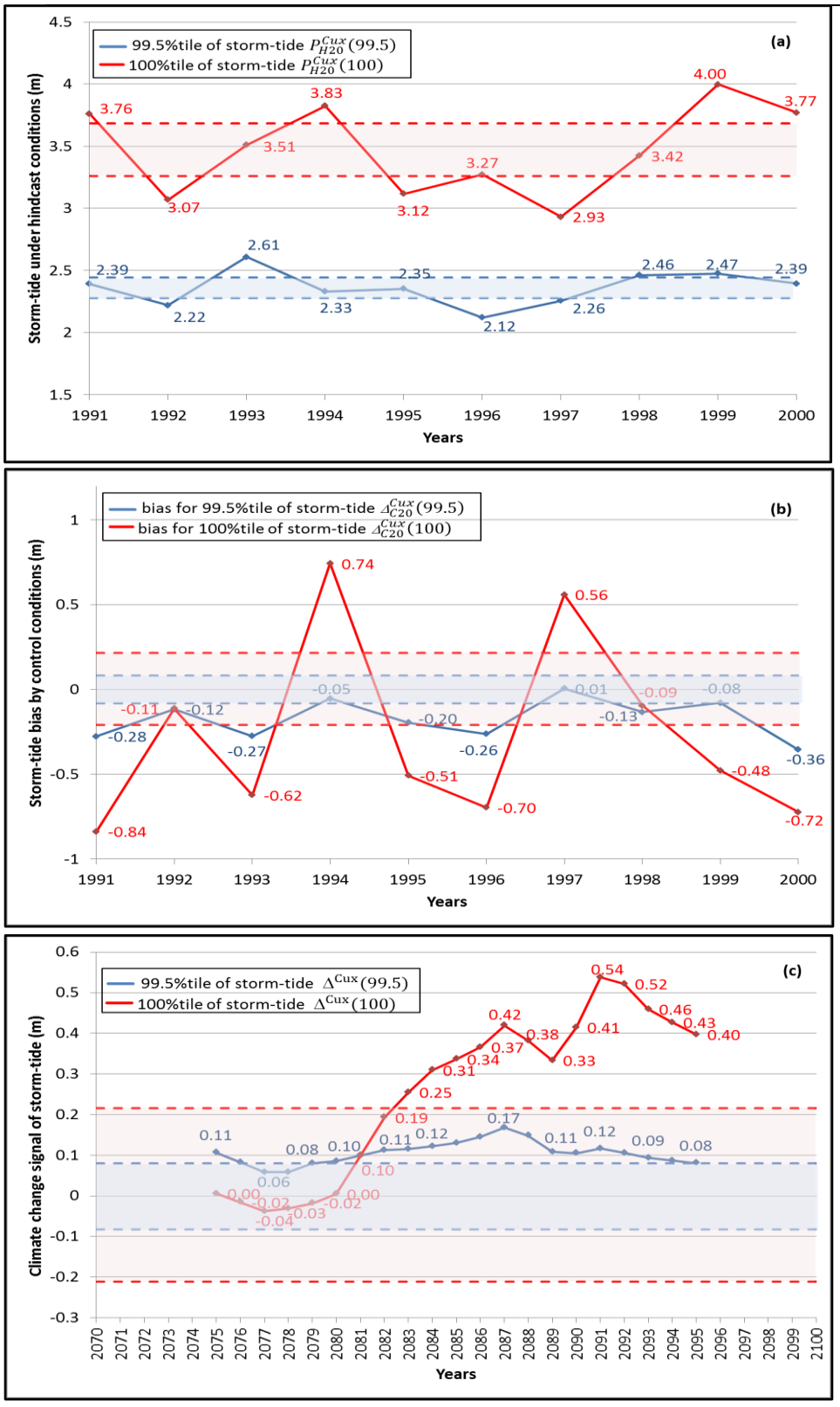

Figure 5.24: Time series of annual storm-tide upper percentiles (99.5% and 100% percentiles) at Cuxhaven under hindcast meteorological conditions 1991-2000 (a) with bias signal under control conditions 1991-2000 as annual difference from the hindcast mean (b) as well as the climate change signal for 10-year running average under future realization 2070-2100 as difference from control mean(c). Shaded areas between blue or red dashed lines correspond to the 95 % confidence interval for the hindcast mean based on bootstrapping of 99.5% and 100% percentiles, respectively.

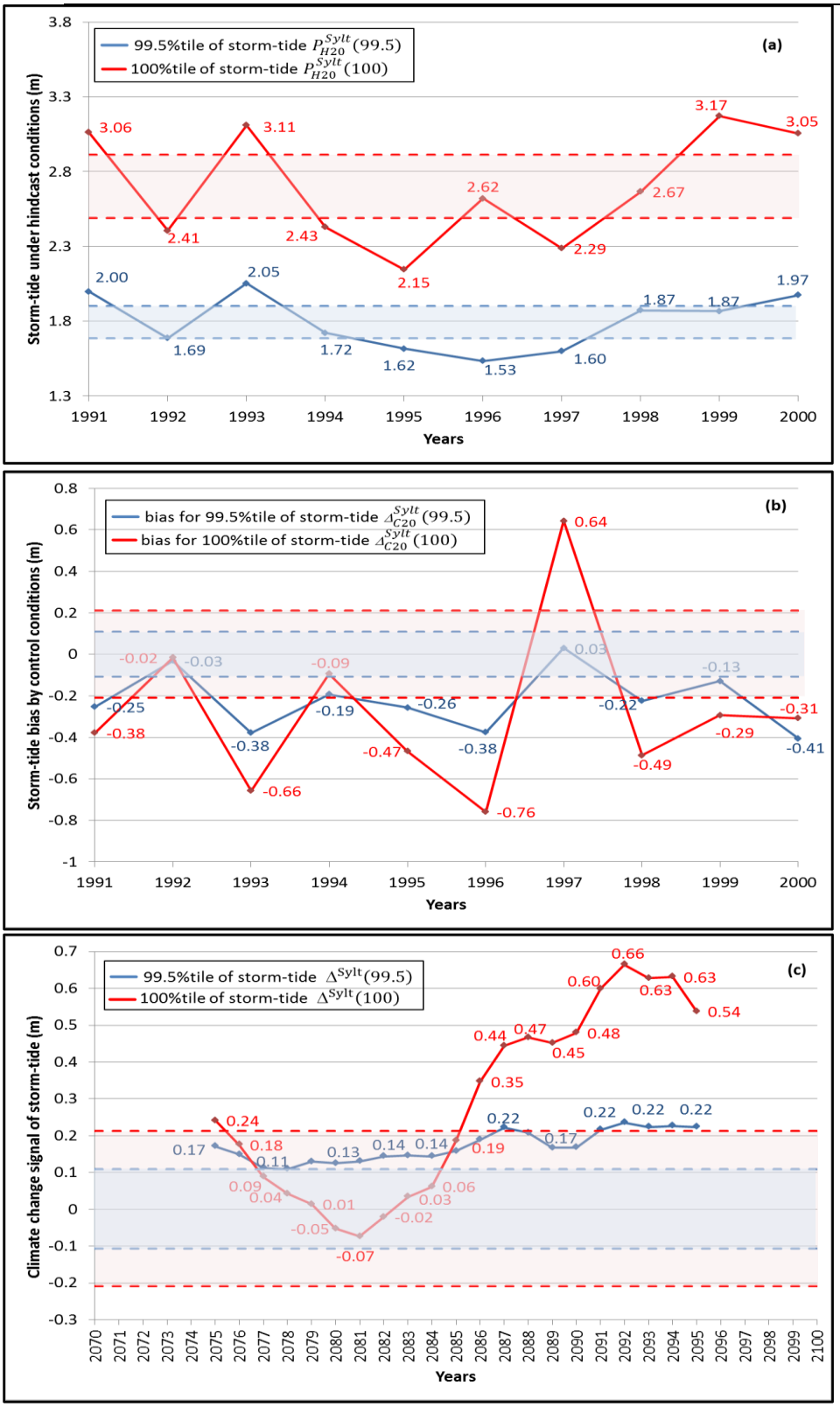

Figure 5.25: Time series of annual storm-tide upper percentiles (99.5% and 100% percentiles) at Sylt under hindcast meteorological conditions 1991-2000 (a) with bias signal under control conditions 1991-2000 as annual difference from the hindcast mean (b) as well as the climate change signal for 10-year running average under future realization 2070-2100 as difference from control mean(c). Shaded areas between blue or red dashed lines correspond to the 95 % confidence interval for the hindcast mean based on bootstrapping of 99.5% and 100% percentiles, respectively.

Figure 5.24(c) and Figure 5.25(c) (steps 5 to7 in Figure 5.23) show the climate change signals of upper percentiles for storm-tide ($\Delta s^x(99.5)$ and $\Delta s^x(100)$, respectively) at Cuxhaven and Sylt, as the difference of 10-year running average of annual future storm-tide from the control mean, as well as the corresponding 95 % confidence interval defined with a bootstrapping method based on annual upper percentiles under hindcast conditions. These signals show a significant increase in $\Delta s^x(99.5)$ at both sites from 2080 to end of 21st century for values ≥ 8 cm at Cuxhaven and ≥ 10 cm at Sylt. While it is significant for $\Delta s^x(100)$ at Cuxhaven and Sylt from 2083 and 2086, respectively, with values ≥ 22 cm at both sites. Furthermore, the increase of $\Delta s^x(99.5)$ and $\Delta s^x(100)$ are stronger at Sylt than their values at Cuxhaven. The highest increase of $\Delta s^x(99.5)$ and $\Delta s^x(100)$ at Sylt occur in year 2092 with 22 cm and 66 cm, respectively, while they occur at Cuxhaven in year 2087 with 17 cm and 2091 with 54 cm, respectively. Moreover, the increase of $\Delta s^x(99.5)$ at both sites shifts up the 99% percentile of storm-tide completely outside of $CIs^x(99.5)$ but still in the range of $CIs^x(100)$, which results in slight increase of extreme storm-tide frequency under future conditions but is not significant (see Figure 5.26 (b)).

The severity of storm-tide depends primarily on wind speed, wind direction and duration. Therefore, its temporal variations are directly related to the combination of local wind speed, direction or duration. The climate change signal of storm-tide at Cuxhaven (see Figure 5.24(c)) is partly related to respective changes in the frequency of extreme wind events, meanwhile it is affected to moderate extend by changes in the duration and speed of extreme wind in these events (see Figure 5.18). For example, the highest increase of $\Delta s^{Cux}(99.5)$ occurs in 2087 of 17 cm, which is related to the significant increase of wind speed (see Figure 5.14) in addition to its moderate increase of frequency and duration (see Figure 5.16 and Figure 5.18, respectively).While at Sylt it is mainly related to the changes in duration of extreme wind events but not their frequencies. The slight increase of extreme wind duration at Sylt in the period 2075-2078 results in significant increase of $\Delta s^{Sylt}(100)$ despite the respective decrease of wind speed and its frequency (see Figure 5.14 and Figure 5.18, respectively).

The average duration and the frequency of extreme storm-tide events under future climate at Cuxhaven and Sylt (see Figure 5.26), which are ≥ 99.5th annual percentile, are determined by the following 3 steps. Since the temporal characteristics of such events are important parameters in the context of coastal protection.

1. extract the average duration and number of extreme storm-tide events in future simulation (2070-2100), which have a period covering one or more hourly intervals and exceeding the 99.5th percentile at Cuxhaven and Sylt ($ds^x_{A1B\_2}(\geq 99.5)$ and $fs^x_{A1B\_2}(\geq 99.5)$, respectively, where *x* is either Cuxhaven or Sylt).
2. Calculate the climate change signal of mean duration or frequency for extreme storm-tide events ($\Delta ds^x_{A1B\_2}(\geq 99.5)$ or $\Delta fs^x_{A1B\_2}(\geq 99.5)$,respectively), which is defined as the difference between the mean value $ds^x_{A1B\_2}(\geq 99.5)$ or $fs^x_{A1B\_2}(\geq 99.5)$,respectively, in the future simulation (A1B_2) and the corresponding mean value $ds^x_{C20\_2}(\geq 99.5)$ or $fs^x_{C20\_2}(\geq 99.5)$,respectively, in the control simulation (C20_2) i.e.:

$$\Delta ds^{x}_{A1B\_2}(\geq 99.5) = ds^{x}_{A1B\_2}(\geq 99.5) - ds^{x}_{C20\_2}(\geq 99.5) \quad (5.13)$$

$$\Delta fs^{x}_{A1B\_2}(\geq 99.5) = fs^{x}_{A1B\_2}(\geq 99.5) - fs^{x}_{C20\_2}(\geq 99.5) \quad (5.14)$$

3. Compare the climate change signals $\Delta ds^{x}_{A1B\_2}(\geq 99.5)$ and $\Delta fs^{x}_{A1B\_2}(\geq 99.5)$ with the corresponding confidence intervals $CIs^{x}_{d}(\geq 99.5)$ and $CIs^{x}_{f}(\geq 99.5)$, respectively, which are based on hindcast simulation, to identify the significant changes in future surge-tide climate at both sites. So a test of the null hypotheses (Eq. (5.15)) are performed to determine if $\Delta ds^{x}_{A1B\_2}(\geq 99.5)$ and $\Delta fs^{x}_{A1B\_2}(\geq 99.5)$ lie in their natural confidence intervals ($CIs^{x}_{d}(\geq 99.5)$ and $CIs^{x}_{f}(\geq 99.5)$ with zero mean, respectively, or not (reject the null hypothesis).

$$H_o: ds^{x}_{A1B\_2}(\geq 99.5) = ds^{x}_{C20\_2}(\geq 99.5) \ \ for\ duration$$
$$H_o: fs^{x}_{A1B\_2}(\geq 99.5) = fs^{x}_{C20\_2}(\geq 99.5) \ \ for\ \ frequency \quad (5.15)$$

The mean duration of extreme storm-tide events increases due to climate change significantly at Sylt ($\Delta ds^{Sylt}_{A1B\_2}(\geq 99.5)$) (see Figure 5.26(a)), while it has no significant change at Cuxhaven ($\Delta ds^{Cux}_{A1B\_2}(\geq 99.5)$). The $\Delta ds^{Sylt}_{A1B\_2}(\geq 99.5)$ is significant above 0.32 hour or less than -0.33 hour. The significant increase of $\Delta ds^{Sylt}_{A1B\_2}(\geq 99.5)$ occurs in the periods 2075-2077 and 2092-2095 with the highest value of 0.43 hour in 2094. This can be related mainly to the increase in duration of extreme wind events at Sylt in these periods of the 21st century (see Figure 5.18). The climate change signals of mean frequency for extreme storm-tide at Cuxhaven and Sylt ($\Delta fs^{Sylt}_{A1B\_2}(\geq 99.5)$ and $\Delta fs^{Cux}_{A1B\_2}(\geq 99.5)$, respectively) are not significant and represent the natural variability of hindcast mean $CIs^{Cux}_{f}(\geq 99.5)$ and $CIs^{Sylt}_{f}(\geq 99.5)$. Moreover, The $\Delta ds^{Sylt}_{A1B\_2}(\geq 99.5)$ and $\Delta ds^{Cux}_{A1B\_2}(\geq 99.5)$ have inverse relation with $\Delta fs^{Sylt}_{A1B\_2}(\geq 99.5)$ and $\Delta fs^{Cux}_{A1B\_2}(\geq 99.5)$, respectively, at both sites. This follows the inverse relation between extreme wind events duration and frequency due to climate change (see Figure 5.18 and Table 5.3). The highest frequency at Cuxhaven reaches 0.38 event/year in 2075 and gradually decreases to the end of 21st century, while it reaches 0.63 event/year at Sylt in 2081 and also decreases afterward.

It has to be mentioned that these patterns for storm-tide upper percentiles are consistent with the increase of storm surge between the German Bight and Denmark, where the changes in the duration and intensity become more important than their slight increase in the western continental coast of the North Sea due to more frequent extremes only (Woth, 2006; Gaslikova et al., 2013). There is an increase in 99.5th percentile of residual surge height toward the coasts of the German Bight. It is higher for the eastern coast (North Frisian Islands), where it reaches

in one realization about 10 % of the reference climate storm surge heights, than for the southern coast (East Frisian Islands), where it is less than 8 % (Gaslikova et al., 2013). This is in coincidence with the increase in frequency of stronger southwesterly and westerly winds (≥17.2 m/s), which enhance the wind-setup toward the east (Gaslikova et al., 2013). The increase in the frequency of extreme events alone would be less relevant for many coastal facilities whereas The increase in duration and magnitude of extreme events could stretch their security limits (Woth, 2006). Table 5.3 shows the higher increase of maximum and 99.5th percentile of mean annual storm-tide at Sylt, which are 24.44% and 12.29%, respectively relative to hindcast means, than their values at Cuxhaven of 14.98% and 4.66%, respectively. This can be related mainly to location of the site in addition to the increase in duration of extreme wind events at Sylt by 5.74% relative to hindcast mean duration, with very weak effect by 99th percentile of wind speed and their frequency. While the location of Cuxhaven results in the duration and frequency of extreme wind events are less than those at Sylt, in spite of the increase of effect by 99th percentile wind speed by 1.15%,.

In order to be able to make statements about the maximum expected climate change effect on storm-tide at Cuxhaven and Sylt, the projections for the Relative Mean Sea Level rise (RMSLr) at both sites (step 8 in Figure 5.23), which are based on results by Wahl et al., (2010, 2011, 2013) and Mudersbach et al. (2012), are used. According to these results, the mean sea level at both sites is expected to increase with approximately 0.20±0.03 m in year 2092 ($[RMSL]_{max}$) relative to the MSL (1991-2000) of 0.121 m and 0.027 m at Cuxhaven and Sylt, respectively. It is assumed that the mean sea level and changing storm-tide are independent and may simply be added at Cuxhaven and Sylt as the mean water depth of both sites is greater than 10 m (Lowe & Gregory, 2005; Woth, 2006; Sterl et al., 2009; Howard et al., 2010; Gaslikova et al., 2013). The highest increase of $\Delta s^x(100)$ at Cuxhaven and Sylt ($[\Delta s^x(100)]_{max}$) occur in 2091 and 2092, respectively, when they reach 0.54 m and 0.66 m (see Figure 5.24 and Figure 5.25). The highest effect by maximum and 99.5th percentile of annual storm-tide are calculated, ($[Ps^x_{A1B\_2}(100)]_{max}$ and $[Ps^x_{A1B\_2}(99.5)]_{max}$, respectively), at each of Cuxhaven and Sylt under future realization (A1B_2), including $[RMSL]_{max}$ as follow :

$$[Ps^x_{A1B\_2}(100)]_{max} = Ps^x_{H20}(100) + [\Delta s^x(100)]_{max} + [RMSL]_{max}$$
$$[Ps^x_{A1B\_2}(99.5)]_{max} = Ps^x_{H20}(99.5) + [\Delta s^x(99.5)]_{max} + [RMSL]_{max} \quad (5.16)$$

with $Ps^x_{H20}(100)$ and $Ps^x_{H20}(99.5)$ are the mean of maximum and 99.5th percentile storm-tide, respectively, as simulated in the hindcast (H20;1991-2000) and with *x* is either Cuxhaven or Sylt. The $Ps^x_{H20}(100)$ and $Ps^x_{H20}(99.5)$ at Cuxhaven are 3.47 m and 2.36 m, respectively, while they are 2.70 m and 1.79 m, at Sylt (see Table 5.3). Therefore, the $[Ps^x_{A1B\_2}(100)]_{max}$ and $[Ps^x_{A1B\_2}(99.5)]_{max}$ are 4.19 m and 2.67 m, respectively, at Cuxhaven in 2091, while they are 3.56 m and 2.21 m at Sylt in 2092. So the $[Ps^x_{A1B\_2}(100)]_{max}$ and $[Ps^x_{A1B\_2}(99.5)]_{max}$ at Cuxhaven are higher than their counterpart values at Sylt in spite of higher rates of subsidence and higher climate change signal of storm-tide at Sylt than those at

Cuxhaven. Since the storm surges and tide at Cuxhaven under hindcast and future conditions are higher than their counterparts at Sylt, thus resulting in water level with less pronounced shoaling effect.

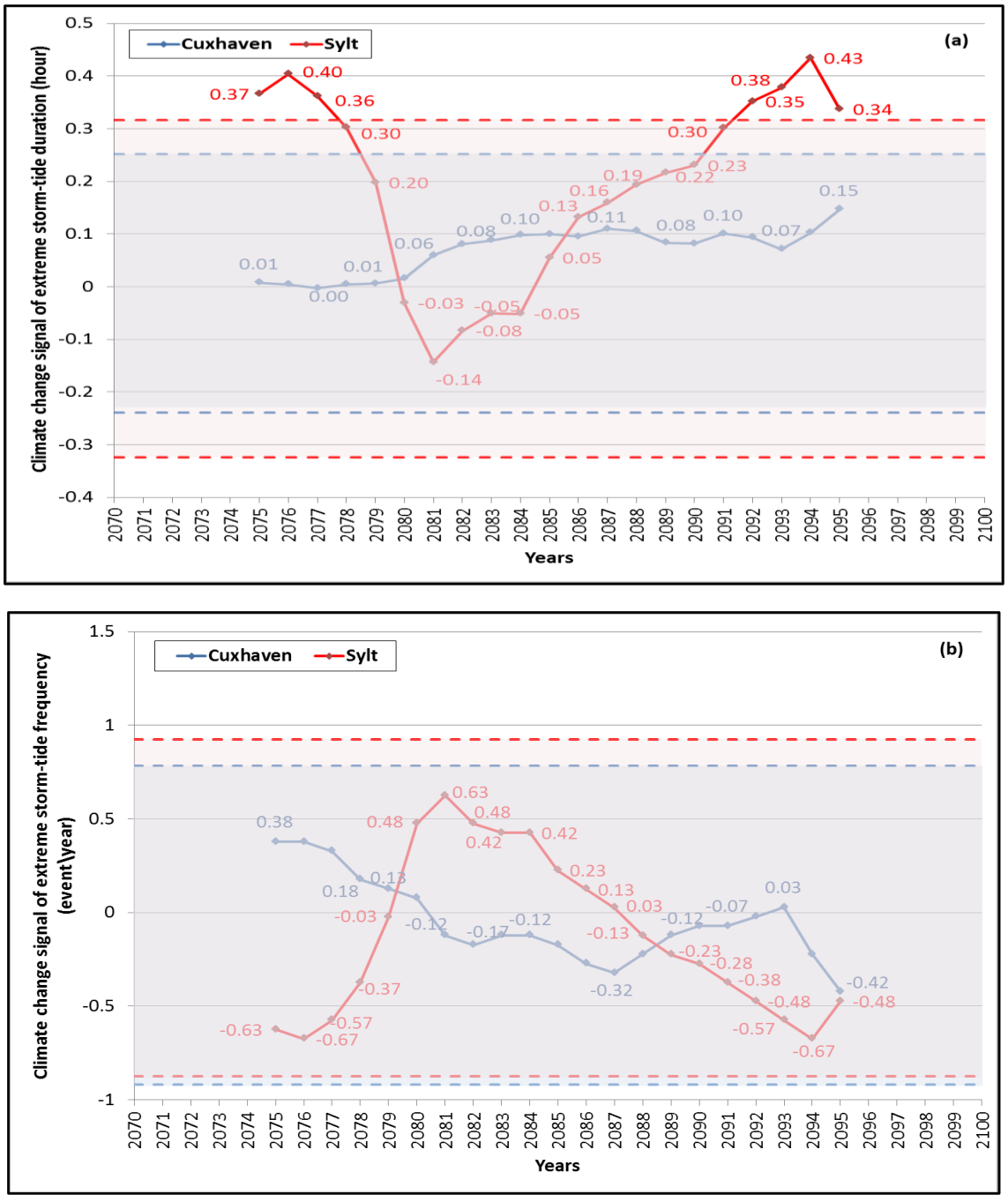

Figure 5.26: Climate change signals for 10-year running averages of extreme storm-tide (storm-tide ≥ annual 99.5th annual percentile) duration (a) and frequency (b) under future realization 2070-2100 as deviations compared to control mean at Cuxhaven and Sylt. Shaded areas between blue or red dashed lines correspond to the 95 % confidence interval for the hindcast mean based on bootstrapping at Cuxhaven or Sylt, respectively.

Table 5.3: Highest effect by the maximum and 99.5th percentile of mean annual storm-tide at each of Cuxhaven and Sylt under future realization (A1B_2; 2070-2100) with their generation forces by 99th percentile of wind speed along with the duration and frequency of extreme events.

sites / parameter	Cuxhaven (2091)			Sylt (2092)		
	Wind speed (99%-tile)	**Maximum storm-tide**	**Storm-tide (99.5%-tile)**	**Wind speed (99%-tile)**	**Maximum storm-tide**	**Storm-tide (99.5%-tile)**
annual mean under hindcast conditions (H20;1991-2000)	17.32 m/s	3.47 m	2.36 m	18.41 m/s	2.70 m	1.79 m
climate change signal	0.20 m/s	0.52 m	0.11 m	0 m/s	0.66 m	0.22 m
Percentage of increase in climate change signal relative to hindcast mean	1.15%	14.98%	4.66%	0%	24.44%	12.29%
mean duration of extreme events* (H20;1991-2000)	7.03 hour	3.07 hour		6.79 hour	3.69 hour	
climate change signal of duration	0.67 hour	0.1 hour		0.39 hour	0.35 hour	
Percentage of increase in duration signal relative to hindcast mean	9.53%	3.26%		5.74%	9.49%	
mean frequency of extreme events* (H20;1991-2000)	12.63 event/year	12.91 event/year		12.88 event/year	11.57 event/year	
climate change signal of frequency	-0.65 event/year	-0.07 event/year		-0.79 event/year	-0.48 event/year	
Percentage of decrease in frequency signal relative to hindcast mean	-5.15%	-0.54%		-6.13%	-4.15%	

* extreme events for wind are those events with wind speed ≥ annual 99th percentile and each event covers one or more hourly interval, while for storm tide are events with height ≥ annual 99.5th percentile and each event covers one or more hourly interval.

The bias signal of annual upper percentiles under the control climate at both sites ($Ps^{xn}_{C20\_2}(99.5)$ and $Ps^{xn}_{C20\_2}(100)$) are generally underestimated and they are significantly different from the range of the natural variability of the results obtained under hindcast conditions ($CIs^{x}(99.5)$ and $CIs^{x}(100)$). This is mainly due to the systematic errors in the simulation results of the present climate obtained by global climate models. Hence, the future storm-tide statistics is subtracted from the control mean, assuming that these runs generate the same biases and that the statistically significant differences are interpreted as the response of the applied emission scenario realization (A1B_2). The climate change signals of the upper percentiles for storm-tide ($\Delta s^{x}(99.5)$ and $\Delta s^{x}(100)$) at both sites show a significant increase approximately from 2080 to the end of the 21st century. The highest increase of $\Delta s^{x}(99.5)$ and $\Delta s^{x}(100)$ at Sylt occur in 2092 with 22 cm and 66 cm, respectively, while at Cuxhaven respectively in 2087 with 17 cm and 2091 with 54 cm. The mean duration of extreme storm-tide events increases due to climate change significantly at Sylt ($\Delta ds^{Sylt}_{A1B\_2}(\geq 99.5)$) (see Figure 5.26(a)), while no significant changes occurs at Cuxhaven ($\Delta ds^{Cux}_{A1B\_2}(\geq 99.5)$). The significant increase of $\Delta ds^{Sylt}_{A1B\_2}(\geq 99.5)$ occurs in the periods 2075-2077 and 2092-2095 with the highest value of 0.43 hour in year 2094. This can be related mainly to the increase in duration of extreme wind events at Sylt in these 21st century periods (see Figure 5.18). The climate change signals of the mean frequency for extreme storm-tide at Cuxhaven ($\Delta fs^{Cux}_{A1B\_2}(\geq 99.5)$) and Sylt ($\Delta fs^{Sylt}_{A1B\_2}(\geq 99.5)$) are not significant and within the range of the natural variability of the hindcast mean ($CIs^{Cux}_{f}(\geq 99.5)$ for Cuxhaven and $CIs^{Sylt}_{f}(\geq 99.5)$ for Sylt).

The mean sea level at both sites is expected to increase with approximately 0.20±0.03 m in 2092 ($[RMSL]_{max}$) relative to the MSL (1991-2000) at Cuxhaven of 0.121 m and Sylt of 0.027 m. It is assumed that the mean sea level and changing storm-tide are independent and may simply be added at Cuxhaven and Sylt as the mean water depth of both sites is greater than 10 m (Lowe & Gregory, 2005; Woth, 2006; Sterl et al., 2009; Howard et al., 2010; Gaslikova et al., 2013). The mean of maximum storm-tide ($[Ps^{x}_{A1B\_2}(100)]_{max}$ is 4.19 m at Cuxhaven in 2091, while it is 3.56 m at Sylt in 2092.

5.3 Summary and Concluding Remarks

The spatial patterns of climate change signals for the 30-year long surge-tide (2070 to 2100, future simulation) were predicted relative to the present-day (1970-2000, control simulation). The future meteorological forcing was based on the IPPC emission A1B scenario (increase of temperature by 2.8^{O}C in 2100). The southeastern part of the North Sea (German Bight) shows higher and statistically significant increase in future surge-tide signal, while the east coast of the UK and the middle of the North Sea are affected by a significant decrease. Similarly the future storm surge signals (2071–2100), which is compared to hindcast simulations (1961–1990), by Woth (2006) and Gaslikova et al. (2013) show an increase in the southeastern North Sea and a slight decrease at some parts of the British coast. The climate change signals for the upper percentiles of surge-tide (99.5 percentile $\Delta^{x}(99.5)$ and 100 percentile $\Delta^{x}(100)$) gradu-

ally increase from the middle of the North Sea toward the Elbe estuary. The highest increase of $\Delta^{x}(100)$ reaches 0.23 m, which is about 6.6% increase as compared to the maximum of control simulation. These results are consistent with the climate change signal of 99.5th percentile of storm surge studied by Woth (2006) within the German Bight along the 10-m bathymetry line under A2 scenario regionalized with 4 different RCMs, in which the increase ranges between 20 cm (the southern coast of German Bight) and 30 cm (the eastern coast of German Bight). This can be related to the increase of westerly wind frequency during storms (Figure 5.15 and Figure 5.16), and their increased duration (Figure 5.18) in the future climate realization. The indicated increase in the height of extreme events would be relevant for the design of coastal defenses in the German Bight.

The climate change signals of upper percentiles for storm-tide ($\Delta s^{x}(99.5)$ and $\Delta s^{x}(100)$) at Cuxhaven and Sylt show a significant increase approximately from 2080 to the end of the 21st century. The highest increase of $\Delta s^{x}(100)$ at Cuxhaven and Sylt occurs approximately in 2092 with 54 cm and 66 cm, respectively. The mean duration of extreme storm-tide events increases due to climate change significantly at Sylt ($\Delta ds^{Sylt}_{A1B\_2}(\geq 99.5)$) (see Figure 5.26(a)), while it does not significantly change at Cuxhaven ($\Delta ds^{Cux}_{A1B\_2}(\geq 99.5)$). The significant increase of $\Delta ds^{Sylt}_{A1B\_2}(\geq 99.5)$ occurs in the periods 2075-2077 and 2092-2095 with the highest value of 0.43 hour in 2094. This can be related mainly to the increase in duration of extreme wind events at Sylt in these periods of the 21st century. The climate change signals of the mean frequency for extreme storm-tide at Cuxhaven and Sylt ($\Delta fs^{Cux}_{A1B\_2}(\geq 99.5)$ and $\Delta fs^{Sylt}_{A1B\_2}(\geq 99.5)$, respectively) are not significant and are within the range of the natural variability of the hindcast mean ($CIs_f^{Cux}(\geq 99.5)$ and $CIs_f^{Sylt}(\geq 99.5)$). The future increase in frequency of extreme storm-tide events alone, which is not significant, would be less relevant for many coastal facilities whereas the increase in duration and/or magnitude of extreme events (both are significant) could decrease their safety.

The highest mean of the annual maximum percentile for storm-tide ($[Ps^{x}_{A1B\_2}(100)]_{max}$) occurs in 2091 with 4.19 m at Cuxhaven, while it is 3.56 m at Sylt in 2092. These values are higher than the maximum of storm-tide ($(\eta_{EFN})_{max}$) at both sites in (1991-2007) by 0.19 m (4.8 %) and 0.54 m (17.9 %), respectively. Furthermore, the $[Ps^{x}_{A1B\_2}(100)]_{max}$ at Cuxhaven is higher than its counterpart value at Sylt, in spite of the stronger effects of subsidence rate and climate change signal on storm-tide at Sylt than those at Cuxhaven. This is due to the higher contribution of storm surge and tide components at Cuxhaven than their counterparts at Sylt under hindcast and future conditions.

6 Summary, concluding remarks and outlook

The increase in storm-tide level during storms is hardly predictable in space as well as time. In fact, it depends on many factors that can be classified in three categories (see Figure 2.15):

(i) Meteorological (highly stochastic) factors such as wind speed and sea level pressure;

(ii) Deterministic factors such as astronomical tides and tidal resonance in the North Sea;

(iii) Local factors in nearshore zones such as local bathymetry and shoreline geometry.

Moreover, the external surges, generated outside the North Sea and propagating to the German Bight, may also noticeably contribute to the observed water level. The contribution of the mutual interactions between the various components to the resulting extreme storm-tide level is still almost fully unknown as these interactions are generally nonlinear and non-stationary. Currently, the nature of these mutual nonlinear interactions and their contribution to the extreme storm-tide cannot yet be solved by conventional hydrodynamic models or statistical models alone.

The current hydrodynamic models have generally been shown to overestimate the maximum water level, and to incorrectly predict the time of its arrival (Higaki et al., 2009)(DERM, 2009). On other hand, the statistical models require long time series of observed water level data (more than 20 years), which is usually not available for all coastal sites, especially in developing countries. Furthermore, serious difficulties arise from the unsteadiness of the processes involved and from the problems associated with the extrapolation of observations to extreme events with an occurrence of 10^{-2}-10^{-5} using statistical distributions without any physical base.

In many other studies, Artificial Neural Networks (ANNs) have been successfully applied for the prediction of water levels, waves and storm surge for short-term periods (e.g. Bajo & Umgiesser, 2010; Makarynskyy et al., 2004; Mandal & Prabaharan, 2006; Prouty et al., 2008; Tissot et al., 2002). These studies generally emphasize the better prediction capabilities of ANNs as compared to the current hydrodynamic and statistical models. However, the prediction capability of any static ANNs model has its limitations, especially in terms of long-term prediction. The long-term dependencies problem (i.e. those systems for which the desired output depends on inputs presented at times far in the past) is lessened for a class of ANNs architectures called *nonlinear autoregressive models with exogenous (NARX) recurrent neural networks*, which have powerful dynamic representational capabilities (Lin et al., 1996). In this PhD study, the hybrid TELEMAC-NARX models for Cuxhaven and Sylt in the German Bight have been developed as an operational tool for modelling the nonlinear complex storm-tide system. Therefore, the hydrodynamic results are included as input for NARX, which reduces the amount of required training data (in this study very good performance with five years data 2000-2005). Combining the strengths of NARX models with those of the TELEMAC models (TELEMAC2D and TOMAWAC) provides a powerful and computationally efficient operational model system. The latter is applied for reconstructing the storm-tide data from the past (e.g. hindcast simulations 1970-2007) and to predict the extreme storm-tide in

the 21st century under future conditions (e.g. under A1B_2 realization 2070-2100) using sequential time series predicted by the hybrid model.

Therefore, the main contributions of this thesis may be summarized as follows:

(i) A hybrid TELEMAC-NARX model system is developed, which, as exemplarily shown in Cuxhaven and Sylt, is capable to account for the nonlinear interactions between the extreme storm-tide components. This enables the substantial errors in both magnitude and timing of the results predicted by the TELEMAC models alone to be corrected.

(ii) A relational NARX model is developed to retrieve missing water level data at one site using observed water level data at a neighbouring site; i.e. it establishes implicitly a nonlinear relationship between the data at two neighbouring sites principally due to the storm surge, tide and external surge. Especially, the two sites are separated by a distance of more than one hundred kilometers, and both sites are affected by the same storms and storm-tide components. The capabilities of this model were exemplarily shown by retrieving the missing storm-tide data from the past (2000-2007) in Sylt by using the available data in Cuxhaven (2000-2007).

(iii) The developed hybrid TELEMAC-NARX model system is exemplarily used for two sites in the German Bight (Cuxhaven and Sylt) to demonstrate its capability to estimate the effects of future climate change projection (e.g.between 2070 and 2100) and relative mean sea level rise on the storm-tide.

Based on the results of the validation of the hybrid model by observed data and its implementation at Cuxhaven and Sylt, recommendations are provided for the practical application of the hybrid TELEMAC-NARX model, the NARX models and the TELEMAC models. Therefore, in the following sections, the main results are *first* summarized and tentative conclusions are drawn. *Second*, the applicability and the limitations of the implemented TELEMAC, NARX and hybrid TELEMAC-NARX models are briefly discussed. *Finally*, recommendations for future research are proposed.

6.1 Summary of main results and conclusions

Along North Sea coasts, reliable storm-tide predictions are of crucial importance as a large portion of the coastal zones is not only below mean sea level but also characterized by frequent storms. As one of the most dramatic impacts of climate change, the threat by extreme storm-tides might increase mainly due to the change in wind climate. Among others, a reliable modelling of extreme storm-tide is crucial for an improved understanding of the contribution of the nonlinear interactions between the diverse storm-tide components on the resulting water level. This is indeed expected to result in improved predictions of extreme water levels, and thus in safer flood defences and in a more efficient flood risk management in a changing climate.

6.1.1 Storm-tide simulation in the North Sea using "TELEMAC2D and TOMAWAC"

The hydrodynamics and wave propagation over the North Sea have been simulated in this study using the selected flow model TELEMAC2D and the wave propagation model TOMAWAC. Both numerical models are parts of the TELEMAC model suite (see Figure 3.1). The models are applied to the North Sea area in order (i) to calibrate and validate the model, and (ii) to identify the relative contributions of storm-tide components at the two study sites (Cuxhaven and Sylt).

Tidal simulations for the North Sea area were performed using TELEMAC2D to define the Chezy friction coefficient as function of water depth in order to calibrate the bottom friction of the model. The friction coefficient was defined according to Eq. (3.29) in four subdomains. The predicted tide of 2006 by TELEMAC2D is validated with the real-tide at three stations in the German Bight: Cuxhaven, Sylt and Helgoland. The observed tides are almost exactly reproduced for the three stations, with a correlation coefficient (CC) of 0.99 and a root mean square error (RMSE) ranging from 0.08 m at Cuxhaven to 0.11 m at Helgoland (see Figure 3.7).

The implementation of the surge-tide simulation using TELEMAC2D is carried out taking into account the meteorological and tidal forces in addition to the effects of the external surge from the Atlantic at the northern boundary of the model (see Figure 3.8). Wick and Lerwick are selected as the most suitable sites to introduce the external surge in the North Sea model, because they have zero time shifts from the northern boundary and better reflect the observed external surge variability in space. Two external surge NARX models are developed for Wick and Lerwick, which are used to fill the gaps in the observed external surge data between 1970 and 2007. Moreover, both models are also used in chapter 5 to predict the external surge for future surge-tide realization 2070-2100. The prediction performance is relatively good for both NARX models with RMSE=0.06 m and CC=0.88 at Lerwick, and RMSE=0.09 m and CC= 0.83 in Wick. Their prediction performance might even be enhanced, if the external surge predicted by the surge-tide model covering the North Atlantic is added to the input deck of the NARX models.

The predicted storm-tide at Cuxhaven and Sylt indicated that the most relevant components are storm surge, tide and external surge. The coupled use of TELEMAC2D and TOMAWAC revealed the contribution of wave setup at both sites. The wave setup due to white-capping dissipation is as expected negligibly small at average water depth of 23 in both sites. In fact, the wave setup (η_w) does not exceed 10 cm (Figure 3.15) during the storm of November 2007 and has no effect during the storms of January 2000 and November 2006. Therefore, the coupling of TELEMAC2D and TOMAWAC is not required for the North Sea model to include the wave setup effect (η_w) at both interested sites, which saves computation time. Nevertheless, inside the surf zone area the contribution of wave setup due to wave breaking dissipation cannot be neglected and use of ARTEMIS model instead of TOMAWAC is more suitable in shallower water (also consider wave reflection and diffraction processes).

The simulated and observed values of surge-tides in 2006 at Cuxhaven and Sylt were compared (see Table 3.5). The standard deviation (σ) of the predicted surge-tide $\eta_{su\text{-}t\ TEL}$ at Sylt is σ =0.69 m, while CC= 0.96 at both stations. The predicted extreme peak values $\eta_{su\text{-}t\ TEL}$ are underestimated as compared to the extreme peak values η_{OB} observed during the storm of November 2006. It is assumed that this might be due to the approximation of the nonlinear interaction between the components of surge-tide predicted by TELEMAC2D (η_{NLT}) that additionally leads to the shift in the arrival time of the predicted extreme peak $\eta_{su\text{-}t\ TEL}$. Based on this assumption, a pragmatic data-driven approach, which can use artificial neural networks (ANNs), is required to assess the contributions of the missing non-linear interactions to the resulting extreme storm-tide (see chapter 4).

6.1.2 Nonlinear interactions of storm-tide components using the hybrid CFD-NARX model

Two types of NARX models were developed for Cuxhaven and Sylt (i) using the Nonlinear Autoregressive with eXogeneous inputs (NARX) (Type-A), (ii) combining the NARX models with TELEMAC2D surge-tide results (Type-B). Furthermore, their ensemble model (hybrid TELEMAC-NARX) is applied to reduce variance and minimize errors during extreme events. The developed models are validated using the observed water level between 1999 and 2007 at both sites. The hybrid TELEMAC-NARX model has the capability to account for nonlinear interaction between the extreme storm-tide components, so the substantial errors in both magnitude and timing of the storm-tide predicted by numerical modelling can be corrected. For Cuxhaven's NARX ensemble model, the lowest RMSE is 0.148 m with a correlation of 0.99. The NARX ensemble model in Sylt has an RMSE of 0.123 m and a correlation of 0.98.

The hybrid TELEMAC-NARX model provides a powerful and computationally efficient operational model system for storm-tide prediction as exemplarily shown in Cuxhaven and Sylt, which allows to:

(i) Reconstruct the missing data using sequential time series predictions for long-term periods,
(ii) Reduce the amount of required observed data for NARX part training (usually five years show very good performance).

The account for nonlinear interaction by the hybrid models may result either in the reduction or increase of the highest water level during storms when compared with the linear superposition of extreme storm-tide components according to the following two situations at both locations (Cuxhaven and Sylt):

(i). If the η_L peak resulting from linear superposition, which occurs directly before the time of $(\eta_{EFN})_{max}$ resulting from the NARX ensemble model, is less than 3 m, then its following peak would overestimate the peak of η_{EFN} at the time of $(\eta_{EFN})_{max}$. Since the peaks of η_{EFN} and η_L, which occur before the time of $(\eta_{EFN})_{max}$, do not increase signif-

icantly the mean water level (MWL) during the storm. Therefore, the following peaks of η_{EFN} and η_L will propagate under more pronounced shoaling effect that increases their heights simultaneously.

(ii). If the η_L peak, which occurs directly before the time of $(\eta_{EFN})_{max}$, is larger than 3.00 m, then its following peak would underestimate the peak of η_{EFN} at the time of $(\eta_{EFN})_{max}$. Since only the peak of η_L, which occurs before the time of $(\eta_{EFN})_{max}$, increases the MWL during the storm to a limit by which its following peak will propagate under less pronounced shoaling effect.

The highest peak of each storm-tide component by TELEMAC2D and the nonlinear interaction (η_{NL}) predicted by the NARX ensemble over the entire time period 1991-2007 at Cuxhaven and Sylt are added together linearly ($(\eta_{all})_{max}$). The result is assumed to represent the highest physical limit of extreme storm-tide over the entire considered time period, though it is very improbable that the peaks of superposed storm-tide components will occur at the same times. The $(\eta_{all})_{max}$ at Cuxhaven, which reaches 7.21 m , is higher than its counterpart at Sylt of 5.66 m. Nevertheless, the maximum effect of the nonlinear interaction $(\eta_{NL})_{max}$ at Cuxhaven, which reaches 21%, is lower than its counterpart of 25.80% at Sylt. Since the storm surges and tide at Cuxhaven are higher than their counterparts at Sylt, thus resulting in higher water level with less pronounced shoaling effect. Therefore, the consideration of $(\eta_{NL})_{max}$ would be relevant for the safety of many coastal facilities, which depends on the magnitude of highest physical limit of extreme storm-tide $(\eta_{all})_{max}$

The recorded near shore water level at Sylt is of great importance in applications such as ocean engineering and safe navigation. Unfortunately, there are gaps in this record at Sylt, which are existed due to the lack of tide-gauge in the past time, failures in the measuring tide-gauge due to strong storms or when it is upgraded. The statistical distributions and properties of meteorological forces (sea level pressure, zonal and meridional wind speed components) for Cuxhaven and Sylt are approximately similar (see section 4.2.1). The Relational NARX model was developed to retrieve the missing data at Sylt using observed water level from Cuxhaven. The prediction by Relational NARX model (η_R) has better performance than the predicted storm-tide by NARX ensemble (η_{EFN}) at Sylt, since the input contains the observed water level at Cuxhaven (see Figure 4.25). It has the lowest normalized RMSE of 0.11 m. Moreover, the highest η_R peaks reach 2.43 m and 2.79 m during the storms of November 2006 and November 2007, respectively, and they slightly overestimate the highest η_{OB} peaks of 2.21 m and 2.65 m.

6.1.3 Extreme storm-tides in the German Bight under future climate change (2070-2100) using the hybrid TELEMAC-NARX model

The majority of the North Sea coasts are low lands and thus highly vulnerable to extreme storm surges, particularly under future climate change. Therefore, potential changes in surge-tide in 2070-2100 are analyzed in order to identify the most threated flood-prone coastal low

lands. The analysis of the impact of future climate change on the water levels is performed in the following two stages by focusing on extreme values (annual 99.5 percentile and maximum surge-tide) and with special emphasis on the German Bight:

- *Stage 1: Simulations of hindcast and control surge-tides (1970-2000) in the North Sea (Figure 5.2):*

  The hindcast and control surge-tide simulations in the North Sea (1970-2000) are performed to examine the similarity of the control simulation, which is representative for the present surge-tides under the meteorological conditions obtained from the ECHAM5-MPIOM/CLM models, with the surge-tides under meteorological conditions obtained from the NCEP/SN-REMO hindcast (Table 5.1). Thus, each simulation is performed using the North Sea model set-up in TELEMAC2D with the same boundary conditions data (Figure 3.8) that represent the surge-tide components (Figure 2.15). The percentiles from control and hindcast surge-tide simulations have a linear correlation of more than 0.99 as exemplarily shown for Cuxhaven and Sylt (Figure 5.6). Moreover, the annual-mean duration and frequency of extreme events in the control simulations compare well with the hindcast over the North Sea (Figure 5.10). The results of this analysis demonstrates that the *control climate*, which is used as *a reference for future climate change impacts*, is well in agreement with the results of the hindcast simulations and has thus a resemblance with the real climate effect on surge-tide. Since the systematic errors (bias) appear in the control simulation as a deviation from the mean of hindcast surge-tide simulation, the difference between the future and control simulations represent the response of the surge-tide under the future emission scenario assuming the same bias in both simulations.

- *Stage 2: Simulation of future surge-tides (2070-2100) for the North Sea (*Figure 5.11*):*

  The changes of the mean 99 percentile wind speed under the A1B scenario resemble the ensemble mean of all future scenarios and preserve a meaningful scale of metrological processes (see Figure 5.12 and Figure 5.13). Therefore, the change in surge-tide statistics over the North Sea due to future climate change is carried under A1B scenario ("future conditions"). The increase in magnitude of the extreme surge-tide due to climate change is significant for the German Bight and the Netherlands coasts, while it decreases significantly toward the middle of the North Sea and along the UK east coast. This is combined with the same spatial increase of the mean duration of extreme surge-tide events ($\Delta d^{x}_{A1B\_2}(\geq 99.5)$). Furthermore, the increase is more pronounced for the eastern German Bight (North Frisian Islands) and the Danish coasts than for the southern German Bight (East Frisian Islands) and the Netherlands coasts. The climate change signal along the 10-m bathymetry line for annual 99.5 percentile of surge-tide ($(\Delta^{x}(99.5))$ in the eastern German Bight ranges from 0.12 m to 0.16 m, while it ranges from 0.08 m to 0.11 m in the southern German Bight. This can be related to the increase of the westerly wind frequency during storms (Figure 5.15 and Figure 5.16), and their increased duration (Figure 5.18) in the future climate realization. In general, the surge-tide climate change signals toward the end of the twenty-

first century (2070–2100) are comparable to those from the storm surge under the A2 scenario over the North Sea by Woth (2006), except for the frequency of the extreme events. Woth (2006) found an increase in the frequency of extreme storm surge events under future climate, while in this study the frequency of storm-tide events not change significantly. This might be due to the nonlinear interaction of tide and external surge with the local surge, which reduces extreme water levels in most of storm events considered in the period (1991-2007).

The temporal variations of the climate change signals for storm-tide at the two pilot sites, Cuxhaven and Sylt, are assessed using the new hybrid modelling approach to consider the nonlinear nature of extreme storm-tide. Moreover, the effect of the mean sea level rise is linearly superimposed on the predicted storm-tide as the water depth is more than 10 m at both considered sites, Cuxhaven and Sylt (Lowe & Gregory, 2005; Woth, 2006; Sterl et al., 2009; Howard et al., 2010; Gaslikova et al., 2013). The maximum storm-tide ($[Ps^{x}_{A1B\_2}(100)]_{max}$) occurs in 2091 with 4.19 m at Cuxhaven, while it is only 3.56 m at Sylt in 2092. These values are higher than the maximum of storm-tide ($(\eta_{EFN})_{max}$) at both sites in the period 1991-2007, by 0.19 m (4.8 %) at Cuxhaven and 0.54 m (17.9 %) at Sylt. The mean duration of extreme storm-tide events increases due to climate change significantly at Sylt ($\Delta ds^{Sylt}_{A1B\_2}(\geq 99.5)$) (see Figure 5.26(a)), while no significant changes occurs at Cuxhaven ($\Delta ds^{Cux}_{A1B\_2}(\geq 99.5)$). The significant increase of $\Delta ds^{Sylt}_{A1B\_2}(\geq 99.5)$ occurs in the periods 2075-2077 and 2092-2095 with the highest value of 0.43 hour in 2094. This can be related mainly to the increase in duration of extreme wind events at Sylt in these periods at the end of 21st century (see Figure 5.18). The climate change signals of the mean frequency of the extreme storm-tides at both sites are within the range of the natural variability of the hindcast mean.

In this study, only one emission scenario (A1B) effect, which is regionalized by the ECHAM5-MPIOM/CLM models, on the spatial and temporal (at Cuxhaven and Sylt) distributions of storm-tide is considered. The use of different emission scenarios and/or global circulation models may have a larger effect on the future changes of the storm-tide. The future increase in frequency of extreme storm-tide events alone, which is not significant, would be less relevant for many coastal facilities whereas the increase in duration and/or magnitude of extreme events (both are significant) could decrease their safety limits.

6.2 Applicability and limitations of the TELEMAC, NARX and hybrid TELEMAC-NARX models

One of the main objectives of this study was to develop a new “operational”, low cost modelling tool for storm-tides in coastal areas and estuaries, which can account for the nonlinear interactions of the storm-tide components, and to exemplarily apply the model for the evaluation of past (1970-2007) and future (2070-2100) storm-tide events in Sylt (open coast) and Cuxhaven (estuary). The new approach combines NARX models with the flow model TELEMAC2D and the wave model TOMAWAC using the observed water level at Cuxhaven and Sylt to train the NARX models, which are available at depth of around 23 m.

- TELEMAC models

The implementation of surge-tide simulation over the North Sea using TELEMAC2D are carried out taking into account the external surge from the Atlantic ocean at the northern boundary (see Figure 3.8). The most suitable sites for considering the external surge of the North Sea model are Wick and Lerwick. Two external surge NARX models were developed for Wick and Lerwick to fill missing observed data. The performance of the two NARX models is relatively good (see Table 3.3). It can be further enhanced, if the observed wind and SLP data at both sites are used. Moreover, their performance can be improved by including as input the external surge predicted by the surge-tide model covering the North Atlantic.

In order to study the nearshore wave field in the German Bight and its effect on surge-tide, the non-steady wave propagation over the North Sea model is performed with TOMAWAC. On the northern open sea boundary the zero spectrum wave energy is prescribed (Figure 3.13), since this boundary is shifted away from the shallow part of the North Sea and the swell effect can be generated by wind over the deeper part. Nevertheless, a more accurate representation of the swell can be obtained by shifting the northern boundary further in deep water to include the part of the North Atlantic Ocean connected to the North Sea model. The predicted significant wave height has a relatively good performance despite the use of the RCM SN-REMO wind field with resolution of 50 km. This might even be enhanced if finer resolution meteorological data of the RCM SN-REMO is available. The TELEMAC2D and TOMAWAC models are coupled to simulate the wave-setup over the North Sea. The application domain of TOMAWAC is in deeper water and does not include shallow water related processes and processes due to the presence of coastal/harbour structures such as reflection and diffraction. The two considered study sites, Cuxhaven and Sylt, are located in water depths h> 20 m (constraint due to the availability of observed water level data). For areas with shallower water (h<10m). the ARTEMIS model from the TELEMAC model suite instead of TOMAWAC should be applied.

For certain extreme storms, such as December 1999 (called Anatol), the extreme of η_{OB} overestimates those computed by TELEMAC ($\eta_{st\text{-}t\ TEL\text{-}TOM}$) at Cuxhaven and Sylt. This is due to the overestimation of the predicted sea level pressure by the climate model SN-REMO as compared to the observed pressure (Nilsson et al., 2007) and/or to η_{NLT}approximation. A substantial improvement might be achieved in the prediction of storm-tide models with a finer spatial resolution (less than 10 km) of the meteorological data predicted by the RCMs in addition to observed meteorological data assimilation over the North Sea.

- NARX model

The capabilities of the developed NARX model depend on the quality and amount of the data available for training the NARX model at the considered site (at least 10 years in high temporal resolution (≤ one hour) without missing data). This is usually not available for all coastal sites, especially in developing countries. The hybrid models at both sites (Cuxhaven and Sylt) perform better (lower RMSE and higher correlation) than NARX models (without

inclusion of storm-tide by TELEMAC2D as input). Moreover, the hybrid models provide long-term prediction with higher performance than NARX models alone.

- Hybrid TELEMAC-NARX model

The capabilities of the new hybrid TELEMAC-NARX model depend on (i) the interested sites from which the observed time series of water level are available for NARX training, including the validity of the purposed physical assumptions about storm-tide components for these sites (ii) the quality and amount of the meteorological data available for numerical storm-tide prediction and NARX model training at the considered sites.

The new hybrid model during NARX training captures the nonlinear nature between extreme storm-tide components using a moderate time span of the observed water levels at the interested sites, Cuxhaven and Sylt (average water depth 23 m). The observed water level data, which has high temporal resolution (from one minute to one hour) in the period 1999-2007, not contain gapes and/or substantial amount of improbable values. Therefore, the hybrid model prediction and conclusions about nonlinear interactions are applicable only for these two sites. The results show that the hybrid model is able to extract the contribution of the nonlinear interaction between the different extreme storm-tide components at both sites as follow:

1. Evaluate each component of the extreme storm-tide $\eta_{st\text{-}t}$ (as defined in Figure 2.15) independently using the North Sea mesh in TELEMAC2D. The two interested sites are far outside of the surf zone and the wave setup component has no contribution on the predicted storm-tide. The long term effect of bathymetric evolution on storm-tide and its components are not taken into account at both sites (Woth, 2006; Gaslikova et al., 2013).
2. The components obtained from step 1 are linearly superposed in order to predict the linear storm-tide for Cuxhaven or Sylt (η_L). This is based on the assumption that the storm-tide components are calculated by TELEMAC with a high accuracy. This assumption is partly validated as the predicted tide reproduces almost exactly the tide measured in the German Bight. Nevertheless, the calculated storm surge and external surge components still need to be verified.
3. Train and develop the hybrid model using the observed water level (1999-2007) at the interested sites. So it cannot provide predictions at other sites where the NARX model is not trained.
4. The nonlinear interaction at both sites is obtained by subtracting the η_L from the predicted storm-tide obtained by the hybrid TELEMAC-NARX model. Moreover, the expected sea level rise is linearly superimposed on the predicted storm-tide as the water depth is larger than 10 m (Lowe & Gregory, 2005; Woth, 2006; Sterl et al., 2009; Howard et al., 2010; Gaslikova et al., 2013).

The training of the hybrid model requires the two wind components and SLP to be included in the input deck in addition to the observed water level at both sites. The observed meteorological data for both sites were not available in acceptable temporal resolution for past conditions (1970-2007). Therefore, these data had to be extracted from the RCMs SN-REMO for both

sites with horizontal resolution of 50 km. For future storm-tide simulation (2070-2100), only one emission scenario (A1B) is considered, which is regionalized by the ECHAM5-MPIOM/CLM models with horizontal resolution of 18 Km. Improvement in the accuracy of the hybrid model might be expected with finer resolution (≤10 km and ≤ one hour) meteorological predictions from the RCMs over the North Sea. The use of different emission scenarios and/or global circulation models for future simulation may have a larger effect on storm-tides. There might be a considerable variability in the response of the extra tropical atmospheric circulation in dependence on the used GCM/RCM and in dependence on the chosen greenhouse gas emission scenario (Woth, 2006; Gaslikova et al., 2013).

6.3 Recommendations for further research and development

- *Improvement of external surge prediction*: Some features of the domain that have not been covered in the numerical modelling might be implemented in a further study. For instance, shifting the northern and western open-sea boundaries of the North Sea model further to deeper water in the North Atlantic will provide a more accurate prediction of the external surge and swell that enter to the North Sea.

- *Application of hybrid TELEMAC-NARX model for shallower sites (h<10m*): For water depth less than 10 m, the ARTEMIS model from the TELEMAC suite, which is able to simulate wave action density (N) taking into account the effects of reflection and diffraction by structures or natural barriers, must be used instead of TOMAWAC. Furthermore, the model geometry should be updated and the bottom elevation of the domain is predicted using SISYPHE (2D sediment transport model (see Figure 3.1), which can be coupled with TELEMAC2D and other wave models of the TELEMAC suite such as ARTEMIS.

- *Nonlinear interaction between storm-tide components*: Since the NARX part of the developed hybrid model is trained using only the observed water level in Sylt and Cuxhaven, the conclusions drawn from the results of the TELEMAC-NARX model on the effect of the nonlinear interaction between the diverse components on the resulting storm-tide level might not be valid for other sites. Therefore, it is suggested to apply the methodology of the hybrid model to other sites over the North Sea, which will provide the assessment of nonlinear interaction contribution. This gives the possibility to accelerate the enhancements of storm-tide numerical modelling.

- *Improvement of the spatial resolution of the RCM meteorological data*: A substantial improvement might be achieved in the prediction of the hybrid TELEMAC-NARX model with a finer spatial resolution (less than 10 km) of the meteorological data predicted by the RCMs over the North Sea. This might also improve the results of the wave models. Furthermore, the use of the observed wind/pressure data as inputs for training the NARX models at the diverse sites (e.g. Wick, Lerwick, Cuxhaven and Sylt) may also improve their prediction performance.

- *Effect of emission scenarios and applied climate models on storm-tide*: The use of different emission scenarios and RCMs may have a larger effect on the changes of storm-tide statistics in the context of climate change. A considerable variability might be expected in the response of the extra tropical atmospheric circulation depending on the applied GCM/RCM and on the chosen greenhouse gas emission scenario. Bringing more light into the possible range of uncertainties involved will represent a major challenge for future climate impact studies.

References

Aelbrecht, D.; Acinas, J. R.; Brebbia, C. A. (1997): 'ARTEMIS 3.0: A finite element model for predicting wave agitation in coastal areas and harbours including dissipation'. *Transactions on the Built Enviroment*, vol. 27.

Aguado, E.; Burt, J. E. (2007): *Understanding weather and climate*. Pearson Prentice Hall Upper Saddle River, NJ, USA,

Alliance, F. H.; Huang, W. (2007): 'Development of a Florida Coastal Neural Network Model For Water Level Predictions'. *Report submitted to Florida Hurricane Alliance, International Hurricane Research Center Florida International University, Miami, Florida*,

Arns, A.; Jensen, J. (2013): 'Extreme water level statistics in the German Bight: A best practice approach'. Presented at the proceeding of International Short Conference on Advances in Extreme Value Analysis and Application to Natural Hazards (EVAN2013)

Arns, A.; Wahl, T.; Dangendorf, S.; Jensen, J. (2015): 'The impact of sea level rise on storm surge water levels in the northern part of the German Bight'. *Coastal Engineering*, vol. 96, pp. 118–131.

Arns, A.; Wahl, T.; Haigh, I. D.; Jensen, J.; Pattiaratchi, C. (2013): 'Estimating extreme water level probabilities: A comparison of the direct methods and recommendations for best practise'. *Coastal Engineering*, vol. 81, pp. 51–66.

Ata, R.; Hervouet, J. M. (2012): 'Telemac version 6.2, release notes'. *Telemac-2D and Telemac-3D*,

Bajo, M.; Umgiesser, G. (2010): 'Storm surge forecast through a combination of dynamic and neural network models'. *Ocean Modelling*, vol. 33, 1, pp. 1–9.

Banner, F. T. (2011): *Physical and Chemical Oceanography, and Physical Resources*. Elsevier,

Battjes, J. A.; Janssen, J. (1978): 'Energy loss and set-up due to breaking of random waves'. *Coastal Engineering Proceedings*, vol. 1, 16.

Beale, M.; Hagan, M.; Demuth, H. (2013): 'Neural network toolbox user's guide Matlab user's guide'

Beniston, M.; Stephenson, D. B.; Christensen, O. B.; Ferro, C. A.; Frei, C.; Goyette, S.; Halsnaes, K.; Holt, T.; Jylhä, K.; Koffi, B. (2007): 'Future extreme events in European climate: an exploration of regional climate model projections'. *Climatic Change*, vol. 81, 1, pp. 71–95.

Benoit, M. (2003): *Logiciel TOMAWAC de modélisation des états de mer en éléments finis. Notice de la version 5.2*. Rapport HP-75/02/065/A, EDF-LNHE

Benoit, M. (2011): *TOMAWAC-Software for sea state modelling on unstructured grids over oceans and coastal seas*. Release,

Benoit, M.; Marcos, F.; Becq, F. (2001): 'Development of a third generation shallow-water wave model with unstructured spatial meshing'. *Coastal Engineering Proceedings*, vol. 1, 25. doi:10.9753/icce.v25.

Brönnimann, S.; Martius, O.; Franke, J.; Stickler, A.; Auchmann, R. (2013): 'Historical weather extremes in the "Twentieth Century Reanalysis"'. *Weather extremes during the past*, vol. 140, pp. 7–17.

Bruss, G.; Gönnert, B.; Mayerle, R. (2011): 'Extreme scenarios at the german North Sea coast a numerical model study'. *Coastal Engineering Proceedings*, vol. 1, 32, p. currents. 26.

Burlace, M. I. (1986): 'The negative North Sea surge of the 19th December 1982'. *Hydrogaphic Journal*, vol. 39, pp. 11–15.

Butler, A.; Heffernan, J. E.; Tawn, J. A.; Flather, R. A.; Horsburgh, K. J. (2007): 'Extreme value analysis of decadal variations in storm surge elevations'. *Journal of Marine Systems*, vol. 67, 1, pp. 189–200.

Chen, W.-B.; Liu, W.-C.; Hsu, M.-H. (2012): 'Predicting typhoon-induced storm surge tide with a two-dimensional hydrodynamic model and artificial neural network model'. *Natural Hazards and Earth System Science*, vol. 12, 12, pp. 3799–3809.

Chini, N. (2012, June 30): 'A contribution towards the analysis of the effect of climate change and sea level rise on hydrodynamic conditions and sediment transport off East Anglian coast'. *[Thesis]. Manchester, UK: The University of Manchester; 2012.*, Retrieved October 19, 2014, from https://www.escholar.manchester.ac.uk/uk-ac-man-scw:163927

Clancy, R. M.; Kaitala, J. E.; Zambresky, L. F. (1986): 'The Fleet Numerical Oceanography Center global spectral ocean wave model'. *Bulletin of the American Meteorological Society*, vol. 67, 5, pp. 498–512.

'Complete neuron cell diagram'. (2013, April 7): In , *Wikipedia, the free encyclopedia*, Retrieved from http://en.wikipedia.org/w/index.php?title=File:Complete_neuron_cell_diagram_en.svg&oldid=370915184

Dangendorf, S.; Müller-Navarra, S.; Jensen, J.; Schenk, F.; Wahl, T.; Weisse, R. (2014): 'North Sea Storminess from a Novel Storm Surge Record since AD 1843*'. *Journal of Climate*, vol. 27, 10, pp. 3582–3595.

Debernard, J.; Røed, L. P. (2008): 'Future wind, wave and storm surge climate in the Northern Seas: a revisit'. *Tellus A*, vol. 60, 3, pp. 427–438.

Debernard, J.; Sætra, Ø.; Røed, L. P. (2003): 'Future wind, wave and storm surge climate in the northern North Atlantic'. In , *EGS-AGU-EUG Joint Assembly*, (Vol. 1, p. 2701)

De Jong, M. S. (2012): *Developing a parametric model for storms to determine the extreme surge level at the Dutch coast*. Ph.D. thesis, TU Delft, Delft University of Technology.

Deltares. (2010): 'Deltares edDelft3D-FLOW'. *Delft, The Netherlands*,

DERM; The Queensland Government Department of Environment and Resource Management. (2009): 'Tropical Cyclone-Induced Water Levels and Waves: Hervey Bay and Sunshine Coast' vol. Queensland Climate Change and Community Vulnerability to Tropical Cyclones, Stage 2 Report, July 2004.

Domingues, C. M.; Church, J. A.; White, N. J.; Gleckler, P. J.; Wijffels, S. E.; Barker, P. M.; Dunn, J. R. (2008): 'Improved estimates of upper-ocean warming and multi-decadal sea-level rise'. *Nature*, vol. 453, 7198, pp. 1090–1093.

Doodson, A. T. (1973): *Admiralty Manual of Tides*. H.M.Stationary Office,

Dronkers, J. J. (1964): 'Tidal computations in rivers and coastal waters'

Dyke, P. (2007): *Modeling coastal and offshore processes*. World Scientific,

Eldeberky, Y.; Battjes, J. A. (1995): 'Parameterization of triad interactions in wave energy models'

Elder, J. W. (1959): 'The dispersion of marked fluid in turbulent shear flow'. *Journal of fluid mechanics*, vol. 5, 04, pp. 544–560.

Fealy, R.; Sweeney, J.; Murphy, C.; McElwain, L. (2012): *The Isle of Man Climate Change Scoping Study: Climate Indicators for acclimatise and the Department of Local Government and the Environment, Isle of Man Government*

Flather, R. A. (2000): 'Existing operational oceanography'. *Coastal Engineering*, vol. 41, 1, pp. 13–40.

Flather, R. A.; Smith, J. A. (1998): 'First estimates of changes in extreme storm surge elevations due to the doubling of CO2'. *The Global Atmosphere and Ocean System*, vol. 6, 2, pp. 193–208.

Flather, R. A.; Williams, J. (2000): 'Climate change effects on storm surges: methodologies and results'. *Climate scenarios for water-related and coastal impacts*, 3, pp. 66–72.

Galland, J.-C.; Goutal, N.; Hervouet, J.-M. (1991): 'TELEMAC: A new numerical model for solving shallow water equations'. *Advances in Water Resources*, vol. 14, 3, pp. 138–148.

Gaslikova, L.; Grabemann, I.; Groll, N. (2013): 'Changes in North Sea storm surge conditions for four transient future climate realizations'. *Natural Hazards*, vol. 66, 3, pp. 1501–1518.

Giardino, A.; Monbaliu, J. (2003): *tidal simulations in the North Sea* (internal report). KATHOLIEKE UNIVERSITEIT LEUVEN, faculteit toegepaste wetenschappen department burgerlijke boukunde laboratorium voor hydraulica Retrieved from http://www.kuleuven.be/hydr/FWOkust/activities/numelab/telemac/telemac.html

Goennert, G.; Sossidi, K. (2011): 'A new approach to calculate extreme storm surges: analysing the interaction of storm surge components' pp. 139–150. doi:10.2495/CP110121

Gönnert, G. (2001): *Sonderheft Global storm surges : theory, observations and applications*. Heide i. Holstein : Westholsteinische Verlagsanst. Boyens,

Gönnert, G.; Thumm, S. (2010): 'Das Risiko von Extremsturmfluten in Ästuaren angesichts globalen Klimawandels'. *From Brazil to Thailand - New Results in Coastal Research. Coastline Reports*, vol. 16, pp. 77–86. EUCC – Die Küsten Union Deutschland e.V., Rostock, 2010.

Hagan, M. T.; Demuth, H. B.; Beale, M. (1996): *Neural network design*. PWS Pub. Co., Boston [etc.].

Hagan, M. T.; Menhaj, M. B. (1994): 'Training feedforward networks with the Marquardt algorithm'. *Neural Networks, IEEE Transactions on*, vol. 5, 6, pp. 989–993.

Hansen, U. A. (1978): 'Wave Setup and Design Water Level'. *Journal of the Waterway Port Coastal and Ocean Division*, vol. 104, 2, pp. 227–240.

Hasselmann, S.; Hasselmann, K.; Allender, J. H.; Barnett, T. P. (1985): 'Computations and parameterizations of the nonlinear energy transfer in a gravity-wave specturm. Part II: Parameterizations of the nonlinear energy transfer for application in wave models'. *Journal of Physical Oceanography*, vol. 15, 11, pp. 1378–1391.

Haykin, S. S. (1999): *Neural networks: a comprehensive foundation*. Prentice Hall, 872.

Hervouet, J.-M. (2007): *Hydrodynamics of Free Surface Flows: Modelling with the Finite Element Method*. John Wiley & Sons, Chichester ; Hoboken, N.J, 378.

Hervouet, J.-M.; Van Haren, E. (1994): *TELEMAC-2D Principle Note. Electrité de France*. Technical Report

Higaki, M.; Hayashibara, H.; Nozaki, F. (2009): 'Outline of the Storm Surge Prediction Model at the Japan Meteorological Agency' vol. RSMC Tokyo - Typhoon Center, Technical Review No.11.

Hofstede, J. (2004): 'A new coastal defence master plan for Schleswig-Holstein'. *Geographie der Meere und Küsten. Coastline Reports*, vol. 1, 2004, pp. 109–117.

Hornik, K. (1993): 'Some new results on neural network approximation'. *Neural Netw.*, vol. 6, 9, pp. 1069–1072. doi:10.1016/S0893-6080(09)80018-X

Horsburgh, K. J.; Wilson, C. (2007): 'Tide-surge interaction and its role in the distribution of surge residuals in the North Sea'. *Journal of Geophysical Research: Oceans*, vol. 112, C8, p. C08003. doi:10.1029/2006JC004033

Houghton, J. T. (1996): *Climate change 1995: The science of climate change: contribution of working group I to the second assessment report of the Intergovernmental Panel on Climate Change*. Cambridge University Press,

Houghton, J. T.; Callander, B. A.; Varney, S. K. (1992): *Climate change 1992: the supplementary report to the IPCC scientific assessment*. Cambridge University Press,

Houghton, J. T.; Ding, Y.; Griggs, D. J.; Noguer, M.; van der Linden, P. J.; Dai, X.; Maskell, K.; Johnson, C. A. (2001): *Climate change 2001: the scientific basis*. Cambridge university press Cambridge,

Howard, T.; Lowe, J.; Horsburgh, K. (2010): 'Interpreting Century-Scale Changes in Southern North Sea Storm Surge Climate Derived from Coupled Model Simulations'. *Journal of Climate*, vol. 23, 23, pp. 6234–6247. doi:10.1175/2010JCLI3520.1

Janssen, P. A. (1989): 'Wave-induced stress and the drag of air flow over sea waves'. *Journal of Physical Oceanography*, vol. 19, 6, pp. 745–754.

Janssen, P. A. (1991): 'Quasi-linear theory of wind-wave generation applied to wave forecasting'. *Journal of Physical Oceanography*, vol. 21, 11, pp. 1631–1642.

Janssen, P. A.; Komen, G. J.; De Voogt, W. J. (1984): 'An operational coupled hybrid wave prediction model'. *Journal of Geophysical Research: Oceans (1978–2012)*, vol. 89, C3, pp. 3635–3654.

Jayawardena, A. W.; Fernando, T. (2001): 'River flow prediction: An artificial neural network approach'. *IAHS PUBLICATION*, pp. 239–246.

Jensen, J.; Mudersbach, C. (2008): 'Simulation of Super Storms in the North Sea'. Presented at the Proceedings of the 7th International Conference on Coastal and Port Engineering in Developing Countries (PIANC COPEDEC VII)

Jensen, J.; Mudersbach, C.; Blasi, C. (2003): 'Hydrological changes in tidal estuaries due to natural and anthropogenic effects'. In , *6th International MEDCOAST 2003 Conference, Ravenna, Italy*, Retrieved from http://www.bau.uni-siegen.de/fwu/wb/forschung/publikationen/medcoast03_estuaries.pdf

Jensen, J.; Mudersbach, C.; Müller-Navarra, S.; Bork, I.; Koziar, C.; Renner, V. (2006): 'Modellgestützte Untersuchungen zu Sturmfluten mit sehr geringen Eintrittswahrscheinlichkeiten an der Deutschen Nordseeküste'. *Die Küste*, vol. 71, pp. 123–167.

Jensen, J.; Mudersbach, C.; Wahl, T. (2008): 'Simulation of super storms for better estimation of design parameters'. *Proceedings of the Coastal Cities Summit 2008, St. Petersburg, USA*,

Joseph, F. (2009): *A Monte Carlo approach to joint probability of wave, tide and surge in extreme water level calculations. Prepared by PhysE Limited for the Health and Safety Executive 2009*. p. 60 Retrieved from http://www.hse.gov.uk/research/rrhtm/rr740.htm

Khan, S. R. (1995): 'Geomorphic characterization of cyclone hazards along the coast of Bangladesh'. *International Institute for Aerospace and Earth Sciences (ITC), The Netherlands (unpublished M. Sc. thesis)*,

Komen, G. J.; Hasselmann, K.; Hasselmann, K. (1984): 'On the existence of a fully developed wind-sea spectrum'. *Journal of physical oceanography*, vol. 14, 8, pp. 1271–1285.

Kösters, F.; Winter, C. (2013): 'Exploring German Bight coastal morphodynamics based on modelled bed shear stress'. *Geo-Marine Letters*, pp. 1–16.

Lautenschlager, M.; Keuler, K.; Wunram, C.; Keup-Thiel, E.; Schubert, M.; Will, A.; Rockel, B.; Boehm, U. (2009): 'Climate Simulation with CLM, Climate of the 20th Century run no. 1 & no. 2, Scenario A1B run no. 1 & no. 2, Scenario B1 run no. 1, Data Stream 2: European region MPI-M'. *MaD. WDCC.[doi: 10.1594/WDCC/CLM_C20_1_D2, CLM_C20_2_D2, CLM_A1B_1_D2, CLM_A1B_2_D2, CLM_B1_1_D2]*,

Lin, T.; Horne, B. G.; Tino, P.; Giles, C. L. (1996): 'Learning long-term dependencies in NARX recurrent neural networks'. *Neural Networks, IEEE Transactions on*, vol. 7, 6, pp. 1329–1338.

Longuet-Higgins, M. S.; Stewart, R. W. (1964): 'Radiation stresses in water waves; a physical discussion, with applications'. In , *Deep Sea Research and Oceanographic Abstracts*, (Vol. 11, pp. 529–562)

Lowe, J. A.; Gregory, J. M. (2005): 'The effects of climate change on storm surges around the United Kingdom'. *Philosophical Transactions of the Royal Society A: Mathematical, Physical and Engineering Sciences*, vol. 363, 1831, pp. 1313–1328. doi:10.1098/rsta.2005.1570

Makarynskyy, O.; Makarynska, D.; Kuhn, M.; Featherstone, W. E. (2004): 'Predicting sea level variations with artificial neural networks at Hillarys Boat Harbour, Western Australia'. *Estuarine, Coastal and Shelf Science*, vol. 61, 2, pp. 351–360.

Mandal, S.; Prabaharan, N. (2006): 'Ocean wave forecasting using recurrent neural networks'. *Ocean Engineering*, vol. 33, 10, pp. 1401–1410. doi:10.1016/j.oceaneng.2005.08.007

Martini, F. H.; Nath, J. L.; Bartholomew, E. F. (2011): *Fundamentals of Anatomy & Physiology*. Benjamin Cummings, 1264.

McCulloch, W. S.; Pitts, W. (1943): 'A logical calculus of the ideas immanent in nervous activity'. *Bulletin of Mathematical Biophysics*, vol. 5, 4, pp. 115–133. doi:10.1007/BF02478259

Meehl, G. A.; Stocker, T. F.; Collins, W. D.; Friedlingstein, P.; Gaye, A. T.; Gregory, J. M.; Kitoh, A.; Knutti, R.; Murphy, J. M.; Noda, A. (2007): 'Global climate projections'. *Climate change*, vol. 3495, pp. 747–845.

Menezes Jr, J. M. P.; Barreto, G. A. (2008): 'Long-term time series prediction with the NARX network: An empirical evaluation'. *Neurocomputing*, vol. 71, 16, pp. 3335–3343.

Mewis, P. (2006): 'Nearshore Wave Simulation for the Hoernum Tideway – Verification and Changes in Wave Climate and Wave Runup Caused by Morphological Evolution'. *Third Chinese-German Joint Symposium on Coastal and Ocean Engineering National Cheng Kung University, Tainan*,

Mitchell, T. M. (1997): *Machine Learning*. McGraw-Hill Science/Engineering/Math, 432.

Mitrovica, J. X.; Gomez, N.; Clark, P. U. (2009): 'The sea-level fingerprint of West Antarctic collapse'. *Science*, vol. 323, 5915, pp. 753–753.

Mudersbach, C.; Wahl, T.; Jensen, J. (2012): 'Estimating future probabilities of extreme sea levels'. In , *Proceedings of the 33rd International Conference on Coastal Engineering*, . Presented at the 33rd International Conference on Coastal Engineering

Munich Re. (2012): *Historical storm surge events* Retrieved from http://www.munichre.com/site/corporate/get/documents_E1318646163/mr/assetpool.shared/Documents/0_Corporate%20Website/6_Media%20Relations/Press%20Dossiers/50th%20anniversary%20storm%20surge%20hamburg/historical-storm-surge-events-en.pdf

Niemeyer, H. D.; Eiben, H.; Rohde, H. (1996): 'History and Heritage of German Coastal Engineering'. In , *N.C. Kraus (ed): History and Heritage of Coastal Engineering, American Society of Civil Engineers*, (pp. 169–214)

Nilsson, C.; Bärring, L.; Goyette, S. (2005): 'Relating Forest Damage Data to the Wind Field from High Resolution RCM Simulations: Case study of Anatol Passing Sweden in December 1999'. In , *Geophysical Research Abstracts*, (Vol. 7, p. 09883)

Nilsson, C.; Goyette, S.; Bärring, L. (2007): 'Relating forest damage data to the wind field from high-resolution RCM simulations: Case study of Anatol striking Sweden in December 1999'. *Global and Planetary Change*, vol. 57, 1, pp. 161–176.

Noorzaei, J.; Hakim, S. J. S.; Jaafar, M. S.; Thanoon, W. A. M. (2007): 'Development of artificial neural networks for predicting concrete compressive strength'. *International Journal of Engineering and Technology*, vol. 4, 2, pp. 141–153.

Open University. (1999): *Waves, tides, and shallow-water processes*. Butterworth-Heinemann, in association with the Open University, Oxford ; Boston, 227.

Otto, L.; Zimmerman, J. T. F.; Furnes, G. K.; Mork, M.; Saetre, R.; Becker, G. (1990): 'Review of the physical oceanography of the North Sea'. *Netherlands Journal of Sea Research*, vol. 26, 2, pp. 161–238.

Oumeraci, H. (2000): 'The sustainability challenge in coastal engineering'. *Keynote lecture. Proc. 4th. IcsnGConG. Hydrodynamics (ICHD) in Yokohama, Japan*, vol. 1, pp. 57–84.

Oumeraci, H. (2004): 'Sustainable coastal flood defences: scientific and modelling challenges towards an integrated risk-based design concept'. In , *Proc. First IMA International Conference on Flood Risk Assessment, IMA-Institute of Mathematics and its Applications, Session*, (Vol. 1, pp. 9–24)

Oumeraci, H. (2009): 'Storm Surge and design water levels (lecture notes in German)'

Pashova, L.; Koprinkova-Hristova, P. D.; Popova, S. (2013): 'Gap filling of daily sea levels by artificial neural networks'. *TransNav: International Journal on Marine Navigation and Safety of Sea Transportation*, vol. 7, 2.

Pawlowicz, R.; Beardsley, B.; Lentz, S. (2002): 'Classical tidal harmonic analysis including error estimates in MATLAB using T_TIDE'. *Computers & Geosciences*, vol. 28, 8, pp. 929–937. doi:10.1016/S0098-3004(02)00013-4

Pedlosky, J. (1982): 'Geophysical fluid dynamics'. *New York and Berlin, Springer-Verlag, 1982. 636 p.*, vol. 1.

Petersen, M.; Rohde, H. (1979): *Sturmflut: die grossen Fluten an den Küsten Schleswig-Holsteins und in der Elbe*. Karl Wachholtz,

Pielke, R. A. (1991): 'A recommended specific definition of" resolution'. *Agric. For. Meteorol*, vol. 55, pp. 345–349.

Plüß, A. (2004): 'Das Nordseemodell der BAW zur Simulation der Tide in der Deutschen Bucht'. *Die Küste*, vol. 67, pp. 83 – 127.

Prandle, D.; Wolf, J. (1978a):. 'The interaction of surge and tide in the North Sea and River Thames'. *Geophysical Journal International*, vol. 55, 1, pp. 203–216.

Prandle, D.; Wolf, J. (1978b):. 'The interaction of surge and tide in the North Sea and River Thames'. *Geophysical Journal International*, vol. 55, 1, pp. 203–216.

Prouty, D. B.; Tissot, P.; Anwer, A. (2008): 'Using ensembles of artificial neural networks for storm surge predictions in the North Sea'. In , *Sixth Conference on Artificial Intelligence Applications to Environmental Science*,

Pugh, D. T. (1996): *Tides, surges and mean sea-level (reprinted with corrections)*. John Wiley & Sons Ltd,

Rakshith, S.; DWARAKISH, G.; NATESAN, U. (2014): 'TIDAL-LEVEL FORECASTING USING ARTIFICIAL NEURAL NETWORKS ALONG THE WEST COAST OF INDIA'. *Journal of JSCE*, vol. 2, 1, pp. 176–187.

Ramachandran, K. (2010): *Tidal Morphodynamic Modelling in the Dee Estuary, UK*. Ph.D. thesis, TU Delft, Delft University of Technology.

Ranganathan, A. (2004): 'The levenberg-marquardt algorithm'. *Tutoral on LM Algorithm*,

Roeckner, E. (2003): 'Coauthors, 2003: The atmospheric general circulation model ECHAM5'. *Part I: Model description. Max Planck Institute for Meteorology Rep*, vol. 349, p. 127.

Sapna, S.; Tamilarasi, A.; Kumar, M. P. (2013): 'Backpropagation Learning Algorithm Based On Levenberg Marquardt Algorithm'. *CS & IT-CSCP*, vol. 2, 2.

Shreenivas, N.; Pradnya, R. (2012): 'Genetic Programming: A Novel Computing Approach in Modeling Water Flows'. In , S. Ventura Soto (Ed.), , *Genetic Programming - New*

Approaches and Successful Applications, Retrieved from http://www.intechopen.com/books/genetic-programming-new-approaches-and-successful-applications/genetic-programming-a-novel-computing-approach-in-modeling-water-flows

siek, michael. (2011): *Predicting Storm Surges Chaos, Computational Intelligence, Data Assimilation and Ensembles: UNESCO-IHE PhD Thesis.* CRC Press,

Siek, M.; Solomatine, D. P. (2011): 'Real-time data assimilation for chaotic storm surge model using NARX neural network'. In , *Proceedings of the 11th International Coastal Symposium*, (pp. 1189–1194)

Solomatine, D. P. (2002): 'Data-driven modelling: paradigm, methods, experiences'. In , *Proc. 5th international conference on hydroinformatics*, (pp. 1–5)

Sossidi, K.; Gönnert, G.; Gerkensmeier, B. (2010): 'The risk and calculation of extreme storm surges due to climate change.'. *Presentation Storm Surges Congress 2010 - Risk and Management of current and future Storm Surges, Hamburg, Germany.*,

Spencer, T.; Brooks, S. M.; Evans, B. R.; Tempest, J. A.; Möller, I. (2015): 'Southern North Sea storm surge event of 5 December 2013: Water levels, waves and coastal impacts'. *Earth-Science Reviews*, vol. 146, pp. 120–145. doi:10.1016/j.earscirev.2015.04.002

Sterl, A.; van den Brink, H.; Vries, H. de; Haarsma, R.; van Meijgaard, E. (2009): 'An ensemble study of extreme storm surge related water levels in the North Sea in a changing climate'. *Ocean Science*, vol. 5, 3, pp. 369–378.

Sündermann, J.; Pohlmann, T. (2011): 'A brief analysis of North Sea physics'. *Oceanologia*, vol. 53, 3, pp. 663–689.

Takayama, T. (2002): *Fundamental study on advancement of storm surge and wave forecasting technology and disaster mitigation*. Disaster Prevention Research Institute, Kyoto University, p. 408

Tayel, M.; Oumeraci, H. (2012a):. *The compilation, configuration and set up of TELEMAC system V6p2 in parallel mode using multiprocessors in a single computer or local area network* (No. 2). LWI internal report, p. 47

Tayel, M.; Oumeraci, H. (2012b):. *Meteorological data preparation from 1970 to 2007 and configuration of the North Sea TELEMAC2D model.* (No. 3). LWI internal report, p. 90

Taylor, K. E. (2001): 'Summarizing multiple aspects of model performance in a single diagram'. *Journal of Geophysical Research*, vol. 106, D7, pp. 7183–7192. doi:10.1029/2000JD900719

Timmerman, H. (1975): 'On the importance of atmospheric pressure gradients for the generation of external surges in the North Sea'. *Deutsche Hydrographische Zeitschrift*, vol. 28, 2, pp. 62–71.

Tissot, P. E.; Cox, D. T.; Michaud, P. (2002): 'Neural Network Forecasting of Storm Surges along the Gulf of Mexico' (pp. 1535–1544) doi:10.1061/40604(273)155

Tomczak, M. (2002): *Lecture Notes in Oceanography*

van Beusekom, J.; Fock, H.; Jong, F. de; Diehl-Christiansen, S.; Christiansen, B. (2001): 'Wadden Sea specific eutrophication criteria'. *Wadden Sea Ecosystem*, vol. 14, pp. 1–115.

Velema, J. J. (2010): 'On the tidal dynamics of the North Sea: an idealised modelling study on the role of bottom friction, the Dover Strait and tidal resonance in the North Sea'

Villaret, C. (2010): 'SISYPHE 6.0 User Manual'. *Modelisation des Apports Hydriques et Transferts Hydro-Sedimentaires-Laboratoire National d'hydraulique et Environnement*,

von Storch, H. (1995): 'Inconsistencies at the interface of climate impact studies and global climate research'. *Meteorologische Zeitschrift*, vol. 4, 2, pp. 72–80.

von Storch, H.; GKSS, G. (2005): 'Veränderliches Küstenklima–die vergangenen und zukünftigen 100 Jahre'. *Kulturlandschaft Marsch: Natur, Geschichte und Gegenwart, Isensee-Verlag, Oldenburg*, pp. 229–245.

von Storch, H.; Langenberg, H.; Feser, F. (2000): 'A spectral nudging technique for dynamical downscaling purposes.'. *Monthly weather review*, vol. 128, 10, pp. 3664–3673.

Wahl. (2012): 'Statistical methods to assess the hydrodynamic boundary conditions for risk based design approaches in coastal engineering'

Wahl; Jensen, J.; Mudersbach, C. (2011): 'A multivariate statistical model for advanced storm surge analyses in the North Sea'. *Coastal Engineering Proceedings*, vol. 1, 32, p. currents. 19.

Wahl; Mudersbach, C.; Jensen, J. (2011): 'Assessing the hydrodynamic boundary conditions for risk analyses in coastal areas: a stochastic storm surge model'. *Natural Hazards and Earth System Science*, vol. 11, 11, pp. 2925–2939.

Wahl, T.; Haigh, I. D.; Woodworth, P. L.; Albrecht, F.; Dillingh, D.; Jensen, J.; Nicholls, R. J.; Weisse, R.; Wöppelmann, G. (2013): 'Observed mean sea level changes around the North Sea coastline from 1800 to present'. *Earth-Science Reviews*, vol. 124, pp. 51–67.

Wahl, T.; Jensen, J.; Frank, T. (2010): 'On analysing sea level rise in the German Bight since 1844'. *Natural Hazards and Earth System Science*, vol. 10, 2, pp. 171–179.

Wahl, T.; Jensen, J.; Frank, T.; Haigh, I. D. (2011): 'Improved estimates of mean sea level changes in the German Bight over the last 166 years'. *Ocean Dynamics*, vol. 61, 5, pp. 701–715.

Wahl, T.; Mudersbach, C.; Jensen, J. (2015): 'Statistical assessment of storm surge scenarios within integrated risk analyses'. *Coastal Engineering Journal*,

Walton, T. L.; Dean, R. G. (2009): 'Influence of discrete step size on wind setup component of storm surge'. *Coastal Engineering*, vol. 56, 9, pp. 1005–1008. doi:10.1016/j.coastaleng.2009.05.003

WAMDI Group, T. W. (1988): 'The WAM model-a third generation ocean wave prediction model'. *Journal of Physical Oceanography*, vol. 18, 12, pp. 1775–1810.

Weaver, R. J.; Slinn, D. N. (2004): 'Effect of wave forcing on storm surge'. In , *COASTAL ENGINEERING CONFERENCE*, (Vol. 29, p. 1532) Retrieved from http://www.worldscientific.com/doi/pdf/10.1142/9789812701916_0122

Weenink, M. P. H. (1956): 'The “twin” storm surges during 21st–24th December, 1954. A case of resonance'. *Deutsche Hydrografische Zeitschrift*, vol. 9, 5, pp. 240–249.

Weisse, R.; Plüß, A. (2006): 'Storm-related sea level variations along the North Sea coast as simulated by a high-resolution model 1958–2002'. *Ocean Dynamics*, vol. 56, 1, pp. 16–25.

Winter, C. (2011): 'Macro scale morphodynamics of the German North Sea coast'. *Journal of Coastal Research, SI*, vol. 64, pp. 706–710.

Wolf, J. (1981): 'Surge-tide interaction in the North Sea and River Thames'. *Floods due to high winds and tides*, pp. 75–94.

Wolf, J. (2009): 'Coastal flooding: impacts of coupled wave–surge–tide models'. *Natural Hazards*, vol. 49, 2, pp. 241–260. doi:10.1007/s11069-008-9316-5

Woth, K. (2006): *Regionalization of global climate change scenarios: An ensemble study of possible changes in the North Sea storm surge statistics* (PhD). Ph.D. thesis, GKSS-Forschungszentrum, Bibliothek, 108.

Woth, K.; Weisse, R.; von Storch, H. (2006): 'Climate change and North Sea storm surge extremes: an ensemble study of storm surge extremes expected in a changed climate projected by four different regional climate models'. *Ocean Dynamics*, vol. 56, 1, pp. 3–15.

YU, C.-S. (1993): *Modelling shelf sea dynamics and estuarine circulations* (Ph.D). Ph.D. thesis, K. U. Leuven, Dept. of Civil Eng.